Reinforced Concrete Beams, Columns and Frames

Reinforced Concrete Beams, Columns and Frames

Mechanics and Design

Charles Casandjian
Noël Challamel
Christophe Lanos
Jostein Hellesland

iSTE WILEY

First published 2013 in Great Britain and the United States by ISTE Ltd and John Wiley & Sons, Inc.

ISTE Ltd
27-37 St George's Road
London SW19 4EU
UK

www.iste.co.uk

John Wiley & Sons, Inc.
111 River Street
Hoboken, NJ 07030
USA

www.wiley.com

Library of Congress Control Number: 2012953072

British Library Cataloguing-in-Publication Data
A CIP record for this book is available from the British Library
ISBN: 978-1-84821-482-8

Printed and bound in Great Britain by CPI Group (UK) Ltd., Croydon, Surrey CR0 4YY

Table of Contents

Preface xi

Chapter 1. Design at Serviceability Limit State (SLS) 1

1.1. Nomenclature 1
1.1.1. Convention with the normal vector orientation 1
1.1.2. Vectorial notation 1
1.1.3. Part of the conserved reference section 2
1.1.4. Frame 2
1.1.5. Compression stress $\sigma_{c,sup}$ in the most compressed fiber 2
1.2. Bending behavior of reinforced concrete beams – qualitative analysis 3
1.2.1. Framework of the study 3
1.2.2. Classification of cross-sectional behavior 5
1.2.3. Parameterization of the response curves by the stress σ_{s1} of the most stressed tensile reinforcement 5
1.2.4. Comparison of σ_{s1} of the tensile reinforcement for a given stress in the most compressed concrete fiber $\sigma_{c,sup}$ 6
1.2.5. Comparison of the bending moments 8
1.3. Background on the concept of limit laws 10
1.3.1. Limit law for material behavior 10
1.3.2. Example of limit laws in physics, case of the transistor 11
1.3.3. Design of reinforced concrete beams in bending at the stress Serviceability Limit State 12
1.4. Limit laws for steel and concrete at Serviceability Limit State 13
1.4.1. Concrete at the cross-sectional SLS 13
1.4.2. Steel at the cross-sectional SLS 13
1.4.3. Equivalent material coefficient 14
1.5. Pivots notion and equivalent stress diagram. 14

1.5.1. Frame and neutral axis 14
1.5.2. Conservation of planeity of a cross-section. 15
1.5.3. Planeity conservation law in term of stress 17
1.5.4. Introduction to pivot concepts 18
1.5.5. Pivot rules 19
1.6. Dimensionless coefficients. 20
1.6.1. Goal 20
1.6.2. Total height of the cross-section 21
1.6.3. Relative position of the neutral axis 21
1.6.4. Shape filling coefficient 22
1.6.5. Dimensionless formulation for the position of the center of pressure 23
1.7. Equilibrium and resolution methodology 24
1.7.1. Equilibrium equations 24
1.7.2. Discussion on the resolution of equations with respect to the number of unknowns 26
1.7.3 Reduced moments 27
1.7.4. Case of a rectangular section 29
1.8. Case of pivot A for a rectangular section 30
1.8.1. Studied section 30
1.8.2. Shape filling coefficient 30
1.8.3. Dimensionless coefficient related to the center of pressure 31
1.8.4. Equations formulation 32
1.8.5. Resolution 33
1.9. Case of pivot B for a rectangular section 35
1.9.1. Studied section 35
1.9.2. Shape filling coefficient 35
1.9.3. Dimensionless coefficient related to the center of pressure 35
1.9.4. Equations formulation 36
1.9.5. Resolution 37
1.9.6. Synthesis 38
1.10. Examples – bending of reinforced concrete beams with rectangular cross-section. 39
1.10.1. A design problem at SLS – exercise 39
1.10.2. Resolution in Pivot A – M_{ser} = 225 kN.m 42
1.10.3. Resolution in Pivot B – M_{ser} = 405 kN.m 45
1.10.4. Resolution in pivot AB 47
1.10.5. Design of a reinforced concrete section, an optimization problem 50
1.10.6. General design at Serviceability Limit State with tensile and compression steel reinforcements 54

1.11. Reinforced concrete beams with T-cross-section 58
1.11.1. Introduction 58
1.11.2. Decomposition of the cross-section 60
1.11.3. Case of pivot A for a T-cross-section 61
1.11.4. Case of pivot B for a T-cross-section 63
1.11.5. Example – design of reinforced concrete beams composed of T-cross-section 65

Chapter 2. Verification at Serviceability Limit State (SLS) 69

2.1. Verification of a given cross-section – control design 69
2.1.1. Position of the neutral axis 69
2.1.2. Equation of static moments for the determination of the position of neutral axis 70
2.1.3. Stress calculation – general case 72
2.1.4. Rectangular cross-section – verification of a given cross-section 74
2.1.5. T-cross-section – verification of a given cross-section 76
2.1.6. Example – verification of a reinforced T-cross-section. 79
2.1.7. Determination of the maximum resisting moment 80
2.2. Cross-section with continuously varying depth. 81
2.2.1. Triangular or trapezoidal cross-section 81
2.2.2. Equilibrium equations – normal force resultant 82
2.2.3. Equilibrium equations – bending resultant moment. 84
2.2.4. Case of pivot A for a triangular cross-section 86
2.2.5. Case of pivot B for a triangular cross-section 87
2.2.6. Static moment equation for a triangular cross-section 87
2.2.7. Design example of a triangular cross-section 88
2.3. Composed bending with combined axial forces 90
2.3.1. Steel reinforcement design for a given reinforced concrete section. 90
2.3.2. Determination of the position of the neutral axis – simple bending. 91
2.3.3. Determination of the position of the neutral axis – composed bending with normal force solicitation 92
2.3.4. Exercises for composed bending with normal force solicitation . . 96
2.4. Deflection at Serviceability Limit State 107
2.4.1. Effect of crack on the bending curvature relationship 107
2.4.2. Simply supported reinforced concrete beam 112
2.4.3. Calculation of deflection – safe approach. 113
2.4.4. Calculation of deflection – a more refined approach; tension stiffening neglected. 114

2.4.5. Calculation of deflection – a more refined approach; tension stiffening included . . . 116
2.4.6. Approximated approach . . . 118
2.4.7. Calculation of deflection – a structural example . . . 119

Chapter 3. Concepts for the Design at Ultimate Limit State (ULS) . . . 123

3.1. Introduction to ultimate limit state . . . 123
3.1.1. Yield design . . . 123
3.1.2. Application of yield design to the cantilever beam . . . 125
3.1.3. Inelastic (plasticity or continuum damage mechanics) bending-curvature constitutive law . . . 129
3.2. Postfailure analysis . . . 133
3.2.1. Historical perspective . . . 133
3.2.2. Wood's paradox . . . 135
3.2.3. Non-local hardening/softening constitutive law, a variational principle . . . 137
3.2.4. Non-local softening constitutive law: application to the cantilever beam . . . 144
3.2.5. Some other structural cases – the simply supported beam . . . 149
3.2.6. Postfailure of reinforced concrete beams under distributed lateral load . . . 152
3.3. Constitutive laws for steel and concrete . . . 156
3.3.1. Steel behavior . . . 156
3.3.2. Concrete behavior . . . 160
3.3.3. Dimensionless parameters at ULS . . . 170
3.3.4. Calculation of the concrete resultant for the rectangular simplified diagram . . . 174
3.3.5. Calculation of the concrete resultant for the bilinear diagram . . . 174
3.3.6. Calculation of the concrete resultant for the parabola–rectangle diagram . . . 179
3.3.7. Calculation of the concrete resultant for the law of Desayi and Krishnan . . . 183
3.3.8. Calculation of the concrete resultant for Sargin's law of Eurocode 2 . . . 187
3.3.9. On the use of the reduced moment parameter . . . 191

Chapter 4. Bending-Curvature at Ultimate Limit State (ULS) . . . 193

4.1. On the bilinear approximation of the moment-curvature relationship of reinforced concrete beams . . . 193
4.1.1. Phenomenological approach . . . 193
4.1.2. Moment-curvature relationship for concrete – brief overview . . . 196
4.1.3. Analytical moment-curvature relationship for concrete . . . 198

4.1.4. A model based on the bilinear moment-curvature approximation . . . 222
4.2. Postfailure of reinforced concrete beams with the initial bilinear moment-curvature constitutive law . . . 226
4.2.1. Elastic-hardening constitutive law . . . 226
4.2.2. Plastic hinge approach . . . 230
4.2.3. Elastic-hardening constitutive law and local softening collapse: Wood's paradox . . . 235
4.2.4. Elastic-hardening constitutive law and non-local local softening collapse . . . 238
4.3. Bending moment-curvature relationship for buckling and postbuckling of reinforced concrete columns . . . 242
4.3.1. A continuum damage mechanics-based moment curvature relationship . . . 242
4.3.2. Governing equations of the problem and numerical resolution . . . 245
4.3.3. Second-order analysis – some analytical arguments . . . 251
4.3.4. Postfailure of the non-local continuum damage mechanics column . . . 258

Appendix 1. Cardano's Method . . . 267

A1.1. Introduction . . . 267
A1.2. Roots of a cubic function – method of resolution . . . 268
A1.2.1. Canonical form . . . 268
A1.2.2. Resolution – one real and two complex roots . . . 269
A1.2.3. Resolution – two real roots . . . 271
A1.2.4. Resolution – three real roots . . . 271
A1.3. Roots of a cubic function – synthesis . . . 273
A1.3.1. Summary of Cardano's method . . . 273
A1.3.2. Resolution of a cubic equation – example . . . 274
A1.4. Roots of a quartic function – principle of resolution . . . 275

Appendix 2. Steel Reinforcement Table . . . 277

Bibliography . . . 279

Index . . . 293

Preface

The authors have written two books on the theoretical and practical design of reinforced concrete beams, columns and frame structures. This book, entitled *Reinforced Concrete Beams, Columns and Frames – Mechanics and Design*, deals with the fundamental aspects of the mechanics and design of reinforced concrete in general, both related to the *Serviceability Limit State (SLS)* and the *Ultimate Limit State (ULS)*. The related book, entitled *Reinforced Concrete Beams, Columns and Frames – Section and Slender Member Analysis*, deals with more advanced *ULS* aspects, along with instability and second-order analysis aspects. The two books are complementary, and, indeed, could have been presented together in one book. However, for practical reasons, it has proved more convenient to present the material in two separate books with the same preface in both titles.

The books are based on an analytical approach for designing usual reinforced concrete structural elements, compatible with most international design rules, including for instance the European design rules *Eurocode 2* for reinforced concrete structures. The presentations have tried to distinguish between what belongs to the philosophy of structural design of such structural elements (related to strength of materials arguments) and the design rules aspects associated with specific characteristic data (for the material or the loading parameters). The *Eurocode 2* design rules are used in most of the examples of applications in the books. Even so, older international rules, as well as national rules such as the old French rules *BAEL* ("Béton Armé aux Etats Limites", or Reinforced Concrete Limit State in English) will sometimes be mentioned, at least for historical reasons.

Whatever the design rules considered, the fundamental concept of *Limit State* will be detailed, and more specifically, the *Serviceability Limit State (SLS)* and *Ultimate Limit State (ULS)* both in bending and in compression will be investigated.

The books are devoted mainly to the bending (flexural) behavior of reinforced concrete elements, including geometrical nonlinear effects (second book). However, two major aspects of reinforced concrete design are not treated. These are shear force effects and the calculation of crack width as dealt with in the *Crack Opening* Limit *State* in *Eurocode 2*. The latter represents a major new contribution as compared to some older European rules such as *BAEL*. The readers are referred to the very good monographs devoted to the general presentation of *Eurocode 2* for these additional parts (see for instance [CAL 05]; [DES 05]; [MOS 07]; [EUR 08]; [PAI 09]; [PER 09]; [ROU 09a]; [ROU 09b]; [THO 09]; [PER 10]; [SIE 10]; [PAU 11]).

We would also like to point out that the calculation of crack widths, even under a simple loading configuration, such as uniform tension loading, still remains a difficult topic. Moreover, the authors are even convinced that meaningful efforts should be addressed in the future, for facilitating the transfer of knowledge from theoretical research in fracture or damage mechanics, to applied, practical design rules. In connection with this, cohesive crack models were introduced in the 1970s to investigate the crack opening in mode I of failure [HIL 76], whereas non-local damage mechanics models were developed in the 1980s for efficient computations of damage softening materials [PIJ 87]. Both appear to belong to the families of non-local models which contain an internal length, for the control of the post-failure process [PLA 93]. Non-local damage mechanics is now widely used in the research community for the study of reinforced concrete structures (see for instance [BAZ 03]; [MAZ 09]). The authors of these books have also conducted some research in this field to better understand the failure of some simple reinforced concrete structural elements (research at INSA of Rennes, University of Rennes I, University of South Brittany or University of Oslo – see for instance [CHA 05]; [CHA 06]; [CHA 07]; [CHA 08]; [CHA 09]; [CHA 10]; [CHA 11]; [CHA 12]). However, the engineering community has not yet necessarily integrated these results into the design process or even into the rules. The gap between the research activity and the engineering methodology is probably too large at present, and researchers will probably have some responsibility in the future to make their results

more tractable to the engineering community. With respect to these books, some very simple concepts of non-local mechanics will be presented when necessary. However, the books are mainly devoted to the design of a reinforced concrete structure at a given limit state, the cracking evolution problem often being considered as a secondary problem. We have chosen to concentrate our efforts on the bending design based on the pivot concept, at both the *Serviceability Limit State (SLS)* and the *Ultimate Limit State (ULS)*. The last part of the second book deals with the design of columns against buckling, and how to take into account second-order effects will be presented for stability design. In particular, some engineering approaches practiced by engineers will be detailed, to replace efficiently, when possible, the nonlinear evolution problem associated with microcracking and failure.

The books are aimed at both undergraduate and graduate (Licence and master) students in civil engineering, engineers and teachers in the field of reinforced concrete design. In addition, researchers and PhD students can find something of interest in the books, including the presentation on elementary applications of non-local damage or plasticity mechanics applied to the ultimate bending of reinforced concrete beams (and columns). We hope that the basic ideas presented in the books can contribute to stimulating the links between the research community in this field (computational modeling and structural analysis) and the design community with practical structural cases. The principles of Limit State design will be introduced and developed first, both at the Serviceability Limit State (SLS) and the Ultimate Limit State (ULS), illustrated by some detailed examples to illustrate the introduced methodology.

Older books (see for instance [HOG 51]; [BAK 56]; [SAR 68]; [ROB 74]; [PAR 75]; [FUE 78]; [LEO 78]; [ALB 81]; [LEN 81]; [BAI 83]; [GYO 88]; [WAL 90]; [PAU 92]; [MAC 97]) have been used in some section of the books for establishing familiar and well-known equations on section design (in particular equations based on the simplified rectangular stress-strain diagram for concrete in compression). In particular, the authors want to acknowledge the very exhaustive work of Professor Robinson, at Ecole Nationale des Ponts et Chaussées, whose reinforced concrete teaching book published in 1974 can still be considered as a main reference with modern insights into reinforced concrete design [ROB 74]. We have also been inspired by the more recent and very exhaustive works of Professor Thonier (see for instance [THO 09]), also at Ecole Nationale des Ponts et Chaussées.

The current book, *Reinforced Concrete Beams, Columns and Frames – Mechanics and Design*, is organized as follows. Chapters 1 and 2 deal with the Serviceability Limit State, for both the design and cross-section verification. The French school of reinforced concrete design have commonly used the concept of "Pivot", which is related to the limit behavior of the cross-section with respect to steel and concrete material characteristics. The Pivot A (where the steel material characteristics control the behavior of the cross-section at the Limit State), and Pivot B (where the concrete material characteristics control the behavior of the cross-section at the Limit State) concepts are introduced with the Serviceability Limit State in Chapter 1. Chapter 1 is mainly focused on the design aspects, whereas Chapter 2 deals with the verification of the reinforced concrete section with both the bending and the normal forces effects. The general theory presented in these first two chapters is valid for arbitrary shapes of reinforced concrete cross-sections including for instance rectangular, triangular, trapezoidal or T-cross-sections. Chapter 2 ends with the presentation of a cubic equation for the determination of the neutral axis in the general loading configuration, including the normal force effects. This elegant equation is also known as the cubic equation of the French reinforced concrete design rules dating from 1906 ("Circulaire du 20 Octobre 1906") (and reported in the book by Magny, 1914 [MAG 14]) or those dating from 1934 ("Règlements des marchés de l'état de 1934" – also in French), also recently reported by Professor Thonier for T-cross-sections [THO 09]. Finally, the tension stiffening phenomenon is introduced in terms of a nonlinear bending moment-curvature constitutive law and some verification examples are given to illustrate the theoretical results obtained in the fundamental parts.

Chapters 3 and 4 focus on the fundamental aspects of the Ultimate Limit State. Chapter 3 starts with a brief introduction to the concept of the Ultimate Limit State for the bending of a reinforced concrete beam. The need to use some non-local theory to correctly model the post-failure behavior of reinforced concrete structural elements is shown in the presence of global curvature softening. The material characteristics of the steel and concrete allowed by Eurocode 2 are listed, and compared with each other. It is possible to derive analytically the normal forces and the resultant bending moment in the compression block for each considered concrete law, including the parabolic-rectangle constitutive law, the simplified rectangular constitutive law, the bilinear constitutive law or Sargin's nonlinear constitutive law. These preliminaries will be used later for the design of reinforced concrete sections at Ultimate Limit State. Chapter 4 discusses

some possible bending moments – curvature law of typical reinforced concrete sections. These cross-sectional behaviors can be deduced from the local characteristics of the steel and concrete constituents. The relevancy of a bilinear approximation for the moment-curvature constitutive law is discussed, with possible tractable analytical results for engineering purposes. Chapter 4 concludes with some buckling and post-buckling results obtained for a reinforced concrete column modeled with a simplified nonlinear bending-curvature constitutive law. It is shown that reinforced concrete columns typically behave like imperfection-sensitive structural systems.

The related book, *Reinforced Concrete Beams, Columns and Frames – Section and Slender Member Analysis*, is organized as follows. The advanced design of general reinforced concrete sections is treated in Chapter 1. The reinforced concrete section can be optimized for a given loading (in terms of minimization of the steel quantity for instance), with some constrained equations. Also discussed is how the Serviceability and the Ultimate Limit States can be compared, depending on the material and loading features of the problem. A design of the cross-section in biaxial bending is also proposed. More generally in this chapter, the reinforced concrete section is designed for various constitutive laws for the behavior of concrete and steel, including possible steel hardening, with possible analytical solutions for the optimized design. Some design examples are included for the various solicitations including simple bending, bending combined with normal forces or bi-axial bending. The last part of Chapter 1 discusses the possible use of moment-normal forces interaction diagrams available in international codes, and some new possible improvements of these simplified diagrams.

Chapter 2 is devoted to general aspects of instability of second-order effects in slender compression members, and in frames that include such members. For such cases, it is necessary to consider second-order load effects in the analysis and design. The concepts of braced, unbraced and partially braced systems as well as associated moment formulations are presented, and the useful distinction between local and global second-order effects discussed. The general principles of analysis and design of individual reinforced concrete columns and frame systems are reviewed in order to provide a general understanding of the problem area. This includes a presentation and discussion of fundamental concepts and theory behind approximate analysis and design methods to provide a reasonable complete basis for relevant analysis and design requirements as given in existing

design rules, such as in Eurocode 2. This also includes a discussion of the applicability of equivalent elastic analysis as an approximation to nonlinear analyses (accounting for both material and geometric nonlinear effects). Local and global slenderness limits, allowing second-order effects to be neglected, are presented and discussed. Chapter 3 deals with approximate analysis methods used for efficient and practical elastic stability calculations, and second-order elastic sway and moment calculations. Included in this chapter are different methods for computing effective lengths, and methods employing the widely used effective length concept in frame analysis. Basic concepts are explained and simple and more complex engineering examples are included to provide a better understanding of the methods.

This book and the first chapter of the related book were mainly written by Charles Casandjian, Noël Challamel and Christophe Lanos, whereas Jostein Hellesland mostly contributed to the final two chapters of *Reinforced Concrete Beams, Columns and Frames – Section and Slender Member Analysis*.

Finally, an appendix is provided that gives further developments on the theoretical background of Cardano's method, useful for the resolution of a cubic equation, often encountered in the designing of reinforced concrete sections at both Serviceability and Ultimate Limit States. An appendix giving a table of steel diameters is also provided for the quick and efficient selection of reinforcement sizes in design calculations.

Charles CASANDJIAN,
Noël CHALLAMEL,
Christophe LANOS and
Jostein HELLESLAND
December 2012

Chapter 1

Design at Serviceability Limit State (SLS)

1.1. Nomenclature

1.1.1. *Convention with the normal vector orientation*

The normal vector is chosen to be oriented toward the external part of the considered body. The usual conventions of mechanics of continuous media are chosen, leading to a positive stress for tension and a negative stress for compression.

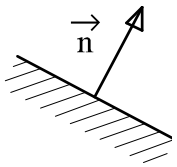

Figure 1.1. *Definition of the normal unit*

1.1.2. *Vectorial notation*

As opposite to the notation used for figures, where vectors are represented with an arrow, in the text, vectors are denoted by bold characters and its components have normal non-bold characters. As an example, we will have "$\mathbf{M} = M_x\mathbf{i} + M_y\mathbf{j} + M_z\mathbf{k}$".

1.1.3. *Part of the conserved reference section*

The conserved reference part of the beam used for the calculation of generalized stress in use of the static theorems is the “right” part.

1.1.4. *Frame*

- Representation of a cross-section.
- Origin of the frame: arbitrary point of the section.
- *x*-axis standing out.
- horizontal*z*-axis, leading to “negative” moments at the support level.
- *y*-axis defined from the orthonormal direct trihedron.

Figure 1.2. *Orientation of the frame for a general section*

1.1.5. *Compression stress $\sigma_{c,sup}$ in the most compressed fiber*

It is admitted that the neutral axis is located inside the cross-section, thus delimiting a tension zone and a compressed zone. This last assumption of a neutral axis inside the cross-section is no more valid when considering additional meaningful normal forces. Typically, under a positive moment (in span), the tension zone is located under the neutral axis, and the compression zone above the neutral axis, as shown in Figure 1.3. Obviously, in the presence of a negative bending moment, the tension zone and the compression zone are permuted with respect to the notation of Figure 1.3. The neutral axis as shown in Figure 1.3 allows the introduction of the concept of extremal compressed fiber, defined from the most distant parallel to the neutral axis belonging to the cross-section. The most compressed fiber in concrete is by definition the fiber associated with the minimal compressive stress in algebraic value, denoted by $\sigma_{c,\sup}$.

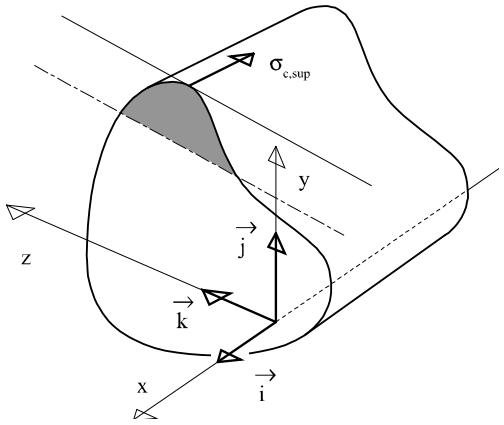

Figure 1.3. *Concept of extremal compressed fiber*

1.2. Bending behavior of reinforced concrete beams – qualitative analysis

1.2.1. *Framework of the study*

1.2.1.1. *Constitutive law of concrete*

The constitutive law of concrete is a strong unsymmetrical law in tension and in compression, both from the strength and the postfailure response, which is characterized by its ductility (see Figure 1.4). As a natural choice, the subscript *c* refers to concrete whereas the subscript *s* refers to the steel material. We adopt by $\sigma_{c,min}$ the extreme stress at the compression peak.

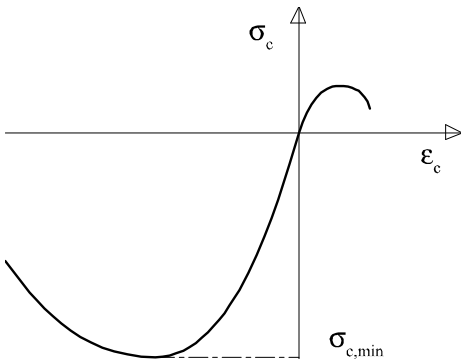

Figure 1.4. *Unsymmetrical response of concrete in uniaxial tension and compression*

1.2.1.2. *Beam theory in simple bending*

In this section, reinforced concrete beams in simple bending are studied (without axial forces), composed of a rectangular cross-section with a total height denoted by h and a width b. This section is reinforced by some steel reinforcement working in tension with a cross-section denoted by A_{s1} and by steel reinforcement working in compression with a cross-section denoted by A_{s2}. The center of gravity of the tensile reinforcement is at a distance d of the upper fiber, and one of the compression reinforcements is at a distance d' of the upper fiber of the cross-section.

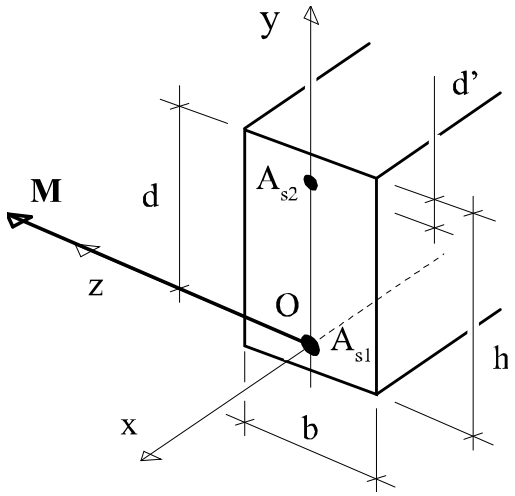

Figure 1.5. *Geometrical parameters of the reinforced cross-section; tensile and compression steel reinforcement*

In this case, again, it is implicitly accepted that the bending solicitation corresponds to a positive moment (the lower fibers are in tension with this convention, typically in span). Designing under negative moment (typically at support, for instance) is formally feasible by permuting the behavior of the cross-section. Furthermore, we can introduce the strain ε_{s1} as the strain of the tensile reinforcement with the largest tensile stress σ_{s1} and with the reinforcement area A_{s1}.

1.2.2. *Classification of cross-sectional behavior*

Three kinds of reinforced concrete beam responses can be distinguished, depending on the steel reinforcement density (Figure 1.6). These responses are explicitly detailed in the space of the bending moment with respect to the stress in the most compressed fiber in concrete.

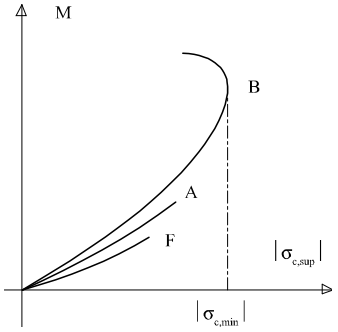

Figure 1.6. *Bending behavior of reinforced concrete beams with respect to the steel reinforcement density*

F: brittle response, which appears when the beam design does not respect the condition of non-brittleness.

A: beam with low steel reinforcement density, characterized by a global ductile response. Failure is induced by a large drawing of the tensile steel reinforcement. As discussed below, the letter *A* refers to Pivot A.

B: beam with high steel reinforcement density, characterized by the breaking up of the compressed part of the upper part concrete. The letter *B* refers to the behavior classified as Pivot B.

In the following, brittle reinforced concrete beams of type F will not be investigated.

1.2.3. *Parameterization of the response curves by the stress σ_{s1} of the most stressed tensile reinforcement*

In Figure 1.7, the response curves are parameterized by the stress σ_{s1} of the most stressed tensile reinforcement. When reading Figure 1.7 in the

sense of increasing the bending moment (the solicitation), the stress value of the tensile steel reinforcement also increases. The stress in the compressed part of the concrete (typically in the upper part of the section for positive bending moment in span) is limited by a material characteristic value f_{cs} defined in the National Annexes to the Eurocode 2 - EC2 [EUR 04] (EC2 7.2.1). This material limitation is defined in the rules for reducing the longitudinal crack level in the tensile part of the cross-section, for reducing the microcacking phenomena of concrete in the compressed part and for limiting the time-dependent induced effects (including the specific creep effect).

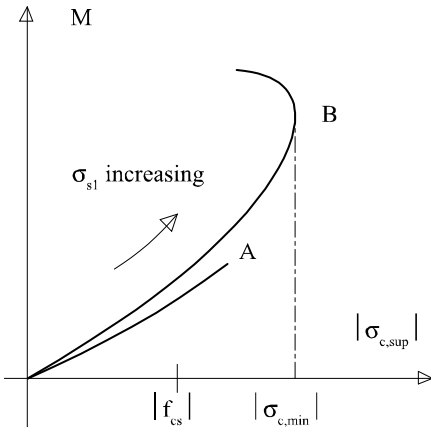

Figure 1.7. *Bending sectional behavior of reinforced concrete beams with respect to the steel reinforcement density; the response curves are parameterized by the stress level in the tensile steel reinforcement*

For the same bending moment, the share taken by tensile reinforcement is more important in case *A*. Consequently, the share taken by the concrete is less important; this generates therefore, in this material, a lower normal stress. This explains the relative position of two curves.

1.2.4. *Comparison of σ_{s1} of the tensile reinforcement for a given stress in the most compressed concrete fiber $\sigma_{c,sup}$*

In this section, the physics of the reinforced concrete beam behavior is discussed with respect to the steel reinforcement density. For a given value of the stress in the most compressed concrete fiber, bending moments for the

two different types of reinforced concrete beams *A* and *B* are different (Figure 1.8). As the reinforced concrete beam of type *A* has a low density of tensile steel reinforcement, the following inequality holds: $M_B > M_A$.

The stress in the most compressed fiber in concrete is being fixed; the linear strain of the upper fibers is the same for the two kinds of reinforced concrete beams. As a result, it is necessary that the compressed part in the section of type *B* has to be larger than the one in the section of type *A*, in order to fulfill the moment inequality. The linear distribution of strains and the associated stress in the tensile reinforcement of section of type *A* are then larger than the section of type *B* (see Figure 1.8).

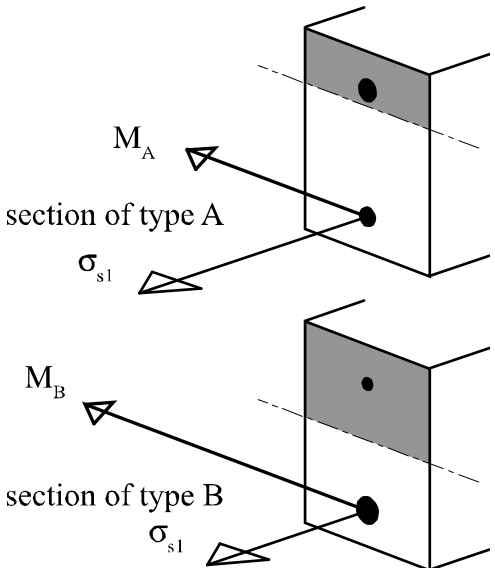

Figure 1.8. *Bending behavior of reinforced concrete beams with respect to the steel tensile reinforcement density; sections of type A and type B*

Reciprocally, if the stress value in the tensile steel reinforcement (in the lower part of the reinforced section) is the same for both types of the section, the section of type *A* will have a lower stress value (in absolute value) in the upper part of the compressed concrete in comparison to the section of type *B* (see Figure 1.9).

Figure 1.9. *Stress in the compression concrete block; sections of type A and type B*

1.2.5. *Comparison of the bending moments*

To reduce the non-elastic strain level (existence of permanent strain for a stress history ended by a vanishing stress value, for instance) leading to some possible large cracks or some possible structural member strains, the steel reinforcement tensile stress is limited to a material characteristic value f_{ss} that is also defined in the National Annexes to Eurocode 2 – EC2 (EC2 7.2.2).

For designing the structural members at the Serviceability Limit State (SLS), we should satisfy the following two simultaneous inequalities that have to be algebraically fulfilled (see also Figure 1.10 or 1.11):

$$\begin{cases} \sigma_{s1} \leq f_{ss} \\ \sigma_{c,\text{sup}} \geq f_{cs} \end{cases} \qquad [1.1]$$

For reinforced concrete beams of kind *A*, slightly reinforced (or with a low tensile steel reinforcement density), the SLS is controlled by the

drawing of the tensile steel reinforcement. The bending moment at the SLS is then calculated for:

$$\begin{cases} \sigma_{s1} = f_{ss} \\ \sigma_{c,\text{sup}} \geq f_{cs} \end{cases} \quad [1.2]$$

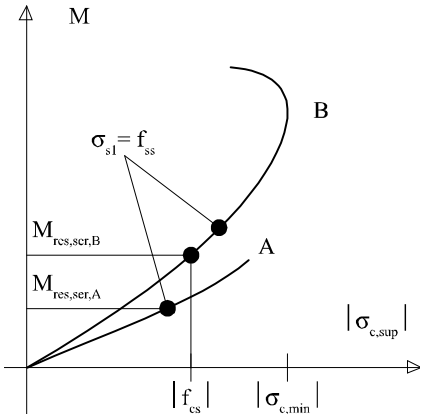

Figure 1.10. *Introduction to the concepts of pivots A and B at the serviceability limit state (SLS); in a Pivot B section, stress limitation in concrete occurs before stress limitation in steel*

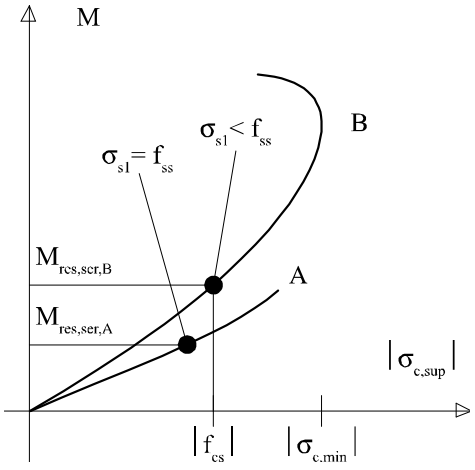

Figure 1.11. *Introduction to the concepts of pivots A and B at the serviceability limit state (SLS)*

For reinforced concrete beams of kind *B*, highly reinforced (or with a high tensile steel reinforcement density), the SLS is controlled by the compression in concrete, considered as unacceptable by the rules. The bending moment at the SLS is then calculated for:

$$\begin{cases} \sigma_{s1} \leq f_{ss} \\ \sigma_{c,\text{sup}} = f_{cs} \end{cases} \quad [1.3]$$

1.3. Background on the concept of limit laws

1.3.1. *Limit law for material behavior*

1.3.1.1. *Definition*

A limit law, for a given material, is defined from the overall possible configurations reached by this material and is compatible with a given state criterion. A limit law, in its essence, is different from a constitutive law; the constitutive law implicitly contains all the successive temporal configurations before reaching the limit state. Therefore, in the concept of limit law, the notion of the stress or strain path is replaced by the notion of the limit state, which is the set of configurations compatible with a given state criterion.

1.3.1.2. *Application to the rectangular parabolic diagram, a limit law of the ultimate limit state*

In the case of a parabola–rectangle diagram applied to concrete modeling (one of the possible limit laws for concrete modeling at the ultimate limit state (ULS)), if the section reaches the concrete limit law, then the Bernoulli assumption leads to a nonlinear stress distribution along the cross-section, as shown by the stress distribution identified by number 5 in Figure 1.11.

In Figure 1.12, for the solicited bending moments $M_1 < M_2 < M_3 < M_4 < M_5 = M_{u,act}$, the stress distribution along the cross-section cannot be ranged as a parabola–rectangle law, for the bending moment M_1–M_4; for these solicitations, the stress response curves are transitory curves between the linear state and the limit state of the parabolic rectangular limit state.

Figure 1.12. *Illustration of the concept of limit law – stress evolution inside the cross-section; Ultimate limit state parabolic-rectangular stress–strain relationship*

However, for the bending moment denoted by M_5 (ultimate limit acting bending moment), the limit state is reached, and the stress limit diagram is known.

1.3.2. *Example of limit laws in physics, case of the transistor*

Figure 1.13. *Electronic example for limit laws in physics: the transistor*

Figure 1.13 shows the setting of a polarized transistor, which is often met in the field of electronics designs. The characteristics of the transistor are given in Figure 1.13. The linear part of Figure 1.14 with a softening slope contains the locus of the static point of this electronic system. In fact, the working point is located on this loading line.

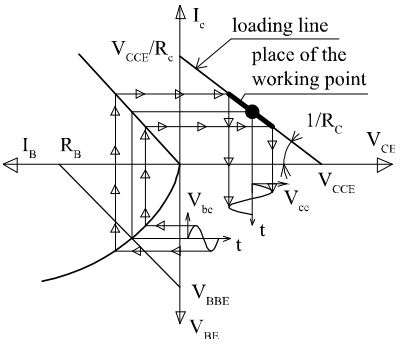

Figure 1.14. *Limit laws in electronics design*

This softening straight line is clearly a limit law: the path from the origin to reach this limit law is not known *a priori*, and only the limit state is of interest.

1.3.3. *Design of reinforced concrete beams in bending at the stress Serviceability Limit State*

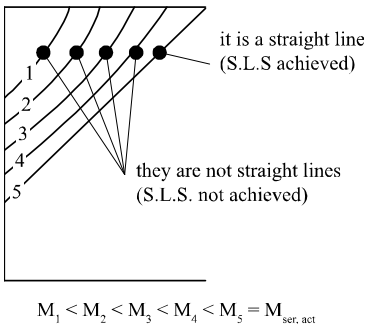

Figure 1.15. *Limit law at the stress serviceability limit state (SLS); stress distribution along the cross-section*

In the case of the limit behavior of concrete at the SLS, a section at its limit state will have a linear distribution of stress in the compressed part of the section (as a consequence of Bernoulli kinematics and elasticity behavior of each material at the SLS), the contribution of concrete in tension being neglected as a fundamental assumption. This “limit” behavior is visualized in Figure 1.15 by the linear stress distribution indicated by number 5.

For the external moments M_1, M_2, M_3, M_4 and M_5 with $M_1 < M_2 < M_3 < M_4 < M_5 = M_{ser,act}$, the stress distribution is theoretically not necessarily linear along the cross-section, for the moments from M_1–M_4; such curves are not known *a priori*. Only for the moment M_5 (limit moment at the SLS), the stress distribution at SLS is known and is linear. However, for this specific limit state, it can be also admitted in this case that the limit case (characterized by linear elasticity) is also reached for the transitory states.

1.4. Limit laws for steel and concrete at Serviceability Limit State

1.4.1. *Concrete at the cross-sectional SLS*

Concrete, at the cross-sectional SLS, is modeled by a linear elastic constitutive law in compression, with a stress limitation denoted by f_{cs}. The strength in tension is neglected (Figure 1.16) and its Young's modulus is denoted by E_c.

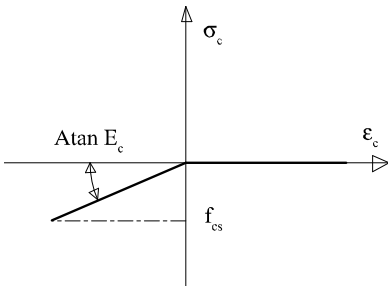

Figure 1.16. *Limit law of concrete at serviceability limit state*

1.4.2. *Steel at the cross-sectional SLS*

Steel at the cross-sectional SLS is also modeled by a linear elastic constitutive law, with a tension limit denoted by f_{ss} (Figure 1.17). A symmetrical behavior in tension and in compression is also accepted for modeling the behavior of the steel reinforcement, which means that the potential buckling of the steel reinforcement in the presence of a crushing phenomena in concrete is generally neglected, except in so far as the spacing of transverse reinforcement. As a result, for the compression steel reinforcement, stress in the absolute value is also limited by the same value f_{ss}. Young's modulus of the steel reinforcement is denoted by E_s.

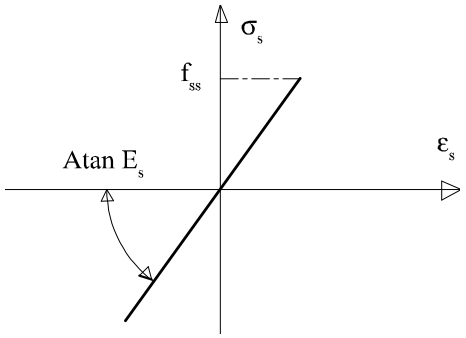

Figure 1.17. *Limit law of steel reinforcement at serviceability limit state*

1.4.3. *Equivalent material coefficient*

The equivalence coefficient (between steel and concrete) is by definition the ratio between the steel modulus and the concrete modulus $\alpha_e = E_s/E_c$. This ratio depends on the short-term or the long-term analysis considered at the SLS. As the Young's modulus is decreasing with the effects of time, the equivalence ratio tends to increase with the effects of time. This ratio is also sometimes denoted by the equivalence coefficient "*n*" in the earlier textbooks on reinforced concrete design. A typical order of magnitude for this ratio is $\alpha_e = 15$.

1.5. Pivots notion and equivalent stress diagram

1.5.1. *Frame and neutral axis*

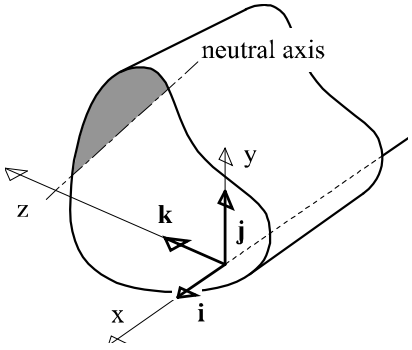

Figure 1.18. *Neutral axis in a general section*

Let us consider a beam in which the direct orthonormal frame *O, x, y,* and *z* is defined. The beam is solicitated by an external screw given at the SLS. The frame is in conformity with section 1.1.3. or 1.1.4. Under the action of the external forces, a neutral axis can be defined (Figure 1.18). It is admitted that the direction of the neutral axis is already known. In the opposite case, some symmetrical considerations have to be added in the reasoning or we can proceed by iterations. The neutral axis separates the tension and the compression parts of the section.

Each of the "*n*" steel bars of the reinforced section will be identified by the subscript *q* with $q \in [1;n]$. Let $\boldsymbol{P_q}$ be the vector whose origin is denoted by *O* and with an extremity defined at the center of gravity of the *q*th reinforcement bar. The oriented angle between the axis *z* and the neutral axis is denoted by ω.

Let d_q be the distance between the center of gravity of the *qth* reinforcement bar and the parallel to the neutral axis assigned to pass through the most compressed fiber. Among the "*n*" steel bars of the reinforced section, the most tensioned reinforcement bar is identified by its subscript *r* and its cross-sectional area A_{sr} with $r \in [1;n]$. The effective height "d_r" of the cross-section can now be defined as the distance between the center of gravity of the most tensioned reinforcement bar, and the parallel to the neutral axis passing through the most compressed fiber (Figure 1.19).

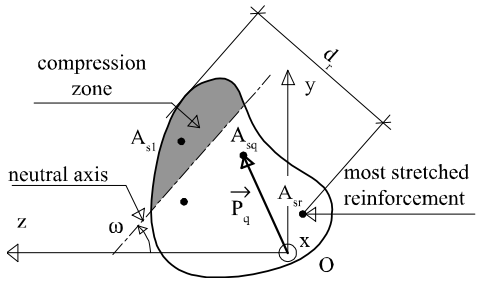

Figure 1.19. *Definition of the notion of effective height* d_r

1.5.2. *Conservation of planeity of a cross-section*

The conservation law of planeity of a cross-section during the deformation process allows us to relate due to some geometrical properties, the strain of each constituent of the cross-section, the compressed part of the

concrete and each steel reinforcement bar. The ordinate axis "*u*" can be defined from a straight line perpendicular to the neutral axis, and oriented from the less compressed to the most compressed concrete fibers. The origin of this axis is located at the basis of this axis, positioned from the projection of the origin point *O* on this line. The stress field in this section is a function of this parameter "*u*". The following scalar variable can be introduced from $u_q = \mathbf{P_q} \cdot (\mathbf{j} \cos \omega + \mathbf{k} \sin \omega)$, where the point denotes the scalar product (dot product) between two vectors (Figure 1.20).

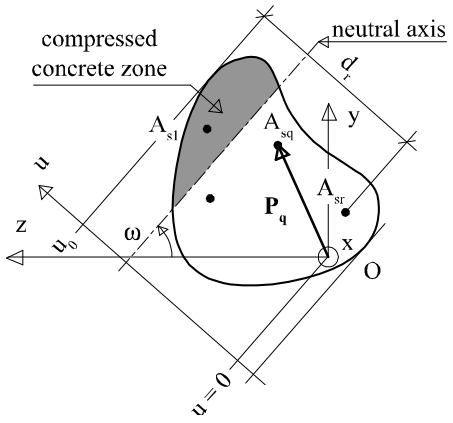

Figure 1.20. *Parameterization of the stress field with the variable u*

The neutral axis is identified by the value $u_r + (1 - \alpha)d_r$ for the variable *u*, where α is a dimensionless distance characterizing the position of the neutral axis. α is a dimensionless parameter normalized by the total height of the cross-section. The most compressed concrete fiber is associated with the projection value u_0 for the variable *u*; the equality $u_0 = d_q + u_q$ is exact whatever the considered subscript $q \in [1;n]$. The strain ε_{sq} in each reinforcement bar and the strain $\varepsilon_c(u)$ in concrete are related with each other by the relationship induced by the planeity conservation of the cross-section:

$$\frac{\varepsilon_{s1}}{d_1 - \alpha d_r} = \frac{\varepsilon_{s2}}{d_2 - \alpha d_r} = \ldots = \frac{\varepsilon_{sq}}{d_q - \alpha d_r} = \ldots$$

$$= \frac{\varepsilon_{sr}}{d_r - \alpha d_r} = \ldots = \frac{\varepsilon_{sv}}{d_v - \alpha d_r} = \frac{-\varepsilon_c(u)}{-u + u_r + (1 - \alpha)d_r} \qquad [1.4]$$

1.5.3. *Planeity conservation law in term of stress*

From equation [1.4], the "limit" laws associated with each material (namely elasticity for each material constituents), at the SLS, allow us to obtain a relationship between the stress in the steel reinforcement bars and the stress in the compressed concrete part along the cross-section. The following equalities finally hold between the stress in the q reinforcement bars σ_{sq} and the stress distribution in the compressed part of concrete $\sigma_c(u)$:

$$\frac{\sigma_{s1} / \alpha_e}{d_1 - \alpha d_r} = \frac{\sigma_{s2} / \alpha_e}{d_2 - \alpha d_r} = \ldots = \frac{\sigma_{sq} / \alpha_e}{d_q - \alpha d_r} = \ldots = \frac{\sigma_{sr} / \alpha_e}{d_r - \alpha d_r} = \ldots = \frac{\sigma_{sv} / \alpha_e}{d_v - \alpha d_r} = \frac{-\sigma_c(u)}{-u + u_r + (1 - \alpha) d_r} \quad [1.5]$$

By setting k the proportionality factor of this last equality (proportional to the curvature), a series of affine relationships for the stress value in both the tensile and the compression steel reinforcement bars, as for the compressed part of concrete is obtained, which can be again written as:

$$\sigma_{sq} / \alpha_e = k(d_q - \alpha d_r) \forall q \in [1; t] \quad [1.6]$$

The calculated stress in the most compressed fiber of concrete is given by:

$$\sigma_c(u) = k[-u + u_r + (1 - \alpha) d_r] \quad [1.7]$$

It is worth mentioning that the characteristic limit values in both the steel and concrete part of the composite section are defined in a algebraic manner, with the mechanics of continuous media convention, that is f_{ss} is positive and f_{cs} is negative. At the limit state formally, the following equalities can be viewed to be valid only in the case $\sigma_{sr} = f_{ss}$ or $\sigma_c(u_0) = f_{cs}$ (see section 1.2.5). We can also consider that the limit state is always reached in elasticity, at least at the SLS.

We finally obtain in Pivot A, with $\sigma_{sr} = f_{ss}$:

$$\sigma_{sq} / \alpha_e = k(d_q - \alpha d_r) \forall q \in [1; t] \text{ and } \sigma_{sr} / \alpha_e = f_{ss} / \alpha_e \text{ for } q = r \quad [1.8a]$$

$$\sigma_c(u) = k[-u + u_r + (1 - \alpha) d_r] \quad [1.8b]$$

In Pivot B, the stress relationships are obtained from $\sigma_c(u_0) = f_{cs}$:

$$\sigma_{sq} / \alpha_e = k(d_q - \alpha d_r) \forall q \in [1; t] \quad [1.9a]$$

$$\sigma_c(u) = k[-u + u_r + (1-\alpha)d_r] \quad [1.9b]$$

1.5.4. *Introduction to pivot concepts*

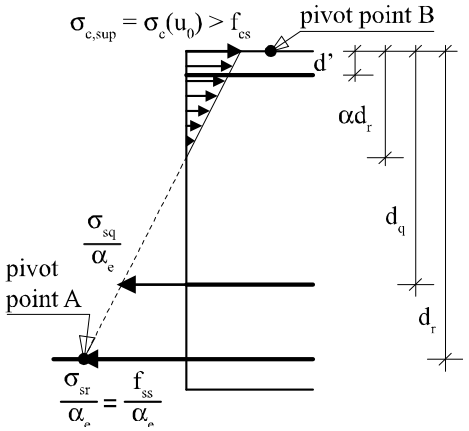

Figure 1.21. *Definition of Pivot A;* $\alpha_e = E_s/E_c$

Designing by h the distance between the two extremal parallels to the neutral axis (h is typically the height of the cross-section), the series of equalities, equation [1.8], can be presented as:

$$\sigma_{sq}/\alpha_e = k(d_q - \alpha d_r) \ \forall \ q \in [1; v\ ]$$
$$\text{and } \sigma_{sr}/\alpha_e = f_{ss} / \alpha_e \text{ for } q = r \quad [1.10a]$$

$$\sigma_c(u) = k[-u + u_r + (1-\alpha)d_r]$$
$$\text{and } 0 > \sigma_c(u) > f_{cs} \forall u \in [u_0 - h;\ u_0] \quad [1.10b]$$

This system of equations can be interpreted as the analytical expression of a plane whose trace in the space *{u,x}* is the straight line appearing in Figure 1.21. This line crosses the fixed point corresponding to the most tensioned steel reinforcement with an equivalent tensile stress equal to f_{ss}/α_e. This point is called Pivot A (Figure 1.21).

The series of equalities, equation [1.9], can be written as:

$$\sigma_{sq} / \alpha_e = k(d_q - \alpha d_r) \; \forall q \in [1; v]$$
$$\text{and } \sigma_{sr} / \alpha_e < f_{ss} / \alpha_e \text{ for } q = r \qquad [1.11a]$$

$$\sigma_c(u) = k[-u + u_r + (1-\alpha)d_r] \text{ and } 0 > \sigma_c(u_0) = f_{cs} \qquad [1.11b]$$

Again, this system of equations can interpreted as the analytical expression of a plane whose trace in the space *{u,x}* is the straight line appearing in Figure 1.22. This line crosses the fixed point, corresponding to the most compressed fiber with an equivalent compression stress equal to f_{cs}. This point is called Pivot B.

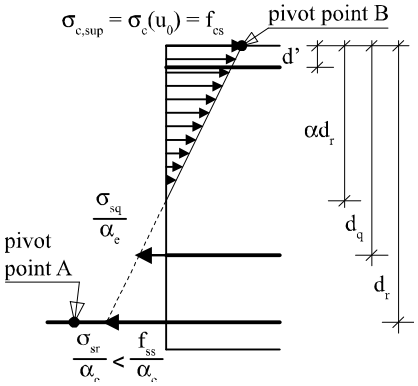

Figure 1.22. *Definition of Pivot B;* $\alpha_e = E_s/E_c$

These fixed points play the role of a turning point or pivot point, around which the equivalent stress lines turn, and define the profile of equivalent stress along the cross-section, which is the stress for the concrete part in compression, and the equivalent or homogenized stress for the steel reinforcement bars, typically the stress divided by the equivalent coefficient α_e.

1.5.5. *Pivot rules*

The planeity conservation assumption at SLS, which is in fact a fundamental kinematics assumption, leads to an equivalent linear stress diagram that contains one of the two Pivot points:

– the point "Pivot A" that corresponds to an equivalent stress f_{ss}/α_e of the most tensioned steel reinforcement bars;

– the point "Pivot B" that corresponds to a compression stress f_{cs} in the most compressed fiber in concrete.

Figure 1.23. *Working zone of the composite cross-section in Pivot A and Pivot B*

This straight line exactly corresponds to the compression stress field in the compressed part of concrete, whereas the stress in the steel reinforcement bars, in tension or in compression, are deduced from the equivalent stress line by introducing the equivalence coefficient $1/\alpha_e$. At the cross-sectional SLS, the diagram of equivalent stresses should cross one of the two pivot points (Pivot A and Pivot B) and should also respect the limit stress requirement for the extremal point at the other pivot point (see Figure 1.23). The limit case between the two pivots is referred as Pivot AB, and is characterized by the limit value for the relative position of the neutral axis α_{AB} defined from the upper fiber of the cross-section as $\alpha_{AB} = \alpha_e f_{cs}/(\alpha_e f_{cs} - f_{ss})$.

1.6. Dimensionless coefficients

1.6.1. *Goal*

To characterize the static equilibrium equations of the cross-section, it is necessary to integrate both the stress field and the moment in the compressed part of concrete, defined at a given point of the cross-section. This calculation will lead to the determination of the internal forces screw

applied to concrete. The total internal screw will then be deduced from the concrete screw, by adding the tensile and the compression steel reinforcement screw evaluated at the same point. The calculation of internal and external screws, both with equilibrium equations will be written, as much as possible, in a dimensionless format, to avoid dimension confusion and try to give the more general presentation. Dimensionless numbers are also important to classify the sectional behavior, in its more general formulation.

1.6.2. *Total height of the cross-section*

As indicated in Part 1.5.4, the total height of the cross-section is denoted by h (h is the distance between two parallels to the neutral axis passing through the extremity of the cross-section). For a rectangular or a T-beam, h has its usual definition and is the height of the cross-section.

1.6.3. *Relative position of the neutral axis*

In section 1.5.2, the position of the neutral axis was identified from the following equation $u = u_r + (1 - \alpha)\, d_r$, where α is the relative height of the neutral axis. Even if the understanding of this relative position is quite intuitive as explained in Figure 1.24, a rigorous mathematical definition can be given based on geometrical arguments. The height parameter d_r can be defined from the distance between two lines parallel to the neutral axis, one passing through the most compressed fiber and the other crossing the most tensioned steel reinforcement. The distance between the most compressed fiber and the neutral axis is denoted by αd_r (Figure 1.24).

Figure 1.24. *Definition of the relative height of the neutral axis*

1.6.4. *Shape filling coefficient*

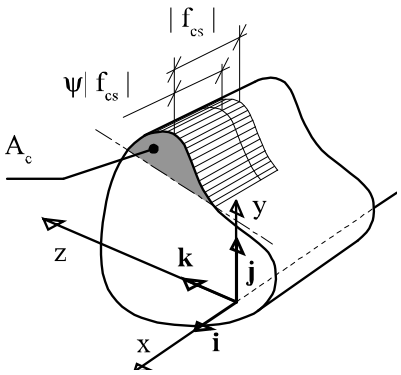

Figure 1.25. *Definition of the shape filling coefficient* ψ

The screw of internal forces applied to concrete is calculated for the normal force N_c, by integration of the compression stress over the domain of the compressed concrete denoted by D_c:

$$\boldsymbol{N_c} = \iint_{D_c} \sigma_c . \boldsymbol{i} . dy . dz = \boldsymbol{i} . \iint_{D_c} \sigma_c . dy . dz \qquad [1.12]$$

The resultant can be written in the following form: $\boldsymbol{N_c} = N_c \boldsymbol{i}$. It is worth mentioning that the stress function $\sigma_c(u)$ is a continuous function within the compression domain D_c. By virtue of the mean value theorem, it can be rigorously deduced that there exists a characteristic variable u^* belonging to the domain of variation of u, such as:

$$N_c = \sigma(u^*) \iint_{D_c} dy . dz \qquad [1.13]$$

The integral in such a definition represents the area of the compression domain D_c, which can be denoted by A_c. The shape filling coefficient ψ can now be defined from this mean value:

$$\psi = \frac{N_c}{f_{cs} A_c} = \frac{\sigma(u^*)}{f_{cs}} \qquad [1.14]$$

The meaning of the shape filling coefficient can be more easily understood from considerations of the volumes highlighted in Figure 1.25, and the intrinsic relationship between the actual stress volume and the

equivalent uniform stress volume. The shape filling coefficient is the ratio between the volume of a cylinder with a basis equal to D_c and a height equal to $\sigma(u^*)$ and the volume of another cylinder of the same basis but with height equal to f_{cs}. It can be remarked that the volume of a cylinder with a basis equal to D_c and with height $\sigma(u^*)$ is equal to N_c. The stress $\sigma(u^*)$ is called the mean stress.

1.6.5. *Dimensionless formulation for the position of the center of pressure*

Figure 1.26. *Notion of center of pressure*

The internal force of the internal screw including the normal force in concrete $\boldsymbol{N_c}$ has been evaluated previously; the internal moment needs now to be calculated for complete equilibrium determination of the cross-section. By designing D_c, the concrete part in compression, the screw of resultant moment $\boldsymbol{M_c}$ calculated, for instance, at the origin of the frame will be given by:

$$\begin{aligned}\boldsymbol{M_c} &= \iint_{D_C} (y\boldsymbol{j} + z\boldsymbol{k}) \wedge (\sigma_c.\boldsymbol{i}).dy.dz \\ &= \boldsymbol{j}.\iint_{D_C} \sigma_c.z.dy.dz - \boldsymbol{k}.\iint_{D_C} \sigma_c.y.dy.dz\end{aligned} \qquad [1.15]$$

Such an expression of the resultant moment, evaluated at the origin of the frame, depends on the stress function $\sigma_c(y,z)$ that possesses a constant sign, in the concrete domain in compression D_c. This stress function has lower and upper bounds, thus also including the vector norm of $y\boldsymbol{j} + z\boldsymbol{k}$ that

parameterizes the point of the studied compression domain. The conditions of application of the second theorem of the generalized mean value are satisfied, and then we can conclude the existence of a vector $\boldsymbol{G} = \xi_{2y}\boldsymbol{j} + \xi_{2z}\boldsymbol{k}$ whose extremity is inside the compression domain D_c (Figure 1.26), and such that:

$$\begin{aligned}\boldsymbol{M}_c &= \iint_{D_C} (y\boldsymbol{j} + z\boldsymbol{k}) \wedge (\sigma_c.\boldsymbol{i}).dy.dz \\ &= \boldsymbol{G}.\iint_{D_C} \sigma_c.\boldsymbol{i}.dy.dz = \boldsymbol{G} \wedge \boldsymbol{N}_c\end{aligned} \quad [1.16]$$

The origin of the frame for calculation of this screw can be chosen to coincide with the center of gravity of the most tensioned steel reinforcement bar (A_{sr}). By dividing the different length (associated with the level arm of the equivalent torque calculation) ξ_{2y} and ξ_{2z} by d_r, the dimensionless parameters δ_{gy} and δ_{gz} appear as:

$$\xi_{2y} = (1 - \alpha\delta_{gy})d_r \text{ and } \xi_{2z} = (1 - \alpha\delta_{gz})d_r \quad [1.17]$$

These size parameters are called the dimensionless coefficient of the center of pressure. Using some symmetry or mechanical considerations, it is possible to calculate these dimensionless parameters by engineering rules. However, in the more general case, for unsymmetrical cross-section, a mathematical integral calculation is often needed.

1.7. Equilibrium and resolution methodology

1.7.1. *Equilibrium equations*

The screw of internal forces can be decomposed into two internal screws, one related to the reinforcement steel bars and the other to the concrete domain in compression. When considering only the internal screw related to the reinforcement steel bars, both in tension and in compression, the normal force resultant $\boldsymbol{N}_s$ and the internal torque resultant $\boldsymbol{M}_s$ are calculated as:

$$\boldsymbol{N}_s = \sum_{q=1}^{n} A_{sq}\sigma_{sq}\,\boldsymbol{i} \text{ (or } N_s = \sum_{q=1}^{n} A_{sq}\sigma_{sq})$$

$$\text{and } \boldsymbol{M}_s = \sum_{q=1}^{n} A_{sq}\sigma_{sq}\boldsymbol{P_q}\wedge\boldsymbol{i} \qquad [1.18]$$

The cross-sectional mechanics equilibrium in bending, at SLS, can then be written in the following form (Figure 1.27):

$$\boldsymbol{M}_{act} = \boldsymbol{M}_s + \boldsymbol{G}\wedge\boldsymbol{N}_c \text{ and } N_{act} = N_s + \psi.A_c.f_{cs} \qquad [1.19]$$

The moment equilibrium equation can be also rewritten as:

$$\boldsymbol{M}_{act} = \boldsymbol{M}_s + \psi(1-\alpha\delta_{gz})d_r A_c f_{cs}\boldsymbol{j} - \psi(1-\alpha\delta_{gy})d_r A_c f_{cs}\boldsymbol{k}$$

$$\text{with } \boldsymbol{M}_s = \sum_{q=1}^{n} A_{sq}\sigma_{sq}\boldsymbol{P_q}\wedge\boldsymbol{i} \text{ and } N_s = \sum_{q=1}^{n} A_{sq}\sigma_{sq} \qquad [1.20]$$

The normal force equilibrium equation is simply reduced to the following scalar equation:

$$N_{act} = N_s + \psi.A_c.f_{cs} \qquad [1.21]$$

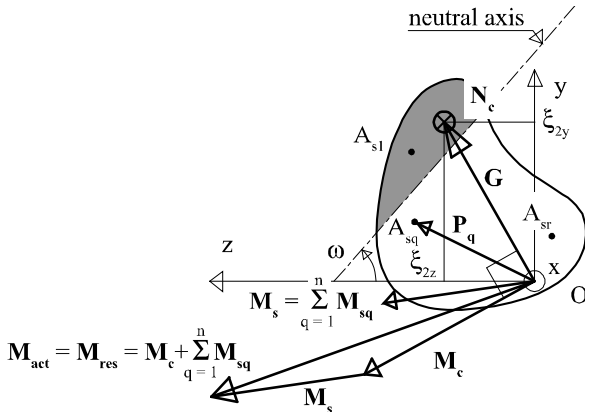

Figure 1.27. *Equilibrium of a general composite section; calculation of the screw of internal action*

1.7.2. *Discussion on the resolution of equations with respect to the number of unknowns*

It has been shown, from the application of the conservation principle of planeity coupled with the notions of limit laws and pivot concepts, that the stress distribution inside the cross-section can be considered as a discretized function of the following characteristic parameters α, $d_q(\forall q \in [1;n])$, f_{ss} or f_{cs}. The equilibrium equations give a system composed of two vectorial equations (three scalar equations) in the general case: $\boldsymbol{M}_{act} = \boldsymbol{M}_s + \boldsymbol{G} \wedge \boldsymbol{N}_c$ and $N_{act} = N_s + N_c$. The mathematical problem, in conformity with the specifications at the SLS, is a well-posed problem only if the number of unknowns is also equal to three in the general case. These unknown variables are of different types and are typically of geometrical nature: steel reinforcement area, position of the neutral axis, etc.

– *General case*: three linearly independent scalar equations;

(two moment scalar equations and one normal force resultant equation).

– *Symmetrical case*: two linearly independent scalar equations;

(one moment scalar equation and one normal force resultant equation).

For symmetrical sections, with symmetrical steel reinforcement, and with symmetrical loading (in this case ω is known), the three-parameter problem is reduced to a two-parameter problem associated with two equations: one scalar moment equation and one resultant equation. Different engineering problems can be envisaged, for reinforced concrete design, which can be illustrated through the following examples:

– Design of a unique unknown steel reinforcement area (in tension or in compression) whose center of gravity is known.

One of the steel reinforcement area A_{si} being unknown (in tension or in compression), two additional parameters have to be chosen, in the unsymmetrical case, such as the relative height of the neutral axis α and the neutral axis direction (angle ω). We have then to solve a problem of three equations with three unknowns A_{si}, ω and α. For a symmetrical section, the two unknown parameters can be the steel reinforcement area and the relative position of the neutral axis α.

– Design of a unique unknown steel reinforcement area (in tension or in compression) with a given neutral axis (related to the variable ω or to the variable α).

One of the steel reinforcement area A_{si} being unknown (in tension or in compression), two additional parameters have to be chosen, in the unsymmetrical case, such as the two spatial coordinates of the considered steel reinforcement. For a symmetrical section, the two unknown parameters can be the steel reinforcement area and the ordinate of the center of gravity of the steel reinforcement. A current case is the case of a symmetrical section, where the neutral axis is fixed at the boundary of Pivot A and Pivot B, to avoid the design of the cross-section at Pivot B (in order to limit the steel reinforcement quantity). In such a case, the two unknown parameters can be the areas of the tension and compression steel reinforcement, for a given fixed location of these steel reinforcements.

1.7.3 *Reduced moments*

From the equilibrium moment equation, we have $\boldsymbol{M}_{act} = \boldsymbol{M}_s + [\xi_{2z}.\boldsymbol{j} - d_r(1-\alpha.\delta_{gy}).\boldsymbol{k}].\psi.A_c.f_{cs}$, which, by dividing each member by the moment quantity $-d_r.A_c.f_{cs}/f(\alpha)$ where $f(\alpha)$ is a function of the dimensionless parameter α, can be formulated as:

$$\frac{-f(\alpha).\boldsymbol{M}_{act}}{d.A_c.f_{cs}} = \frac{-f(\alpha).\boldsymbol{M}_s}{d.A_c.f_{cs}} - \frac{f(\alpha).\psi.\xi_{2z}.\boldsymbol{j}}{d} + f(\alpha).\psi.(1-\alpha.\delta_g).\boldsymbol{k}. \qquad [1.22]$$

From this dimensionless equilibrium equation, the dimensionless reduced moment can be introduced:

$$\mu_{act,ser} = \frac{-f(\alpha).\boldsymbol{M}_{act}}{d.A_c.f_{cs}} \text{ and } \mu_{res,ser} = f(\alpha).\psi.(1-\alpha.\delta_{gy}) \qquad [1.23]$$

with $\mu_{act,ser}$ is the acting reduced moment and $\mu_{res,ser}$ is the reduced concrete contribution moment.

The function $f(\alpha)$ can be chosen such as the reduced acting moment which does not contain explicitly the variable α; it is quite efficient to take $f(\alpha) = d_r.A_c/(d_r^2.b)$ where b is a characteristic length of the cross-section. For instance, for a rectangular section solicited in its symmetry plane, the natural choice $f(\alpha) = \alpha$ leads to the following acting reduced moment:

$$\mu_{act} = \frac{-M_{act}}{b.d_r^2.f_{cs}} \quad [1.24]$$

and the reduced concrete contribution moment is written as:

$$\mu_{res} = \alpha.\psi.(1 - \alpha.\delta_{gy}) \quad [1.25]$$

Another example can illustrate the role played by the function $f(\alpha)$ to highlight the role of the dimensionless parameters. Let us take the example of a *T*-section, solicited in its plan of symmetry. It is possible to choose the function $f(\alpha)$ is such a way:

$$f(\alpha) = (\frac{b}{b_w} - 1).\frac{h_0}{d_r} + \alpha \quad [1.26]$$

leading to:

$$\mu_{act} = \frac{-M_{act}}{b_w.d_r^2.f_{cs}} \quad [1.27]$$

The reduced bending moment is then formulated as:

$$\mu_{res} = [(\frac{b}{b_w} - 1).\frac{h_0}{d_r} + \alpha].\psi.(1 - \alpha.\delta_{gy}) \quad [1.28]$$

Another choice for the function $f(\alpha)$ in the case of the *T*-section would be based on:

$$f(\alpha) = (1 - \frac{b_w}{b}).\frac{h_0}{d_r} + \alpha \quad [1.29]$$

With this alternative of the function $f(\alpha)$, the reduced bending moment is normalized with respect to the width of the concrete slab:

$$\mu_{act} = \frac{-M_{act}}{b.d_r^2.f_{cs}} \quad [1.30]$$

The reduced bending moment is then formulated as:

$$\mu_{res} = [(1 - \frac{b_w}{b}).\frac{h_0}{d_r} + \alpha\frac{b_w}{b}].\psi.(1 - \alpha.\delta_{gy}) \quad [1.31]$$

In the symmetrical loading case with symmetrical cross-section, we finally obtain, for the reduced moment equation:

$$\frac{-f(\alpha).M_{act}}{d_r.A_c.f_{cs}} = \frac{-f(\alpha).M_s}{d_r.A_c.f_{cs}} + f(\alpha).\psi.(1-\alpha\delta_{gy}.) \qquad [1.32]$$

In this relationship, it is convenient to define the physical meaning of each term:

$\frac{-f(\alpha).M_{act}}{d.A_c.f_{cs}} = \mu_{act,ser}$ reduced acting moment

$\frac{-f(\alpha).M_s}{d.A_c.f_{cs}} = \mu_{res,ser,s}$ reduced steel reinforcement moment

$f(\alpha).\psi.(1-\alpha.\delta_g) = \mu_{res,ser,c}$ reduced concrete contribution moment

The total moment equilibrium equation is simply obtained by the sum of each contribution of the steel and the concrete part of the reinforced concrete section:

$$\mu_{act,ser} = \mu_{res,ser,s} + \mu_{res,ser,c} \qquad [1.33]$$

1.7.4. *Case of a rectangular section*

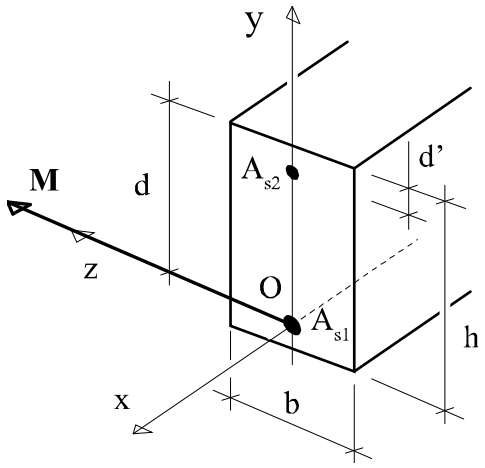

Figure 1.28. *Characteristics of a rectangular reinforced concrete section*

Using the notations of Figure 1.28, the two equilibrium equations both for the normal force and the bending moment (only two equations for symmetrical reasons) are written as:

$$N_{act} = A_{s1}\sigma_{s1} + A_{s2}\sigma_{s2} + \alpha\psi bdf_{cs} \quad [1.34]$$

$$M_{act} = -A_{s2}\sigma_{s2}(d - d') - \alpha\psi(1 - \alpha\delta_g)bd^2 f_{cs} \quad [1.35]$$

1.8. Case of pivot A for a rectangular section

1.8.1. *Studied section*

The case of a rectangular cross-section reinforced by both tensile (area A_{s1}) and compressive (area A_{s2}) steel reinforcements symmetrically disposed along the median axis y is now considered. The origin of the frame is located at the center of gravity of the tensile steel reinforcement. The geometrical characteristics of the cross-section are denoted by b, h, d and d' and are illustrated in Figure 1.28. The concrete and steel material stress limits are given at the SLS by f_{ss} for the steel reinforcement, and f_{cs} for the concrete, the equivalence coefficient being classically denoted by α_e. The acting solicitation is evaluated at the point O and is characterized by two components, the acting bending moment $\boldsymbol{M}_{act} = M_{act}\boldsymbol{k}$ and the normal force resultant $\boldsymbol{N}_{act} = N_{act}.\boldsymbol{i}$. The unknown of the problem are, respectively, the tensile reinforcement area A_{s1} and the relative height of the neutral axis α.

1.8.2. *Shape filling coefficient*

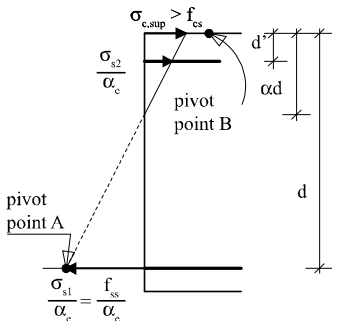

Figure 1.29. *Stress diagram in the homogenized section of the reinforced concrete section for Pivot A*

The variable α varies in the interval $[0; \alpha_e f_{cs}/(\alpha_e f_{cs} - f_{ss})]$, which depends on both the elastic and the stress limit values at the SLS. Stresses inside the composite cross-section are related by the equalities:

$$\frac{-\sigma_{s2}}{\alpha d - d'} = \frac{f_{ss}}{d - \alpha d} = \frac{-\alpha_e . \sigma_{csup}}{\alpha d} \qquad [1.36]$$

The stress diagram in the homogenized section is shown in Figure 1.29. By definition, the normal force in the compressed part of concrete is calculated as $N_c = \alpha \psi . b . d f_{cs}$., which is also equivalent after calculation to $N_c = 0{,}5 . \sigma_{c,sup} . \alpha . b . d$. The shape filling coefficient ψ is then simply expressed by:

$$\psi = \frac{-\alpha}{2\alpha_e(1 - \alpha)} \cdot \frac{f_{ss}}{f_{cs}} \qquad [1.37]$$

1.8.3. *Dimensionless coefficient related to the center of pressure*

At the SLS, the pressure center of the compressed part of concrete is at a distance $\alpha d/3$ of the most compressed fiber (the upper fiber of concrete), leading to the dimensionless coefficient $\delta_g = 1/3$ (Figure 1.30).

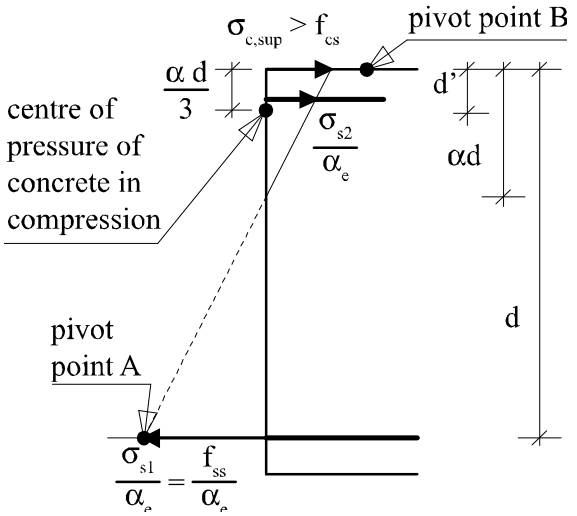

Figure 1.30. *Position of the center of pressure at the serviceability limit state; Pivot A*

1.8.4. *Equations formulation*

A third-order polynomial equation of the unknown neutral axis position has to be solved at the SLS. This polynomial equation is obtained from writing the equilibrium equations in bending moment and normal forces, coupled with the kinematics assumptions of the cross-section and the elastic behavior of the steel and concrete constituents of the composite cross-section:

$$N_{act} = A_{s1}\sigma_{s1} + A_{s2}\sigma_{s2} + \alpha\psi bdf_{cs} \qquad [1.38]$$

$$M_{act} = -A_{s2}\sigma_{s2}(d - d') - \alpha\psi(1 - \alpha\delta_g)bd^2 f_{cs} \qquad [1.39]$$

The stress in the compression steel reinforcement σ_{s2} also depends on the unknown α.

$$\sigma_{s2} = \frac{-f_{ss}.(\alpha d - d')}{d - \alpha d} \qquad [1.40]$$

It means that only the second bending moment, equation [1.39], contains one single unknown α out of the two unknowns of the design problem, respectively, the tensile reinforcement area A_{s1} and the relative height of the neutral axis α. As the filling shape coefficient ψ is given by:

$$\psi = \frac{-\alpha}{2\alpha_e(1-\alpha)} \cdot \frac{f_{ss}}{f_{cs}} \qquad [1.41]$$

and by setting the section equilibrium $M = M_{ser}$, equation of the equilibrium bending moment finally leads to:

$$M = \frac{A_{s2}(d-d')(\alpha d-d')f_{ss}}{d(1-\alpha)} + \frac{\alpha^2(3-\alpha)}{6\alpha_e(1-\alpha)} bd^2 f_{ss} \qquad [1.42]$$

We recognize a third-order polynomial equation:

$$\alpha^3 - 3\alpha^2 + 6\alpha_e\left(\frac{-M}{bd^2 f_{cs}}\frac{f_{cs}}{f_{ss}} - \frac{(d-d')A_{s2}}{bd^2}\right)\alpha +$$

$$6\alpha_e\left(\frac{M}{bd^2 f_{cs}}\frac{f_{cs}}{f_{ss}} + \frac{d'(d-d')A_{s2}}{bd^3}\right) = 0 \qquad [1.43]$$

Some other dimensionless coefficients can be introduced as:

$$\delta' = \frac{d'}{d}\ ,\ \rho'_{cs} = \frac{A_{s2}}{bd} \text{ and } \mu_{act} = \frac{-M}{bd^2 f_{cs}} \qquad [1.44]$$

We note that all these dimensionless coefficients δ', ρ'_{cs} and μ_{act} are positive numbers. The third-order polynomial equation can finally be written as:

$$\alpha^3 - 3\alpha^2 + 6\alpha_e[(f_{cs}/f_{ss})\mu_{act} - (1-\delta')\rho'_{cs}]\alpha + 6\alpha_e\,[-(f_{cs}/f_{ss})\mu_{act} + \delta'(1-\delta')\rho'_{cs}] = 0 \qquad [1.45]$$

Algebraically, this third-order equation can easily be solved using Cardano's method (see Appendix 1).

1.8.5. *Resolution*

Following Cardano's method, such a third-order polynomial equation can be presented in a canonical format using canonical parameters:

$$p = -3 - 6\alpha_e[(-f_{cs}/f_{ss})\mu_{act} + (1-\delta')\rho\delta'_{cs}] \text{ and}$$
$$q = -2 - 6\alpha_e(1-\delta')^2\rho'_{cs} \qquad [1.46]$$

Both canonical parameters p and q are negative numbers. The solution α can be extracted from Cardano's formula as one of the three real equations, whose solution of interest, for physical reasons, is:

$$\alpha = 1 + 2\sqrt{\frac{-p}{3}}\cos\left[\frac{Arc\cos\left(-\frac{q}{2}\left|\frac{p}{3}\right|^{-1.5}\right) - 2\pi}{3}\right] \qquad [1.47]$$

which can be equivalently written as:

$$\alpha = 1 + 2\sqrt{\frac{-p}{3}}\cos\left[\frac{Arc\cos\left(\frac{3q}{2p}\sqrt{\frac{3}{-p}}\right) - 2\pi}{3}\right] \qquad [1.48]$$

If there is no compression steel reinforcement (A_{s2} = 0), the neutral axis equation to be solved is still a third-order polynomial equation that is now simplified in:

$$\alpha^3 - 3\alpha^2 - 6\alpha_e\,\mu_{act}\left(\frac{-f_{cs}}{f_{ss}}\right)\alpha + 6\alpha_e\,\mu_{act}\left(\frac{-f_{cs}}{f_{ss}}\right) = 0 \qquad [1.49]$$

The canonical parameters in this particular case (A_{s2} = 0) are also simplified:

$$p = -3 - 6\alpha_e(-f_{cs} / f_{ss})\mu_{act} \text{ and } q = -2 \qquad [1.50]$$

In the absence of compression steel reinforcement (A_{s2} = 0), the solution for the position of neutral axis α in Pivot A is then calculated as:

$$\alpha = 1 + 2\sqrt{1 + 2\alpha_e\left(-\frac{f_{cs}}{f_{ss}}\right)\mu_{act}} \times \cos\left[\frac{Arc\cos\left[\left(1 + 2\alpha_e\left(-\frac{f_{cs}}{f_{ss}}\right)\mu_{act}\right)^{-1.5}\right] - 2\pi}{3}\right] \qquad [1.51]$$

Once the neutral axis position α is calculated, the axial force equilibrium equation gives the tensile steel area:

$$A_{s1} = \frac{N_{act}}{f_{ss}} + \frac{\alpha - \delta'}{1 - \alpha}A_{s2} + \frac{\alpha^2 bd}{2\alpha_e(1 - \alpha)} \qquad [1.52]$$

In the absence of compression steel reinforcement (A_{s2} = 0), the tensile steel area in Pivot A is given by:

$$A_{s1} = \frac{N_{act}}{f_{ss}} + \frac{\alpha^2 bd}{2\alpha_e(1 - \alpha)} \qquad [1.53]$$

The stress SLS has been then solved in Pivot A.

1.9. Case of pivot B for a rectangular section

1.9.1. *Studied section*

The case of a rectangular cross-section reinforced by both tensile (area As_1) and compressive (area As_2) steel reinforcements symmetrically disposed along the median axis y is considered, but now the section is ruled by Pivot B. The geometrical characteristics of the cross-section are also denoted by b, h, d and d', and are illustrated in Figure 1.28. The concrete and steel material stress limits are given at the SLS by f_{ss} for the steel reinforcement, and f_{cs} for the concrete, the equivalence coefficient being classically denoted by α_e. The acting solicitation is evaluated at the point O, and is characterized by two components, the acting bending moment $\boldsymbol{M}_{act} = M_{act}\boldsymbol{k}$ and the normal force resultant $\boldsymbol{N}_{act} = N_{act}.\boldsymbol{i}$. The unknown of the problem are, respectively, the tensile reinforcement area A_{s1} and the relative height of the neutral axis α.

1.9.2. *Shape filling coefficient*

In a case of simple bending solicitation (without combined axial forces), the variable α varies in the interval $[\alpha_e f_{cs}/(\alpha_e f_{cs} - f_{ss}); h/d]$, which depends on both the elastic and the stress limit values at the SLS. In case of bending with combined axial forces, the neutral axis can be located outside the cross-section. However, in the simple bending case, the neutral axis is inside the cross-section, which gives the upper bound variation of the dimensionless coefficient α. By definition, the normal force in the compression part N_c is calculated from:

$$N_c = \psi . f_{cs} . \alpha . b . d \qquad [1.54]$$

As the stress diagram is linear at the SLS, it can be easily deduced that the filling shape coefficient ψ in Pivot B is equal to $\psi = 1/2$, as $N_c = 0{,}5.\alpha. f_{cs}.b.d$.

1.9.3. *Dimensionless coefficient related to the center of pressure*

At the SLS, the pressure center of the compressed part of concrete is at a distance $\alpha d/3$ of the most compressed fiber (the upper fiber of concrete), leading to the dimensionless coefficient of $\delta_g = 1/3$ (Figure 1.31).

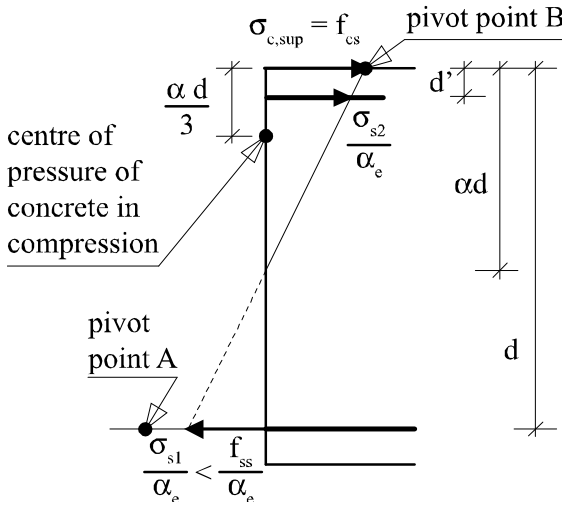

Figure 1.31. *Position of the center of pressure at the serviceability limit state; Pivot B*

1.9.4. *Equations formulation*

In the more general case, at Pivot B, a third-order polynomial equation of the unknown neutral axis position α has also to be solved at the SLS. This polynomial equation is obtained from writing the equilibrium equations in moment and normal forces, coupled with the kinematics assumptions of the cross-section and the elastic behavior of the steel and concrete constituents of the composite cross-section:

$$N_{act} = A_{s1}\sigma_{s1} + A_{s2}\sigma_{s2} + \alpha\psi bdf_{cs} \qquad [1.55]$$

$$M_{act} = -A_{s2}\sigma_{s2}(d - d') - \alpha\psi(1 - \alpha\delta_g)bd^2 f_{cs} \qquad [1.56]$$

The stress in the compression steel reinforcement σ_{s2} also depends on the unknown α.

$$\sigma_{s2} = \frac{\alpha_e f_{cs}(\alpha d - d')}{\alpha d} \qquad [1.57]$$

It is worth mentioning that the stress expression in the compression steel reinforcement is different in Pivot A and Pivot B. Inserting the value of the

shape filling coefficient ψ at Pivot B, ψ = ½, and the equilibrium moment equation is finally given by:

$$M = -A_{s2}\frac{(d\text{-}d')(\alpha d\text{-}d')}{\alpha d}\alpha_e f_{cs} - \frac{\alpha(3 - \alpha)}{6}bd^2 f_{cs} \qquad [1.58]$$

This equation is equivalent to the third-order polynomial equation, which allows us to calculate algebraically the position of the neutral axis at Pivot B:

$$\alpha^3 - 3\alpha^2 + 6\left(\frac{-M}{bd^2 f_{cs}} - \frac{(d\text{-}d')\ \alpha_e A_{s2}}{bd^2}\right)\alpha + \frac{6\alpha_e d'(d\text{-}d')A_{s2}}{bd^3} = 0 \qquad [1.59]$$

The dimensionless coefficients can be introduced as:

$$\delta' = \frac{d'}{d},\ \rho_{cs} = \frac{\alpha_e A_{s2}}{bd} \text{ and } \mu_{act} = \frac{-M}{bd^2 f_{cs}} \qquad [1.60]$$

We note that all these dimensionless coefficients δ', ρ'_{cs} and μ_{act} are also positive numbers. The third-order polynomial equation can finally be written as:

$$\alpha^3 + 3\alpha^2 + 6\ [\mu_{act} - (1 - \delta')\rho_{cs}]\alpha + 6\delta'(1 - \delta')\rho_{cs} = 0 \qquad [1.61]$$

In this case, again, this third-order equation can be easily algebraically solved using Cardano's method (see Appendix 1). It can be outlined that the third-order equation in Pivot B is different from the third-order equation in Pivot A, and the two resolutions are indeed two different mathematical problems.

1.9.5. *Resolution*

Following Cardano's method, such a third-order polynomial equation can be presented in canonical format using the canonical parameters:

$$p = 6[\mu_{act} - \rho_{cs}(1 - \delta')] - 3 \text{ and } q = 6[\mu_{act} - \rho_{cs}(1 - \delta')^2] - 2 \qquad [1.62]$$

Both canonical parameters p and q are generally negative numbers. The solution α can be extracted from Cardano's formula as:

$$\alpha = 1 + 2\sqrt{\frac{-p}{3}}\cos\left[\frac{Arc\cos\left(\frac{3q}{2p}\sqrt{\frac{3}{-p}}\right) - 2\pi}{3}\right] \qquad [1.63]$$

If there is no compression steel reinforcement ($A_{s2} = 0$), the neutral axis equation to be solved is now a second-order polynomial equation which can be written as:

$$\alpha^2 - 3\alpha + 6\mu_{act} = 0 \qquad [1.64]$$

whose solution is well known in reinforced concrete designs:

$$\alpha = 1{,}5\left(1 - \sqrt{1 - \frac{8}{3}\mu_{act}}\right). \qquad [1.65]$$

Once the neutral axis position α has been calculated, the axial force equilibrium equation gives the tensile steel area:

$$A_{s1} = \frac{-\alpha N_{act}}{\alpha_e f_{cs}(1-\alpha)} + \frac{\alpha - \delta'}{1 - \alpha} A_{s2} + \frac{\alpha^2 bd}{2\alpha_e(1-\alpha)} \qquad [1.66]$$

In the absence of compression steel reinforcement ($A_{s2} = 0$), the tensile steel area in Pivot B is given by:

$$A_{s1} = \frac{-\alpha N_{act}}{\alpha_e f_{cs}(1-\alpha)} + \frac{\alpha^2 bd}{2\alpha_e(1-\alpha)} \qquad [1.67]$$

The stress SLS has been then solved in Pivot B.

1.9.6. *Synthesis*

In Pivot A, the calculation of the position of the neutral axis at the stress SLS needs the resolution of a third-order polynomial equation, whatever compression steel reinforcements are incorporated in the cross-section

(A_{s2} = 0 or $A_{s2} \neq 0$). In Pivot B, the calculation of the position of the neutral axis at the stress SLS needs the resolution of a polynomial third-order polynomial equation, when compression steel reinforcement are incorporated in the cross-section ($A_{s2} \neq 0$). However, only in Pivot B, the third-order equation degenerates to a second-order polynomial equation in absence of compression steel reinforcement ($A_{s2} = 0$).

1.10. Examples – bending of reinforced concrete beams with rectangular cross-section

1.10.1. *A design problem at SLS – exercise*

1.10.1.1. *Structural problem*

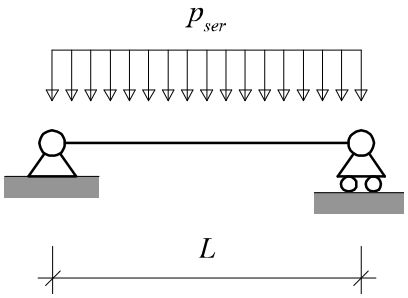

Figure 1.32. *Simply supported reinforced concrete beam*

As a first application of the presented theory, we would like to design the reinforcement of a given beam with a given rectangular cross-section (see Figures 1.32 and 1.33). This is a simply supported beam of length L = 6 m.

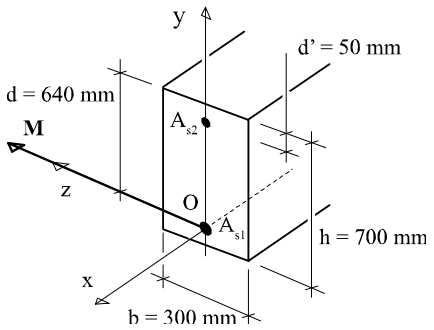

Figure 1.33. *Characteristics of the rectangular cross-section*

The geometrical characteristics are given in Figure 1.33 and detailed below:

$$b = 300 \text{ mm}; h = 700 \text{ mm}; d = 640 \text{ mm}; d' = 50 \text{ mm} \quad [1.68]$$

For engineering design, the order of magnitude for both the position of the center of gravity of the tensile steel reinforcement and the compression steel reinforcement is usually taken as:

$$d \sim 0.9\, h;\ d' \sim 0.1\, h \quad [1.69]$$

which is almost satisfied in our present case.

1.10.1.2. *Material parameters*

The reinforced concrete section is composed of *B500B* steel bars and a *C25/30* type of concrete. In the nomenclature of steel classification *B500B*, the first *B* stands for steel for reinforced concrete. The next three digits represent the specified characteristic value of upper yield strength f_{yk} = 500 MPa. The last symbol *B* stands for ductility class. In the nomenclature of concrete classification *C25/30*, the first *C* stands for concrete. The next digits are related to characteristic strengths. The first characteristic compression strength is the cylinder characteristic strength f_{ck} = 25MPa, whereas the second characteristic compression strength is the cubic characteristic strength. Hence, we calculate the limit stresses at the SLS as:

$$\begin{aligned} f_{ss} &= 0.8\, f_{yk} = 0.8 \times 500 = 400 \text{ MPa and} \\ f_{cs} &= -0.6\, f_{ck} = -0.6 \times 25 = -15 \text{ MPa} \end{aligned} \quad [1.70]$$

The equivalence coefficient is given for this problem as: α_e = 15. The steel Young's modulus is equal to *Es* = 200,000 MPa.

There could be some discussions on the calculation of the concrete Young modulus E_c. From EC2 (Eurocode 2) [EUR 04], we have (in MPa):

$$E_c = \frac{E_{cm}}{1 + \varphi(\infty, t_0)} \text{ with } E_{cm} = 22{,}000 \left(\frac{f_{cm}}{10} \right)^{0.3} \text{ and } f_{cm} = f_{ck} + 8 \quad [1.71]$$

where φ is the creep coefficient (time-dependent effects) and the subscript m represents the mean value of the considered variable. The order of magnitude of φ typically varies between 1 and 2. The formula in this equation is not homogeneous from a dimensional point of view, except for the numbers 22,000, 10 and 8 can be viewed as specific stress values given in megapascals (MPa). We calculate for the mean value of the concrete Young modulus:

$$E_{cm} = 22{,}000\left(\frac{33}{10}\right)^{0.3} = 31475.81\,\text{MPa} \qquad [1.72]$$

For a specific concrete, the calculation of the equivalent coefficient α_e depends on the creep coefficient φ. For a given value of the equivalent coefficient α_e, the creep coefficient can be calculated as:

$$\phi(\infty, t_0) = \frac{\alpha_e E_{cm}}{E_s} - 1 = \frac{15 \times 31{,}475.81}{200{,}000} - 1 = 1.361 \qquad [1.73]$$

It means, in this example, that the value of $\alpha_e = 15$ corresponds to a creep coefficient φ of approximately 1.361. The determination of the equivalence coefficient is still debated, actually (see also [THO 09] or [PAI 09], for instance), and the typical value of α_e = 15, which was the usual value employed in the old French rules BAEL 91, which is still relevant to use with the new EC2 rules.

More generally, the creep coefficient depends on the type of concrete and on the type of analysis, namely the short-term or the long-term analyses.

1.10.1.3. *Loading parameters*

The simply supported reinforced concrete beam is loaded by some uniform distributed loads:

– permanent loads (without the own weight): $g_1 = 24.75$ kN/m;

– variable loads: $q = 20$ kN/m.

The volumetric density of the reinforced concrete beam can be taken as $\overline{\omega} = 25\,\text{kN/m}^3$. The permanent loads are then calculated as the sum of g_1 and the own weight g_2:

$$g = g_1 + g_2 = g_1 + \overline{\omega} bh = 24.75 + 25 \times 0.3 \times 0.7 = 30\,\text{kN/m} \qquad [1.74]$$

The combination of action at the SLS is usually one for the permanent load and one for the variable load, leading to the serviceability distributed load:

$$p_{ser} = g + q = 30 + 20 = 50\,\text{kN/m} \qquad [1.75]$$

The critical section of this problem is the one where the bending moment is maximum, that is at mid-span, leading to the bending solicitation for designing at the SLS:

$$M_{ser} = p_{ser} \frac{L^2}{8} = 50 \times \frac{6^2}{8} = 225\,\text{kN.m} \qquad [1.76]$$

1.10.1.4. *Steel reinforcement at SLS*

The exercice consists of designing the steel reinforcement of the reinforced concrete beam at the Stress SLS for this solicitation M_{ser}= 225 kN.m, and for a higher solicitation:

– M_{ser} = 225 kN.m;

– M_{ser} = 405 kN.m.

We first start from the first solicitation M_{ser} = 225 kN.m.

1.10.2. *Resolution in Pivot A – M_{ser} = 225 kN.m*

As presented in section 1.5.5, the limit value of the neutral axis position at the boundary of the two pivots, Pivot A and Pivot B, is given from:

$$\alpha_{AB} = \frac{\alpha_e}{\alpha_e - \dfrac{f_{ss}}{f_{cs}}} = \frac{15}{15 + \dfrac{400}{15}} = \frac{9}{25} = 0.36 \qquad [1.77]$$

The bending moment solicitation at the boundary of Pivot A and Pivot B can be calculated from:

$$M_{AB} = -N_{c,AB} \times \left(d - \frac{\alpha_{AB} d}{3} \right) = -bd^2 f_{cs} \frac{\alpha_{AB}}{2} \left(1 - \frac{\alpha_{AB}}{3} \right)$$
$$= 0.3 \times 0.64^2 \times 15 \times \frac{0.36}{2} \times \left(1 - \frac{0.36}{3} \right) = 0.29196 \text{ MN.m} \quad [1.78]$$

It is also possible to introduce the dimensionless reduced moment at the boundary between Pivot A and Pivot B as:

$$\mu_{AB} = \frac{M_{AB}}{-bd^2 f_{cs}} = \frac{\alpha_{AB}}{2} \left(1 - \frac{\alpha_{AB}}{3} \right)$$
$$= \frac{0.36}{2} \times \left(1 - \frac{0.36}{3} \right) = 0.1584 \quad [1.79]$$

It can be easily checked, for this solicitation, that Pivot A rules the behavior of the cross-section at SLS as:

$$M_{ser} = 0.225 \text{ MN.m} \le M_{AB} = 0.29196 \text{ MN.m or}$$
$$\mu_{ser} = \frac{M_{ser}}{-bd^2 f_{cs}} = 0.122 \le \mu_{AB} = 0.1584 \quad [1.80]$$

Then, the dimensionless position of the neutral axis given by parameter α should be the solution of the following third-order polynomial equation:

$$\alpha^3 - 3\alpha^2 - 6\alpha_e \mu_{act} \left(\frac{-f_{cs}}{f_{ss}} \right) \alpha + 6\alpha_e \mu_{act} \left(\frac{-f_{cs}}{f_{ss}} \right) = 0, \text{ or}$$

$$\alpha^3 - 3\alpha^2 - 0.41175\alpha + 0.41175 = 0 \quad [1.81]$$

The canonical parameters needed for the resolution of this third-order polynomial equation by Cardano's method are then calculated:

$$p = -3 - 6\alpha_e (-f_{cs} / f_{ss}) \mu_{act} = -3.41175 \text{ and } q = -2 \quad [1.82]$$

The solution for the position of neutral axis α in Pivot A, for this cross-section, is calculated as:

$$\alpha = 1 + 2\sqrt{\frac{-p}{3}}\cos\left[\frac{Arc\cos\left(\frac{3q}{2p}\sqrt{\frac{3}{-p}}\right) - 2\pi}{3}\right] \text{ or}$$

$$\alpha = 1 + 2\sqrt{\frac{3.41175}{3}}\cos\left[\frac{0.601393 - 2\pi}{3}\right] = 0.322737 \qquad [1.83]$$

Finally, the tensile steel reinforcement area is obtained from equilibrium of the normal force component as:

$$A_{s1} = \frac{\alpha^2 bd}{2\alpha_e(1-\alpha)} = \frac{\alpha^2 \times 0.3 \times 0.64}{2 \times 15 \times (1-\alpha)} = 9.84289 \times 10^{-4} \text{ m}^2 \qquad [1.84]$$

The tensile steel reinforcement area of 9.843 cm^2 is needed to verify the stress SLS of this cross-section for the bending solicitation M_{ser} = 225 kN.m. Using the abacus of Appendix 2, we can choose 5ϕ16 (10.053 cm^2), which has to be an upper bound of the minimum tensile steel area of 9.843 cm^2. An example of steel reinforcement location is presented in Figure 1.34.

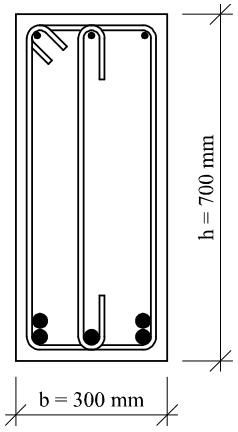

Figure 1.34. *5ϕ16 tensile steel reinforcement for M_{ser} = 225 kN.m at serviceability limit state*

1.10.3. *Resolution in Pivot B – M_{ser} = 405 kN.m*

By comparing the reduced moment μ_{ser} with the reduced frontier moment between Pivot A and Pivot B, $\mu_{AB} = 0.1584$, we see that for this solicitation M_{ser} = 405 kN.m, the section will behave in Pivot B:

$$\mu_{ser} = \frac{M_{ser}}{-bd^2 f_{cs}} = 0.2197 \geq \mu_{AB} = 0.1584 \qquad [1.85]$$

In Pivot B, and without additional compression steel reinforcement, the position of the neutral axis is obtained from resolution of a second-order polynomial equation whose root of interest is:

$$\alpha = \frac{3}{2}\left[1 - \sqrt{1 - \frac{8}{3}\mu_{ser}}\right] = \frac{3}{2}\left[1 - \sqrt{1 - \frac{8}{3} \times 0.2197}\right] = 0.53478 \qquad [1.86]$$

Finally, the tensile steel reinforcement area is obtained from equilibrium of the normal force component as:

$$A_{s1} = \frac{\alpha^2 bd}{2\alpha_e (1-\alpha)} = \frac{\alpha^2 \times 0.3 \times 0.64}{2 \times 15 \times (1-\alpha)} = 39.34 \times 10^{-4} \ \text{m}^2 \qquad [1.87]$$

The tensile steel reinforcement area of 39.34 cm^2 is needed to verify the stress SLS of this cross-section for the bending solicitation M_{ser} = 405 kN.m. Using the abacus of Appendix 2, we can choose 5ϕ32 (40.212 cm^2), which has to be an upper bound of the minimum tensile steel area of 39.34 cm^2.

It can be seen that for a solicitation M_{ser} = 405 kN.m less than twice the other solicitation M_{ser} = 225 kN.m, the steel reinforcement quantity has been multiplied by approximately four (from approximately 10 cm^2 to 40 cm^2). Even if physically possible, it is generally not interesting to design a section at Pivot B for economical reasons. This can be explained by Figure 1.35, where the variation of the steel reinforcement quantity measured by ρ_{s1} is compared in Pivot A and Pivot B without compression steel reinforcement (A_{s2} = 0).

Figure 1.35. *Evolution of the dimensionless steel quantity ρ_{s1} with respect to the solicitation expressed with the reduced moment μ_{ser}*

In Pivot A, we have the following relationships for the calculation of the dimensionless steel reinforcement area ρ_{s1}:

$$\rho_{s1} = \frac{\alpha_e A_{s1}}{bd} = \frac{\alpha^2}{2(1-\alpha)} \text{ and } \mu_{ser} = \frac{3\alpha^2 - \alpha^3}{6\alpha_e \left(-\frac{f_{cs}}{f_{ss}}\right)(1-\alpha)} \quad [1.88]$$

In Pivot B, we have the following relationships for the calculation of the dimensionless steel reinforcement area:

$$\rho_{s1} = \frac{\alpha_e A_{s1}}{bd} = \frac{\alpha^2}{2(1-\alpha)} \text{ and } \mu_{ser} = \frac{3\alpha - \alpha^2}{6} \quad [1.89]$$

Figure 1.35 shows the change of the slope of the steel area variation with respect to the solicitation represented by the reduced bending moment.

To avoid a design in Pivot B with too much steel reinforcement, it is suggested to add some compression steel reinforcement and to design the section at the boundary between the two pivots: Pivot AB.

1.10.4. *Resolution in pivot AB*

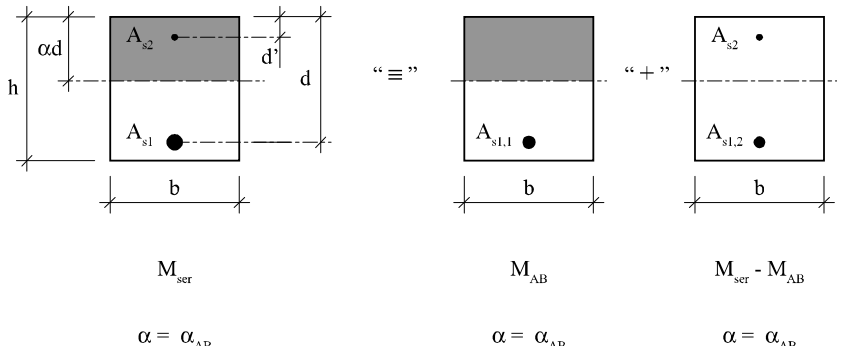

Figure 1.36. *Decomposition of the cross-section into two parts; Design at Pivot AB*

We choose to add some additional compression steel reinforcement with a section area A_{s2}, located at a distance d' from the upper fiber of the cross-section ($d' \approx 0.1$ h; in the present case, we choose $d' = 5$ cm). In order to keep the design problem as a well-posed mathematical problem, we have to fix an additional parameter by adding the unknown of the compression steel reinforcement area. Following the previous analysis, it has been shown that we have interest to fix the position of the neutral axis in order to behave in Pivot A. It is chosen to fix the position of the neutral axis such as:

$$\alpha = \alpha_{AB} \quad \Rightarrow \quad \begin{cases} \sigma_{s1} = f_{ss} \\ \sigma_{c,\text{sup}} = f_{cs} \end{cases} \qquad [1.90]$$

The section is decomposed into parts as shown in Figure 1.36, one section with the compressed part of the concrete and only the tensile reinforcement, whereas the other section is composed of some tensile and compression steel reinforcement. The total area of tensile steel reinforcement is equal to:

$$A_{s1} = A_{st1} + A_{st2} \qquad [1.91]$$

The calculation of the tensile steel reinforcement in the first part of the cross-section (see Figure 1.36) is obtained from the normal force equilibrium

equation, having in mind that this cross-section is solicitated by a fictitious bending moment equal to M_{AB}:

$$A_{st1} = \alpha_{AB} \frac{bd}{2} \left(-\frac{f_{cs}}{f_{ss}} \right) = \frac{{\alpha_{AB}}^2 bd}{2\alpha_e \left(1-\alpha_{AB}\right)} \Rightarrow A_{st1}$$

$$= 0.36 \times \frac{0.3 \times 0.64}{2} \times \frac{15}{400} = 12.96 \times 10^{-4}\,\text{m}^2 \qquad [1.92]$$

Considering the second part of the cross-section (see also Figure 1.36), the stress in the compression steel reinforcement is calculated from the compatibility of strain in the deformed cross-section:

$$\sigma_{s2} = \alpha_e f_{cs} \left(1 - \frac{d'}{\alpha_{AB} d} \right) \Rightarrow$$

$$\sigma_{s2} = -15 \times 15 \times \left(1 - \frac{0.05}{0.36 \times 0.64} \right) = -176.17\ \text{MPa} \qquad [1.93]$$

The moment equilibrium equation written at the center of gravity of the tensile steel reinforcement induces:

$$A_{s2} = \frac{M_{ser} - M_{AB}}{-\sigma_{s2}\left(d - d'\right)} \Rightarrow$$

$$A_{s2} = \frac{0.405 \times 10^6 - 0.292 \times 10^6}{176.17 \times 10^6 \times \left(0.64 - 0.05\right)} = 10.87 \times 10^{-4}\,\text{m}^2 \qquad [1.94]$$

The normal force equilibrium equation gives the tension steel reinforcement:

$$f_{ss} A_{st1} + \sigma_{s2} A_{st2} = 0 \Rightarrow A_{st2} = A_{s2} \frac{-\sigma_{s2}}{f_{ss}}$$

$$= 10.87 \times 10^{-4} \times \frac{176.17}{400} = 4.79 \times 10^{-4}\,\text{m}^2 \qquad [1.95]$$

We finally obtain for this cross-section designed at Pivot AB by adding some compression steel reinforcement: A_{s1} = 12.96 + 4.79 = 17.75 cm^2 and A_{s2} = 10.87 cm^2. We can take 6ϕ20 (18.85 cm^2) for the tensile steel reinforcement, and 2ϕ20 + 1ϕ25 (11.19 cm2) for the compression steel

reinforcement. The total steel quantity for this alternative less consuming design is 30.04 cm^2 (with $A_{s2} \neq 0$) compared to 40.21cm^2 obtained before in Pivot B without the use of compression steel reinforcement (with $A_{s2} = 0$). In this case, adding some compression steel reinforcement allows us to gain approximately 25% of the total steel reinforcement.

In fact, the interest of adding compression steel reinforcement can be clearly seen in Figure 1.37 for sufficiently large bending solicitation $\mu_{ser} \geq \mu_{AB}$. In the case where compression steel reinforcements are added to the upper part of the cross-section and the section is designed at Pivot AB, the total dimensionless steel area ρ_s is given by:

$$\rho_s = \frac{\alpha_{AB}^2}{2(1-\alpha_{AB})} + \frac{\mu_{ser} - \mu_{AB}}{\left(1-\frac{d'}{\alpha_{AB} d}\right)\left(1-\frac{d'}{d}\right)}\left[1+\alpha_e\left(\frac{-f_{cs}}{f_{ss}}\right)\left(1-\frac{d'}{\alpha_{AB} d}\right)\right]$$

$$\text{with } \rho_s = \frac{\alpha_e}{bd}\left(A_{s1} + A_{s2}\right) \qquad [1.96]$$

As shown by Figure 1.37, adding some compression steel reinforcement in this case makes the variation of the steel quantity linear with respect to the bending solicitation, whereas a design at Pivot B without additional compression steel reinforcement leads to a strongly nonlinear curve, which may overestimate significantly the steel quantity needed at SLS.

Figure 1.37. *Evolution of the total dimensionless steel quantity ρ_s with respect to the solicitation expressed with the reduced moment μ_{ser}*

1.10.5. *Design of a reinforced concrete section, an optimization problem*

In fact, designing the section at Pivot AB at SLS may lead to the optimized solution with respect to the total steel quantity used in the reinforced section. It can be shown that the position of the neutral axis (see Chapter 2 on the so-called "static moment equation") is obtained from a second-order polynomial equation written as:

$$\alpha = -(\rho_{s1} + \rho_{s2}) + \sqrt{(\rho_{s1} + \rho_{s2})^2 + 2(\rho_{s1} + \delta'\rho_{s2})} \qquad [1.97]$$

where the dimensionless coefficient $\delta' = d'/d$ has been used. We can introduce the change of variable:

$$\rho_{s1} = \rho_s \cos^2\theta \text{ and } \rho_{s2} = \rho_s \sin^2\theta \qquad [1.98]$$

It is easy to check that $\rho_S = \rho_{s1} + \rho_{s2}$ and $\tan^2\theta = \rho_{s2}/\rho_{s1}$. The optimization consists of finding the optimized value θ so that the SLS capacity reduced moment μ is maximized for a given quantity of steel reinforcement ρ_s. This optimization problem is illustrated in Figure 1.38 for the problem with geometrical parameters defined in Figure 1.33.

Figure 1.38. *Optimization of the reduced moment μ_{ser} with respect to the steel reinforcement ratio; $\rho_{s2}/\rho_{s1} = \tan^2\theta$ for a given quantity $\rho_S \in \{0.1; 0.2; 0.3; 0.4; 0.5\}$; $\delta' = 0.078125$; B500B steel bars and C25/30 type of concrete*

The optimization problem can be explicitly formulated from the analytical expression of the neutral axis position and the reduced moment

parameters. The position of the neutral axis is then expressed with respect to the new optimization variables:

$$\alpha(\rho_s,\theta) = -\rho_s + \sqrt{\rho_s^2 + 2\rho_s\left(\cos^2\theta + \delta'\sin^2\theta\right)} \qquad [1.99]$$

The reduced moment in Pivot A, for $\alpha(\rho_s,\theta) \le \alpha_{AB}$, is given by:

$$\mu(\rho_s,\theta) = \frac{\alpha^2(3-\alpha)}{6\alpha_e(1-\alpha)}\left(\frac{f_{ss}}{-f_{cs}}\right) + \frac{\rho_s\sin^2\theta}{\alpha_e}\frac{(1-\delta')(\alpha-\delta')}{1-\alpha}\left(\frac{f_{ss}}{-f_{cs}}\right) \qquad [1.100]$$

The reduced moment in Pivot B, for $\alpha(\rho_s,\theta) \ge \alpha_{AB}$, is given by:

$$\mu(\rho_s,\theta) = \rho_s\left(\sin^2\theta\right)(1-\delta')\frac{\alpha-\delta'}{\alpha} + \frac{\alpha}{2}\left(1-\frac{\alpha}{3}\right) \qquad [1.101]$$

As shown by Figure 1.38, the optimization problem is a singular optimization problem and the optimization parameter is associated with Pivot AB, leading to the transcendental equation:

$$\alpha(\rho_s,\theta) = -\rho_s + \sqrt{\rho_s^2 + 2\rho_s\left(\cos^2\theta + \delta'\sin^2\theta\right)} = \alpha_{AB} \qquad [1.102]$$

which can be analytically solved from:

$$\theta = \arccos\sqrt{\frac{\alpha_{AB}^2 + 2(\alpha_{AB}-\delta')\rho_s}{2\rho_s(1-\delta')}} \text{ for}$$

$$\rho_s \ge \frac{\alpha_{AB}^2}{2(1-\alpha_{AB})} = 0.10125 \qquad [1.103]$$

For $\mu_{ser} \le \mu_{AB} = 0.1584$, that is for a Pivot A section with only tensile steel reinforcement, the best solution is obtained for $\theta = 0$, that is, there is no need to add some compression steel reinforcement in the reinforced concrete section.

However, it can be shown that designing the section at SLS at the boundary between Pivot A and Pivot B for $\mu_{ser} \geq \mu_{AB}$ is not necessarily the best solution for all the range of parameters. The optimization problem coincides with the Pivot AB design in the problem handled in Figure 1.38, based on *B500B* steel bars and the *C25/30* type of concrete, and with $\delta' = 0.078125$. However, for the same materials but changing the value of the geometrical ratio δ' up to 0.15, it can be seen in Figures 1.39 and 1.40 that the optimized solution is different from the optimized solutionof Pivot AB.

For instance, this geometrical ratio $\delta' = 0.15$ corresponds to the reinforced section based on the following parameters:

b (m)..... 0.5
d′ (m)..... 0.06
d (m)..... 0.4
h (m)..... 0.46
f_{ss} (MPa)..... 400
f_{cs} (MPa)..... −15
M_{ser} (MN.m)..... 0.22
α_e.....15 [1.104]

Figure 1.39. *Optimization of the reduced moment μ_{ser} with respect to the steel reinforcement ratio; $\rho_{s2} / \rho_{s1} = \tan^2 \theta$ for a given quantity $\rho_s \in \{0.1; 0.2; 0.3; 0.4; 0.5\}$; $\delta' = 0.15$; B500B steel bars and C25/30 type of concrete*

Figure 1.40. *Optimization of the reduced moment μ_{ser} with respect to the steel reinforcement ratio; $\rho_{s2} / \rho_{s1} = \tan^2 \theta$ for a given quantity $\rho_s \in \{0.1; 0.15; 0.2\}$; $\delta' = 0.15$; B500B steel bars and C25/30 type of concrete*

As an example related to the sensitivity analysis shown by Figures 1.39 and 1.40, we give below an example of an reinforced concrete section in Pivot B with a total steel quantity lesser than the one associated with the design in Pivot AB. For this solicitation $\mu_{ser} = 0.183$, the design at Pivot AB leads to:

$$\alpha = \alpha_{AB} = 0.36; A_{s2} = 6.705 \text{ cm}^2; A_{s1} = 15.700 \text{ cm}^2;$$
$$A_s = 22.405 \text{ cm}^2 \text{ and then } \rho_s = 0.168 \qquad [1.105]$$

whereas the optimized solution, for the same solicitation $\mu_{ser} = 0.183$ is given in Pivot B, for:

$$\alpha_{opt} = 0.416 > \alpha_{AB} = 0.36; A_{s2} = 1.065 \text{ cm}^2; A_{s1} = 20.181 \text{ cm}^2;$$
$$A_s = 21.246 \text{ cm}^2 \text{ and then } \rho_s = 0.159 \qquad [1.106]$$

In this case, the optimized solution allows the gain of more than 5% of steel area with respect to the design at Pivot AB.

1.10.6. *General design at Serviceability Limit State with tensile and compression steel reinforcements*

In this section, the design of a reinforced concrete section at SLS with both tensile and compression steel reinforcements is presented. The section is not necessarily designed at Pivot AB, as developed in section 1.10.4. In the general case, the section is decomposed into two parts (see Figure 1.41).

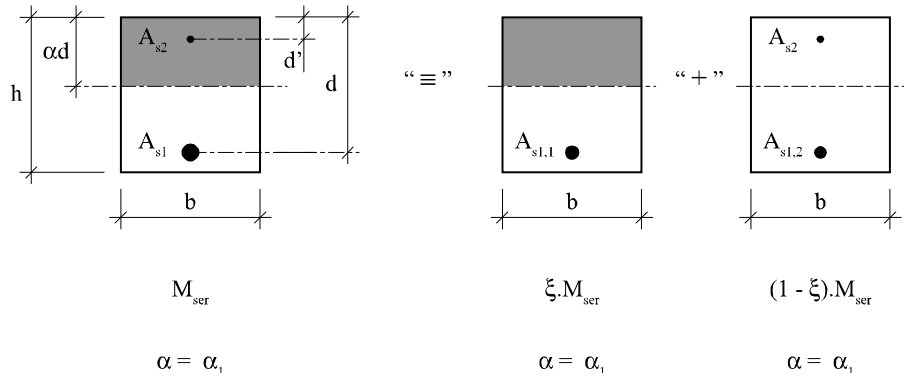

Figure 1.41. *Decomposition of the cross-section into two parts; general design*

It is assumed to write the total bending solicitation into two terms:

$$M_{ser} = M_1 + M_2 \text{ with } M_1 = \xi M_{ser} \text{ and } M_2 = (1-\xi) M_{ser} \qquad [1.107]$$

where ξ is a free dimensionless parameter that fixes the neutral axis position. For instance, if the neutral axis position is fixed at $\alpha = \alpha_{AB}$, then the parameter ξ is equal to $\xi_{AB} = M_{AB} / M_{ser}$. But this last case is of course a particular case. The design of the first fictitious section with only tensile steel reinforcements is first presented (solicitation $M_1 = \xi M_{ser}$). For a given value of the dimensionless coefficient ξ, the steel quantity $A_{s1,1}$ is calculated for the reduced moment $\mu_{ser,1} = \dfrac{-\xi M_{ser}}{b.d^2.f_{cs}}$. If $\mu_{ser,1} \le \mu_{AB}$, the calculation of the dimensionless neutral axis position α_1 is computed from the cubic equation:

$$\alpha_1^3 - 3\alpha_1^2 - 6\alpha_e \mu_{ser,1} \left(\frac{-f_{cs}}{f_{ss}}\right) \alpha_1 + 6\alpha_e \mu_{ser,1} \left(\frac{-f_{cs}}{f_{ss}}\right) = 0 \quad [1.108]$$

leading to the root:

$$\alpha_1 = 1 + 2\sqrt{1+2\alpha_e\left(-\frac{f_{cs}}{f_{ss}}\right)\mu_{ser,1}}\cos\left\{\frac{\text{Arc}\cos\left[1+2\alpha_e\left(-\frac{f_{cs}}{f_{ss}}\right)\mu_{ser,1}\right]^{-1.5} - 2\pi}{3}\right\} \quad [1.109]$$

If $\mu_{ser,1} \geq \mu_{AB}$, the calculation of the dimensionless neutral axis position α_1 is computed from the second-order polynomial equation:

$$\alpha_1^2 - 3\alpha_1 + 6\mu_{ser,1} = 0 \quad [1.110]$$

leading to the solution:

$$\alpha_1 = 1{,}5\left(1-\sqrt{1-\frac{8}{3}\mu_{ser,1}}\right) \quad [1.111]$$

In both cases, in Pivot A or Pivot B, the tensile steel area of section $A_{s1,1}$is obtained from:

$$A_{s1,1}=\frac{\alpha_1^2 bd}{2\alpha_e(1-\alpha_1)} \quad [1.112]$$

Now considering the second fictitious section with some tensile steel reinforcement (area $A_{s1,2}$), compression steel reinforcements (area A_{s2}), without any concrete in compression and solicited by the moment $M_2=(1-\xi)M_{ser}$. If α_1 corresponds to Pivot A, then the stresses in the tensile and compression steel reinforcements are calculated from:

$$\sigma_{s2} = -\frac{\alpha-\delta'}{1-\alpha}f_{ss}$$

$$\sigma_{s1,1} = \sigma_{s1,2} = f_{ss} \quad [1.113]$$

The bending moment equilibrium equation can be written at the center of the gravity of each steel reinforcement:

$$-A_{s2}\sigma_{s2}(1-\delta')d = (1-\xi)M_{ser}$$
$$A_{s1,2}\sigma_{s1,2}(1-\delta')d = (1-\xi)M_{ser} \qquad [1.114]$$

It is worth mentioning that a combination of each of these equations is in fact equivalent to the normal force equilibrium equation $A_{s1,2}\sigma_{s1} + A_{s2}\sigma_{s2} = 0$. The tensile and compression steel area can be finally obtained from:

$$A_{s2} = \frac{(1 - \xi)M_{ser}(1 - \alpha_1)}{(1 - \delta')(\alpha_1 - \delta')\, d\, f_{ss}}$$

$$A_{s1,2} = \frac{(1 - \xi)M_{ser}}{(1 - \delta')\, d\, f_{ss}} \text{ and } A_{s1,1} = \frac{\alpha_1^2 bd}{2\alpha_e(1 - \alpha_1)}$$

$$A_{s1} = \frac{(1 - \xi)M_{ser}}{(1 - \delta')d\, f_{ss}} + \frac{\alpha_1^2 bd}{2\alpha_e(1 - \alpha_1)} \qquad [1.115]$$

If α_1 corresponds to Pivot B, then the stresses in the steel reinforcements are obtained from:

$$\sigma_{s2} = \frac{\alpha_1 - \delta'}{\alpha_1}\alpha_e f_{cs}$$

$$\sigma_{s1,1} = \sigma_{s1,2} = -\frac{1 - \alpha_1}{\alpha_1}\alpha_e f_{cs} \qquad [1.116]$$

Also, using the bending moment equilibrium equation [1.114], the steel reinforcement areas can be calculated in Pivot B from:

$$A_{s2} = -\frac{\alpha_1(1 - \xi)M_{ser}}{(1 - \delta')(\alpha_1 - \delta')\, d\, \alpha_e f_{cs}}$$

$$A_{s1,2} = -\frac{\alpha_1(1 - \xi)M_{ser}}{(1 - \delta')(1 - \alpha_1)\, d\, \alpha_e f_{cs}} \text{ and } A_{s1,1} = \frac{\alpha_1^2 bd}{2\alpha_e(1 - \alpha_1)}$$

$$A_{s1} = -\frac{\alpha_1(1 - \xi)M_{ser}}{(1 - \delta')(1 - \alpha_1)\, d\, \alpha_e f_{cs}} + \frac{\alpha_1^2 bd}{2\alpha_e(1 - \alpha_1)} \qquad [1.117]$$

Using these equations, it would be possible to compute the total steel area $A_{s1} + A_{s2}$ with respect to the dimensionless free parameter ξ. It is also possible to optimize the design of the reinforced concrete section with respect to the total steel area by studying the evolution of the total steel area $A_{s1} + A_{s2}$ with respect to the dimensionless position of the neutral axis α_1. In Pivot A, the dimensionless compression steel area ρ_{s2} is obtained from:

$$\rho_{s2} = \frac{\alpha_1^3 - 3\alpha_1^2 + 6\alpha_e (f_{cs}/f_{ss})\mu_{ser}\alpha_1 - 6\alpha_e (f_{cs}/f_{ss})\, \mu_{ser}}{6(1-\delta')(\alpha_1 - \delta')} \quad [1.118]$$

and the total dimensionless steel area ρ_s is then equal to:

$$\rho_s = \frac{\alpha_1^3 - 3\alpha_1^2 + 6\alpha_e (f_{cs}/f_{ss})\mu_{ser}\alpha_1 - 6\alpha_e (f_{cs}/f_{ss})\, \mu_{ser}}{6(1 - \alpha_1)(\alpha_1 - \delta')} + \frac{\alpha_1^2}{2(1 - \alpha_1)} \quad [1.119]$$

In Pivot B, the dimensionless compression steel area ρ_{s2} is obtained from:

$$\rho_{s2} = \frac{\alpha_1^3 - 3\alpha_1^2 + 6\,\mu_{ser}\alpha_1}{6(1-\delta')\,(\alpha_1 - \delta')} \quad [1.120]$$

and the total dimensionless steel area ρ_s is then equal to:

$$\rho_s = \frac{\alpha_1^3 - 3\alpha_1^2 + 6\,\mu_{ser}\alpha_1}{6(1 - \alpha_1)\,(\alpha_1 - \delta')} + \frac{\alpha_1^2}{2(1 - \alpha_1)} \quad [1.121]$$

Figure 1.42. *Evolution of the steel quantity with respect to the dimensionless position of the neutral axis; B500B steel bars and C25/30 type of concrete;* $\mu_{ser} = 0.183; \delta' \in \{0.078125; 0.15\}$

The optimization problem consists of finding the smallest steel quantity ratio ρ_s with respect to α, for a given reduced moment $\mu_{ser} = 0.183$. It is clearly shown in Figure 1.42 that the optimization problem is sensible regarding the value of the parameter $\delta' = d'/d$. For the parameter $\delta' = 0.078125$ (problem analyzed in Figure 1.38), it is confirmed that the optimization solution is the solution associated with the design at Pivot AB, whereas for $\delta' = 0.15$ (problem analyzed in Figures 1.39 and 1.40), the optimized solution is different from the solution at the boundary between Pivot A and Pivot B. The optimal solution $\alpha_{opt} = 0.416 > \alpha_{AB} = 0.36$ is obtained in this case for the branch ruled by Pivot B, from the quartic equation:

$$\frac{\partial \rho_s}{\partial \alpha}(\alpha = \alpha_{opt}) = 0 \quad \Rightarrow$$

$$\alpha_{opt}^4 - 2(1+\delta')\alpha_{opt}^3 - \frac{3}{4}(-6\delta' - \delta'^2 - 1 + 2\mu_{ser})\alpha_{opt}^2 - \frac{3}{2}\delta'(1+\delta')\alpha_{opt} + \frac{3}{2}\delta'\mu_{ser} = 0 \qquad [1.122]$$

where ρ_s is given by equation [1.121] in Pivot B. For this value of $\delta' = 0.15$, we find $\alpha_{opt} \geq \alpha_{AB}$ and $\alpha = \alpha_{opt}$ is the solution of the constrained optimization problem. On the other hand, if the solution of the quartic equation [1.122] was less than α_{AB}, then the optimized solution would be the one of Pivot AB, as already mentioned for the case with $\delta' = 0.078125$.

1.11. Reinforced concrete beams with T-cross-section

1.11.1. *Introduction*

A T-cross-section is analyzed where both compression (with area A_{s2}) and tensile (with area A_{s1}) steel bars reinforce the composite cross-section (see Figure 1.43).

The geometry of the cross-section is characterized by the different length parameters b, b_w, h, h_0, d and d', where b is the width of the concrete slab, h_0 is the depth of the flange (slab) thickness, and the width of the web is

denoted by b_w. The position of the neutral axis is as usual, characterized by αd from the upper fiber of the cross-section.

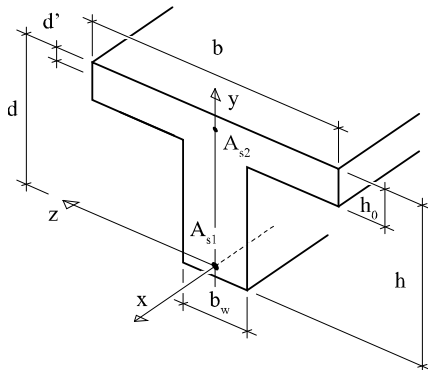

Figure 1.43. *Geometry of a T-cross-section*

If the depth of the compression block is within the flanged portion of the beam, that is the neutral axis depth αd is less than the flange (slab) thickness h_0, measured from the top of the slab ($\alpha d < h_0$), then the section can be calculated as an "equivalent" rectangular cross-section with the width equal to b (as tensile concrete contribution is neglected in the analysis). Then, we find again the configuration previously investigated, for the design of reinforced concrete beams with rectangular cross-section at the SLS. However, when the depth of the compression block is larger than the flange (slab) thickness, the neutral axis is located in the web of the T-cross-section, and the calculation has to be based on the T-cross-section calculation, as detailed in this section.

The concrete and steel material stress limits are given at the SLS by f_{ss} for the steel reinforcement, and f_{cs} for the concrete, the equivalence coefficient being classically denoted by α_e. The acting solicitation is evaluated at point O and is characterized by two components, the acting moment $\boldsymbol{M}_{act} = M_{act}\boldsymbol{k}$ and the normal force resultant $\boldsymbol{N}_{act} = N_{act}.\boldsymbol{i}$. The unknowns of the problem are, respectively, the tensile reinforcement area A_{s1} and the relative height of the neutral axis α. It is assumed that the neutral axis is located inside the web, that is $h_0 \le \alpha d \le h$.

To simplify the theoretical study of the T-cross-section analysis, the summation of the forces resistant screw is induced by a decomposition of the total cross-section within piecewise rectangular cross-sections, without forgetting the steel reinforcements, both in tension and compression.

1.11.2. *Decomposition of the cross-section*

The cross-section S is decomposed into three rectangular parts: two rectangular parts, S_1 that can be added, and S_2 that can be subtracted, plus the additional steel reinforcement S_3 that has to be added to the total cross-section (see Figure 1.44). These subsections have the same neutral axis and the same curvature for compatibility reasons.

Figure 1.44. *Decomposition of the T-cross-section*

The characteristics of each subdomain are given in Table 1.1.

	S	S_1	S_2	S_3
Effective depth	d	d	$d-h_0$	/
Relative depth of the neutral axis	α	α	$\alpha' = (\alpha d-h_0)/(d-h_0)$	/
Force	/	$\alpha.\psi.b.d.f_{cs}$	$\alpha'.\psi'.(b-b_w).(d-h_0).f_{cs}$	$A_{s1}.\sigma_{s1}+A_{s2}.\sigma_{s2}$
Moment with respect to O	/	$-\alpha.\psi.(1-\alpha.\delta_g).b.d^2.f_{cs}$	$-\alpha'.\psi'.(1-\alpha'.\delta_g).(b-b_w).(d-h_0)^2.f_{cs}$	$-A_{s2}.\sigma_{s2}.(d-d')$

Table 1.1. *Characterization of each subdomain of the T-cross-section*

The center of pressure of the compression block in concrete is at a distance $\alpha d/3$ of the most compressed fiber of the cross-section, that is the upper concrete fiber, and then $\delta g = 1/3$. As for the rectangular cross-section, the shape filling coefficient ψ has been introduced in Table 1.1. The normal force in the compressed part of concrete can be expressed through this dimensionless coefficient:

$$N_c = \psi f_{cs} \alpha b d \qquad [1.123]$$

In Table 1.1, the dimensionless shape filling coefficient ψ depends on the considered pivot, Pivot A or Pivot B.

$$\psi = \frac{-\alpha}{2\alpha_e(1-\alpha)} \cdot \frac{f_{ss}}{f_{cs}} \text{ in Pivot A, and } \psi = 1/2 \text{ in Pivot B} \qquad [1.124]$$

In Table 1.1, the dimensionless parameter ψ' denotes another shape filling coefficient that also depends on the considered pivot, Pivot A or Pivot B:

$$\psi' = -(\alpha - h_0/d) f_{ss} / [2\alpha_e(1-\alpha) f_{cs}] \text{ in Pivot A,}$$
$$\text{and } \psi' = (\alpha - h_0/d) / (2\alpha_e \alpha) \text{ in Pivot B} \qquad [1.125]$$

1.11.3. *Case of pivot A for a T-cross-section*

1.11.3.1. *Equations formulation*

By setting $M = M_{ser}$, the bending moment equilibrium consideration leads to a nonlinear equation of the dimensionless relative depth α, similar to what has been found for the rectangular cross-section in section 1.8.4 as:

$$M = \frac{A_{s2}(d-d')(\alpha d - d')f_{ss}}{d(1-\alpha)} + \frac{\alpha^2(3-\alpha)}{6\alpha_e(1-\alpha)} b d^2 f_{ss} -$$
$$\frac{(\alpha - h_0/d)^2(3 - 2h_0/d - \alpha)}{6\alpha_e(1-\alpha)} (b - b_w) d^2 f_{ss} \qquad [1.126]$$

or, equivalently, by using the dimensionless coefficients:

$$M = [\alpha_e (1 - \delta')(\alpha - \delta')dA_{s2} + \frac{\alpha^2(3 - \alpha)}{6}bd^2 -$$

$$\frac{(\alpha - h_0/d)^2(3 - 2\,h_0/d - \alpha)}{6}(b - b_w)d^2]\,\frac{f_{ss}}{\alpha_e(1-\alpha)} \qquad [1.127]$$

A third-order polynomial equation is finally obtained for the determination of the neutral axis position, characterized by α, for a given cross-section:

$$a_0\alpha^3 + a_1\alpha^2 + a_2\alpha + a_3 = 0 \text{ with}$$

$$\begin{cases} a_0 = \dfrac{b_w}{b} \\ a_1 = -\dfrac{3b_w}{b} \\ a_2 = -6\alpha_e\left(\dfrac{M}{bd^2 f_{ss}} + \dfrac{(1-\delta')A_{s2}}{bd}\right) - 3\left(\dfrac{h_0}{d}\right)\left(2 - \dfrac{h_0}{d}\right)\left(1 - \dfrac{b_w}{b}\right) \\ a_3 = +6\alpha_e\left(\dfrac{M}{bd^2 f_{ss}} + \dfrac{\delta'(1-\delta')A_{s2}}{bd}\right) + \left(\dfrac{h_0}{d}\right)^2\left(3 - \dfrac{2h_0}{d}\right)\left(1 - \dfrac{b_w}{b}\right) \end{cases} \qquad [1.128]$$

where the dimensionless coefficient $\delta' = d'/d$ has been used.

1.11.3.2. *Resolution – Pivot A*

Cardano's method can be used for the resolution of this third-order polynomial equation (see Appendix 1). The canonical parameters are:

$$p = \frac{3a_0a_2 - a_1^2}{3a_0^2} \text{ and } q = \frac{27a_0^2a_3 + 2a_1^3 - 9a_0a_1a_2}{27a_0^3} \qquad [1.129]$$

Typically, for the physical parameters associated with reinforced concrete design application, the third-order polynomial equation in α has three roots, which the one of interest in our study is:

$$\alpha = 2\sqrt{\frac{-p}{3}}\cos\left[\frac{Arc\cos\left(\frac{3q}{2p}\sqrt{\frac{3}{-p}}\right)+4\pi}{3}\right]-\frac{b}{3a} \qquad [1.130]$$

Once the neutral axis position α is numerically calculated, the normal force equilibrium equation gives the area of tensile steel reinforcement as found in section 1.8.5 for the rectangular cross-section:

$$A_{s1} = \frac{N_{act}}{f_{ss}} + \frac{\alpha - \delta'}{1 - \alpha} A_{s2} + \frac{\alpha^2\, bd}{2\alpha_e(1-\alpha)} - \frac{(\alpha - h_0/d)^2\,(b-b_w)d}{2\alpha_e(1-\alpha)} \qquad [1.131]$$

Different specific cases can be deduced from this general equation valid for T-cross-section. In the case of simple bending N_{act}= 0, the steel area equation is reduced to:

$$A_{s1} = \frac{\alpha - \delta'}{1 - \alpha} A_{s2} + \frac{\alpha^2\, bd}{2\alpha_e(1-\alpha)} - \frac{(\alpha - h_0/d)^2\,(b-b_w)d}{2\alpha_e(1-\alpha)} \qquad [1.132]$$

In the case of simple bending N_{act}= 0, and with only tensile steel reinforcement (A_{s2} = 0), this equation is simplified into:

$$A_{s1} = \frac{\alpha^2\, bd}{2\alpha_e(1-\alpha)} - \frac{(\alpha - h_0/d)^2\,(b-b_w)d}{2\alpha_e(1-\alpha)} \qquad [1.133]$$

Finally, in the case of simple bending N_{act}= 0, with only tensile steel reinforcement (A_{s2} = 0), and for rectangular cross-section (b_w = b), we find again what has been found in sections 1.8 and 1.9:

$$A_{s1} = \frac{\alpha^2\, bd}{2\alpha_e(1-\alpha)} \qquad [1.134]$$

1.11.4. *Case of pivot B for a T-cross-section*

1.11.4.1. *Equations formulation*

By setting $M = M_{ser}$, the bending moment equilibrium consideration leads to a nonlinear equation of the dimensionless relative depth α, similar to what has been found for the rectangular cross-section in section 1.9.4 as:

$$M = -\frac{\alpha_e A_{s2}(d-d')(\alpha d-d')f_{cs}}{\alpha d} - \frac{\alpha(3-\alpha)}{6}bd^2 f_{cs} +$$

$$\frac{(\alpha - h_0/d)^2(3 - 2\,h_0/d - \alpha)}{6\alpha}(b-b_w)d^2 f_{cs} \qquad [1.135]$$

or, equivalently, by using the dimensionless coefficients:

$$M = [\alpha_e (1-\delta')(\alpha-\delta')dA_{s2} + \frac{\alpha^2(3-\alpha)}{6}bd^2 -$$

$$\frac{(\alpha - h_0/d)^2(3 - 2\,h_0/d - \alpha)}{6}(b-b_w)d^2] \frac{f_{cs}}{\alpha} \qquad [1.136]$$

A third-order polynomial equation is finally obtained for the determination of the neutral axis position, characterized by α, for a given cross-section:

$$a_0\alpha^3 + a_1\alpha^2 + a_2\alpha + a_3 = 0 \text{ with}$$

$$\begin{cases} a_0 = \dfrac{b_w}{b} \\ a_1 = -\dfrac{3b_w}{b} \\ a_2 = -6\left(\dfrac{M}{bd^2 f_{cs}} + \dfrac{\alpha_e(1-\delta')A_{s2}}{bd}\right) - 3\left(\dfrac{h_0}{d}\right)\left(2 - \dfrac{h_0}{d}\right)\left(1 - \dfrac{b_w}{b}\right) \\ a_3 = +\dfrac{6\alpha_e\delta'(1-\delta')A_{s2}}{bd} + \left(\dfrac{h_0}{d}\right)^2\left(3 - \dfrac{2h_0}{d}\right)\left(1 - \dfrac{b_w}{b}\right) \end{cases} \qquad [1.137]$$

whose solution is also given by Cardano's method (see section 1.11.3).

1.11.4.2. *Resolution*

Once the neutral axis position α is numerically calculated, the normal force equilibrium equation gives the area of tensile steel reinforcement as found in section 1.9.5 for the rectangular cross-section:

$$A_{s1} = \frac{-\alpha N_{act}}{\alpha_e f_{cs}(1-\alpha)} + \frac{\alpha - \delta'}{1 - \alpha}A_{s2} + \frac{\alpha^2\, bd}{2\,\alpha_e(1-\alpha)} - \frac{(\alpha - h_0/d)^2\,(b-b_w)d}{2\,\alpha_e(1-\alpha)} \qquad [1.138]$$

The stresses in the tensile and in the compression steel reinforcements are obtained from the equivalent stress diagram:

$$\sigma_{s1} = -\frac{\alpha_e(1-\alpha)}{\alpha} f_{cs} \quad \text{and} \quad \sigma_{s2} = \frac{\alpha_e(\alpha-\delta')}{\alpha} f_{cs} \qquad [1.139]$$

It is worth mentioning that a third-order polynomial equation is generally obtained for the determination of the position of the neutral axis at Pivot B, as in the case of Pivot A (even if the third-order equations in both pivots are not the same). However, in the specific case of a rectangular cross-section ($b_w = b$) without compression steel reinforcement ($A_{s2} = 0$), the last term a_3 vanishes in the third-order equation and the third-order equation degenerates mathematically into a second-order equation:

$$a_3 = 0 \quad \Rightarrow \quad \alpha^3 - 3\alpha^2 - \frac{6M}{bd^2 f_{cs}}\alpha = 0 \qquad [1.140]$$

We recognize the second-order equation for the determination of the position of the neutral axis at Pivot B in the case of a rectangular cross-section without compression steel reinforcement. However, in the case of a T-cross-sectional, with $b \neq b_w$, a third-order equation is obtained for the determination of the position of neutral axis α, even in a case without compression steel reinforcement, which is a notable difference with the case of a rectangular cross-section.

Finally, in the case of simple bending $N_{act} = 0$, with only tensile steel reinforcement ($A_{s2}=0$), and for a rectangular cross-section ($b_w=b$), we find again, as in the case of Pivot A:

$$A_{s1} = \frac{\alpha^2 bd}{2\alpha_e(1-\alpha)} \qquad [1.141]$$

1.11.5. *Example – design of reinforced concrete beams composed of T-cross-section*

1.11.5.1. *Data of the design problem*

The geometrical characteristics of the T-cross-section are given in Figure 1.45 and detailed below:

$$b = 800 \text{ mm}; b_w = 300 \text{ mm}; h_0 = 200 \text{ mm};$$
$$d = 920 \text{ mm}; d' = 40 \text{ mm}; A_{s2} = 0 \text{ mm}^2. \quad [1.142]$$

The reinforced concrete section is composed of steel bars with f_{yk} = 300 MPa and *C25/30* type of concrete. Hence, we calculate the limit stresses at the SLS as:

$$f_{ss} = 0.8 f_{yk} = 0.8 \times 300 = 240 \text{ MPa}$$
$$\text{and } f_{cs} = -0.6 f_{ck} = -0.6 \times 25 = -15 \text{ MPa} \quad [1.143]$$

The equivalence coefficient is given for this problem as: α_e = 15. The steel Young's modulus is equal to *Es* = 200,000 MPa.

The solicitation is a simple bending solicitation characterized at the center of gravity of the tensile steel reinforcement by M_{ser} = 0.49 MN.m and N_{ser} = 0 MN. In simple bending, the solicitation would have been the same in another point of the cross-section.

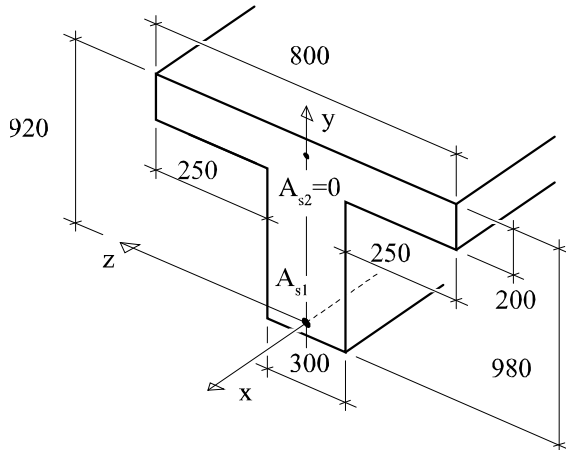

Figure 1.45. *Steel reinforcement design of a reinforced concrete T-cross-section at SLS; lengths given in meters*

It is assumed that there is no compression steel reinforcement (A_{s2} = 0 m^2). The exercise consists of designing the tensile reinforcement of this *T*-cross-section at the stress SLS.

1.11.5.2. *Resolution*

As presented in Chapter 5.5, the limit value of the neutral axis position at the boundary of the two pivots, Pivot A and Pivot B, is given from:

$$\alpha_{AB} = \frac{\alpha_e}{\alpha_e - \frac{f_{ss}}{f_{cs}}} = \frac{15}{15 + \frac{240}{15}} = 0.48387 \qquad [1.144]$$

The bending moment solicitation at the boundary of Pivot A and Pivot B can be calculated from:

$$M_{AB} = \frac{A_{s2}(d\text{-}d')(\alpha_{AB}d\text{-}d')f_{ss}}{d(1 - \alpha_{AB})} + \frac{\alpha_{AB}^2(3 - \alpha_{AB})}{6\,\alpha_e(1 - \alpha_{AB})}bd^2f_{ss}$$

$$- \frac{(\alpha_{AB} - h_0/d)^2(3 - 2\,h_0/d - \alpha_{AB})}{6\,\alpha_e(1 - \alpha_{AB})}(b - b_w)d^2f_{ss} = 1.737\ 78 \text{ MN.m}$$

$$> M_{ser,act} = 0.49 \text{ MN.m} \qquad [1.145]$$

Hence, the T-cross-section has to be calculated with the Pivot A rule. The dimensionless neutral axis position is the solution of a third-order equation given by equation [1.128] and written with the numerical application as:

$$0.375\ \alpha^3 - 1.125\ \alpha^2 - 0.997976725\ \alpha + 0.347138392 = 0 \qquad [1.146]$$

The three solutions can be computed from Cardano's method according to Appendix 1 – see equation [A1.23].

$$\alpha_1 = -0.930295125;\ \alpha_2 = 0.272002024;\ \alpha_3 = 3.658293101 \qquad [1.147]$$

Only $\alpha_2 = 0.2720$ is of interest for physical reasons. Furthermore, we can check that for this value of the neutral axis, the T-cross-section does not behave as a rectangular cross-section as:

$$\alpha d = 0.272 \times 0.92 = 0.25024 \text{ m} \geq h_0 = 0.2 \text{ m} \qquad [1.148]$$

In other words, it is confirmed that the neutral axis is located in the web of the T-cross-section, which justifies the calculation with the web part of the T-cross-section. In Pivot A, the stress in the tensile steel reinforcement

σ_{s1} is equal to the serviceability limit stress f_{ss} and the steel area A_{s1} can be calculated from equation [1.132]:

$$\sigma_{s1} = f_{ss} = 240 \text{ MPa} \quad \text{and}$$

$$A_{s1} = \frac{\alpha^2 bd}{2\alpha_e(1-\alpha)} - \frac{(\alpha - h_0/d)^2 (b-b_w)d}{2\alpha_e(1-\alpha)} = 24.304\ 10^{-4}\ \text{m}^2 \qquad [1.149]$$

We finally obtain for this cross-section designed at Pivot A, A_{s1} = 24.30 cm^2. We can take *3ϕ32* (A_{s1} = 24.13cm^2) for the tensile steel reinforcement (see Appendix 2). But *5ϕ25* (A_{s1} = 24.54cm^2) would probably be safer, even if the first solution based on *3ϕ32* could also be used, if the anticipated value of *d,* the distance from the center of gravity of the tensile steel reinforcement to the upper fiber of the cross-section, is a little bit larger than 0.92 m.

Chapter 2

Verification at Serviceability Limit State (SLS)

2.1. Verification of a given cross-section – control design

2.1.1. *Position of the neutral axis*

Figure 2.1. *Position of the neutral axis at serviceability limit state*

In this section, we assume a given reinforced concrete cross-section at its serviceability limit state (SLS), with a given area of tensile steel reinforcement A_{s1} and a given area of compression steel reinforcement A_{s2}. To check the correctness of the reinforced concrete design, the stresses in each part of the cross-section have to be calculated and compared to the serviceability limit stresses.

For a given reinforced concrete cross-section, the position of the neutral axis can be calculated at the SLS (see Figure 2.1). It is found that this position does not depend on the solicitation level, at least in simple bending without a normal force. This fundamental property is not true at the ultimate limit state (ULS), where the position of the neutral axis, in fact, depends on the solicitation level. The neutral axis is used to define the *z*-axis along which the frame axis is defined (see Figure 2.1). The upper part of the cross-section is assumed in compression, which corresponds to the positive moment in span. The axis origin is chosen arbitrarily along this neutral axis. The frame is completed by the *x*-axis, perpendicular to the plane of the cross-section, and oriented towards the external part of the considered body (convention of positive traction). In the plane of the cross-section, the frame is completed by a vertical *y*-axis oriented toward the compressed part of concrete.

2.1.2. *Equation of static moments for the determination of the position of neutral axis*

Starting for the conservation law of planeity, the strain relationship in both the steel and the concrete part is linearly related through:

$$\frac{\varepsilon_{c,sup}}{\alpha d} = \frac{\varepsilon_c(y)}{\mathrm{y}} = \frac{\varepsilon_{s2}}{\alpha d\text{-}d'} = \frac{\varepsilon_{s1}}{\alpha d\text{-}d} \qquad [2.1]$$

The equivalent stress equations are deduced from the strain relationship by introducing the elasticity constitutive law in the steel $\sigma_s = E_s\,\varepsilon_s$ and the concrete part $\sigma_c = E_c\,\varepsilon_c$ of the cross-section, and using the equivalence coefficient $\alpha_e = E_s/E_c$, as:

$$\frac{\alpha_e\sigma_{c,sup}}{\alpha d} = \frac{\alpha_e\sigma_c(y)}{y} = \frac{\sigma_{s2}}{\alpha d\text{-}d'} = \frac{-\,\sigma_{s1}}{d\text{-}\alpha d} \qquad [2.2]$$

The normal force in the compressed part of concrete D_c, denoted by N_c, is calculated through an integral operator as:

$$N_c = \iint_{D_c} \sigma_c(y).dy.dz. = \frac{\sigma_{c,sup}}{\alpha d} \iint_{D_c} y.dy.dz = \frac{\sigma_{c,sup}}{\alpha d}\, S_c \qquad [2.3]$$

where S_c is the static moment calculated with respect to the neutral axis of the compressed area of concrete D_c. It is also possible to calculate the normal forces N_{s1} and N_{s2} in both the tensile steel reinforcement of area A_{s1} and compression steel reinforcement of area A_{s2}:

$$N_{s1} = \sigma_{s1} A_{s1} = \frac{\sigma_{c,sup}}{\alpha d} \alpha_e (\alpha d - d) A_{s1}$$

$$= \frac{\sigma_{c,sup}}{\alpha d} S_{s1} \text{ with } S_{s1} = \alpha_e (\alpha d - d) A_{s1} \quad [2.4]$$

$$N_{s2} = \sigma_{s2} A_{s2} = \frac{\sigma_{c,sup}}{\alpha d} \alpha_e (\alpha d - d') A_{s2}$$

$$= \frac{\sigma_{c,sup}}{\alpha d} S_{s2} \text{ with } S_{s2} = \alpha_e (\alpha d - d') A_{s2} \quad [2.5]$$

where, with respect to the neutral axis Oz, S_{s1} is the static moment of "α_e" times the area of the tensile steel reinforcement with an area A_{s1} and S_{s2} is the static moment of "α_e" times the area of the compression steel reinforcement with an area A_{s2}. The normal force equilibrium equation at the SLS then leads to a static moment relationship:

$$N_{act} = N_c + N_{s1} + N_s \Leftrightarrow \frac{N_{act} \alpha d}{\sigma_{c,sup}} = S_c + S_{s1} + S_{s2} \quad [2.6]$$

In the case of simple bending without additional normal force N_{act}= 0, this equation is reduced to the static moment equation:

$$0 = S_c + S_{s1} + S_{s2} \quad [2.7]$$

The concept of a homogenised section may be introduced at this stage, by affectation a unity coefficient on the concrete part and by the equivalent Young's modulus coefficient α_e, the steel reinforcements both in tension and compression. It is worth mentioning that this notion of a homogenized section no longer holds at the ULS where the nonlinear behaviors of the steel and the concrete parts are not compatible in general with elasticity. After having introduced this concept of a homogenized section, the meaning of the static moment equation can now be discussed. This equation expresses the fact that the sum of the homogenized static moments with respect to

the neutral axis is vanishing in a reinforced concrete section at the SLS. We can also say that the neutral axis crosses the center of gravity of the homogenized cross-section, neglecting of course the tensile part of concrete. The static moment equation allows the determination of the neutral axis position, for a given reinforced concrete cross-section. This static moment equation is a second-order equation for a cross-section with piecewise constant width, including for instance a rectangular cross-section or T-cross-sections.

2.1.3. *Stress calculation – general case*

Once the neutral axis position has been calculated thanks to the *static moment equation*, the stresses in each part of the reinforced cross-section can be calculated. The moment equilibrium equation has to now be used:

$$M_c + M_{s1} + M_{s2} = M_{act} \qquad [2.8]$$

where the resultant moment with respect to the compression block of concrete is M_c, the resultant moment with respect to the tensile steel reinforcements is M_{s1} and the resultant moment with respect to the compression steel reinforcement is M_{s2}. The moment resultant in the compression part of concrete, denoted by M_c, is calculated with respect to the neutral axis as:

$$M_c = \iint_{D_c} - \sigma_c(y).y.dy.dz. = \frac{- \sigma_{c,sup}}{\alpha d} \iint_{D_c} y^2.dy.dz = \frac{- \sigma_{c,sup}}{\alpha d} I_c \qquad [2.9]$$

where I_c is the quadratic moment with respect to the neutral axis of the compression block of concrete D_c. The resultant moment in the tensile and the compression steel reinforcements, denoted by M_{s1} and M_{s2}, can also be calculated with respect to the neutral axis as:

$$M_{s1} = - \sigma_{s1} A_{s1} (\alpha d - d) = \frac{- \sigma_{c,sup}}{\alpha d} \alpha_e (\alpha d - d)^2 A_{s1}$$

$$= \frac{- \sigma_{c,sup}}{\alpha d} I_{s1} \text{ with } I_{s1} = \alpha_e (\alpha d - d)^2 A_{s1} \qquad [2.10]$$

$$M_{s2} = -\sigma_{s2} A_{s2} (\alpha d - d') = \frac{-\sigma_{c,sup}}{\alpha d} \alpha_e (\alpha d - d')^2 A_{s2} =$$

$$\frac{-\sigma_{c,sup}}{\alpha d} I_{s2} \text{ with } I_{s2} = \alpha_e (\alpha d - d')^2 A_{s2} \qquad [2.11]$$

where I_{s1} is the quadratic moment with respect to the neutral axis of the tensile reinforcement homogenized by the equivalence coefficient α_e and I_{s2} is the quadratic moment with respect to the neutral axis of the compression reinforcement homogenized by the equivalence coefficient α_e. These quadratic moments are the exact quadratic moments of the homogenized steel reinforcements, assuming that the principal quadratic moment of each steel cross-section can be neglected (only the transport term is meaningful in application of Huygens's formulae). Going back to the equilibrium moment equation, the maximum compression stress in the compression block can now be calculated from:

$$M_{act} = M_c + M_{s1} + M_{s2} \Leftrightarrow \frac{M_{act} \alpha d}{-\sigma_{c,sup}} =$$

$$I_c + I_{s1} + I_{s2} \Leftrightarrow \sigma_{c,sup} = \frac{-M_{act} \alpha d}{I_c + I_{s1} + I_{s2}} = \frac{-M_{act} \alpha d}{I} \qquad [2.12]$$

where I is the quadratic moment of the homogenized section (neglecting the tensile part of concrete) with respect to the neutral axis. The stresses in the steel reinforcement and compression block are finally obtained from the equivalent linear diagram in the homogenized section:

$$\begin{cases} \sigma_{c,\sup} = -\dfrac{M_{act} \alpha d}{I} \\ \sigma_{s1} = -\alpha_e \dfrac{M_{act} (\alpha d - d)}{I} \\ \sigma_{s2} = -\alpha_e \dfrac{M_{act} (\alpha d - d')}{I} \end{cases} \qquad [2.13]$$

This equation can easily be compared to the usual equation valid in linear elasticity for a homogeneous cross-section $\sigma = \pm Mv/I$. However, in this case, as a main difference with linear elasticity, the contribution of concrete in tension has been neglected.

2.1.4. *Rectangular cross-section – verification of a given cross-section*

2.1.4.1. *Rectangular cross-section – stress equations*

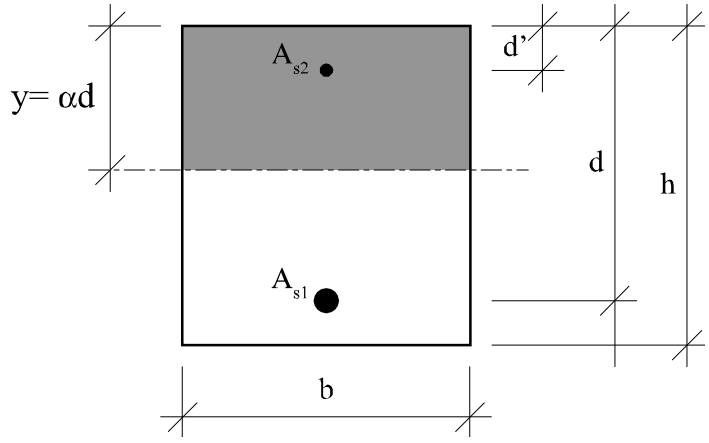

Figure 2.2. *Position of the neutral axis at serviceability limit state; rectangular cross-section*

The rectangular cross-section has the geometrical characteristics denoted by b, h, d and d', and are illustrated in Figure 2.2. The equation $y = \alpha d$ is the distance from the neutral axis to the upper compression fiber of the cross-section, whereas $y = \alpha d$ is the unknown of the design problem that can be determined using the *static moment equation*:

$$\frac{b}{2}y^2 + \alpha_e(A_{s1} + A_{s2})y - \alpha_e(A_{s1}d + A_{s2}d') = 0 \qquad [2.14]$$

This second-order equation can be easily solved, and it leads to the root of the physical interest, as:

$$y = \frac{-\alpha_e(A_{s1} + A_{s2}) + \sqrt{\alpha_e^2(A_{s1} + A_{s2})^2 + 2\alpha_e b(A_{s1}d + A_{s2}d')}}{b} \qquad [2.15]$$

The stresses are then calculated from equation [2.13], where the equivalent moment quadratic for the rectangular cross-section is equal to:

$$I = \frac{by^3}{3} + \alpha_e A_{s1}(y - d)^2 + \alpha_e A_{s2}(y - d')^2 \quad \text{with } y=\alpha d \qquad [2.16]$$

2.1.4.2. *Example – rectangular cross-section*

As an example, the rectangular cross-section is reinforced by tensile steel reinforcement with area A_{s1} = 12.57 cm^2 (*4ϕ20*) and by compression steel reinforcement with area A_{s2} = 1.57 cm^2 (*2ϕ10*). The cross-section has the following characteristics: b = 25 cm; h = 40 cm; d = 35 cm; d' = 3.5 cm. The reinforced concrete section is composed of *B500B* steel bars and the *C25/30* type of concrete. The equivalence coefficient is given for this problem as: α_e = 15. The beam is solicitated in simple bending with M_{ser}= 80 kN·m. The exercise consists of controlling the design of this reinforced rectangular cross-section at the stress SLS.

The static moment equation [2.14], in this case, gives the second-order polynomial equation:

$$0.125y^2 + 0.02121y - 6.6817\times10^{-3} = 0 \Rightarrow y = 0.1614\,\text{m} \qquad [2.17]$$

The calculation of the quadratic moment of the homogenized section is given in equation [1.138] and detailed for the specific studied cross-section:

$$\begin{aligned} I &= \frac{by^3}{3} + \alpha_e A_{s1}(y-d)^2 + \alpha_e A_{s2}(y-d')^2 \\ &= 3.504\times10^{-4} + 3.7626\times10^{-4} + 6.7067\times10^{-4} = 10.59\times10^{-4}\ \ m^4 \end{aligned} \qquad [2.18]$$

The stresses are finally calculated in each part of the reinforced concrete section:

$$\begin{cases} \sigma_{c,\text{sup}} = -\dfrac{M_{ser}\,y}{I} = -12.19\ \ \text{MPa} \\ \sigma_{s1} = -\alpha_e \dfrac{M_{ser}\,(y-d)}{I} = 213.7\ \ \text{MPa} \\ \sigma_{s2} = -\alpha_e \dfrac{M_{ser}\,(y-d')}{I} = -143.2\ \ \text{MPa} \end{cases} \Rightarrow \begin{cases} \left|\sigma_{c,\text{sup}}\right| = 12.19\ \ \text{MPa} \le \left|f_{cs}\right| = 15\ \ \text{MPa} \\ \left|\sigma_{s1}\right| = 213.7\ \ \text{MPa} \le f_{ss} = 400\ \ \text{MPa} \\ \left|\sigma_{s2}\right| = 143.2\ \ \text{MPa} \le f_{ss} = 400\ \ \text{MPa} \end{cases} \qquad [2.19]$$

It can be checked that this reinforced concrete cross-section is correctly designed with respect to the SLS.

2.1.5. *T-cross-section – verification of a given cross-section*

2.1.5.1. *T-cross-section or rectangular cross-section?*

Figure 2.3. *Position of the neutral axis at serviceability limit state; T-cross-section*

A T-cross-section is analyzed where both the compression (with area A_{s2}) and tensile (with area A_{s1}) steel bars reinforce the composite cross-section. The geometry of the cross-section is characterized by the different length parameters b, b_w, h, h_0, d and d'. b is the width of the concrete slab and h_0 is the depth of the flange (slab) thickness. The width of the web is denoted by b_w. The position of the neutral axis is as usual characterized by $y = \alpha d$ from the upper fiber of the cross-section.

If the depth of the compression block is within the flanged portion of the beam, that is the neutral axis depth αd is less than the flange (slab) thickness h_0, and measured from the top of the slab ($y = \alpha d < h_0$), then the section can be calculated as an "equivalent" rectangular cross-section with the width equal to b (as tensile concrete contribution is neglected in the analysis). Then, we find again the configuration previously investigated for the design of reinforced concrete beams with a rectangular cross-section at the SLS. However, when the depth of the compression block is larger than the flange (slab) thickness, the neutral axis is located in the web of the T-cross-section ($y = \alpha d > h_0$) and the calculation has to be based on the T-cross-section calculation. The transitory case between these two kinds of behavior is obtained for $y = \alpha d = h_0$ (see Figure 2.3).

To evaluate the type of configuration (rectangular or T-cross-section calculation), it is required to assume a rectangular cross-section and see

when the rectangular assumption $y = \alpha d < h_0$ is fulfilled. The position of the neutral axis for a rectangular cross-section is already given in equation [2.14] and the condition of the rectangular assumption for the calculation is then written as:

$$y = \frac{-\alpha_e (A_{s1} + A_{s2}) + \sqrt{\alpha_e^2 (A_{s1} + A_{s2})^2 + 2\alpha_e b (A_{s1} d + A_{s2} d')}}{b} \leq h_0 \quad [2.20]$$

which is equivalent to:

$$\frac{b}{2} h_0^2 + \alpha_e (A_{s1} + A_{s2}) h_0 - \alpha_e (A_{s1} d + A_{s2} d') \geq 0 \quad [2.21]$$

The following compression and tensile static moments can be introduced as:

$$\tilde{\mu}_c = \frac{b h_0^2}{2} + \alpha_e A_{s2} (h_0 - d') \quad \text{and} \quad \tilde{\mu}_t = \alpha_e A_{s1} (d - h_0) \quad [2.22]$$

Hence, if the condition $\tilde{\mu}_c \geq \tilde{\mu}_t$ is fulfilled, then the depth of the compression block is within the flanged portion of the beam, that is the neutral axis depth αd is less than the flange (slab) thickness h_0 ($y = \alpha d < h_0$). The section can be calculated as an "equivalent" rectangular cross-section with the width equal to b. On the contrary, if the condition $\tilde{\mu}_c \leq \tilde{\mu}_t$ is fulfilled, then the depth of the compression block is larger than the flange (slab) thickness, the neutral axis is located in the web of the T-cross-section ($y = \alpha d > h_0$) and the calculation is based on the T-cross-section calculation, as detailed below.

$$\begin{aligned} &\tilde{\mu}_c \geq \tilde{\mu}_t \rightarrow \text{Calculation based on a rectangular cross-section} \\ &\tilde{\mu}_c \leq \tilde{\mu}_t \rightarrow \text{Calculation based on a T} - \text{cross-section} \end{aligned} \quad [2.23]$$

It is useful to note that these conditions are independent of the solicitation and depend only on the properties of the cross-section.

2.1.5.2. *Calculation of the position of neutral axis – T-cross-section*

It is assumed that the neutral axis is located inside the web, that is $h_0 \leq \alpha d \leq h$. The static moment of the compression block S_c is obtained as

the sum of the static moment of the compression part of the web $b_w.y.y/2$, with one of the flanges $(b - b_w).h_0.(y - h_0/2)$:

$$S_c = \frac{b_w}{2} y^2 + 2 \times \frac{b - b_w}{2} h_0 \left(y - \frac{h_0}{2} \right) \qquad [2.24]$$

The static moment equation is then written as:

$$\frac{b_w y^2}{2} + [\alpha_e.(A_{s1} + A_{s2}) + (b-b_w).h_0].y - \alpha_e.(A_{s1}.d + A_{s2}.d') - \frac{(b - b_w)h_0^2}{2} = 0 \qquad [2.25]$$

whose positive solution is:

$$y = \frac{-[\alpha_e(A_{s1} + A_{s2}) + h_0(b - b_w)] + \sqrt{[\alpha_e(A_{s1} + A_{s2}) + h_0(b - b_w)]^2 + 2b_w \left[\alpha_e(A_{s1}d + A_{s2}d') + \frac{(b - b_w)h_0^2}{2} \right]}}{b_w} \qquad [2.26]$$

Once the position y of the neutral axis is obtained, the quadratic moment of the homogenized section is calculated as:

$$I = \frac{b.y^3}{3} - \frac{(b - b_w)(y-h_0)^3}{3} + \alpha_e.A_{s1}(y-d)^2 + \alpha_e A_{s2}(y-d')^2 \qquad [2.27]$$

The stresses are then calculated for the most compression concrete fiber, the tensile steel reinforcement and the compression steel reinforcement from equation [2.13], which still remains valid. Now by using the dimensionless coefficients:

$$\alpha = \frac{y}{d}, \quad \rho_{s1} = \frac{\alpha_e A_{s1}}{b_w d}, \quad \rho_{s2} = \frac{\alpha_e A_{s2}}{b_w d} \quad \text{and} \quad \delta' = \frac{d'}{d} \qquad [2.28]$$

the position of the neutral axis expressed in dimensionless format is given by:

$$\alpha = -\left[\rho_{s1} + \rho_{s2} + \frac{h_0}{d} \left(\frac{b}{b_w} - 1 \right) \right] + \sqrt{\left[\rho_{s1} + \rho_{s2} + \frac{h_0}{d} \left(\frac{b}{b_w} - 1 \right) \right]^2 + 2\left(\rho_{s1} + \delta' \rho_{s2} \right) + \left(\frac{h_0}{d} \right)^2 \left(\frac{b}{b_w} - 1 \right)} \qquad [2.29]$$

The case of the rectangular cross-section is simply deduced by putting $b_w = b$:

$$b_w = b \Rightarrow \alpha = -(\rho_{s1} + \rho_{s2}) + \sqrt{(\rho_{S1} + \rho_{s2})^2 + 2(\rho_{s1} + \delta'\rho_{s2})} \quad [2.30]$$

When the reinforced concrete section is designed without compression steel reinforcement $(\rho_{s2} = 0)$, the case of the rectangular cross-section $b_w = b$ leads to:

$$\rho_{s2} = 0 \quad \text{and} \quad b_w = b \Rightarrow \alpha = -\rho_{S1} + \sqrt{\rho_{S1}(\rho_{s1} + 2)} \quad [2.31]$$

2.1.6. *Example – verification of a reinforced T-cross-section*

The cross-section characteristics of the T-cross-section are the characteristics given in Figure 2.1. As an example, the rectangular cross-section is reinforced by tensile steel reinforcement with area A_{s1} = 24.54 cm^2 (*5φ25*) and by compression steel reinforcement with area A_{s2} = 0 cm^2 (no compression steel reinforcement). The cross-section has the following characteristics: b = 0.8 m; d = 0.92 m; d' = 0.04 m; b_w= 0.3 m; and h_0= 0.2 m. The reinforced concrete section is composed of *B300B* steel bars (f_{yk}= 300 MPa) and *C25/30* type of concrete (f_{ck}= 25MPa). The equivalence coefficient is given for this problem as: α_e = 15. The beam is solicitated in simple bending with M_{ser}= 0.49 MN·m. The exercise consists of controlling the design of this reinforced T-cross-section at the stress SLS.

The following compression and tensile static moments can be calculated from equation [2.22]:

$$\tilde{\mu}_c = \frac{bh_0^2}{2} + \alpha_e A_{s2}(h_0 - d') = \frac{0.8}{2} \times 0.2^2 = 0.016\,\text{m}^3 \quad \text{and}$$
$$\tilde{\mu}_t = \alpha_e A_{s1}(d - h_0) = 15 \times 24.54 \times 10^{-4} \times (0.92 - 0.2) = 0.0265\ \text{m}^3 \quad [2.32]$$

The two static moments can be compared and we obtain $\tilde{\mu}_c < \tilde{\mu}_t$, which means that the depth of the compression block is larger than the flange (slab) thickness: the neutral axis is located in the web of the T-cross-section ($y = \alpha d > h_0$) and the calculation is based on the T-cross-section calculation. The static moment equation [2.25] in this case gives the second-order

polynomial equation with respect to the unknown position of the neutral axis measures with $y = \alpha d$:

$$\frac{0.3 \times y^2}{2} + (0.03682 + 0.5 \times 0.2\ ) \times y - 0.03682 \times 0.92 - \frac{0.5 \times 0.2^2}{2} = 0$$

$$\text{or equivalently } 0.15 \times y^2 + 0.13682 \times y - 0.0438744 = 0 \qquad [2.33]$$

whose positive root is $y = 0.251$ m, which is indeed greater than $h_0 = 0.2$ m. The quadratic moment of the homogenized section with respect to the neutral axis is equal to:

$$I = \frac{0.8 \times y^3}{3} - \frac{0.5 \times (y-0.2)^3}{3} + 0.03682 \times (y - 0.92)^2 = 0.0207 \text{ m}^4 \qquad [2.34]$$

The stress values in both the tensile steel reinforcement and the compression block in concrete are then calculated as:

$$\sigma_{c,sup} = \frac{-M_{act}.y}{I} = \frac{-0.49 \times y}{0.020\,673\ldots} = -5{,}96 \text{ MPa}$$

$$\sigma_{s1} = \alpha_e \frac{-M_{act}.(y-d)}{I} = \alpha_e \frac{-0.49 \times (y-0.92)}{0.020\,673\ldots} = 237{,}7 \text{ MPa} \qquad [2.35]$$

$$\Rightarrow \begin{cases} |\sigma_{c,sup}| = 5.96\ MPa \le |f_{cs}| = 15 \text{ MPa} \\ |\sigma_{s1}| = 237.7\ MPa \le f_{ss} = 240 \text{ MPa} \end{cases} \qquad [2.36]$$

It can be checked that this reinforced concrete cross-section is correctly designed with respect to the SLS. This reinforced concrete section has been clearly designed at Pivot *A*.

2.1.7. *Determination of the maximum resisting moment*

It has been shown above how to design a reinforced concrete section by determining the steel quantity for a given solicitation in simple bending, according to the SLS. We have also shown how to check that a given reinforced concrete section verifies the stress SLS. In this section, we present the methodology to compute the maximum solicitation that a given reinforced concrete section can support at the SLS.

For a given reinforced concrete section, the neutral axis position expressed with the dimensionless parameter α can be determined by using the moment static equation leading to the solution given by equation [2.29]. The parameter α has to be compared to $\alpha_{AB} = \alpha_e f_{cs}/(\alpha_e f_{cs} - f_{ss})$ to determine the type of pivot that should pilot the reinforced concrete section at the SLS.

If $\alpha < \alpha_{AB}$ (Pivot *A*), the resistant moment at the SLS is calculated from:

$$M_{res} = [\alpha_e (1 - \delta')(\alpha - \delta')dA_{s2} + \frac{\alpha^2(3 - \alpha)}{6} bd^2 - \frac{(\alpha - h_0/d)^2(3 - 2\,h_0/d - \alpha)}{6} (b - b_w)d^2] \frac{f_{ss}}{\alpha_e(1-\alpha)} \quad [2.37]$$

If $\alpha > \alpha_{AB}$ (Pivot *B*), the resitant moment at the SLS is calculated from:

$$M_{res} = [\alpha_e (1 - \delta')(\alpha - \delta')dA_{s2} + \frac{\alpha^2(3 - \alpha)}{6} bd^2 - \frac{(\alpha - h_0/d)^2(3 - 2\,h_0/d - \alpha)}{6} (b - b_w)d^2] \frac{f_{cs}}{\alpha} \quad [2.38]$$

2.2. Cross-section with continuously varying depth

2.2.1. *Triangular or trapezoidal cross-section*

Even if rectangular or T-cross-sections have a wide area of applications in civil engineering or building, some specific engineering problems with continuous varying depth cross-sections can be met, especially in bridge engineering, with prestressed concrete caissons, for instance (see Figure 2.4).

Figure 2.4. *Different kinds of cross-section with rectangular, triangular or trapezoidal cross-sections*

In these cases, the use of the T-cross-section analogy is not always possible and an exact calculation with an integration over the prismatic cross-section is needed. In this section, we will study a reinforced concrete triangular cross-section (see Figure 2.5), designed at its SLS. In a certain sense, this case englobes some other trapezoidal variation cross-section, at least from a methodology point of view.

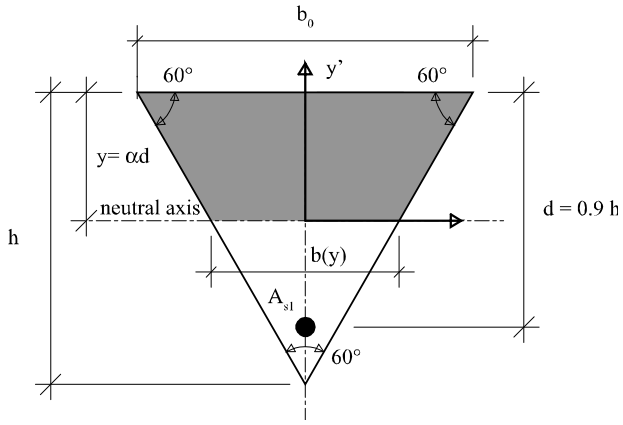

Figure 2.5. *Reinforced concrete triangular cross-section with tensile steel reinforcement*

The triangular cross-section is reinforced by some tensile steel reinforcement (with area A_{s1}). The geometry of the cross-section is characterized by the different length parameters b_0, h and d, where b_0 is the width of the upper part triangle base and h is the total depth of the triangle. The position of the neutral axis is as usual, characterized by $y = \alpha d$ from the upper fiber of the cross-section.

At the neutral axis level, the width of the cross-section is equal to:

$$b(\alpha) = b_0\left(1 - \alpha\frac{d}{h}\right) \qquad [2.39]$$

2.2.2. *Equilibrium equations – normal force resultant*

The equilibrium equations are expressed both for the normal force component and the moment at the center of gravity of the tensile steel reinforcement as:

$$N_{act} = A_{s1}\sigma_{s1} + \iint_{D_c} \sigma_c(y')\ dS = 0 \quad \text{and}$$
$$M_{act} = -\iint_{D_c} [y' + d(1-\alpha)]\ \ \sigma_c(y')\ dS = 0 \qquad [2.40]$$

In linear elasticity, at SLS, the compression stress in the concrete block linearly evolves as:

$$\sigma_c(y') = \frac{y'}{\alpha d}\sigma_{c,\text{sup}} \qquad [2.41]$$

The width of the cross-section at the fiber parameterized by the ordinate y' in the compression block ($y' = 0$ at the neutral axis – see Figure 2.5) is given by:

$$b(y') = \frac{b_0}{h}(y' + h - \alpha d); \quad y' \in [0; \alpha d] \qquad [2.42]$$

The normal force in the concrete block can then be calculated as:

$$N_c = \iint_{D_c} \sigma_c(y')dy'dz = \frac{\sigma_{c,\text{sup}}}{\alpha d}\iint_{A_c} y'dy'dz =$$
$$\frac{\sigma_{c,\text{sup}}}{\alpha d}\int_0^{\alpha d}\int_{-\frac{b(y')}{2}}^{\frac{b(y')}{2}} y'dy'dz \qquad [2.43]$$

The double integral can be easily converted into a single integral with the slice integration technique:

$$N_c = \frac{\sigma_{c,\text{sup}}}{\alpha d}\int_0^{\alpha d} b(y')dy' = \frac{b_0\sigma_{c,\text{sup}}}{\alpha dh}\int_0^{\alpha d} y'^2 + (h - \alpha d)\,y'\,dy' \qquad [2.44]$$

The normal force in the concrete compression block can then be calculated as:

$$N_c = \sigma_{c,\text{sup}}\frac{b_0}{h}\left[-\frac{(\alpha d)^2}{6} + h\frac{\alpha d}{2}\right] \qquad [2.45]$$

The normal force equilibrium equation is then written as:

$$N_{act} = A_{s1}\sigma_{s1} + \sigma_{c,\sup}\frac{b_0}{h}\left[-\frac{(\alpha d)^2}{6} + h\frac{\alpha d}{2}\right] = 0 \qquad [2.46]$$

It would also be possible to have used a geometrical proof for this normal force expression. In fact, the calculation of the double integral for the determination of the normal force in concrete is equivalent to the calculation of the volume of a pentahedron composed of a regular pentahedron and two symmetrical tetrahedral (see Figure 2.6). The total volume of the pentahedron V can be decomposed as the sum of two other volumes $V = V_3 + 2V_4$, with V_3 as the volume of the regular pentahedron and V_4 as the volume of each tetrahedron. The volume V_3 of the regular pentahedron with a width $b(\alpha)$ and depth αd can be calculated as:

$$V_3 = b(\alpha)\alpha d\sigma_{c,\sup}\frac{1}{2} \text{ with } b(\alpha) = b_0\left(1-\alpha\frac{d}{h}\right) \qquad [2.47]$$

The volume V_4 of each tetrahedron is equal to the product of the base area multiplying a third of the depth, which is expressed as:

$$V_4 = \frac{b_0 - b(\alpha)}{2}\sigma_{c,\sup}\frac{\alpha d}{3} \qquad [2.48]$$

It can easily be verified that $N_c = V_3 + 2V_4$ (or equivalently $N_c = V_1 - 2V_2$ with the notation of Figure 2.6).

2.2.3. *Equilibrium equations – bending resultant moment*

The bending moment in the concrete block can then be calculated at the center of gravity of the tensile steel reinforcement as:

$$\begin{aligned} M_c &= -\iint_{D_c} y\sigma_c(y)dydz \\ &= -\frac{\sigma_{c,\sup}}{\alpha d}\int_0^{\alpha d}\int_{-\frac{b(y')}{2}}^{\frac{b(y')}{2}} y'\left[y' + d(1-\alpha)\right]\ dydz \end{aligned} \qquad [2.49]$$

The double integral can be easily converted into a single integral with the slice integration technique:

$$M_c = -\frac{b_0 \sigma_{c,\sup}}{h \alpha d} \int_0^{\alpha d} (y' + h - \alpha d) \ [y'^2 + y' d(1-\alpha)] \ dy' \qquad [2.50]$$

We finally obtain from this integral equation:

$$\frac{M_{act}}{-b_0 d^2 \sigma_{c,\sup}} = \frac{d}{h}\left[\frac{\alpha^3}{12} - \left(1 + \frac{h}{d}\right)\frac{\alpha^2}{6} + \frac{h}{2d}\alpha\right] \qquad [2.51]$$

This result can also be shown from geometrical arguments, as detailed in Figure 2.6.

Figure 2.6. *Linear stress diagram in the concrete compression block of the triangular cross-section – serviceability limit state*

The calculation of the bending moment can also be based on geometrical arguments:

$$M_c = V_3 d_3 + 2V_4 d_4 \quad \text{with} \quad \begin{cases} d_3 = d(1-\alpha) + \dfrac{2}{3}\alpha d \\ d_4 = d(1-\alpha) + \dfrac{3}{4}\alpha d \end{cases} \qquad [2.52]$$

where d_3 and d_4 are the distance from the center of gravity of each volume to the center of gravity of the tensile steel reinforcement. It can be checked that equation [2.52] is equivalent to the mathematical expression of equation [2.51].

2.2.4. *Case of pivot A for a triangular cross-section*

At Pivot *AB* (boundary between Pivot *A* and Pivot *B*), we have the characteristic values:

$$\alpha_{AB} = \frac{\alpha_e f_{cs}}{\alpha_e f_{cs} - f_{ss}} \quad \text{and}$$

$$\mu_{AB} = \frac{d}{h}\left[\frac{\alpha_{AB}{}^3}{12} - \left(1+\frac{h}{d}\right)\frac{\alpha_{AB}{}^2}{6} + \frac{h}{2d}\alpha_{AB}\right] \qquad [2.53]$$

For $\mu \le \mu_{AB}$, the section has to be designed with respect to Pivot *A*. At Pivot *A*, the compression stress in concrete in the most compressed fiber is related to the tensile stress in the tensile steel reinforcement as:

$$\sigma_{s1} = f_{ss} \quad \Rightarrow \quad \sigma_{c,\text{sup}} = -\frac{\alpha}{1-\alpha}\frac{f_{ss}}{\alpha_e} \qquad [2.54]$$

Inserting equation [2.54] in to equation [2.51] leads to the dimensionless reduced moment μ, which is expressed as:

$$\mu = -\frac{\alpha}{1-\alpha}\frac{d}{h}\frac{f_{ss}}{\alpha_e f_{cs}}\left(\frac{\alpha^3}{12} - \frac{\alpha^2}{6}\left(1+\frac{h}{d}\right) + \frac{\alpha}{2}\frac{h}{d}\right)$$

$$\text{with} \quad \mu = -\frac{M_{ser}}{b_0 d^2 f_{cs}} \qquad [2.55]$$

Equation [2.55] is a fourth-order polynomial equation in α and is written as:

$$\frac{\alpha^4}{12}-\frac{1}{6}\left(1+\frac{h}{d}\right)\alpha^3+\frac{h}{2d}\alpha^2+\frac{h}{d}\alpha_e\mu\left(\frac{-f_{cs}}{f_{ss}}\right)\alpha-\left(\frac{-f_{cs}}{f_{ss}}\right)\frac{h}{d}\alpha_e\mu=0 \quad [2.56]$$

2.2.5. *Case of pivot B for a triangular cross-section*

For $\mu \geq \mu_{AB}$, the section has to be designed with respect to Pivot *B*. At Pivot *B*, the compression stress in concrete is equal to the limit compressive stress at SLS $\sigma_{c,\text{sup}} = f_{cs}$, and the dimensionless reduced moment μ is directly obtained from equation [2.51] as:

$$\mu=\frac{d}{h}\left[\frac{\alpha^3}{12}-\left(1+\frac{h}{d}\right)\frac{\alpha^2}{6}+\frac{h}{2d}\alpha\right] \quad [2.57]$$

Equation [2.57] is a third-order polynomial equation in α, and is written as:

$$\frac{\alpha^3}{12}-\frac{1}{6}\left(1+\frac{h}{d}\right)\alpha^2+\frac{h}{2d}\alpha-\frac{h}{d}\mu=0 \quad [2.58]$$

It is shown that in the particular case of a triangular reinforced concrete section, the order of the neutral axis position polynomial equation is higher in Pivot *A* than in Pivot *B*, as for the rectangular cross-section without compression steel reinforcement. Furthermore, it is interesting to note that the order of the polynomial equation is 1^o higher for the triangular section than it is for the rectangular section.

2.2.6. *Static moment equation for a triangular cross-section*

For a given reinforced concrete triangular cross-section, the determination of the position of the neutral axis can be obtained from the static moment equation, which is simply written as:

$$S_{s1}+S_c=0 \quad \text{with} \quad S_{s1}=\alpha_e(y-d)A_{s1} \quad \text{and}$$
$$S_c=b(y)y\frac{y}{2}+2\left[\frac{b_0-b(y)}{2}\frac{y}{2}\frac{2y}{3}\right] \quad \text{and} \quad b(y)=b_0\left(1-\frac{y}{h}\right) \quad [2.59]$$

As a result, a third-order equation is obtained for the determination of the position of the neutral axis:

$$-\frac{b_0}{6h}y^3+\frac{b_0}{2}y^2+\alpha_e A_{s1}y-\alpha_e A_{s1}d=0 \qquad [2.60]$$

In this case, again, the order of the polynomial equation issued of the static moment equation is one degree higher for the triangular section than it is for the rectangular section.

2.2.7. *Design example of a triangular cross-section*

The cross-section characteristics of the triangular cross-section are shown in Figure 1.43. The cross-section has the following characteristics: b_0= 0.8 m; d = 0.9 × h. The reinforced concrete section is composed of *B500B* steel bars (f_{yk}= 500 MPa) and the *C30/37* type of concrete (f_{ck}= 30MPa). The equivalence coefficient is given for this problem as: α_e = 15. The beam is solicitated in simple bending with M_{ser}= 1 MN·m. The exercise consists of controlling the design of this reinforced triangular cross-section at the stress SLS.

As the triangular cross-section is an equilateral triangle, the depth h is related to the width b_0 as:

$$h=b_0\frac{\sqrt{3}}{2}=0.6928\,\text{m} \quad \text{and} \quad d=0.9h=0.62354\,\text{m} \qquad [2.61]$$

The critical parameters α_{AB} and μ_{AB} are first calculated from equation [2.53] as:

$$\alpha_{AB}=\frac{\alpha_e f_{cs}}{\alpha_e f_{cs}-f_{ss}}=\frac{15\times 18}{15\times 18+400}=\frac{27}{67}=0.402985 \quad \text{and}$$
$$\mu_{AB}=0.15498 \qquad [2.62]$$

We then calculate the reduced moment μ, which is compared to the critical reduced moment μ_{AB}:

$$\mu=\frac{1\times 10^6}{0.8\times 0.62354^2\times 18\times 10^6}=0.17861>\mu_{AB}=0.15498 \qquad [2.63]$$

As $\mu \geq \mu_{AB}$, the section has to be designed with respect to Pivot *B*. The determination of the position of neutral axis needs to solve a third-order equation in α given by equation [2.58], and numerically presented in the following format:

$$\begin{aligned} &a\alpha^3 + b\alpha^2 + c\alpha + d = 0 \quad \text{with} \\ &a = 0.08333, b = -0.35185, c = 0.55555 \text{ and } d = -0.19846 \end{aligned} \qquad [2.64]$$

We use Cardano's method to compute the root of this cubic. The canonical parameters are calculated from:

$$\begin{aligned} p &= \frac{3ac - b^2}{3a^2} = 0.72428 \quad \text{and} \\ q &= \frac{27a^2d + 2b^3 - 9abc}{27a^3} = 1.42564 \end{aligned} \qquad [2.65]$$

It can be checked that $4p^3 + 27q^2 = 56.3963 > 0$, and the cubic admits only one real solution (see Appendix 1):

$$\begin{aligned} \alpha &= \sqrt[3]{-\frac{q}{2} + \sqrt{\frac{q^2}{4} + \frac{p^3}{27}}} + \sqrt[3]{-\frac{q}{2} - \sqrt{\frac{q^2}{4} + \frac{p^3}{27}}} - \frac{b}{3a} \\ &= 0.493376 > \alpha_{AB} = 0.402985 \end{aligned} \qquad [2.66]$$

The tensile steel reinforcement area A_{s1} is then deduced from the consideration of the normal force equilibrium equation:

$$N_{act} = A_{s1}\sigma_{s1} + \sigma_{c,\sup}\frac{b_0}{h}\left[-\frac{(\alpha d)^2}{6} + h\frac{\alpha d}{2}\right] = 0 \qquad [2.67]$$

As the section is designed under Pivot *B*, the stresses of the extremal fibers are given by:

$$\sigma_{s1} = -\frac{1-\alpha}{\alpha}\alpha_e f_{cs} \quad \text{and} \quad \sigma_{c,\sup} = f_{cs} \qquad [2.68]$$

The area of tensile steel reinforcement is then calculated as:

$$A_{s1} = \frac{\alpha}{1-\alpha}\frac{b_0}{h}\frac{1}{\alpha_e}\left[\frac{-(\alpha d)^2}{6} + h\frac{\alpha d}{2}\right]$$
$$= \frac{\alpha}{1-\alpha}\frac{0.8}{0.6928\times 15} \times \left[-\frac{\alpha^2}{6}\times 0.623538^2 + 0.6928 \times \frac{0.623538}{2}\alpha\right]$$
$$= 6.8066\times 10^{-3}\, m^2 \qquad [2.69]$$

We finally obtain for this cross-section designed at Pivot *B*, A_{s1}= 68.07 cm^2. We can consider *4ϕ25 + 4ϕ40* (A_{s1} = 69.9 cm^2*)* for the tensile steel reinforcement (see Appendix 2).

2.3. Composed bending with combined axial forces

2.3.1. *Steel reinforcement design for a given reinforced concrete section*

Equations of sections 1.8, 1.9 and 1.11 (Chapter 1) are valid both in simple bending and in composed bending with combined axial forces. The bending moment and normal forces components are given at the center of gravity of the tensile steel reinforcement (M_{act},N_{act}) (see Figure 2.7 for rectangular cross-section and Figure 2.8 for T-cross-section).

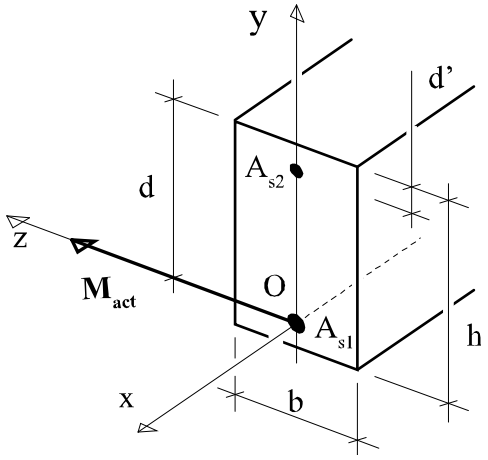

Figure 2.7. *Design of a rectangular reinforced concrete cross-section at serviceability limit state for composed bending state with combined axial forces*

When dealing with the design of the steel reinforcement quantity for a given solicitation, depending on the pivot nature of the reinforced concrete section, the equations given for the position of the neutral axis are different in Pivot *A* and Pivot *B*. In Pivot *A*, for a T-cross-section (the rectangular cross-section is considered as a particular case of a T-cross-section with $b_w = b$), the determination of the position of the neutral axis needs to solve the cubic equation [1.102], and the tensile steel reinforcement can then be calculated in composed bending from equation [1.105]. In Pivot *B*, for a T-cross-section, the determination of the position of the neutral axis also needs to solve a cubic equation given by equation [1.111], and the tensile steel reinforcement can then be calculated in composed bending from equation [1.112]. The limit case between the two pivots is referred to as pivot *AB*, and is characterized by the limit value for the relative position of the neutral axis α_{AB} defined from the upper fiber of the cross-section as $\alpha_{AB} = \alpha_e f_{cs}/(\alpha_e f_{cs} - f_{ss})$.

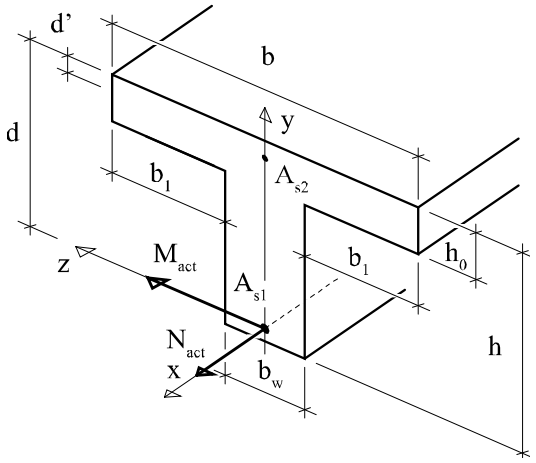

Figure 2.8. *Design of a reinforced concrete T-cross-section at serviceability limit state for composed bending state with combined axial forces*

2.3.2. *Determination of the position of the neutral axis – simple bending*

As shown in section 2.1, Chapter 2, the calculation of the stresses for a given reinforced composite cross-section is a different problem, which is associated with the determination of the position of neutral axis inside the cross-section with the given steel reinforcement. For simple bending

solicitation, without normal force (N_{ser} = 0), this problem is solved with the so-called static moment equation, which leads to a second-order polynomial equation given by equation [2.25] for a T-cross-section. Again, the rectangular cross-section can be viewed as a particular case of a T-cross-section with $b_w = b$. The stresses in each part of the cross-section are then calculated from the equivalent linear stress diagram given by equation [2.13]. Note that the determination of the position of neutral axis in this case does not require the specific notion of Pivot *A* or Pivot *B*. For simple bending solicitation, without normal force (N_{ser} = 0), the position of the neutral axis is summarized below for a T-cross-section as:

$$b_w d\alpha^2 + 2[\alpha_e(A_{s1} + A_{s2}) + h_0(b - b_w)]\alpha -$$

$$2\alpha_e(A_{s1} + \delta' A_{s2}) - h_0^2(b - b_w)/d = 0 \Rightarrow$$

$$\alpha = -[\rho_{s1} + \rho_{s2} + \frac{h_0}{d}(\frac{b}{b_w} - 1)] +$$

$$\sqrt{[\rho_{s1} + \rho_{s2} + \frac{h_0}{d}(\frac{b}{b_w} - 1)]^2 + 2(\rho_{s1} + \delta'\rho_{s2}) + (\frac{h_0}{d})^2(\frac{b}{b_w} - 1)} \qquad [2.70]$$

with the steel reinforcement ratio defined from $\rho_{s1} = \frac{\alpha_e A_{s1}}{b_w d}$ and $\rho_{s2} = \frac{\alpha_e A_{s2}}{b_w d}$. In the particular case of a rectangular cross-section, this equation is simplified as:

$$\alpha = -(\rho_{s1} + \rho_{s2}) + \sqrt{(\rho_{s1} + \rho_{s2})^2 + 2(\rho_{s1} + \delta'\rho_{s2})} \qquad [2.71]$$

2.3.3. *Determination of the position of the neutral axis – composed bending with normal force solicitation*

2.3.3.1. *Rectangular cross-section*

The acting solicitation evaluated at the center of gravity of the tensile steel reinforcement, leading to the equilibrium equation:

$$M_{act} = M_c + M_{s2} \quad \text{and} \quad N_{act} = N_c + N_{s1} + N_{s2} \qquad [2.72]$$

The static moment equation [2.6] can still be used for the normal force component, and is detailed below for the case of the rectangular cross-section:

$$\frac{N_{act}\alpha d}{\sigma_{c,sup}} = S_c + S_{s1} + S_{s2} = \frac{b}{2}(\alpha d)^2 + \alpha_e (\alpha d - d) A_{s1} + \alpha_e (\alpha d - d') A_{s2} \qquad [2.73]$$

The bending moment equation evaluated at the center of gravity of the tensile steel reinforcement can be developed as:

$$M_{act} = -\iint_{D_c} \sigma_c(y).dy.dz - \sigma_{s2} A_{s2}(d - d') \Rightarrow$$
$$\frac{M_{act}\alpha d}{\sigma_{c,\sup}} = -\alpha_e(\alpha d - d')(d - d')A_{s2} - b(\alpha d)^2 \left(\frac{3d - \alpha d}{6}\right) \qquad [2.74]$$

For a rectangular cross-section, we finally obtain the ratio between the bending moment and normal force:

$$\frac{M_{act}}{d \times N_{act}} = \frac{-\rho_{s2}(\alpha - \delta')(1 - \delta') - \dfrac{\alpha^2(3-\alpha)}{6}}{\dfrac{\alpha^2}{2} + \rho_{s1}(\alpha - 1) + \rho_{s2}(\alpha - \delta')} \qquad [2.75]$$

As in the case of a simple bending moment, this equation is independent on the pivot nature of the cross-section. For a loading with constant eccentricity e_{act}, we have:

$$\frac{e_{act}}{d} = \frac{M_{act}}{d \times N_{act}} \qquad [2.76]$$

In this case, the neutral axis position should be the solution of a cubic, which is independent of the solicitation except through the eccentricity parameter e_{act}:

$$\alpha^3 - 3\left(1 + \frac{e_{act}}{d}\right)\alpha^2 - 6\left[\rho_{s2}(1 - \delta') + \frac{e_{act}}{d}(\rho_{s1} + \rho_{s2})\right]\alpha +$$
$$6\rho_{s2}\delta'(1 - \delta') + 6\frac{e_{act}}{d}(\rho_{s1} + \delta'\rho_{s2}) = 0 \qquad [2.77]$$

This cubic equation can then be solved using Cardano's method. Such a cubic equation can be found in some other textbooks such as in [WAL 90] for rectangular cross-sections or in [ROB 74] for both rectangular and T-cross-sections [ROB 74]. This equation can be understood as the generalization of the *static moment equation* for composed bending with the combined normal force effect.

This equation is also known as the cubic equation of the French reinforced concrete design rules, dating from 1906 (*Circulaire du 20 Octobre 1906*) (and reported in the book of Magny [MAG 14]) or the French reinforced concrete design rules dating from 1934 (*règlements des marchés de l'état de 1934* – in French), which was recently reported in [THO 09], and is presented in the following canonical format for rectangular reinforced concrete cross-sections:

$$\begin{aligned} &y^3 + py + q = 0 \quad \text{with} \quad y = \alpha d - c; \quad c = d + e_{act}; \\ &p = -3c^2 + \frac{6\alpha_e A_{s1}}{b}(d-c) + \frac{6\alpha_e A_{s2}}{b}(d'-c) \\ &\text{and} \quad q = -2c^3 - \frac{6\alpha_e A_{s1}}{b}(d-c)^2 - \frac{6\alpha_e A_{s2}}{b}(d'-c)^2 \end{aligned} \qquad [2.78]$$

It can be easily shown that equations [2.78] and [2.77] are equivalent. We note that the simple bending case can be deduced asymptotically with an infinite eccentricity leading to:

$$\frac{e_{act}}{d} \to \infty \quad \Rightarrow \quad -3\alpha^2 - 6\left(\rho_{s1} + \rho_{s2}\right)\alpha + 6\left(\rho_{s1} + \delta'\rho_{s2}\right) = 0 \qquad [2.79]$$

whose solution has been already given in equation [2.30]. The cubic equation [2.77] can be simplified in case of tensile steel reinforcement without compression steel reinforcement $A_{s2} = 0$ as:

$$\alpha^3 - 3\left(1 + \frac{e_{act}}{d}\right)\alpha^2 - 6\frac{e_{act}}{d}\rho_{s1}\alpha + 6\frac{e_{act}}{d}\rho_{s1} = 0 \qquad [2.80]$$

2.3.3.2. *T-cross-section*

The static moment equation [2.6] can still be used for the normal force component, and is detailed below for the case of a T-cross-section:

$$\frac{N_{act}\,\alpha d}{\sigma_{c,sup}} = \frac{b}{2}(\alpha d)^2 - \frac{b-b_w}{2}(\alpha d - h_0)^2 + \alpha_e(\alpha d - d)A_{s1} + \alpha_e(\alpha d - d')A_{s2} \quad [2.81]$$

The bending moment equation evaluated at the center of gravity of the tensile steel reinforcement can be developed as:

$$M_{act} = -\iint_{D_c}\sigma_c(y).dy.dz - \sigma_{s2}A_{s2}(d-d') \Rightarrow$$
$$\frac{M_{act}\alpha d}{\sigma_{c,\sup}} = -\alpha_e(\alpha d - d')(d-d')A_{s2} - b(\alpha d)^2\left(\frac{3d-\alpha d}{6}\right) + \frac{(\alpha - h_0/d)^2(3d-2h_0-\alpha d)}{6}(b-b_w)d^2 \quad [2.82]$$

The position of the neutral axis given by the dimensionless parameter α can be computed from the fractional equation for a loading with constant eccentricity e_{act}:

$$\frac{e_{act}}{d} = \frac{-\alpha_e(1-\delta')(\alpha-\delta')A_{s2} - \frac{\alpha^2(3-\alpha)}{6}bd + \frac{(\alpha - h_0/d)^2(3-2\,h_0/d-\alpha)}{6}(b-b_w)d}{-\alpha_e(1-\alpha)A_{s1} + \alpha_e(\alpha-\delta')A_{s2} + \frac{\alpha^2}{2}bd - \frac{(\alpha-h_0/d)^2}{2}(b-b_w)d} \quad [2.83]$$

We also obtain a cubic equation with respect to the parameter α:

$$\alpha^3 - 3\left(1+\frac{e_{act}}{d}\right)\alpha^2 - 6\left[\rho_{s2}(1-\delta') + \left(\frac{b}{b_w}-1\right)\left(\frac{h_0}{d} - \frac{1}{2}\left(\frac{h_0}{d}\right)^2\right) + \frac{e_{act}}{d}\left(\rho_{s1}+\rho_{s2}+\frac{h_0}{d}\left(\frac{b}{b_w}-1\right)\right)\right]\alpha + 6\rho_{s2}\delta'(1-\delta') + \left(\frac{b}{b_w}-1\right)\left(3-2\frac{h_0}{d}\right)\left(\frac{h_0}{d}\right)^2 + 6\frac{e_{act}}{d}\left[\rho_{s1}+\delta'\rho_{s2}+\frac{1}{2}\left(\frac{h_0}{d}\right)^2\left(\frac{b}{b_w}-1\right)\right] = 0 \quad [2.84]$$

which, again, can be solved using Cardano's method.

This equation is also known as the cubic equation of the French reinforced concrete design rules dating from 1906 (*Circulaire du 20 Octobre 1906*) (see also [MAG 14]) or the French reinforced concrete design rules dating from 1934 (*règlements des marchés de l'état de 1934* – in French), which was recently reported in [THO 09] for T-cross-sections, and is presented in the following canonical format:

$$y^3 + py + q = 0 \quad \text{with} \quad y = \alpha d - c; \quad c = d + e_{act};$$
$$p = -3\frac{b}{b_w}c^2 + 3\left(\frac{b}{b_w} - 1\right)(c - h_0)^2 + \frac{6\alpha_e A_{s1}}{b_w}(d - c) + \frac{6\alpha_e A_{s2}}{b_w}(d' - c) \quad \text{and}$$
$$q = -2\frac{b}{b_w}c^3 + 2\left(\frac{b}{b_w} - 1\right)(c - h_0)^3 - \frac{6\alpha_e A_{s1}}{b_w}(d - c)^2 - \frac{6\alpha_e A_{s2}}{b_w}(d' - c)^2 \qquad [2.85]$$

It can be easily shown that equations [2.84] and [2.85] are equivalent. It is worth mentioning that equation [2.85] is presented directly in canonical format so that Cardano's method can be directly applied without variable transformation.

We note that the simple bending case can be deduced asymptotically from equation [2.84], with an infinite eccentricity leading to:

$$\frac{e_{act}}{d} \to \infty \quad \Rightarrow \quad -3\alpha^2 - 6\left[\rho_{s1} + \rho_{s2} + \frac{h_0}{d}\left(\frac{b}{b_w} - 1\right)\right]\alpha$$
$$+6\left[\rho_{s1} + \delta'\rho_{s2} + \frac{1}{2}\left(\frac{h_0}{d}\right)^2\left(\frac{b}{b_w} - 1\right)\right] = 0 \qquad [2.86]$$

whose solution has been already given in equation [2.26].

2.3.4. *Exercises for composed bending with normal force solicitation*

2.3.4.1. *Design of a specific rectangular cross-section*

2.3.4.1.1. Data of the problem

A rectangular cross-section of a reinforced concrete beam is solicited in composed bending with normal forces. The external screw elements are given at the point G of the rectangular cross-section (see Figure 2.9). The

point G is located at the center of gravity of the full rectangular cross-section (see Figure 2.9). The data of the problem are given below:

$M_G = 0.11$ MN·m $\quad$ $|N_G| = 95$ kN in compression

$b = 0.3$ m $\quad$ $d = 0.45$ m

$h = 0.50$ m $\quad$ $A_{s2} = 0$ cm^2

$f_{ss} = 320$ MPa $\quad$ $f_{cs} = -11.7$ MPa

$\alpha_e = 16.5$ [2.87]

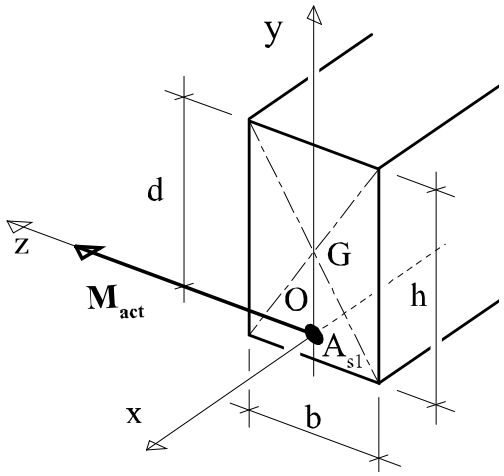

Figure 2.9. *Design of a reinforced concrete rectangular cross-section at serviceability limit state for composed bending state with combined axial forces; solicitation defined at the center of gravity of the cross-section*

The exercise consists of designing the tensile steel reinforcement of this reinforced concrete beam solicitated in composed bending with normal compression. In the second part of the problem, it is suggested to control the design of a given reinforced concrete section for a given solicitation in composed bending with normal compression, or equivalently for a given loading eccentricity (see Figure 2.10). For an easier resolution of the problem, the design is decomposed into different steps that can be helpful for optimizing the design of this reinforced cross-section at SLS.

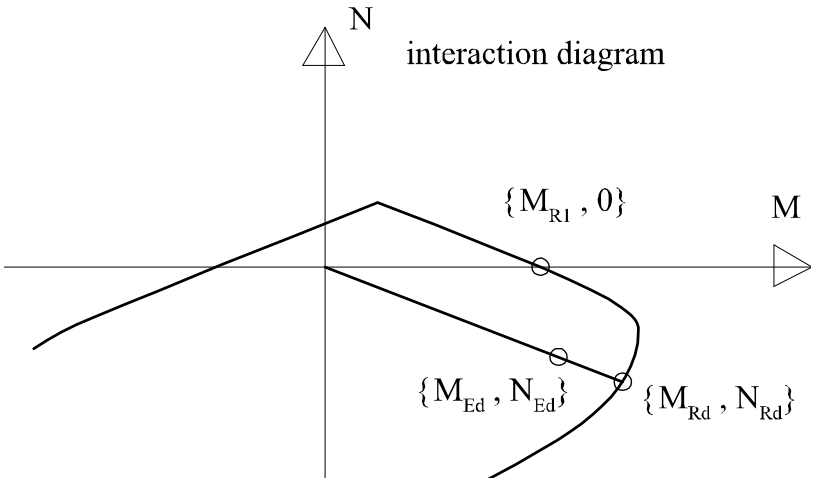

Figure 2.10. *Interaction diagram in the normal force – bending moment space*

1) Determine the screw reduction elements (moment M_{Ed} and normal force N_{Ed}) of the external screw forces evaluated at the frame origin.

2) In this question, the characterization of the pivot *AB* is investigated. It is recalled that the pivot *AB* is defined at the boundary of Pivot *A* and Pivot *B* from a stress at the upper fiber equal to f_{cs} and a stress at the center of gravity of the tensile steel reinforcement (lower fiber) equal to f_{ss}. Give the value α_{AB} of the relative depth of this limit case. By considering that M_{AB} is the associated moment of this limit case, calculate this bending moment and conclude on the type of pivot that controls the design of this rectangular cross-section with this solicitation.

3) Give the analytical expression of the nonlinear equation for this pivot with respect to the dimensionless position of the neutral axis, and solve this polynomial equation with the given data of the problem, especially with the external solicitation given by $\{M_{Ed}, N_{Ed}\}$.

4) Under the action of the external screw $\{M_{Ed}, N_{Ed}\}$, calculate the stress level in the upper fiber of concrete $\sigma_{c,sup}$, the stress in the tensile steel reinforcement σ_{s1} and the steel area A_{s1} of the steel reinforcement needed at the SLS. This will conclude the design of the reinforced concrete section for the given solicitation.

5) For the following, we would like to control the design of a given reinforced concrete section, with the tensile steel reinforcement composed of

6HA 14 (with A_{s1}= 9.236 cm^2). Under the action of the external screw $\{M_{Ed}, N_{Ed}\}$, calculate the stress level in the upper fiber of concrete $\sigma_{c,sup}$, the stress in the tensile steel reinforcement σ_{s1} and check the design of this reinforced concrete section at the SLS.

2.3.4.1.2. Resolution

1) The external screw forces evaluated at the origin point *O* are calculated from the screw forces given at the point *G* from the transport rule:

$$\begin{cases} M_{Ed} = M_G - N_G\left(d - \dfrac{h}{2}\right) = 0.11 + 0.095 \times (0.45 - 0.25) = 0.129 \ \text{MN.m} \\ N_{Ed} = N_G = -0.095 \ \text{MN} \end{cases} \quad [2.88]$$

It can be checked that $M_{Ed} \geq M_G$, which is physically consistent with respect to the applied load. The equivalent eccentricity of the external screw forces is also calculated from:

$$e_{Ed} = \frac{M_{Ed}}{N_{Ed}} = \frac{M_G}{N_G} - d + \frac{h}{2} = -1.35789\,\text{m} \quad [2.89]$$

2) The limit case at Pivot *AB* is characterized by the limit values:

$$\alpha_{AB} = \frac{\alpha_e f_{cs}}{\alpha_e f_{cs} - f_{ss}} = 0.376279 \Rightarrow \text{M}_{\text{AB}} = \frac{\alpha_{AB}^2 (3 - \alpha_{AB})}{6\,\alpha_e (1 - \alpha_{AB})} b d^2 f_{ss}$$

$$= -\frac{\alpha_{AB}(3 - \alpha_{AB})}{6} b d^2 f_{cs} = 0.11695 \ \text{MN·m} \quad [2.90]$$

It is easy to check that $M_{Ed} \geq M_{AB}$ and the section behaves at Pivot *B* at the SLS.

3) At Pivot *B*, the dimensionless position α of the neutral axis is expressed in dimensionless format with:

$$\alpha = 1{,}5\left(1 - \sqrt{1 - \frac{8}{3} \cdot \frac{-\text{M}_{\text{ser}}}{\text{bd}^2 \text{f}_{\text{cs}}}}\right) = 0.42248; \ \sigma_{c,sup} = f_{cs} = -11.7 \ \text{MPa}$$

$$\text{and} \ \sigma_{s1} = -\frac{\alpha_e (1 - \alpha)}{\alpha} \text{f}_{\text{cs}} = 263.89 \ \text{MPa} \quad [2.91]$$

4) The tensile steel reinforcement area needed at the SLS is then calculated from:

$$A_{s1} = \frac{-\alpha N_{act}}{\alpha_e f_{cs}(1-\alpha)} + \frac{\alpha^2 bd}{2\ \alpha_e(1-\alpha)} = 9.04356 \text{ cm}^2 \qquad [2.92]$$

5) For the verification of the reinforced concrete cross-section, a cubic equation has to be solved from:

$$\alpha^3 - 3\left(1+\frac{e_{Ed}}{d}\right)\alpha^2 - 6\frac{e_{Ed}}{d}\rho_{s1}\alpha + 6\frac{e_{Ed}}{d}\rho_{s1} = 0$$

$$\text{with} \quad \frac{e_{Ed}}{d} = -3.0175 \quad \text{and} \quad \rho_{s1} = 0.11288 \qquad [2.93]$$

Cardano's method is used to solve this cubic equation.

$$a\alpha^3 + b\alpha^2 + c\alpha + d = 0 \text{ with}$$

$$a = 1, b = +6.0526, c = 2.0438 \text{ and } d = -c \qquad [2.94]$$

We use Cardano's method to compute the root of this cubic. The canonical parameters are calculated from:

$$p = \frac{3ac - b^2}{3a^2} = -10.1676 \text{ and}$$

$$q = \frac{27a^2d + 2b^3 - 9abc}{27a^3} = 10.2575 \qquad [2.95]$$

It can be checked that $4p^3 + 27q^2 = -1363.73 < 0,$ and the cubic equation admits three real solutions (see Appendix 1), calculated from the following term $Arc\cos\left(3q/2p\sqrt{-3/p}\right) = 2.5357,$ and leads to:

$$\begin{cases} \alpha_1 = 2\sqrt{\dfrac{-p}{3}}\cos\left[\dfrac{Arc\cos\left(\dfrac{3q}{2p}\sqrt{\dfrac{3}{-p}}\right)+2\pi}{3}\right]-\dfrac{b}{3a}=-5.6246 \\ \alpha_2 = 2\sqrt{\dfrac{-p}{3}}\cos\left[\dfrac{Arc\cos\left(\dfrac{3q}{2p}\sqrt{\dfrac{3}{-p}}\right)+4\pi}{3}\right]-\dfrac{b}{3a}=-0.8536 \\ \alpha_3 = 2\sqrt{\dfrac{-p}{3}}\cos\left[\dfrac{Arc\cos\left(\dfrac{3q}{2p}\sqrt{\dfrac{3}{-p}}\right)}{3}\right]-\dfrac{b}{3a}=0.42567 \end{cases} \quad [2.96]$$

The third solution is the physical solution of the problem $\alpha = 0.42567$. The stress in the most compressed fiber of concrete is calculated from:

$$\sigma_{c,\sup} = \frac{N_{ser}\alpha d}{\frac{b}{2}(\alpha d)^2 + \alpha_e(\alpha d - d)A_{s1} + \alpha_e(\alpha d - d')A_{s2}}$$

$$= \frac{-0.095\times10^6\times0.42567\times0.45}{\frac{0.3}{2}\times(0.42567\times0.45)^2 + 16.5\times(0.42567\times0.45-0.45)\times9.326\times10^{-4}} = -11.63 \text{ MPa}$$

and

$$\sigma_{s1} = \frac{(d-\alpha d)}{\alpha d}\left(-\alpha_e\sigma_{c\sup}\right) = \frac{0.45-0.42567\times0.45}{0.42567\times0.45}\times16.5\times11.63\times10^6 = 258.9 \text{ MPa} \quad [2.97]$$

It is easy to check that $|\sigma_{s1}| \le f_{ss}$ and $|\sigma_{c,\sup}| \le |f_{cs}|$. Clearly, the section is correctly designed at the SLS, and its behavior is close to the one in Pivot *B*.

2.3.4.2. *Design of a specific T-cross-section*

2.3.4.2.1. Data of the problem

A T-cross-section of a reinforced concrete beam is solicited in composed bending with normal forces. The external screw elements are given at the

point *O* chosen at the center of gravity of the tensile steel reinforcement (see Figure 2.8). The data of the problem are given below:

$M_O = 0{,}49$ MN.m	$N_O = -0.49$ MN	
$b = 0.7$ m	$d = 1.$ m	
$b_w = 0.3$ m	$d' = 0.05$ m	
$h = 1{,}10$ m	$h_0 = 0.18$ m	
$f_{ss} = 240$ MPa	$f_{cs} = -15$ MPa	
$\alpha_e = 8$	$A_{s2} = 0.848$ cm^2 $(3\phi 6)$	[2.98]

The exercise consists of designing the tensile steel reinforcement of this reinforced concrete beam solicitated in composed bending with normal compression. The calculation of the tensile steel area needs to determine analytically and numerically the function $M_{res,s}(\alpha)$, where $M_{res,s}$ is the resistant moment of the cross-section at SLS, evaluated at the center of gravity of the tensile steel reinforcement and α is as usual the dimensionless depth of the neutral axis position.

It can be shown that the function $M_{res,s}(\alpha)$ is continuous in the domain $[0,\ h/d]$ and is exactly known at least in each sub-interval as a piecewise function. The total domain for the variation of the neutral axis position α is subdivided into sub-domains connected at some characteristic points associated with a material or a geometrical discontinuity. These characteristic values can be classified in a formal suite $(\alpha_0,\ \alpha_1,\ \alpha_2,\ \ldots,\alpha_n)$ of $[0,h/d]$ with $\alpha_0 = 0 < \alpha_1 < \alpha_2 < \ldots < \alpha_n = h/d$ such that for each $i \in \{1,\ 2,...,n\}$, there exists an application $M_{bi}(\alpha)$, that is continuous in $[\alpha_{i-1},\ \alpha_i]$ and verifies:

$$
\begin{aligned}
&M_{res,s}(\alpha) = M_{bi}(\alpha) \forall\, \alpha[\alpha_{i-1}, \alpha_i] \\
&M_{res,s}(\alpha_i) = M_{bi}(\alpha_i) = M_{bi+1}(\alpha_i) \forall\ i \in \{0,\ 1,\ 2, \ldots, n-1\} \\
&M_{res,s}(\alpha_0) = M_{b1}(\alpha_0) \\
&M_{res,s}(\alpha_n) = M_{bn}(\alpha_n)
\end{aligned}
$$

Each function $M_{bi}(\alpha)$ can be called a "branch" of $M_{res,s}(\alpha)$, which differs from each other from the discontinuous nature of the material or the geometrical characteristics of the reinforced cross-section. The choice of the relevant branch with respect to the design of a given reinforced concrete section can be done from the comparison of the boundary moments with

respect to the serviceability moment $M_{act,s}$, leading to a unique nonlinear equation to be solved for the determination of the position of neutral axis α.

For an easier resolution of the problem, the design is decomposed into different steps that can be helpful for optimizing the design of this reinforced cross-section at SLS.

1) Let us fix $\varepsilon_{c,sup} = 0$ (or equivalently $\alpha = 0$). Determine for this particular position of the neutral axis, the expression of the resistant moment M_0 with respect to the variables of the problem.

2) We are now interested in calculating the resistant moment M_t at *SLS*, which corresponds to the position of the neutral axis located at the distance h_0 from the upper fiber of the cross-section (boundary between the flanged portion of the beam and the web). After explaining the pivot associated with this limit case, it is suggested, to find analytically, this bending moment M_t.

3) In this question, the characterization of the pivot *AB* is investigated. It is recalled that the pivot *AB* is defined at the boundary of Pivot *A* and Pivot *B* from a stress at the upper fiber equal to f_{cs} and a stress at the center of gravity of the tensile steel reinforcement (lower fiber) equal to f_{ss}. Give the value α_{AB} of the relative depth of this limit case. By considering that M_{AB} is the associated moment of this limit case, calculate this bending moment and specify how the section can be calculated for this limit case (rectangular cross-section or T-cross-section calculations).

4) After having classified different characteristic cases, analyze the type of pivot and the type of calculation (rectangular cross-section or T-cross-section calculations), which is needed for the design of this T-cross-section at SLS. Give the analytical expression of the nonlinear equation for this pivot with respect to the dimensionless position of the neutralaxis α.

5) Under the action of the external screw $\{M_O, N_O\}$, calculate the stress level in the upper fiber of concrete $\sigma_{c,sup}$, the stress in the tensile steel reinforcement σ_{s1} and the steel area A_{s1} of the steel reinforcement needed at the SLS.

2.3.4.2.2. Resolution

1) In this case, the neutral axis is located at the upper fiber of the reinforced concrete section, $\alpha = 0$, meaning that the cross-section is fully in compression or in tension. At Pivot *A*, the lower steel reinforcements of area

A_{s1} are in tension with a strain value $\varepsilon_{s1} = f_{ss}/E_s$. By neglecting the tensile part of the concrete, the bending moment M_0 is simply calculated from:

$$M_0 = -A_{s2}E_s\varepsilon_{s2}\left(d-d'\right) = -A_{s2}f_{ss}\delta'\left(d-d'\right) = -9.6672\times10^{-4}\ \text{MN}\cdot\text{m} \quad [2.99]$$

This negative sign of the bending moment is linked to the tension behavior of the upper steel reinforcement of area A_{s2}. The reduced moment $\mu_0 = M_0 \Big/ \left[b_w d^2\left(-f_{cs}\right)\right]$ is equal to $\mu_0 = -2.148\times10^{-4}$.

2) The limit case at the boundary between the rectangular cross-section and the T-cross-section is obtained from $\alpha_t = h_0/d = 0.18 < \alpha_{AB} = \alpha_e.f_{cs}/(\alpha_e.f_{cs} - f_{ss}) = 0.3333$. It means that this case is typically ruled by Pivot *A* for a rectangular cross-section:

$$M_t = \frac{\alpha-\delta'}{1-\alpha}(d-d')A_{s2}.f_{ss} + \frac{\alpha^2(3-\alpha)}{6\,\alpha_e(1-\alpha)}bd^2f_{ss} \Rightarrow M_t = 0.39305\ \text{MN}\cdot\text{m} \quad [2.100]$$

We calculate, in this case, the reduced moment $\mu_t = M_t \Big/ \left[b_w d^2\left(-f_{cs}\right)\right] = 0.08734$.

3) As $\alpha_t = h_0/d < \alpha_{AB}$, the calculation of the resistant moment at Pivot *AB* is necessarily associated with the T-cross-section formulae as:

$$M_{AB} = \frac{\alpha_{AB}-\delta'}{1-\alpha_{AB}}(d-d')A_{s2}.f_{ss} + \frac{\alpha_{AB}^2(3-\alpha_{AB})}{6\,\alpha_e(1-\alpha_{AB})}bd^2f_{ss}$$

$$-\frac{(\alpha_{AB}-h_0/d)^2(3-2\,h_0/d-\alpha_{AB})}{6\,\alpha_e(1-\alpha_{AB})}(b-b_w)d^2f_{ss}$$

$$\Rightarrow M_{AB} = 1.401076\ \text{MN}\cdot\text{m} \quad [2.101]$$

We calculate, for Pivot *AB*, the reduced moment equal to $\mu_{AB} = M_{AB} \Big/ \left[b_w d^2\left(-f_{cs}\right)\right] = 0.31135$.

4) For the solicitation (M_0 = 0.49 MN·m; N_0 = 0.49 MN), we have $M_0 \in \left[M_t; M_{AB}\right]$ and then the section is controlled by Pivot A with a T-cross-sectional calculation. The cubic equation for the determination of the

position of the neutral axis at Pivot *A* for a T-cross-section is given by equation [1.102] with the coefficients numerically calculated as:

$$a_0\alpha^3 + a_1\alpha^2 + a_2\alpha + a_3 = 0 \text{ with}$$

$$\begin{cases} a_0 = \dfrac{b_w}{b} = 0.428571 \\ a_1 = -\dfrac{3b_w}{b} = 1.285714 \\ a_2 = -6\alpha_e\left(\dfrac{M}{bd^2 f_{ss}} + \dfrac{(1-\delta')A_{s2}}{bd}\right) - 3\left(\dfrac{h_0}{d}\right)\left(2-\dfrac{h_0}{d}\right)\left(1-\dfrac{b_w}{b}\right) = -0.707124 \\ a_3 = +6\alpha_e\left(\dfrac{M}{bd^2 f_{ss}} + \dfrac{\delta'(1-\delta')A_{s2}}{bd}\right) + \left(\dfrac{h_0}{d}\right)^2\left(3-\dfrac{2h_0}{d}\right)\left(1-\dfrac{b_w}{b}\right) = 0.189154 \end{cases} \quad [2.102]$$

Cardano's method is used (see Appendix 1), with the canonical parameters calculated as:

$p = -4.649956$; $q = -3.208597$ and finally,

$$\alpha = 2\sqrt{-\frac{p}{3}}\cos\left[\frac{\text{Arc}\cos\left(\frac{3q}{2p}\sqrt{-\frac{3}{p}}\right) + 4\pi}{3}\right] - \frac{b}{3a}$$

$$= 0.199768 \quad [2.103]$$

5) At Pivot *A*, the stress in the tensile steel reinforcement is equal to the steel serviceability stress limit $\sigma_{s1} = f_{ss}$. The steel area is obtained from the normal force equilibrium equation:

$$A_{s1} = \frac{N_{act}}{f_{ss}} + \frac{\alpha_1 - \delta'}{1 - \alpha_1} A_{s2} + \frac{\alpha_1^2\, bd}{2\alpha_e(1-\alpha_1)} - \frac{(\alpha_1 - h_0/d)^2\,(b-b_w)d}{2\alpha_e(1-\alpha_1)}$$

$$= 1.438\,008 \text{ cm}^2 \quad [2.104]$$

We finally obtain for this T-cross-section designed at Pivot *A*, A_{s1} = 1.44 cm^2. We can design the cross-section with $3\phi 8$ (1.508 cm^2).

In this case, as shown in Figure 2.11, the section behaves in Pivot *A* and is quite far from the Pivot *AB*. Equations of each branch can be analytically given. For instance, the expression of the reduced moment branch in Pivot *A* when the cross-section behaves as rectangular cross-section is given by:

$$\mu = \frac{\rho_{s2}}{\alpha_e}\frac{(1-\delta')(\alpha-\delta')}{1-\alpha}\left(\frac{-f_{ss}}{f_{cs}}\right)+\frac{\alpha^2(3-\alpha)}{6\alpha_e(1-\alpha)}\frac{b}{b_w}\left(\frac{-f_{ss}}{f_{cs}}\right)$$

$$\text{with } \mu = \frac{M}{b_w d^2(-f_{cs})},\ \delta' = \frac{d'}{d} \text{ and } \rho_{s2} = \frac{\alpha_e A_{s2}}{b_w d} \qquad [2.105]$$

The branch in Pivot *A* but with a complete T-cross-sectional behavior is given by:

$$\mu = \frac{\rho_{s2}}{\alpha_e}\frac{(1-\delta')(\alpha-\delta')}{1-\alpha}\left(\frac{-f_{ss}}{f_{cs}}\right)+\frac{\alpha^2(3-\alpha)}{6\alpha_e(1-\alpha)}\frac{b}{b_w}\left(\frac{-f_{ss}}{f_{cs}}\right)-$$
$$\frac{\left(\alpha-\frac{h_0}{d}\right)^2\left(3-2\frac{h_0}{d}-\alpha\right)}{6\alpha_e(1-\alpha)}\left(\frac{b}{b_w}-1\right)\left(\frac{-f_{ss}}{f_{cs}}\right) \qquad [2.106]$$

Finally, the branch in Pivot *B* but with a complete T-cross-sectional behavior is given by:

$$\mu = \frac{\rho_{s2}}{\alpha}(1-\delta')(\alpha-\delta')+\frac{\alpha(3-\alpha)}{6}\frac{b}{b_w}-\frac{\left(\alpha-\frac{h_0}{d}\right)^2\left(3-2\frac{h_0}{d}-\alpha\right)}{6\alpha}\left(\frac{b}{b_w}-1\right) \qquad [2.107]$$

The continuous branches shown in Figure 2.11 are specific of the cross-section. For the solicitation investigated in the problem, the cross-sectional behavior is materialized by a point with the coordinates $(\alpha,\mu)=(0.1998;0.1088)$.

Figure 2.11. *Moment versus the position of neutral axis for each branch; design of a reinforced concrete T-cross-section*

2.4. Deflection at Serviceability Limit State

2.4.1. *Effect of crack on the bending curvature relationship*

2.4.1.1. *Tension stiffening phenomenon*

As reported in Eurocode 2, the appearance and utility of the structure may be impaired when the calculated sag of a beam, slab or cantilever subjected to quasi-permanent loads exceeds a beam's span/250. The sag is relative to the supports. Deflections that can damage adjacent parts of the structure should be limited. For the deflection after construction, a beam's span/500 is normally an appropriate limit for quasi-permanent loads.

The deflection control at SLS is then formulated as:

$$f \leq \overline{f} \qquad [2.108]$$

where $\overline{f} = L/500$ for structures where adjacent parts should not be affected by the deflection of the beam (with a span length equal to L) or $\overline{f} = L/250$ in the other cases. The deflections are computed from an applied load with a nonlinear bending-curvature constitutive law that takes into account both the reduction of stiffness due to the cracking process in the tension part of

concrete and the time-dependent phenomena such as creep that softens the apparent stiffness of the reinforced concrete beam. Consider the bending behavior of a reinforced concrete beam, as shown in Figure 2.12.

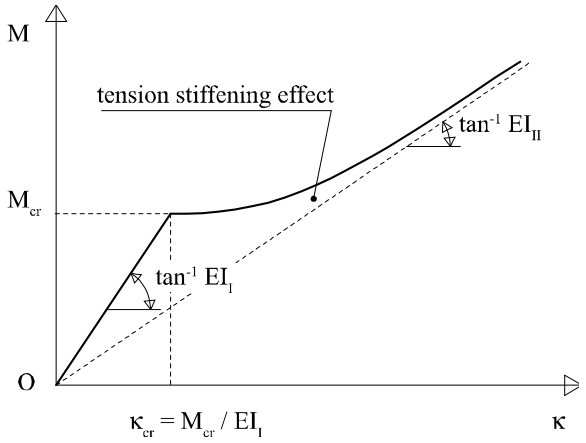

Figure 2.12. *Moment-curvature relationship at serviceability limit state for the calculation of deflection including tension stiffening phenomenon*

The law to calculate the reduction of stiffness is the following:

$$\kappa = \zeta \frac{M}{EI_{II}} + (1-\zeta)\frac{M}{EI_I} \qquad [2.109]$$

where κ is the curvature, M is the bending moment, EI_I is the bending stiffness of the uncracked beam, and EI_{II} is the bending stiffness of the cracked beam. For physical reasons linked to the micro-cracking process, the stiffness of the damaged beam is smaller than the stiffness of the undamaged beam $EI_{II} \leq EI_I$.

Note that this law can also be formulated as:

$$M = EI_e \kappa \text{ with } EI_e = \frac{EI_I \times EI_{II}}{\zeta EI_I + (1-\zeta) EI_{II}} \qquad [2.110]$$

The contribution of the cracking part of concrete in the global stiffness of the reinforced concrete beam is called the tension stiffening effect.

In Eurocode 2, the distribution coefficient is an empirical coefficient that is assumed to be dependent on the bending variable as:

$$\zeta = \left\langle 1 - \beta_1 \left(\frac{M_{cr}}{M} \right)^2 \right\rangle \text{ with } \langle x \rangle = \frac{x + |\ x\ |}{2} \qquad [2.111]$$

In the above equation, $\zeta = 0$ corresponds to the uncracked section and $\zeta = 1$ corresponds to the cracked section. β_1 is a coefficient that takes into account the time-dependent effects: $\beta_1 = 1$ for short-term analyses and $\beta_1 = 1/2$ for long-term analyses (typically in case of permanent or quasi-permanent loading). In fact, ζ could be interpreted as a cross-sectional bending damage parameter, even if the law is essentially a hardening law. M_{cr} is the cracking moment that is associated with a stress value in the lower fiber of concrete $\sigma_{c,\inf}$ equal to the uniaxial tensile strength of concrete f_{ctm} in the uncracked section.

With respect to deflection control, the long-term analysis is the most unfavorable, and creep effects have to be taken into account with the creep coefficient φ given in equation [1.71] to derive the effective Young's modulus of concrete $E_{c,eff} = E_{cm} / \left[1 + \phi(\infty, t_0) \right]$. Shrinkage effects should also be added for an exhaustive design.

2.4.1.2. *Uncracked section*

2.4.1.2.1. Uncracked section – rectangular cross-section

Consider a rectangular cross-section as shown in Figure 1.28. This section is the uncracked section, meaning that we do take into account the tension part of concrete. We calculate the parameters of the uncracked homogenized section as follows. The position of the neutral axis is obtained from the upper fiber of the cross-section as:

$$y_I = \alpha_I d = \frac{\dfrac{bh^2}{2} + \alpha_e \left(A_{s1} d + A_{s2} d' \right)}{bh + \alpha_e \left(A_{s1} + A_{s2} \right)} \text{ and}$$

$$I_I = \frac{b y_I^3}{3} + \frac{b \left(h - y_I \right)^3}{3} + \alpha_e \left[A_{s1} \left(d - y_I \right)^2 + A_{s2} \left(y_I - d' \right)^2 \right] \qquad [2.112]$$

The equivalent stiffness of the uncracked section is then $EI_I = E_{c,eff} \times I_I$. The cracking moment can be explicitly calculated from:

$$\sigma_{c,\inf} = f_{ctm} \quad \Rightarrow \quad M_{cr} = \frac{f_{ctm} \times I_I}{h - y_I} \qquad [2.113]$$

We note that this critical moment does not depend on the solicitation, but only depends on the material and geometrical parameters of the reinforced concrete cross-section.

2.4.1.2.2. Uncracked section – T-cross-section

For a T-cross-section, the formula valid for the rectangular cross-section can be generalized as following, when the neutral axis of the uncracked section is located in the web:

$$y_I = \alpha_I d = \frac{\frac{b_w h^2}{2} + \frac{(b - b_w) h_0^2}{2} + \alpha_e \left(A_{s1} d + A_{s2} d' \right)}{b_w h + (b - b_w) h_0 + \alpha_e \left(A_{s1} + A_{s2} \right)} \text{ and}$$

$$I_I = \frac{b y_I^3}{3} - \frac{(b - b_w)(y_I - h_0)^3}{3} + \frac{b_w (h - y_I)^3}{3} + \alpha_e \left[A_{s1} (d - y_I)^2 + A_{s2} (y_I - d')^2 \right] \qquad [2.114]$$

The equivalent stiffness of the uncracked section is then $EI_I = E_{c,eff} \times I_I$. The cracking moment can be explicitly calculated from:

$$\sigma_{c,\inf} = f_{ctm} \quad \Rightarrow \quad M_{cr} = \frac{f_{ctm} \times I_I}{h - y_I} \qquad [2.115]$$

2.4.1.3. *Cracked section*

2.4.1.3.1. Cracked section – rectangular cross-section

In the cracked section with rectangular cross-section, we use the equation of "static moment" to derive the neutral axis position from equations [2.15] and [2.16] that are rewritten as:

$$y_{II} = \alpha_{II} d = \frac{-\alpha_e (A_{s1} + A_{s2}) + \sqrt{\alpha_e^2 (A_{s1} + A_{s2})^2 + 2\alpha_e b (A_{s1} d + A_{s2} d')}}{b} \quad [2.116]$$

The inertia of the homogenized cracked section is calculated from:

$$I_{II} = \frac{b y_{II}^3}{3} + \alpha_e A_{s1} (y_{II} - d)^2 + \alpha_e A_{s2} (y_{II} - d')^2 \quad [2.117]$$

The equivalent stiffness of the cracked section is then $EI_{II} = E_{c,eff} \times I_{II}$. We also note that the parameters of the cracked section do not depend on the solicitation, but depend only on the material and geometrical parameters of the reinforced concrete cross-section.

2.4.1.3.2. Cracked section – T-cross-section

In the cracked section with T-cross-section, we use the equation of "static moment" to derive the neutral axis position from equations [2.26] and [2.27] that are rewritten here as:

$$y_{II} = \alpha_{II} d = \frac{-\left[\alpha_e (A_{s1} + A_{s2}) + h_0 (b - b_w)\right] + \sqrt{\left[\alpha_e (A_{s1} + A_{s2}) + h_0 (b - b_w)\right]^2 + 2 b_w \left[\alpha_e (A_{s1} d + A_{s2} d') + \frac{(b - b_w) h_0^2}{2}\right]}}{b_w} \quad [2.118]$$

The inertia of the homogenized cracked section is calculated from:

$$I_{II} = \frac{b y_{II}^3}{3} - \frac{(b - b_w)(y_{II} - h_0)^3}{3} + \alpha_e A_{s1} (y_{II} - d)^2 + \alpha_e A_{s2} (y_{II} - d')^2 \quad [2.119]$$

The equivalent stiffness of the cracked section is then $EI_{II} = E_{c,eff} \times I_{II}$.

2.4.1.4. *On the nonlinear bending-curvature constitutive law at SLS*

In the post-cracked section, a nonlinear bending curvature constitutive law appears that can be presented as a damage law.

$$\kappa \le \kappa_{cr} = \frac{M_{cr}}{EI_I} \Rightarrow \kappa = \frac{M}{EI_I} \text{ and}$$

$$\kappa \ge \kappa_{cr} = \frac{M_{cr}}{EI_I} \Rightarrow \kappa = \frac{M}{EI_{II}} - \beta_1 M_{cr}\left(\frac{1}{EI_{II}} - \frac{1}{EI_I}\right)\frac{M_{cr}}{M} \qquad [2.120]$$

The nonlinear post-cracked curvature-bending moment is continuous for $\beta_1 = 1$.

2.4.2. *Simply supported reinforced concrete beam*

A simply supported reinforced concrete beam is studied, loaded by some uniform distributed load at the SLS denoted by p_{ser}. The beam has a length L. The bending moment is parabolic in this statically determinate system, and is given, for $x \in [0;L]$, by:

$$M(x) = \frac{p_{ser}L^2}{2}\left[\frac{x}{L} - \left(\frac{x}{L}\right)^2\right] \qquad [2.121]$$

It is assumed that the reinforcement is homogeneous along the beam. For symmetrical reasons, two symmetrical parts of the beam of length L_I can be highlighted with an uncracked behavior (see Figure 2.13):

$$M = EI_I\kappa \text{ for } x \in [0;L_I] \text{ and } x \in [L - L_I; L] \qquad [2.122]$$

The length L_I corresponds to a bending moment that is equal to the critical moment:

$$M(L_I) = M_{cr} \quad \Rightarrow \quad \left(\frac{L_I}{L}\right)^2 - \left(\frac{L_I}{L}\right) + \frac{2M_{cr}}{p_{ser}L^2} = 0 \qquad [2.123]$$

The smallest solution is of interest, with respect to the notation of Figure 2.13, which is written as:

$$\frac{L_I}{L} = \frac{1 - \sqrt{1 - \dfrac{8M_{cr}}{p_{ser}L^2}}}{2} \text{ for } \frac{p_{ser}L^2}{8} \geq M_{cr} \qquad [2.124]$$

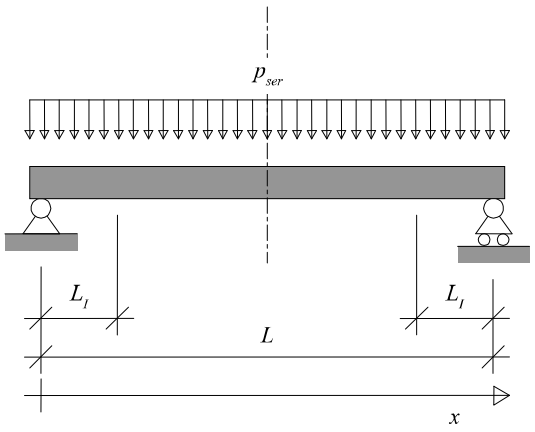

Figure 2.13. *Simply supported reinforced concrete beam loaded by uniform loads; definition of cracked and uncracked portion of the beam*

For the cracked part of the beam, namely for $x \in [L_I; L - L_I]$, a detailed structural analysis is needed for the integration of the nonlinear constitutive law along the beam.

2.4.3. *Calculation of deflection – safe approach*

The safer approach (approach in security) would consist of neglecting the tension stiffening effect of concrete. In this simplified approach, the cracked section is assumed along the entire beam:

$$M = EI_{II}\kappa \text{ for } x \in [0; L] \qquad [2.125]$$

In this case, this simplified approach leads to the deflection of the cracked beam:

$$f_{II} = \frac{5p_{ser}L^4}{384EI_{II}} \leq \overline{f} \qquad [2.126]$$

This approach is equivalent to neglecting the tension stiffening effect and to neglecting the uncracked contribution of the beam around the supports. If this inequality is checked, it is not necessarily to refine the approaches to control the deflection.

2.4.4. *Calculation of deflection – a more refined approach; tension stiffening neglected*

A more refined approach would be based on the following constitutive law:

$$M = EI_I \kappa \text{ for } x \in [0; L_I] \text{ and } x \in [L - L_I; L], \text{ and}$$
$$M = EI_{II} \kappa \text{ for } x \in [L_I; L - L_I] \qquad [2.127]$$

The uncracked contribution of the beam around the supports is taken into account, but the tension stiffening effect in the cracked portion of the beam is neglected, and approximated by the fully cracked section behavior. For homogeneous reinforcement along the beam, this engineering approach is in fact equivalent to a piecewise homogeneous beam with two different stiffnesses EI_I and EI_{II}. In this case, the deflection in the beam can be calculated from the integration of second-order differential equations given by:

$$EI_I w'' = \frac{-p_{ser} L^2}{2}\left[\frac{x}{L} - \left(\frac{x}{L}\right)^2\right] \text{ for } x \in [0; L_I], \text{ and}$$
$$EI_{II} w'' = \frac{-p_{ser} L^2}{2}\left[\frac{x}{L} - \left(\frac{x}{L}\right)^2\right] \text{ for } x \in \left[L_I; \frac{L}{2}\right] \qquad [2.128]$$

For a symmetrical reason, only half of the beam is considered in the study. The boundary conditions at the connection $x = L_I$ express the continuity of the deflection $w(x)$ and the slope angle $w'(x)$:

$$w(0) = 0, w'\left(\frac{L}{2}\right) = 0, w(L_I^-) = w(L_I^+) \text{ and } w'(L_I^-) = w'(L_I^+) \qquad [2.129]$$

The deflections in each part of the beam are finally calculated as:

$$w(x)=\frac{-p_{ser}L^2}{2EI_I}\left[\frac{x^3}{6L}-\frac{x^4}{12L^2}\right]+\frac{p_{ser}}{2EI_I}\left(1-\frac{EI_I}{EI_{II}}\right)\left(\frac{LL_I^2}{2}-\frac{L_I^3}{3}\right)x+$$

$$\frac{p_{ser}L^3x}{24EI_{II}} \text{ for } x\in[0;L_I], \text{ and}$$

$$w(x)=\frac{-p_{ser}L^2}{2EI_{II}}\left[\frac{x^3}{6L}-\frac{x^4}{12L^2}\right]+\frac{p_{ser}L^3x}{24EI_{II}}+$$

$$\frac{p_{ser}}{2EI_{II}}\left(\frac{EI_{II}}{EI_I}-1\right)\left(\frac{L_I^3L}{3}-\frac{L_I^4}{4}\right) \text{ for } x\in\left[L_I;\frac{L}{2}\right] \quad [2.130]$$

The deflection at mid-span $f=w(L/2)$ is presented in the following format:

$$f=f_{II}-\Delta f \text{ with } f_{II}=\frac{5p_{ser}L^4}{384EI_{II}} \text{ and}$$

$$\Delta f=\frac{p_{ser}L^4}{2EI_{II}}\left(1-\frac{EI_{II}}{EI_I}\right)\left[\frac{1}{3}\left(\frac{L_I}{L}\right)^3-\frac{1}{4}\left(\frac{L_I}{L}\right)^4\right] \quad [2.131]$$

As anticipated, the deflection with this model is smaller than the deflection of the cracked section $f\le f_{II}$. It is also easy to check the correctness of these formulas for the limit cases:

$$EI_{II}=EI_I \Rightarrow f=f_{II}=f_I, L_I=0 \Rightarrow f=f_{II} \text{ and } L_I=\frac{L}{2} \Rightarrow f=f_I \quad [2.132]$$

It is quite interesting to outline that the deflection f in equation [2.131] is a nonlinear function of the load p_{ser} due to the nonlinear dependence of L_I with respect to p_{ser}, as given by equation [2.124]. Clearly, this calculation is not based on elastic constitutive laws.

With this model, the deflection, Δf, has to be subtracted from the deflection f_{II} of the cracked beam, which can be finally presented as:

$$\frac{\Delta f}{f_{II}-f_I}=\frac{384}{10}\left[\frac{1}{3}\left(\frac{L_I}{L}\right)^3-\frac{1}{4}\left(\frac{L_I}{L}\right)^4\right] \text{ with}$$

$$\frac{L_I}{L}=\frac{1-\sqrt{1-\frac{8M_{cr}}{p_{ser}L^2}}}{2}, f_I=\frac{5p_{ser}L^4}{384EI_I} \text{ and } f_{II}=\frac{5p_{ser}L^4}{384EI_{II}} \quad [2.133]$$

2.4.5. *Calculation of deflection – a more refined approach; tension stiffening included*

It is possible to take into account the tension stiffening effect with the nonlinear bending-curvature constitutive law.

A more refined approach would be based on the following constitutive law:

$$M=EI_I\kappa \text{ for } x\in[0;L_I] \text{ and } x\in[L-L_I;L],$$
$$\text{and } \kappa=\frac{M}{EI_{II}}-\beta_1 M_{cr}\left(\frac{1}{EI_{II}}-\frac{1}{EI_I}\right)\frac{M_{cr}}{M} \text{ for } x\in[L_I;L-L_I] \quad [2.134]$$

In this case, the deflection in the beam can be calculated from the integration of second-order differential equations given by:

$$w''=\frac{-p_{ser}L^2}{2EI_I}\left[\frac{x}{L}-\left(\frac{x}{L}\right)^2\right] \text{ for } x\in[0;L_I], \text{ and}$$
$$w''=\frac{-p_{ser}L^2}{2EI_{II}}\left[\frac{x}{L}-\left(\frac{x}{L}\right)^2\right]+\beta_1 M_{cr}\left(\frac{1}{EI_{II}}-\frac{1}{EI_I}\right)\frac{2M_{cr}}{p_{ser}L^2\left[\frac{x}{L}-\left(\frac{x}{L}\right)^2\right]} \text{ for } x\in\left[L_I;\frac{L}{2}\right] \quad [2.135]$$

Integrating each second-order differential equation, and introducing the same boundary conditions as in equation [2.129], leads to the deflection solution:

$$w(x)=\frac{-p_{ser}L^2}{2EI_I}\left[\frac{x^3}{6L}-\frac{x^4}{12L^2}\right]+\frac{p_{ser}}{2EI_I}\left(1-\frac{EI_I}{EI_{II}}\right)\left(\frac{LL_I^2}{2}-\frac{L_I^3}{3}\right)x+\frac{p_{ser}L^3x}{24EI_{II}}$$
$$+\beta_1 xM_{cr}\left(\frac{1}{EI_{II}}-\frac{1}{EI_I}\right)\frac{2M_{cr}}{p_{ser}L}\ln\left(\frac{\frac{L_1}{L}}{1-\frac{L_1}{L}}\right)\quad\text{for } x\in[0;L_I],$$

and

$$w(x)=\frac{-p_{ser}L^2}{2EI_{II}}\left[\frac{x^3}{6L}-\frac{x^4}{12L^2}\right]+\frac{p_{ser}L^3x}{24EI_{II}}$$
$$+\beta_1 M_{cr}\left(\frac{1}{EI_{II}}-\frac{1}{EI_I}\right)\frac{2M_{cr}}{p_{ser}L^2}\left[Lx\ln\left(\frac{\frac{x}{L}}{1-\frac{x}{L}}\right)+L^2\ln\left(1-\frac{x}{L}\right)\right]$$
$$+\frac{p_{ser}}{2EI_{II}}\left(\frac{EI_{II}}{EI_I}-1\right)\left(\frac{L_I^3L}{3}-\frac{L_I^4}{4}\right)-\beta_1 M_{cr}\left(\frac{1}{EI_{II}}-\frac{1}{EI_I}\right)\frac{2M_{cr}}{p_{ser}}\ln\left(1-\frac{L_1}{L}\right)$$
$$\text{for } x\in\left[L_I;\frac{L}{2}\right] \qquad [2.136]$$

The deflection at mid-span $f=w(L/2)$ can be presented in the following format:

$$f=f_{II}-\Delta f \text{ with } f_{II}=\frac{5p_{ser}L^4}{384EI_{II}}$$
$$\text{and } \Delta f=\frac{p_{ser}L^4}{2EI_{II}}\left(1-\frac{EI_{II}}{EI_I}\right)\left[\frac{1}{3}\left(\frac{L_I}{L}\right)^3-\frac{1}{4}\left(\frac{L_I}{L}\right)^4\right]+$$
$$\frac{\beta_1 M_{cr}}{EI_{II}}\left(1-\frac{EI_{II}}{EI_I}\right)\frac{2M_{cr}}{p_{ser}}\ln\left[2\left(1-\frac{L_I}{L}\right)\right] \qquad [2.137]$$

Finally, when the tension stiffening phenomenon is taken into account, the deflection correction Δf has to be subtracted from the deflection f_{II} of the cracked beam, which can be finally presented as:

$$\frac{\Delta f}{f_{II}-f_I}=\frac{384}{10}\left[\frac{1}{3}\left(\frac{L_I}{L}\right)^3-\frac{1}{4}\left(\frac{L_I}{L}\right)^4\right]+\frac{12}{5}\beta_1\left(\frac{8M_{cr}}{p_{ser}L^2}\right)^2\ln\left[2\left(1-\frac{L_I}{L}\right)\right] \text{ with}$$

$$\frac{L_I}{L}=\frac{1-\sqrt{1-\dfrac{8M_{cr}}{p_{ser}L^2}}}{2}, f_I=\frac{5p_{ser}L^4}{384EI_I} \text{ and } f_{II}=\frac{5p_{ser}L^4}{384EI_{II}} \qquad [2.138]$$

This result coincides with the deflection calculation presented in the worked examples of EC2 [EUR 08a].

Of course, in the most general configuration, including, for instance, variable steel reinforcement along the beam, an analytical integration is not always feasible, and a numerical integration has to be performed.

2.4.6. *Approximated approach*

Another engineering approach presented in the literature consists of expressing the deflection as a combination of the deflection of the cracked and the uncracked section as:

$$\tilde{f}=\zeta f_{II}+(1-\zeta)f_I=f_{II}-\Delta\tilde{f} \text{ with}$$

$$\Delta\tilde{f}=(1-\zeta)(f_{II}-f_I) \text{ and } \zeta=\left\langle 1-\beta_1\left(\frac{M_{cr}}{M_{\max}}\right)^2\right\rangle \qquad [2.139]$$

Applying this engineering approach to the present simply supported beam leads to the correction deflection:

$$\frac{\Delta\tilde{f}}{f_{II}-f_I}=1-\zeta=\left(\frac{M_{cr}}{M_{\max}}\right)^2=\left(\frac{8M_{cr}}{p_{ser}L^2}\right)^2 \text{ for } \beta_1=1 \qquad [2.140]$$

The two approaches (the exact one with and without tension stiffening effect) and the engineering approach are compared in Figure 2.14. It can be

seen that the engineering approach gives a safer result than the exact one including the stiffening effect, as the correction deflection is smaller for the engineering approach than for the exact one. It is also shown that the tension stiffening effect is significant with respect to the deflection correction term neglecting this phenomenon.

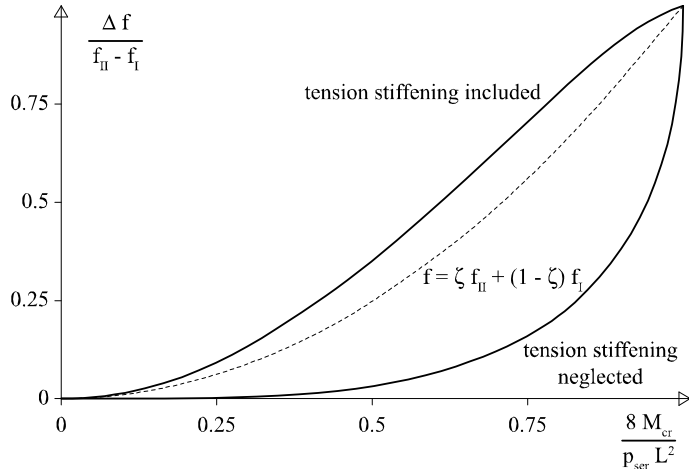

Figure 2.14. *Effect of the tension stiffening phenomenon on the deflection behavior of the cracked beam;* $\beta_1 = 1$

2.4.7. *Calculation of deflection – a structural example*

2.4.7.1. *Data of the problem*

We consider a reinforced concrete beam with a rectangular cross-section. As shown in Figure 2.13, the simply supported beam is loaded by some uniform serviceability load p_{ser}.

The data of the problem are the following:

$f_{ck} = 25$ MPa	$L = 10$ m	
$b = 0.5$ m	$d = 0.65$ m	
$h = 0.70$ m	$A_{s1} = 31.67$ cm^2 ($7\phi 24$)	
$\varphi = 2$.....	$p_{ser} = 38.$ kN/m	[2.141]

This reinforced concrete section has no compression steel reinforcement, $A_{s2} = 0$.

Given the creep coefficient $\varphi = 2$, the equivalent coefficient α_e can be calculated.

$$\alpha_e = \frac{E_s}{E_{cm}}(1+\phi) = \frac{200,000}{31,475.81} \times 3 = 19.06 \qquad [2.142]$$

where the mean value of the concrete Young's modulus has been given for this *C25/30* type concrete in equation [1.72]. The question is to check the SLS for the deflection control.

2.4.7.2. *Characteristics of the uncracked section*

From equation [2.112], we calculate the position of the neutral axis of the uncracked section y_I and the associated homogenized inertia I_I as:

$$y_I = \frac{\frac{0.5\times 0.7^2}{2} + 19.06\times 31.67\times 10^{-4}\times 0.65}{0.5\times 0.7 + 19.06\times 31.67\times 10^{-4}} = 0.3941 \text{ m and}$$

$$I_I = \frac{0.5\times 0.3941^3}{3} + \frac{0.5\times(0.7-0.3941)^3}{3} + 19.06\times 31.67\times 10^{-4}\times(0.65-0.3941)^2 = 1.8925\times 10^{-2} \text{ m}^4 \qquad [2.143]$$

The cracking moment can be explicitly calculated from:

$$f_{ctm} = 0.30\times(25)^{2/3} = 2.565 \text{ MPa} \Rightarrow M_{cr} = \frac{2.565\times 10^6 \times 1.8925\times 10^{-2}}{0.7-0.3941} = 0.15869 \text{ MN.m} \qquad [2.144]$$

We calculate the load ratio as:

$$\frac{M_{cr}}{M_{\max}} = \frac{8M_{cr}}{p_{ser}L^2} = \frac{8\times 0.15869\times 10^6}{38\times 10^3\times 10^2} = 0.33408 \qquad [2.145]$$

The length of the uncracked part of the beam, denoted by L_I, is calculated from equation [1.247] as:

$$\frac{L_I}{L} = \frac{1-\sqrt{1-0.33408}}{2} = 0.09198 \qquad [2.146]$$

The stiffness of the uncracked section is obtained from:

$$EI_I = \frac{31475.81\times10^6}{3}\times1.8925\times10^{-2} = 1.985599\times10^8\ \text{N.m}^2 \qquad [2.147]$$

2.4.7.3. *Characteristics of the cracked section*

The characteristics of the cracked section are given by equations [2.116] and [2.117] and are detailed below:

$$y_{II} = \frac{-19.06\times31.67\times10^{-4} + \sqrt{\left(19.06\times31.67\times10^{-4}\right)^2 + 2\times19.06\times0.5\times31.67\times10^{-4}\times0.65}}{0.5}$$
$$= 0.29342\ \text{m}$$
$$I_{II} = \frac{0.5\times0.29342^3}{3} + 19.06\times31.67\times10^{-4}\times\left(0.65-0.29342\right)^2 = 1.1885\times10^{-2}\ \text{m}^4 \qquad [2.148]$$

The stiffness of the cracked section is obtained from:

$$EI_{II} = \frac{31475.81\times10^6}{3}\times1.1885\times10^{-2} = 1.246967\times10^8\ \text{N.m}^2 \qquad [2.149]$$

2.4.7.4. *Calculation of deflection*

We compute the characteristics deflection f_I, f_{II} and $\overline{f}$ from:

$$f_I = \frac{5\times38\times10^3\times10^4}{384\times1.985599\times10^8} = 24.92\times10^{-3}\ \text{m} = 24.92\ \text{mm};$$
$$f_{II} = \frac{EI_I}{EI_{II}}f_I = \frac{1.985599}{1.1885}\times24.92 = 41.63\ \text{mm and}\ \overline{f} = \frac{L}{250} = 40\ \text{mm} \qquad [2.150]$$

It can be seen that $f_{II} > \overline{f}$ and the deflection control needs to take into account the tension stiffening effect to check the admissible maximum deflection.

From equation [2.137], the correction deflection induced by the tension stiffening phenomenon is calculated for $\beta = 1$ as:

$$\frac{\Delta f}{f_{II}-f_I}=\frac{384}{10}\left[\frac{1}{3}\times 0.09198^3-\frac{1}{4}\times 0.09198^4\right]$$
$$+\frac{12}{5}\times 0.33408^2\ln\left[2\times\left(1-0.09198\right)\right]=0.169 \qquad [2.151]$$

We calculate the total deflection including the tension stiffening effect as:

$$f=f_{II}-\Delta f=41.63-0.169\times\left(41.63-24.92\right)=38.80\text{ mm}<\overline{f}=40\text{ mm} \qquad [2.152]$$

We conclude that this beam is correctly designed with respect to the deflection control at SLS. Note that the approximated engineering formula (which is safe with respect to the exact one including rigorously the tension stiffening effect) would lead in this case to:

$$\tilde{f}=f_{II}-\Delta\tilde{f}=\text{ with }\frac{\Delta\tilde{f}}{f_{II}-f_I}=\left(\frac{M_{cr}}{M_{\max}}\right)^2$$
$$=0.33408^2\Rightarrow\tilde{f}=39.77\text{ mm}<\overline{f}=40\text{ mm} \qquad [2.153]$$

In this case, the deflection SLS would have been possibly checked with this simplified engineering formula.

Chapter 3

Concepts for the Design at Ultimate Limit State (ULS)

3.1. Introduction to ultimate limit state

3.1.1. *Yield design*

The purpose of designing a reinforced concrete structure is to achieve acceptable probabilities that this structure under a given load will not reach a limit state, namely the serviceability limit state (SLS) or the ultimate limit state (ULS). In this chapter, the strength of ULS is presented for general in-plane bending loading including the normal force coupling. The ULS is characterized by the requirement that the structure must be able to withstand, with an adequate factor of safety against collapse, to ensure the safety of both the building's occupants and the structure itself. The possibility of buckling phenomenon or other kinds of structural instabilities has formally also to be taken into account. However, in this chapter, we only focus on sectional ULS without considering possible structural instabilities. The ULS design can be based on the concept of yield design, where the maximum capacity of a given structure under a given loading system can be evaluated from the strength of its constituents (for a reinforced concrete structure, the strength of the steel reinforcement, the strength of the concrete and the strength of the interface between these constituents).

As greatly analyzed by Timoshenko [TIM 83], Yu and Zhang [YU 96], Heyman [HEY 99] or Salençon ([SAL 90], [SAL 02] or [SAL 06]),

Galileo's dialogs (1638) are often considered as a fundamental pioneering study of the strength of materials at the beam scale [GAL 02]. As detailed by Salençon [SAL 06]:

> *"The main topic treated in the First Day and the Second Day of Galileo's Dialogs is the resistance that solids offer to fracture with special consideration to prisms and cylinders submitted to axial tensile loading or to "transverse", i.e. bending forces. Without any consideration to the deformation of the considered solid before fracture, Galileo's reasoning implicitly introduces the concept of a Continuum within which coherence forces do act in order to maintain the filaments, fibres or any constituent particles together: one may say that Galileo opens the way to the concept of stress, which was settled explicitly some 200 years later. Having recognised that coherence forces and gravity forces in a solid are not related in the same way to its geometric scale, he performs what can be considered as the first striking example of dimensional analysis with application to similarity. In its celebrated analysis of the resistance of a cantilever beam submitted to bending, Galileo gives a first attempt to deriving the resistance of a whole solid submitted to some kind of loading from the resistance of its constituent material determined from another test."*

Galileo's cantilever beam (shown in Figure 3.1) can be classified as a structural paradigm as this structural model contains some stress gradient along the beam, allowing for the so-called localization effect that we will detail later.

Figure 3.1. *The cantilever beam studied by Galileo (1638)*

"This approach must also be associated with Coulomb's celebrated essay (1773) as one of milestones of the theory of yield design, implicitly evidencing the duality between forces and virtual velocity fields, which is presently implemented in the virtual rate of work method. The theory of yield design is the fundamental root of the Ultimate Limit State design now introduced in international codes for civil engineering".

3.1.2. *Application of yield design to the cantilever beam*

3.1.2.1. *A cantilever beam with general inelastic bending-curvature constitutive law*

The homogeneous cantilever beam of length L is loaded by a vertical concentrated load P at its end (Figure 3.2). We recognize Galileo's cantilever beam previously solved by Galileo himself (1564–1642) using equilibrium, strength and dimensional arguments. The cantilever beam loaded by a concentrated force can be viewed as a typical case of plastic beam with non-constant bending moment. The beam is assumed to behave with a complex nonlinear bending-curvature constitutive law, including possible irreversible phenomena.

The nonlinear bending-curvature constitutive law is considered as in Figure 3.3. The bending strength criterion is simply given by the following inequality:

$$\left| M(x) \right| \leq M_p \text{ for } x \in [0; L] \qquad [3.1]$$

where M_p is the yield moment (strength capacity of the cross-section).

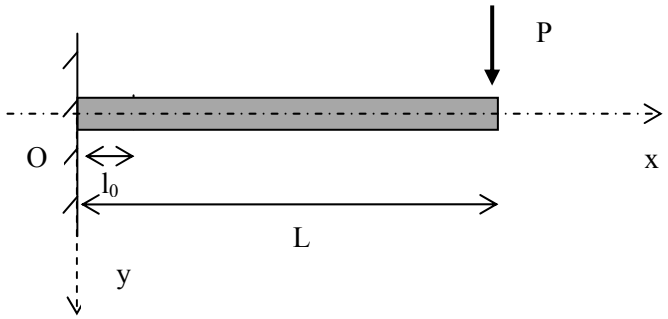

Figure 3.2. *The cantilever beam*

The reasoning that we will present here includes all kinds of structural applications (reinforced concrete design, steel structural design, timber engineering, etc.). When considering reinforced concrete design, the strength capacity of the cross-section depends on the strength of the steel reinforcement and the one of the concrete in compression. The reasoning is independent of the constitutive law of the material and only depends on the strength parameter M_p, which is the upper bending moment value. The reasoning is independent of the history path in the bending-curvature space.

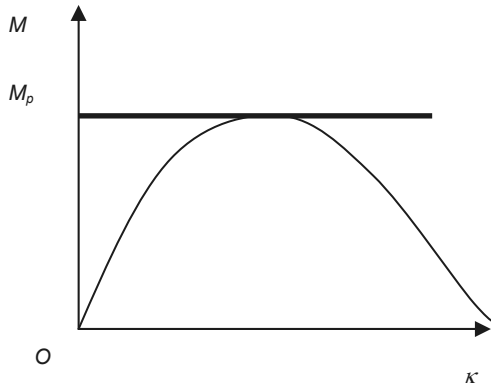

Figure 3.3. *Possible nonlinear bending M-curvature κ law for a reinforced concrete member*

Figure 3.4 also shows other possible bending-curvature constitutive law included in the yield design reasoning, which is quite independent of the path used to reach the strength limit M_p.

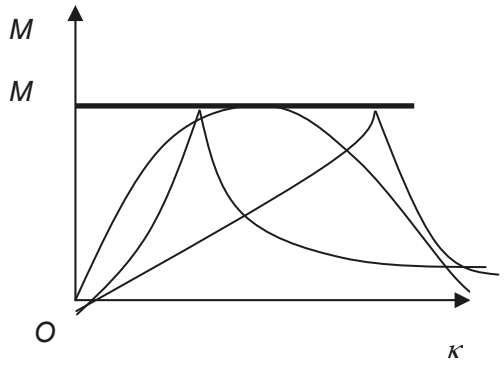

Figure 3.4. *Possible nonlinear bending-curvature law for a reinforced concrete member*

3.1.2.2. *Static approach by inside*

In the case of the cantilever beam, the structural system is statically determinate, and the bending moment is then calculated without any difficulties as a linearly decreasing function associated with a constant shear force:

$$M(x) = -P(L-x) \qquad [3.2]$$

Introducing the bending moment expression in the strength criterion leads to the optimization problem:

$$\text{Find the largest } P \text{ such as } \left| P(L-x) \right| \leq M_p \; \forall \; x \in [0;L] \qquad [3.3]$$

which is also equivalent to the following inequality:

$$P = M_p / L \leq P^+ \qquad [3.4]$$

P^+ is the yield load or the maximum capacity of the beam with respect to its local sectional strength constituent dependent on M_p. This approach is called a static approach, and gives a lower bound of the value P^+. However, from equation [3.3], as the moment distribution is the exact one of the problem for this statically determinate problem, an upper bound of the maximum capacity of the beam can also be obtained:

$$P^+ \leq \frac{M_p}{L} \qquad [3.5]$$

This is also called static approach by outside (as detailed by Salençon [SAL 02]).

3.1.2.3. *Kinematic approach by outside*

The same result can be obtained from direct application of the principle of virtual work:

$$P\delta w(L) = \int_0^L M\delta\kappa \; dx + \sum_i M\left[\delta\theta\right]_i \qquad [3.6]$$

where $[\delta\theta]$ denotes the jump of any quantity $\delta\theta$ at the point of abscissa s_i. The fundamental reasoning of the kinematic approach of yield design is based on the surrounding of the internal work with respect to the strength capacity of the beam [SAL 02]:

$$P\delta w(L) \leq \int_0^L M_p \left|\delta\kappa\right| dx + \sum_i M_p \left|[\delta\theta]_i\right| \qquad [3.7]$$

The simplest virtual displacement field is the rigid mechanism defined by one conventionally positive kinematic parameter $\delta\theta_0$:

$$\delta\theta(x) = \delta\theta_0 \qquad [3.8]$$

The inequality equation [3.6] is then reduced to:

$$PL\delta\theta_0 \leq M_p \delta\theta_0 \quad \Rightarrow \quad P^+ \leq \frac{M_p}{L} \qquad [3.9]$$

The present reasoning can be generalized to geometrically nonlinear problems (see, for instance, [CHA 09a]).

3.1.2.4. *Discussion on the meaning of the capacity load*

In this simple statically determinate case, both static and kinematic approaches give the same capacity load of the cantilever beam:

$$P \leq P^+ \text{ with } P^+ = M_p / L \qquad [3.10]$$

Note that no constitutive law arguments have been introduced in the reasoning. Only the ultimate limit moment denoted by M_p has been used. The yield design theory gives us information about the maximum strength capacity of this cantilever beam in bending, without answering the complex problem of what would happen beyond this strength limit. It means that designing this cantilever beam with respect to this strength capacity would be safe, whatever the bending constitutive law considered at the sectional level. The yield design theory also does not answer, generally speaking, whether the strength capacity will be reached during the deformation process. Only in the case of perfect plasticity (no hardening/softening

processes) with associated flow rule, we can relate the capacity load with the limit load of the elastic–plastic evolution problem.

3.1.3. *Inelastic (plasticity or continuum damage mechanics) bending-curvature constitutive law*

3.1.3.1. *Softening plasticity moment-curvature constitutive law*

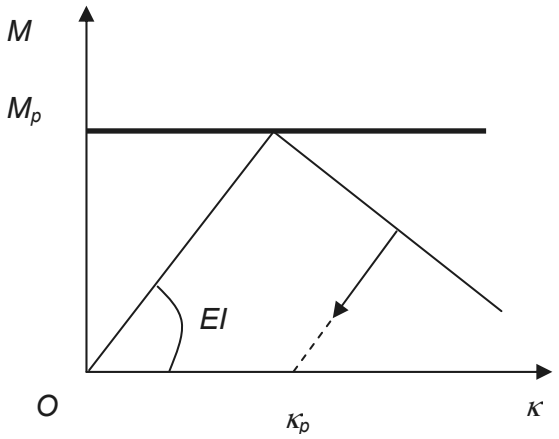

Figure 3.5. *Softening plasticity constitutive law with plastic curvature* κ_p

In this section, we will present two commonly used inelastic constitutive laws, namely the plasticity and the damage constitutive laws. These two constitutive laws can be viewed as two particular cases of the more general laws introduced in Figure 3.4. The bending-curvature elastoplastic model represented in Figure 3.5 is a standard plasticity model with negative hardening (softening). Softening here means that the strength decreased during the inelastic process.

Using the decomposition of the total curvature κ into an elastic part and a plastic part, the moment-elastic curvature relation gives:

$$M = EI\left(\kappa - \kappa_p\right) \qquad [3.11]$$

where the slope of the bending moment-curvature curve is initially equal to EI and κ_p is the plastic curvature (see Figure 3.5). The plasticity yield function f is given by:

$$f\left(M, M^*\right) = |M| - \left(M_p + M^*\right) \quad [3.12]$$

where M^* is an additional moment variable that accounts for the loading history. The plastic curvature rate $\dot{\kappa}_p$ is obtained using the normality rule:

$$\dot{\kappa}_p = \dot{\lambda}\frac{\partial f}{\partial M} = \dot{\lambda}\,\mathrm{sgn}\left(M\right) \quad [3.13]$$

The plastic multiplier $\dot{\lambda}$ must satisfy the complementary conditions:

$$\dot{\lambda} \geq 0, f\left(M, M^*\right) \leq 0, \dot{\lambda} f\left(M, M^*\right) = 0 \quad [3.14]$$

Equation [3.14] can be viewed as the so-called optimality Kuhn–Tucker conditions (see, for instance, [JIR 02] for a discussion on Kuhn–Tucker conditions for inelastic analysis). For monotonic loading with positive or negative bending moments, the plastic multiplier λ is simply related to the absolute value of the plastic curvature $\lambda = \left|\kappa_p\right|$.

The hardening/softening being linear, the following relation holds for the "local" case:

$$M^*\left(\kappa_p\right) = k\left|\kappa_p\right| \quad [3.15]$$

According to the sign of the plastic modulus k, we can get a softening for $k = k^- < 0$ (as shown in Figure 3.5), or a hardening for $k = k^+ > 0$.

Note that the plasticity softening branch is obtained by combining equation [3.11] with equation [3.12] leading to the linear relationship between the bending moment and the curvature, which is expressed in the case of softening plasticity as:

$$M = \frac{EI}{EI + k^-}\left(M_p + k^- \kappa\right) \text{ for } M \geq 0, \text{ and}$$
$$M = \frac{EI}{EI + k^-}\left(-M_p + k^- \kappa\right) \text{ for } M \leq 0 \qquad [3.16]$$

The slope of the softening part of the bending-curvature relationship is then equal to:

$$M'(\kappa) = \frac{EI \times k^-}{EI + k^-} \qquad [3.17]$$

We will show later that such a "local" bending-curvature constitutive law leads to the so-called Wood's paradox where the propagation of the plasticity inelastic zone cannot hold beyond the peak load. To avoid "local" snapback, the following condition should be verified:

$$EI + k^- \geq 0 \qquad [3.18]$$

3.1.3.2. *Softening damage moment-curvature constitutive law*

The continuum damage mechanics (CDM) moment-elastic curvature relation is written as:

$$M = EI(1 - D)\kappa \qquad [3.19]$$

where the slope of the bending moment-curvature curve is initially equal to EI and D is the cross-sectional damage parameter that evolves between 0 and 1 (see Figure 3.6). The damage yield function f is given by:

$$f(\kappa, \kappa^*) = |\ \kappa\ | - (\kappa_Y + \kappa^*) \text{ with } \kappa_Y = \frac{M_p}{EI} \qquad [3.20]$$

where κ^* is an additional curvature variable that accounts for the loading history. The damage rate $\dot{D}$ is obtained using the normality rule:

$$\dot{D} = \dot{\lambda}\frac{\partial f}{\partial |\kappa|} = \dot{\lambda} \qquad [3.21]$$

The plastic multiplier $\dot{\lambda}$ must satisfy the complementary conditions:

$$\dot{\lambda} \geq 0, f\left(\kappa, \kappa^*\right) \leq 0, \dot{\lambda} f\left(\kappa, \kappa^*\right) = 0 \qquad [3.22]$$

The hardening/softening being linear, the following relation holds for the "local" case:

$$\kappa^*(D) = \frac{M_p}{EI} \frac{D}{1 - D - \dfrac{k}{EI + k}} \qquad [3.23]$$

This damage law in the softening part is equivalent to equation [3.16].

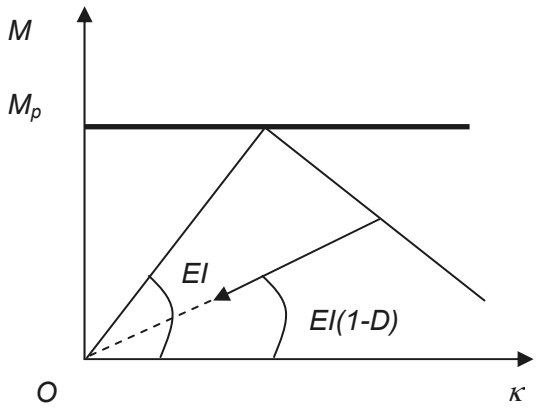

Figure 3.6. *Softening damage constitutive law with damage variable D*

We will also show later that such a "local" bending-curvature constitutive law leads to the so-called Wood's paradox where the propagation of the damage inelastic zone cannot hold beyond the peak load.

As far as no elastic unloading appears during the evolution problem, the two plasticity and damage mechanics models presented above are mathematically equivalent. However, in both cases, these kind of softening models (plasticity or CDM models) cannot be used in such a local format, as the structural problem to be solved, even for the simple cantilever case, is ill-posed, as the inelastic localization zone cannot propagate in both cases. Whatever the softening inelastic model considered, it can be shown that the

beam cannot collapse with such kinds of models, as detailed in the next section.

3.2. Postfailure analysis

3.2.1. *Historical perspective*

This section deals with the propagation of localization in hardening–softening plasticity beams. The propagation of plasticity along a bending beam is studied for a piecewise hardening–softening moment-curvature relationship. Historically, moment-curvature relationships with softening branch were first introduced for reinforced concrete beams [WOO 68]. Wood [WOO 68] did point out some specific difficulties occurring during the solution of the evolution problem for plastic softening models. More precisely, he highlighted the impossibility of the plastic softening beam to flow, if the plastic curvature is assumed to be a continuous function in space, a phenomenon sometimes called Wood's paradox. Hardening–softening plasticity models may concern a wide class of structural mechanics problems. Such simplified models can be useful for the fundamental understanding of bending of structural members at their ultimate state (reinforced concrete members, timber beams, composite members, etc.). The plastic buckling of tubes in bending can be also modeled with a hardening–softening moment-curvature relationship. The bending response of thin-walled members can also experience a softening phenomenon induced by the local buckling phenomenon (see also [CHA 10b]).

Wood's paradox is met for local softening moment-curvature relationship. A non-local (gradient) moment-curvature constitutive relation was introduced by Challamel [CHA 03] associated with some scale effects for controlling the postfailure of softening beams. Non-local models at the beam scale abandon the classical assumption of locality, and admit that the bending moment depends not only on the state variables (curvature, plastic curvature) at that point. Non-local inelastic models (damage or plasticity models) were successfully used as a localization limiter with a regularization effect on softening structural response in the 1980s. The non-local character of the constitutive law, generally introduced through an internal length, is restricted to the loading function (damage loading function or plasticity loading function). Pijaudier-Cabot and Bažant [PIJ 87] first elaborated a non-local damage theory, based on the introduction of the non-locality in the

damage loading function. This theory has the advantage of leaving the initial elastic behavior unaffected, and to control the localization process in the post-peak regime. It is worth mentioning that this idea was already used before to model shear bands. Gradient plasticity models (also called explicit gradient plasticity models) and integral plasticity models may be distinguished. In the case of explicit gradient plasticity models, the plasticity loading function depends on the plastic strain and its derivative, whereas for integral plasticity models, the plasticity loading function is expressed from an integral operator of the plastic strain. Moreover, it can be shown, as in the case of non-local elastic models ([ERI 83], see also [ELI 12]), that some relevant integral plasticity models can be cast in a differential form [ENG 03]. These models are called implicit gradient plasticity models, but can be viewed as particular cases of integral plasticity models with specific weight functions defined as Green's function of the differential operator [ENG 03].

More recently, an implicit gradient plasticity model was used at the beam scale to solve Wood's paradox in beams with moment gradient and without hardening range ([CHA 08b] or [CHA 08c]). The localization phenomenon is controlled by a non-local softening plasticity model, based on a combination of the local and the non-local plastic variables (as suggested by Vermeer and Brinkgreve [VER 94], see also [JIR 02]). It has been shown on simple structural examples that the softening evolution problem was well posed with this non-local constitutive law. In particular, the uniqueness of the evolution problem is clearly obtained in the presence of gradient moment, typically for a cantilever beam solicited by a vertical force. Note that this uniqueness result of the evolution problem would not be obtained for homogeneous structures with constant generalized stress (constant moment) (see [DEB 92] for gradient plasticity models, or more recently for the non-local beam problem [CHA 08c]). The same kind of results (loss of uniqueness with uniform state of stress) has also been recently noticed by Benallal and Marigo [BEN 07] for damage problems. Introduction of some heterogeneities can restore the uniqueness property for these non-local damage problems [CHA 09b]. Most of the presented theoretical results deal with softening media without hardening range. Hence, up to now, very few results are available for hardening–softening non-local plasticity media, even if this configuration is of fundamental importance from an engineering point of view.

3.2.2. *Wood's paradox*

The axial and transversal coordinates are denoted by x and y, respectively, and the transverse deflection is denoted by w. The stiffness of the already cracked beam is denoted by *EI* (the tension stiffening effect is neglected with respect to the specific reinforced concrete behavior). At the end of the beam, the displacement $v = w(L)$ of concentrated force *P* is used to control the loading process. The local moment-curvature relationship (M, κ) considered is bilinear with a linear elastic part and a linear softening part (Figure 3.5). The curvature κ is related to the displacement field thanks to the kinematics $\kappa = -w''$. This model is first considered in a local form, that is standard plasticity model with negative hardening. The non-local extension will be investigated later in the chapter. M_p is the limit elastic moment, and κ_Y is the limit elastic curvature, related through $M_p / \kappa_Y = EI$. In practice, the curvature cannot increase indefinitely and is limited by κ_u (the ultimate admissible curvature). However, such limitation is not taken into account in the present study.

The maximum bending moment occurs at $x = 0$, where the beam is clamped. Plastic rotation starts as soon as the bending moment reaches the plastic bending moment M_p. The maximum elastic displacement at the beam end v_Y and the corresponding load P_Y are given by:

$$v_Y = \frac{M_p L^2}{3EI} \text{ and } P_Y = P^+ = \frac{M_p}{L} \qquad [3.24]$$

For displacement v smaller than v_Y $(v \le v_Y)$, the beam remains elastic and the deflection can be calculated using the elasticity solution. For v greater than v_Y $(v \ge v_Y)$, the plastic regime starts and the beam can be split into an elastic and a plastic domain. The size of the plastic domain is denoted by $l_0 \le L$ (see Figure 3.2). We can introduce the notation of l_0^- for the softening domain and l_0^+ for the hardening domain. Considering only the softening problem in this section, the governing equations in the plastic domain are:

$$x \in \left[0; l_0^-\right]: \quad \begin{cases} EI\left(-w^{-''}(x) - \kappa_p(x)\right) = -P(L-x) \\ \left|\kappa_p(x)\right| = \dfrac{P(L-x) - M_p}{k^-} \end{cases} \qquad [3.25]$$

where w^- denotes the deflection in the plastic region. The elastic adjacent domain is governed by:

$$x \in \left[l_0^-; L\right]: EIw^{+''}(x) = P(L-x) \qquad [3.26]$$

w^+ is the deflection in the elastic region. The boundary conditions can be summarized as:

$$\begin{cases} w^-(0) = 0 \\ w^{-'}(0) = 0 \end{cases} \text{ and } \begin{cases} w^-\left(l_0^-\right) = w^+\left(l_0^-\right) \\ w^{-'}\left(l_0^-\right) = w^{+'}\left(l_0^-\right) \end{cases} \qquad [3.27]$$

The deflection $w(x)$ and the rotation $w'(x)$ must be continuous functions of x (in particular at the intersection of the elastic and the plastic domains). Enforcing that κ_p is also a continuous function of x $(\kappa_p(l_0^-) = 0)$, leads to:

$$\begin{cases} P\left(L - l_0^-\right) = M_p \\ PL \le M_p \end{cases} \Rightarrow \quad l_0^- = 0 \qquad [3.28]$$

This additional assumption gives Wood's paradox. The unloading elastic solution is the only possible solution of the local softening problem, if the plastic curvature is assumed to be a continuous function in space (Figure 3.7). This paradox can also be interpreted as the appearance of plastic curvature increments localized into one single section, leading to the physically non-reasonable phenomenon of failure with zero dissipation. This paradox is well documented in the literature ([WOO 68], [BAZ 76], [ROY 01], [BAZ 03] and [CHA 05d]). A possible way to overcome Wood's paradox is to introduce a non-local plastic softening constitutive law (see [CHA 08b], [CHA 08c]).

Figure 3.7. *Wood's paradox – local softening plasticity models*

Exactly the same reasoning can hold for the local damage softening beam problem (with the constitutive law shown in Figure 3.6, for instance), which is also associated with Wood's paradox. For this kind of constitutive law, a non-local damage softening also allows us to solve this apparent paradox.

3.2.3. *Non-local hardening/softening constitutive law, a variational principle*

For the implicit gradient plasticity model, the non-local plastic curvature $\overline{\kappa_p}$ is defined as the solution of the differential equation:

$$\overline{\kappa_p} - l_c^{\,2}\,\overline{\kappa_p}'' = \kappa_p \qquad [3.29]$$

Therefore, a characteristic length l_c is introduced in the definition of the non-local plastic curvature $\overline{\kappa_p}$. As shown by Eringen [ERI 83] for non-local elasticity, this differential equation clearly shows that the non-local plastic curvature $\overline{\kappa_p}$ is a spatial weighted average of the variable κ_p. This spatial weighted average is calculated on the plastic domain:

$$\overline{\kappa_p}(x) = \int_0^{l_0} G(x,y)\,\kappa_p(y)\,dy \qquad [3.30]$$

where the weighting function $G(x,y)$ is Green's function of the differential system with appropriate boundary conditions. The non-local hardening/softening constitutive law of modulus k ($k = k^+$ for hardening evolutions, $k = k^-$ for softening evolutions) including the associated boundary conditions can be obtained from a variational principle, as already obtained in the rate form for gradient plasticity [MUH 91]. The extension to non-local plasticity is inspired by the micromorphic approach recently developed for elastic and inelastic media, in a consistent thermodynamic framework [FOR 09]. The following energy functional can be chosen:

$$W\left[w,\chi_p\right]=\int_0^L \frac{1}{2}EI\left(-w''-\kappa_p\right)^2+M_p\lambda+\frac{k}{2}\lambda^2+\frac{k}{2}(\zeta-1)\left(\lambda-\overline{\lambda}\right)^2+\frac{k}{2}l_c^{\,2}(\zeta-1)\left(\overline{\lambda}'\right)^2\,dx\;-\;Pw(L)\;\text{ with }\;\lambda=\left|\kappa_p\right| \qquad [3.31]$$

where ζ is a dimensionless parameter that appears in the hardening/softening evolution law. Following a classical procedure, also used for explicit gradient plasticity models (see, for instance, [MUH 91]), the overall domain can be divided into a plastic domain and an elastic domain. The first variation of this energy functional leads to the extremal condition:

$$\begin{aligned}\delta W\left[w,\kappa_p\right]=&\int_0^L EI\left(-w''-\kappa_p\right)\delta\left(-w''\right)\,dx+\int_0^{l_0}-EI\left(-w''-\chi_p\right)\delta\kappa_p+M_p\delta\lambda+\\&k\left(\zeta\lambda+(1-\zeta)\overline{\lambda}\right)\delta\lambda dx-k(\zeta-1)\int_0^{l_0}\left(\lambda-\overline{\lambda}+l_c^{\,2}\overline{\lambda}''\right)\delta\overline{\lambda}+\\&\frac{k}{2}l_c^{\,2}(\zeta-1)\left[\overline{\lambda}'\delta\overline{\lambda}\right]_0^{l_0}-P\delta w(L)=0\end{aligned} \qquad [3.32]$$

Moreover, following a Green-type identity associated with the self-adjoint property of the regularized operator for relevant boundary conditions, and according to the definition of the non-local plastic curvature, the following identity holds:

$$\int_0^{l_0}\left(\lambda-\overline{\lambda}+l_c^{\,2}\overline{\lambda}''\right)\delta\overline{\lambda}dx=\int_0^{l_0}\overline{\left(\lambda-\overline{\lambda}+l_c^{\,2}\overline{\lambda}''\right)}\delta\lambda dx=0 \qquad [3.33]$$

Therefore, using $M\delta\kappa_p = |M|\delta\lambda$, the first variation of the energy functional can be also simplified as:

$$\delta W\left[w,\kappa_p\right] = \int_0^L -M\delta w''\ dx\ -\ \int_0^{l_0} |M| - \left(M_p + M^*\right)\ \delta\lambda dx + \frac{k}{2} l_c^{\,2}\left(\zeta - 1\right)\left[\bar{\lambda}'\delta\bar{\lambda}\right]_0^{l_0} - P\delta w(L) = 0 \qquad [3.34]$$

with the associated constitutive law for the elastic, and the non-local hardening/softening law:

$$M = EI\left(\kappa - \kappa_p\right) \text{and}\, M^* = k\left(\zeta\lambda + \left(1-\zeta\right)\bar{\lambda}\right) \qquad [3.35]$$

The following integration by part can be considered for the deflection:

$$\int_0^L M\delta w''\ dx = \left[M\delta w'\right]_0^L - \left[M'\delta w\right]_0^L + \int_0^L M''\delta w\ dx \text{ with } M = EI\left(w'' - \kappa_p\right) \qquad [3.36]$$

The extremal condition leads to the equilibrium equation and the yield function:

$$M'' = 0 \text{and} |M| = M_p + M^* \qquad [3.37]$$

with the natural boundary conditions:

$$M(L) = 0,\ M'(L) = P,\ w(0) = w'(0),\ \bar{\lambda}'(0) = \bar{\lambda}'(l_0) = \kappa_p(l_0) = 0 \qquad [3.38]$$

The high-order boundary conditions of the non-local plasticity model are included in these equations, and are applied at the boundary of the elastoplastic domain. Considering the higher order boundary conditions at the elastoplastic boundary has the advantage to be variationally and physically motivated. In this case, the non-local plastic variable is calculated over the plastic domain (see equation [3.30] as for most integral-based non-local plasticity models – see also Polizzotto *et al.* [POL 98] for the thermodynamics background of integral-based non-local plasticity models). For instance, a uniform plastic variable in the plastic domain would lead to a

non-local variable that is identical. The introduction of the higher order boundary conditions at the physical boundary of the solid would lead to different results, as detailed in [CHA 10b]. Note that the non-local plastic curvature does not necessarily vanish at the boundary of the elastoplastic domain, whereas the plastic curvature is a continuous variable of the spatial coordinate and vanishes at the boundary between the elastic and the plastic domain.

Note that a different functional was considered in [CHA 08b] leading to the same constitutive behavior with the same boundary conditions [CHA 10b]:

$$W[w,\kappa_p] = \int_0^L \frac{1}{2} EI(-w'' - \kappa_p)^2 + \frac{k}{2}\zeta \; l_c^{\,2}\,\overline{\lambda}'\,\lambda' + M_p\lambda + \frac{k}{2}\overline{\lambda} \;\; \lambda \;\; dx \;\; - Pw(L) \qquad [3.39]$$

The non-local plastic constitutive law appearing from the variational principle is based on a combination of the local plastic curvature and the non-local plastic curvature.

$$M^* = k\tilde{\lambda} \text{ with } \tilde{\lambda} = \zeta\lambda + (1-\zeta)\overline{\lambda} = \overline{\lambda} - \zeta l_c^2 \overline{\lambda}'' \qquad [3.40]$$

Such a combination of local and non-local plastic variables was initially proposed by Vermeer and Brinkgreve [VER 94] for softening evolutions. In the present case, this model can also be written in the form of a differential equation:

$$M^* - l_c^{\,2} M^{*''} = k[\lambda - \zeta\, l_c^{\,2}\lambda''] \qquad [3.41]$$

In the case of the cantilever beam, it is worth mentioning that the non-local differential format looks like a gradient plasticity model:

$$M'' = 0 \;\; \Rightarrow \;\; M^{*''} = 0 \;\; \Rightarrow \;\; M^* = k[\lambda - \zeta\, l_c^{\,2}\lambda''] \qquad [3.42]$$

However, the boundary conditions written in equation [3.38] for the non-local plastic curvatures are different from the boundary conditions of the usual gradient plasticity models dealing with only the derivative of

the plastic curvatures. Equation [3.41] is the plasticity generalization of the mixed elastic constitutive law investigated for a one-dimensional non-local elastic bar ([CHA 09d]; see also [AIF 03] or more recently [AIF 11] and [ELI 12]):

$$\sigma - l_c^{\,2}\sigma'' = E\left[\varepsilon - \zeta l_c^2 \varepsilon''\right] \qquad [3.43]$$

where σ and ε are the uniaxial stress and the uniaxial strain, respectively. Equation [3.43] gives satisfactory results for a dispersive wave equation of lattice models.

The sign of ζ controls the well-posedness of the plasticity evolution problem for both hardening and softening behaviors (as shown in [CHA 08c]). Typically, ζ can be understood as a regularization parameter. For hardening evolutions, ζ^+ has to be positive, leading to the non-local hardening constitutive law:

$$M^* - l_c^{\,2} M^{*''} = k^+\left[\lambda - a^2\lambda''\right] \text{ with } \zeta^+ = \left(\frac{a}{l_c}\right)^2 \qquad [3.44]$$

This model comprises the purely non-local plastic softening model $(a = 0)$, and the gradient plasticity model for hardening evolution $(l_c = 0)$. The differential format equation [3.44] has been already used in the past in structural engineering for some specific applications:

$$M - l_c^{\,2} M'' = EI\left[\kappa - a^2\kappa''\right] \text{ or } p - l_c^{\,2} p'' = k_0\left(y - a^2 y''\right) \qquad [3.45]$$

Interestingly, the moment-curvature (M, κ) constitutive model equation [3.45] has been proposed for applications in composite beams with imperfect connections between the two elements (such as steel-concrete composite structures, timber-concrete elements and layered wood systems with interlayer slip) ([GIR 07], [CHA 11a], [CHA 11b]). Note the similarity with the non-local bending constitutive law recently studied for the elastic problems ([CHA 08a], [ZHA 10]). As recently shown by di Paola *et al*. [DIP 09], models of elastic foundation can also involve some non-locality. In fact, the soil–structure interaction model of Reissner [REI 58] is also based

on the differential equation [3.33], where p and y are the foundation reaction and the deflection, respectively (see also [CHA 10c]).

On the opposite, for softening evolutions, ζ^- has to take negative values [CHA 08c], leading to the non-local softening constitutive law:

$$M^* - l_c^2 M^{*''} = k^- \left[\lambda + a^2 \lambda'' \right] \text{ with } \zeta^- = -\left(\frac{a}{l_c} \right)^2 \quad [3.46]$$

A relevant choice often assumed in the softening constitutive behavior is to assume that a is equal to l_c ($\zeta^- = -1$) (see also [CHA 08c]). In the following, a local hardening moment-curvature relationship is incorporated in the model, leading to a well-posed evolution problem. In fact, it is not necessary to introduce some non-locality in the hardening range from a mathematical point of view. However, it is also possible to introduce some non-locality during hardening, to introduce some scale effects in the hardening range. For the non-local hardening plasticity model, M^* is related to the combined non-local plastic curvature variable $\tilde{\lambda}$ through the linear model:

$$M^* = k^+ \tilde{\lambda} \text{ with } \tilde{\lambda} = \overline{\lambda} - a^2 \overline{\lambda}'' \quad [3.47]$$

Introducing the combined non-local plastic curvature into the loading function leads to a differential equation:

$$\overline{\lambda} - a^2 \overline{\lambda}'' = \frac{P(L-x) - M_p}{k^+} \quad [3.48]$$

The general solution of this differential equation is written as:

$$x \in \left[0; l_0^+ \right] : \overline{\lambda}(x) = A \cosh \frac{x}{a} + B \sinh \frac{x}{a} + \frac{P(L-x) - M_p}{k^+} \quad [3.49]$$

with the boundary conditions obtained from the variational principle:

$$\lambda\left(l_0^+\right) = 0, \overline{\lambda}'\left(l_0^+\right) = 0 \text{ and } \overline{\lambda}'(0) = 0, \quad [3.50]$$

The nonlinear system of three equations with three unknowns A, B and l_0^+ is finally obtained:

$$\begin{cases} A\left(1-\left(\frac{l_c}{a}\right)^2\right)\cosh\frac{l_0^+}{a}+B\left(1-\left(\frac{l_c}{a}\right)^2\right)\sinh\frac{l_0^+}{a}+\frac{P\left(L-l_0^+\right)-M_p}{k^+}=0 \\ \frac{A}{a}\sinh\frac{l_0^+}{l_c}+\frac{B}{a}\cosh\frac{l_0^+}{l_c}-\frac{P}{k^+}=0 \\ \frac{B}{a}-\frac{P}{k^+}=0 \end{cases} \quad [3.51]$$

The following dimensionless parameters may be introduced as:

$$\beta=\left(1-\frac{P_Y}{P}\right)\frac{L}{l_c}\geq 0 \text{ and } \xi=\frac{l_0^+}{l_c}\geq 0 \quad [3.52]$$

leading to the localization relation:

$$\beta=\xi+\frac{1-\zeta}{\zeta}\frac{\cosh\xi-1}{\sinh\xi} \quad [3.53]$$

The plastic zone ξ versus the loading parameter β is shown in Figure 3.8 and is parameterized by the dimensionless parameter ζ.

Figure 3.8. *Evolution of the plastic zone ξ versus the loading parameter β – non-local hardening plasticity model: $\zeta > 0$*

The gradient plasticity model (in the hardening range) is recovered from this relationship as an asymptotic law ($l_c \to 0$ in equation [3.53]):

$$\zeta \to \infty \quad \Rightarrow \quad \beta = \xi - \frac{\cosh \xi - 1}{\sinh \xi} \qquad [3.54]$$

The width of the plastic zone associated with the non-local models is larger than the reference width of the local model, for ζ larger than unity, whereas this width is smaller than the one of the local model for ζ smaller than unity. The local hardening plastic zone relation is obtained by setting $\zeta = 1$.

3.2.4. *Non-local softening constitutive law: application to the cantilever beam*

For the non-local softening plasticity model, M^* is related to the combined non-local plastic curvature variable $\tilde{\lambda}$ through the linear model (see, for instance, equation [3.46]):

$$M^* = k^- \tilde{\lambda} \text{ with } \tilde{\lambda} = \overline{\lambda} + a^2 \overline{\lambda}'' \qquad [3.55]$$

Introducing the combined non-local plastic curvature (with $a = l_c$) into the loading function leads to a linear differential equation:

$$\overline{\lambda} + l_c^{\,2} \overline{\lambda}'' = \frac{P(L-x) - M_p}{k^-} \qquad [3.56]$$

The general solution of this differential equation is written as:

$$x \in \left[0; l_0^-\right] : \overline{\lambda}(x) = A \cos \frac{x}{l_c} + B \sin \frac{x}{l_c} + \frac{P(L-x) - M_p}{k^-} \qquad [3.57]$$

with the boundary conditions obtained from the variational principle:

$$\lambda(l_0) = 0 \; \overline{\lambda}'\left(l_0^-\right) = 0 \text{ and } \overline{\lambda}'(0) = 0 \qquad [3.58]$$

The nonlinear system of three equations with three unknowns A, B and l_0^- is finally obtained:

$$\begin{cases} 2A\cos\dfrac{l_0^-}{l_c}+2B\sin\dfrac{l_0^-}{l_c}+\dfrac{P\left(L-l_0^-\right)-M_p}{k^-}=0 \\ -\dfrac{A}{l_c}\sin\dfrac{l_0^-}{l_c}+\dfrac{B}{l_c}\cos\dfrac{l_0^-}{l_c}-\dfrac{P}{k^-}=0 \\ \dfrac{B}{l_c}-\dfrac{P}{k^-}=0 \end{cases} \quad [3.59]$$

The following dimensionless parameters may be introduced as:

$$\beta=\left(1-\frac{P_Y}{P}\right)\frac{L}{l_c}\le 0 \text{ and } \xi=\frac{l_0^-}{l_c}\ge 0 \quad [3.60]$$

and the load-plastic zone relationship is finally written as:

$$\beta=\xi-2\frac{1-\cos\xi}{\sin\xi} \text{ for } \sin(\xi)\neq 0 \quad [3.61]$$

In other words, Wood's paradox is overcome for the non-local softening cantilever case and uniqueness prevails for the softening evolution considered in the chapter. Figure 3.9 shows the evolution of the plastic zone ξ in terms of the positive dimensionless parameter $|\beta|$.

The parameter $|\beta|$ varies between 0 and tends toward an infinite value when P tends toward zero. Moreover, the size of the plastic zone tends toward an asymptotic value for large values of $|\beta|$ (and sufficiently small values of P). $\xi_0=\pi$ is the limiting value of the maximum width of the localization zone. The plastic zone evolves from a transitory regime toward a material (or section) scale that does not depend anymore on the loading range. The results reveal that the evolution tends toward one unique solution with a finite energy dissipation that depends only on the characteristic length. The maximum width of the localization zone l_0^- directly depends on the characteristic length of the non-local model via the relation $l_0^-=\pi l_c$ (for

the cantilever beam). The determination of the characteristic length l_c (or the maximum width of the localization zone l_0^-) is related to the question of the finite-length hinge model, a central question of the present non-local model. Wood [WOO 68], inspired by the works of Barnard and Johnson [BAR 65], suggested the term of discontinuity length. Many papers have been published on the experimental or theoretical investigation of such a length [WOO 68, BAZ 76, BAZ 87, PAU 92, BAZ 03 LEE 09] for reinforced concrete beams. It is generally acknowledged that the value of l_c (or the maximum localization zone l_0^-) must be related to the depth of the cross-section h. The rigid body moment-rotation mechanism detailed in [DAN 08] or [HAS 09] may be used to calibrate this characteristic length for reinforced concrete beams. Therefore, it is recommended that the maximum width of the localization zone l_0^- is chosen in the order of magnitude of the depth of the cross-section h. This implies for the cantilever beam that the characteristic length l_c is in the order of magnitude of h/π. This theoretical aspect certainly merits some further investigations. However, the existence of the finite size fracture process zone leads to the specific structural size effect.

Figure 3.9. *Evolution of the plastic zone ξ versus the loading parameter β – non-local hardening plasticity model: $\zeta > 0$*

The deflection in the plastic zone $x \in \left[0; l_0^-\right]$ is obtained by integrating twice the elastic curvature:

$$w^-(x) = \left(\frac{PL}{EI} + \frac{PL - M_p}{k^-}\right)\frac{x^2}{2} - \left(\frac{P}{EI} + \frac{P}{k^-}\right)\frac{x^3}{6} - 2\frac{Pl_c^{\,3}}{k^-}\frac{\cos\left(\frac{l_0^-}{l_c}\right) - 1}{\sin\left(\frac{l_0^-}{l_c}\right)}\left[\cos\left(\frac{x}{l_c}\right) - 1\right] - 2\frac{Pl_c^{\,3}}{k^-}\left[\sin\left(\frac{x}{l_c}\right) - \frac{x}{l_c}\right] \quad [3.62]$$

The deflection in the elastic zone $x \in \left[l_0^-; L\right]$ is derived from the continuity condition given by equation [3.27]:

$$w^+(x) = \frac{PLx^2}{2EI} - \frac{Px^3}{6EI} + \left[w^{-\prime}\left(l_0^-\right) - \frac{PLl_0^-}{EI} + \frac{P\left(l_0^-\right)^2}{2EI}\right]x + \left[w^-\left(l_0^-\right) - \left(l_0^-\right)w^{-\prime}\left(l_0^-\right) + \frac{PL\left(l_0^-\right)^2}{2EI} - \frac{P\left(l_0^-\right)^3}{3EI}\right] \quad [3.63]$$

Figure 3.10 shows the resolution of Wood's paradox with the non-local softening plastic model. After the peak load, the softening plasticity propagates along the beam, leading to the global softening phenomenon.

The influence of the characteristic length, which controls the propagation of the localization zone, is shown in Figure 3.11.

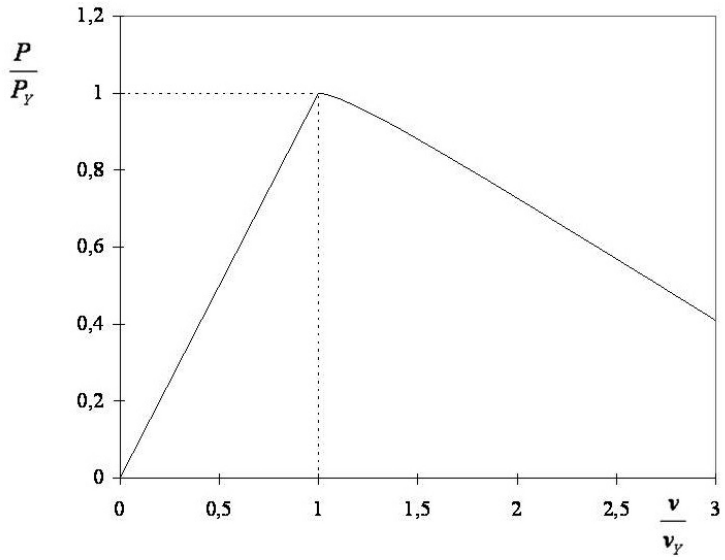

Figure 3.10. *Response of the elastoplastic non-local softening beam;* $\frac{EI}{k^-} = -5;\ \frac{l_c}{L} = 0.1$

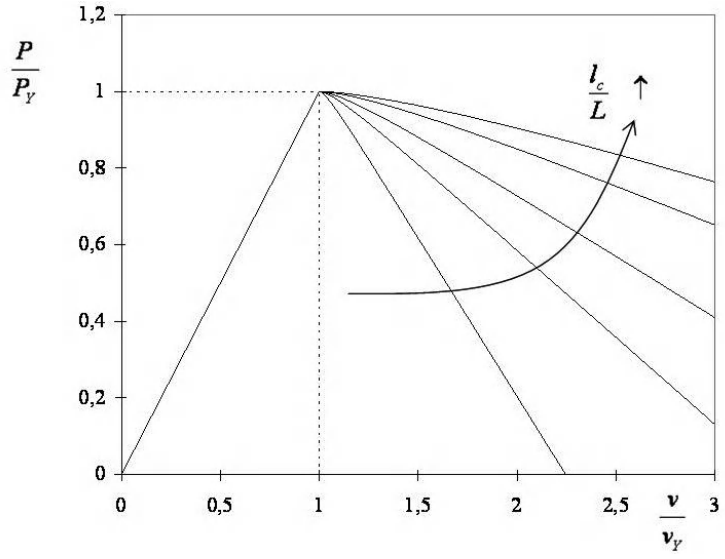

Figure 3.11. *Influence of the characteristic length on the softening response of the elastoplastic beam* P / P_Y *versus* v / v_Y*;* $\frac{EI}{k^-} = -5$

The global ductility increases as the stiffness ratio $|EI/k|$ increases, or the length ratio l_c/L increases. Evolution of the plastic zone during the plastic softening process is shown in Figure 3.12.

Figure 3.12. *Evolution of the plastic zone during the softening process; deflection of the cantilever beam;* $\frac{EI}{k^-} = -5$; $\frac{l_c}{L} = 0.1$

3.2.5. *Some other structural cases – the simply supported beam*

Another simple statically determinate model is the simply supported beam under central concentrated load (Figure 3.13). We will show that this case can be analyzed from the cantilever case. More specifically, the plastic zone parameterized by the length l_0 is related to the loading parameter through a similar law. For symmetrical reasons, the bending moment is symmetrical with respect to the central axis (bending moment is positive in this case):

$$M(x) = \frac{PL}{4} - \frac{P}{2}|x| \text{ with } P \geq 0 \text{ and } x \in \left[-\frac{L}{2}; \frac{L}{2}\right] \qquad [3.64]$$

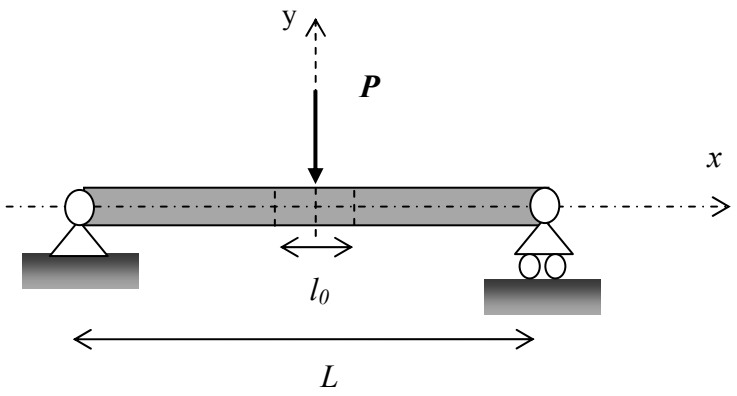

Figure 3.13. *Simply supported beam*

Using symmetrical considerations, it is sufficient to analyze half a structure, leading to the differential equation for the non-local plastic curvature:

$$\overline{\lambda} + l_c^{\,2}\overline{\lambda}'' = \frac{\frac{PL}{4} - \frac{P}{2}x - M_p}{k^-} \text{ with } x \in \left[0; \frac{l_0}{2}\right] \qquad [3.65]$$

In this case, and using symmetrical arguments, the boundary conditions are written as:

$$\lambda\left(\frac{l_0}{2}\right) = 0, \overline{\lambda}'\left(\frac{l_0}{2}\right) = 0 \text{ and } \overline{\lambda}'(0) = 0 \qquad [3.66]$$

Let us introduce the change of variable:

$$\hat{P} = \frac{P}{2}, \hat{L} = \frac{L}{2}, \hat{l}_0 = \frac{l_0}{2}, \hat{P}_Y = \frac{M_p}{\hat{L}}, \hat{\xi} = \frac{\hat{l}_0}{l_c} \text{ and } \hat{\beta} = \left(1 - \frac{\hat{P}_Y}{\hat{P}}\right)\frac{\hat{L}}{l_c} \qquad [3.67]$$

The new differential system is obtained:

$$\overline{\lambda} + l_c^{\,2}\overline{\lambda}'' = \frac{\hat{P}\left(\hat{L} - x\right) - M_p}{k^-} \text{ with } \lambda\left(\hat{l}_0\right) = 0, \overline{\lambda}'\left(\hat{l}_0\right) = 0 \text{ and } \overline{\lambda}'(0) = 0 \qquad [3.68]$$

We recognize the cantilever problem with the new variables introduced in equation [3.67]. The load-plastic zone relationship is given by equation [3.61] corrected with the new variables:

$$\hat{\beta} = \hat{\xi} - 2\frac{1-\cos\hat{\xi}}{\sin\hat{\xi}} \text{ for } \sin\left(\hat{\xi}\right) \neq 0 \qquad [3.69]$$

Figure 3.9 obtained for the cantilever beam is still valid for the simply supported beam (with the new notation of equation [3.67]). However, in the case of a simply supported beam, the boundary conditions dealing with the displacement function differ from the one of the cantilever case:

$$w\left(\hat{L}\right) = 0 \text{ and } w'(0) = 0 \qquad [3.70]$$

This means that the solution of the cantilever case can be used for the rotation function, but not for the displacement function. The rotation in the plastic zone is obtained from:

$$\theta^{-}(x) = -\hat{P}\left(\frac{1}{EI} + \frac{1}{k^{-}}\right)\left(\hat{L}x - \frac{x^2}{2}\right) + \frac{M_p}{k^{-}}x - 2\frac{\hat{P}l_c^{\,2}}{k^{-}}\frac{\cos\left(\frac{\hat{l}_0}{l_c}\right)-1}{\sin\left(\frac{\hat{l}_0}{l_c}\right)}\sin\left(\frac{x}{l_c}\right)$$
$$+ 2\frac{\hat{P}l_c^{\,2}}{k^{-}}\left[\cos\left(\frac{x}{l_c}\right)-1\right] \text{ if } x \in \left[0;\hat{l}_0\right] \qquad [3.71]$$

The rotation in the elastic zone is derived from the continuity of the rotation along the elastoplastic boundary:

$$\theta^{+}(x) = -\frac{\hat{P}\hat{L}}{EI}\left(x - \hat{l}_0\right) + \frac{\hat{P}}{2EI}\left(x^2 - \hat{l}_0^{\,2}\right) + \theta^{-}\left(\hat{l}_0\right) \text{ if } x \in \left[\hat{l}_0;\hat{L}\right] \qquad [3.72]$$

The deflection in the elastic domain can be written as:

$$w^{+}(x) = -\frac{\hat{P}}{EI}\left(\hat{L}\frac{x^2}{2} - \frac{x^3}{6} - \frac{\hat{L}^3}{3}\right) - \left(x - \hat{L}\right)\left(\frac{\hat{P}\hat{l}_0^{\,2}}{2EI} - \frac{\hat{P}\hat{L}\hat{l}_0}{EI} - \theta^{-}\left(\hat{l}_0\right)\right)$$

$$\text{if } x \in \left[\hat{l}_0; \hat{L}\right] \qquad [3.73]$$

3.2.6. *Postfailure of reinforced concrete beams under distributed lateral load*

The failure process of the cantilever beam solicited by its own weight (or under uniform distributed lateral load) can also be studied (Figure 3.14).

In this case, the bending moment varies no more as a linear function, but as a parabolic function:

$$M(x) = -\frac{q}{2}(L - x)^2 \text{ with } q \geq 0 \text{ and } x \in [0; L] \qquad [3.74]$$

The differential equation for the non-local plastic curvature is now written as:

$$\overline{\lambda} + l_c^{\,2}\overline{\lambda}'' = \frac{\frac{q}{2}(L - x)^2 - M_p}{k^{-}} \qquad [3.75]$$

The solution of such a differential equation is obtained from:

$$x \in [0; l_0]: \overline{\lambda}(x) = A\cos\frac{x}{l_c} + B\sin\frac{x}{l_c} + \frac{q}{2k^{-}}(L - x)^2 - \frac{M_p}{k^{-}} - \frac{q l_c^{\,2}}{k^{-}} \qquad [3.76]$$

with the three constants (A, B, l_0) identified from the three boundary conditions given by equation [3.68].

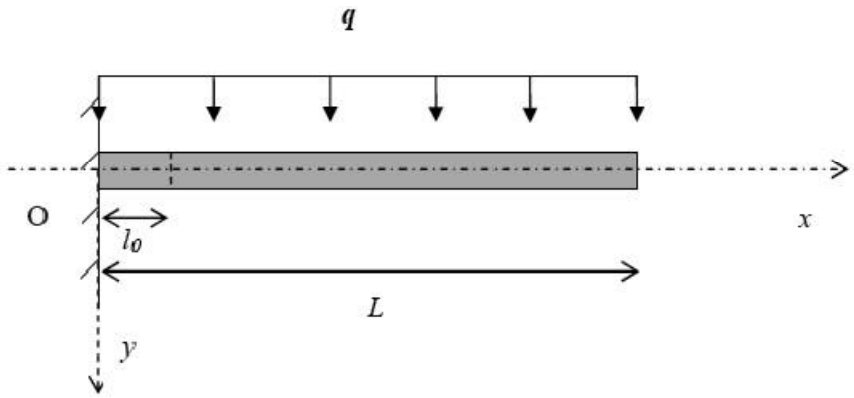

Figure 3.14. *Cantilever beam under distributed load*

The following dimensionless parameters may be introduced as:

$$\beta = \left(1 - \frac{q_Y}{q}\right)\frac{L}{l_c} \le 0, \xi = \frac{l_0}{l_c}, l_c^* = \frac{l_c}{L} \text{ with } q_Y = \frac{2M_p}{L^2} \qquad [3.77]$$

and the load-plastic zone relationship is finally written as (see Figure 3.16):

$$\beta = -4\frac{1 + \left(l_c^* \xi - 1\right)\cos\xi}{\sin\xi} - l_c^* \xi^2 + 2\xi + 4l_c^* \text{ for} \sin\left(\xi\right) \neq 0 \qquad [3.78]$$

Another simple statically determinate model is the simply supported beam under uniform distributed lateral load (Figure 3.15). We will show that this case is not analogous to the cantilever case under distributed load. For symmetrical reasons, the bending moment is symmetric with respect to the central axis (bending moment is positive in this case):

$$M\left(x\right) = \frac{qL^2}{8} - \frac{qx^2}{2} \text{ with } x \in \left[-\frac{L}{2}; \frac{L}{2}\right] \qquad [3.79]$$

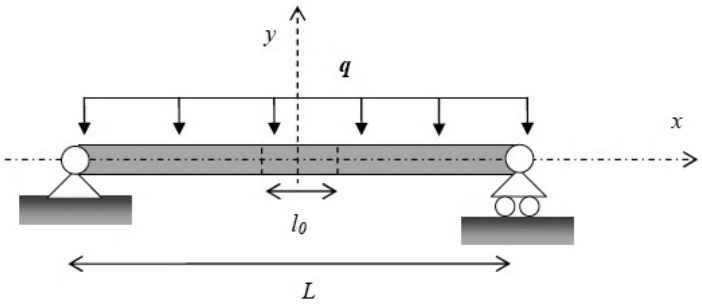

Figure 3.15. *Simply supported beam under distributed load*

Using symmetrical considerations, it is sufficient to analyze half a structure, leading to the differential equation for the non-local plastic curvature:

$$\overline{\lambda} + l_c^2 \overline{\lambda}'' = \frac{\frac{qL^2}{8} - \frac{qx^2}{2} - M_p}{k^-} \text{ with } \lambda\left(\frac{l_0}{2}\right) = 0, \overline{\lambda}'\left(\frac{l_0}{2}\right) = 0 \text{ and } \overline{\lambda}'(0) = 0 \quad [3.80]$$

The following change of variable can be adopted:

$$\hat{L} = \frac{L}{2}, \hat{l}_0 = \frac{l_0}{2}, \hat{q}_Y = \frac{2M_p}{\hat{L}^2}, \hat{\xi} = \frac{\hat{l}_0}{l_c}, \hat{l}_c^* = \frac{l_c}{\hat{L}} \text{ and } \hat{\beta} = \left(1 - \frac{\hat{q}_Y}{q}\right)\frac{\hat{L}}{l_c} \quad [3.81]$$

The new differential system is obtained:

$$\overline{\lambda} + l_c^2 \overline{\lambda}'' = \frac{\frac{q}{2}\left(\hat{L}^2 - x^2\right) - M_p}{k^-} \text{ with } \lambda\left(\hat{l}_0\right) = 0, \overline{\lambda}'\left(\hat{l}_0\right) = 0 \text{ and } \overline{\lambda}'(0) = 0 \quad [3.82]$$

This system cannot be cast in the form given by equation [3.78], and there is no equivalence between the cantilever case and the simply supported beam in case of uniform loading. The load-plastic zone relationship is finally written as (see Figure 3.16):

$$\hat{\beta} = 4\hat{\xi}\hat{l}_c^* \frac{\cos\hat{\xi}}{\sin\hat{\xi}} + \hat{l}_c^* \hat{\xi}^2 - 4\hat{l}_c^* \text{ for } \sin(\xi) \neq 0 \quad [3.83]$$

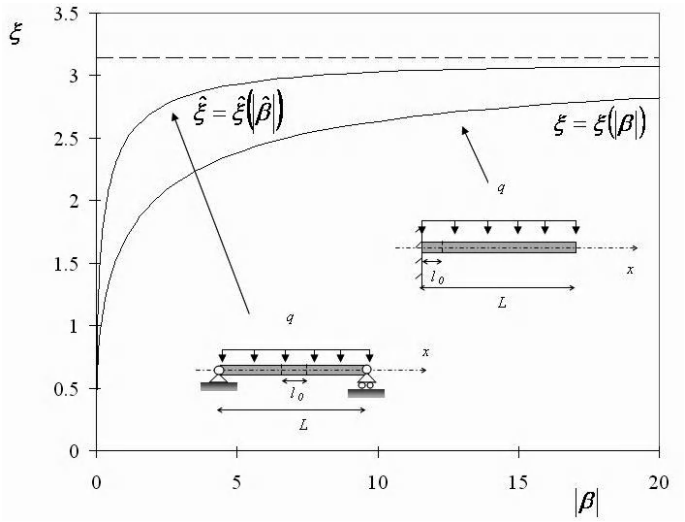

Figure 3.16. *Evolution of the plastic zone* ξ *(or* $\hat{\xi}$*) versus the loading parameter* β *(or* $\hat{\beta}$*) – beam under distributed load –* $l_c^* = 0.1$

To summarize, the numerical description of the postfailure of reinforced concrete members needs the use of non-local mechanics theory (in this chapter, non-local plasticity mechanics has been used). However, the same arguments would be needed for the bending analysis of damage beams, where non-local damage mechanics models are needed in presence of softening in order to avoid Wood's paradox (see, for instance, [CHA 10a]).

The bending damage law can be generalized in a non-local format by correcting the damage loading function, as suggested by Pijaudier-Cabot and Bažant [PIJ 87]:

$$M = EI(1-D)\ \ \kappa \text{ and } f(\kappa, \kappa^*) = \left| \ \overline{\kappa} \ \right| - (\kappa_Y + \kappa^*) \qquad [3.84]$$

where the non-local variable is the non-local curvature-driven variable $\overline{\kappa}$. But other kinds of variationally based damage models can also be used, such as [CHA 10a]:

$$M = EI\left(1-\overline{D}\right)\ \ \kappa \text{ and } f\left(Y, Y^*\right) = \overline{Y} - \left(Y_Y + Y^*\right) \text{ with } Y = \frac{1}{2} EI\kappa^2 \qquad [3.85]$$

where $\overline{Y}$ is the non-local damage energy release rate at the cross-sectional level. However, in the following, we will be mainly concerned with the yield characterization of the reinforced concrete cross-section before softening, and non-locality in this case is not necessary to be introduced.

3.3. Constitutive laws for steel and concrete

3.3.1. *Steel behavior*

3.3.1.1. *Design values for steel at Ultimate Limit State*

The design yield strength of reinforcement f_{yd} also denoted by f_{su}, is related to the characteristic yield strength of reinforcement f_{yk} through the partial factor γ_s for reinforcing steel as:

$$f_{su} = f_{yd} = \frac{f_{yk}}{\gamma_s} \qquad [3.86]$$

γ_s is equal to *1.15*, except for combinations with accidental actions (for combinations with accidental action, γ_s is equal to unity). In the following, we will mainly use the value $\gamma_s = 1.15$. As usual (see also the SLS), the Young's modulus of steel E_s is taken equal to 200,000 MPa.

As an example, let us consider a reinforced concrete section composed of *B500B* steel bars. In the nomenclature of steel classification *B500B*, the first *B* stands for steel for reinforced concrete. The next three digits represent the specified characteristic value of upper yield strength f_{yk} = 500 MPa. The last symbol *B* stands for ductility class.

3.3.1.2. *Perfect elastoplasticity*

Two possibilities are offered to model the steel behavior in *Eurocode 2*. The first possibility is based on perfect plasticity (hardening neglected – see Figure 3.17).

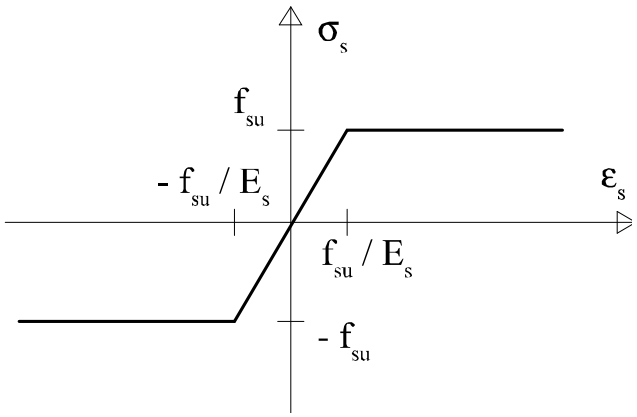

Figure 3.17. *Perfect elastoplasticity diagram for the steel reinforcements*

Even if the old French rules, such as *Béton Armé aux Etats Limites* (BAEL) dated 1983 and modified in 1999 (or some other international rules such as the ACI design rules) introduced a limitation of the tensile strain (typically ε_{ud} = 10‰), the new rules – *Eurocode* 2 do not limit the strain in the steel reinforcement. The steel in the reinforcement is modeled with a perfect plasticity rule without any limitation in strain. It also means that the pivot *A* concept does not exist anymore with such a modeling of the steel reinforcement. For monotonic loading, the stress–strain relationship of the steel behavior is then given by:

$$\begin{aligned} &\sigma_s = E_s \varepsilon_s \text{ for} \left| \ \varepsilon_s \ \right| \le \varepsilon_{su} = \frac{f_{su}}{E_s} \text{and} \\ &\sigma_s = f_{su} \operatorname{sgn}\left(\varepsilon_s\right) \text{for} \left| \ \varepsilon_s \ \right| \ge \varepsilon_{su} = \frac{f_{su}}{E_s} \end{aligned} \qquad [3.87]$$

where f_{su}, also denoted by f_{yd}, is the design yield strength of reinforcement.

3.3.1.3. *Hardening elastoplasticity*

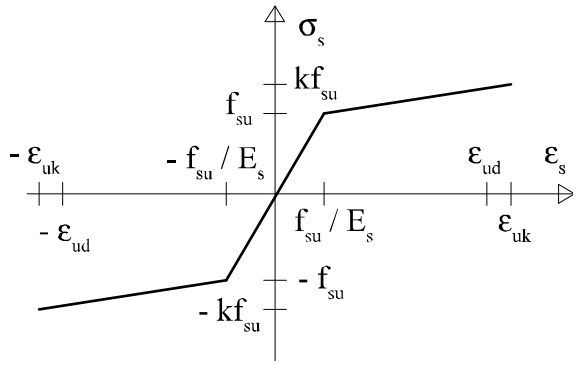

Figure 3.18. *Elastoplasticity with linear hardening for the steel reinforcements*

It is correct to take into account the steel hardening in *Eurocode* 2 (see Figure 3.18). In this case, the characteristic ultimate limit strain is bounded ε_{uk} (typically ε_{uk} = 50‰). The design ultimate limit strain is calculated from the characteristic strain of reinforcement at maximum load through a partial coefficient:

$$\varepsilon_{ud} = 0.9\varepsilon_{uk} \qquad [3.88]$$

For monotonic loading, the stress–strain law can be written as a piecewise linear law:

$$\sigma_s = m\varepsilon_s + m' \qquad [3.89]$$

where value of the parameters (m,m') depends on the branch considered. These parameters can be expressed by:

$$\begin{aligned} &m = q \text{ and } m' = q' \text{ for } \varepsilon_s \in [\varepsilon_{su};\varepsilon_{ud}] \\ &m = E_s \text{ and } m' = 0 \text{ for } \varepsilon_s \in [-\varepsilon_{su};\varepsilon_{su}] \\ &m = q \text{ and } m' = -q' \text{ for } \varepsilon_s \in [-\varepsilon_{ud};-\varepsilon_{su}] \end{aligned} \qquad [3.90]$$

Only the strain inside the interval $\left|\varepsilon_s\right| \le \varepsilon_{ud}$ is allowed. The plasticity hardening parameters are defined below:

$$q = \frac{(k-1) f_{su}}{\varepsilon_{uk} - \varepsilon_{su}}, q' = f_{su}\left(1 - \frac{q}{E_s}\right) \text{ and } \varepsilon_{su} = \frac{f_{su}}{E_s} \quad [3.91]$$

The linear branches have been calculated from continuity with the elastic branches, with the following characteristic points:

$$\sigma_s(\varepsilon_{su}) = f_{su},\ \sigma_s(\varepsilon_{uk}) = kf_{su},\ \sigma_s(-\varepsilon_{su}) = -f_{su} \text{ and } \sigma_s(-\varepsilon_{uk}) = -kf_{su} \quad [3.92]$$

The coefficient k depends on the steel ductility, and is given in *Eurocode 2* as:

k = 1.05 for steel with standard ductility,
k = 1.08 for steel with high ductility. [3.93]

Note that we do not focus on cycling behavior with possible unloading–reloading, and then, the type of hardening (isotropic, kinematic or mixed hardening) is not of importance for the design of the reinforced concrete section, at least in the static range.

With this constitutive law, the Pivot *A* is defined for the maximum design ultimate strain in the tensile steel reinforcement as:

$$\varepsilon_s = \varepsilon_{ud} \text{ and } \sigma_s = q\varepsilon_{ud} + q' < kf_{su} \quad [3.94]$$

As a result using Eurocode 2, Pivot *A* is less present than Pivot *B*, due to the allowed large ductility of steel, a significant change with respect to the older European rules, for instance. Typically, $\varepsilon_{ud} = 45‰$ is allowed in Eurocode 2, whereas $\varepsilon_{ud} = 10‰$ was the limited value in the old French rules (*Béton Armé aux Etats Limites BAEL 83* which was modified in 1999).

It can be interesting also to have some other material characteristics for the steel reinforcement, such as the density $\rho = 7{,}850$ kg/m^3, or the thermic dilatation coefficient $\alpha = 10^{-5}$ K^{-1} (the dilatation coefficient for the steel and the concrete part of the reinforced concrete section are almost identical).

3.3.1.4. *Numerical application*

As an example, for steel reinforcement bars made of *B500B* steel bars, the steel material parameters at the ULS are:

$$f_{su} = \frac{f_{yk}}{\gamma_s} = \frac{500}{1.15} = 434.783 \text{ MPa}; k = 1.08; E_s = 200,000 \text{ MPa}; \varepsilon_{ud} = 45‰;$$
$$q = \frac{(1.08-1)\times 434.783}{\frac{50}{1000} - \frac{434.783}{200000}} = 727.273 \text{ MPa and } q' = 434.783 \times \left(1 - \frac{727.273}{200000}\right)$$
$$= 433.202 \text{ MPa} \qquad [3.95]$$

3.3.2. *Concrete behavior*

3.3.2.1. *Design values for concrete at Ultimate Limit State*

Concrete has complex unsymmetrical material responses in tension and in compression, both from the strength and the ductility properties (see Figure 3.19).

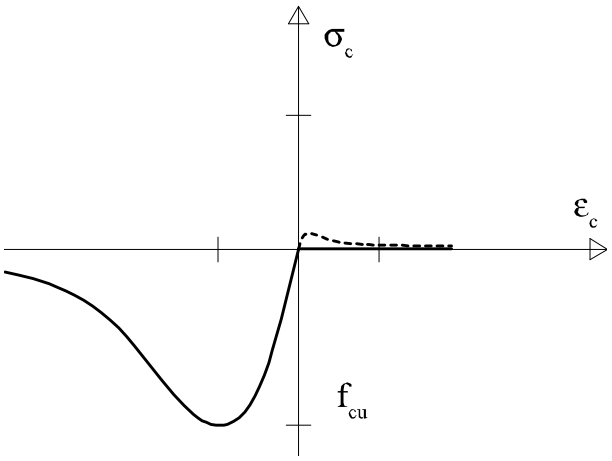

Figure 3.19. *Unsymmetrical response of concrete in uniaxial tension and compression*

As for the SLS, the tension strength of concrete will be neglected at ULS.

The design compression yield strength of concrete f_{cd}, also denoted by f_{cu}, is related to the characteristic yield strength of concrete f_{ck} through the partial factor γ_c for concrete as:

$$f_{cu} = f_{cd} = -\alpha_{cc} \frac{f_{ck}}{\gamma_c} \qquad [3.96]$$

γ_c is equal to 1.5, except for the combination with accidental actions combinations (for combination with accidental action, γ_s is equal to 1.2). α_{cc} is a reducing coefficient for including the time-dependent cracking process at large stress values. Typically, this coefficient α_{cc} varies between 0.8 and 1, and is available in the national Annexes of Eurocode 2 for each country.

This coefficient was initially included to take into account the possible creep failure phenomenon (tertiary creep) for large stress values, typically for compressive stress values higher than 85% of the instantaneous compressive strength. This time-dependent phenomenon has been experimentally studied in details by Rüsch [RUS 60], and recently modeled with a simple creep damage model [CHA 05a]. It is shown in [CHA 05a] or [CHA 05c] that the creep failure phenomenon is associated with the existence of a limit point in the stress–strain diagram at a very slow loading rate, and then creep failure is interpreted as a loss of equilibrium solution associated with the constitutive law.

In the French National Annexes (each annex has different rules), this coefficient is equal to $\alpha_{cc} = 1$ in most design cases (for building design, for instance) except, for instance, in bridge design, or for prestressed design. For bridge design, the value $\alpha_{cc} = 0.85$ is recommended. For the next applications presented in this chapter, we will focus on building applications, and then $\alpha_{cc} = 1$. Historically speaking, the old French rules *Béton Armé aux Etats Limites BAEL 83*, gave $\alpha_{cc} = 0.85$ (this value $\alpha_{cc} = 0.85$ also appears in the American rules ACI for reinforced concrete structure design, or in the CEB-FIP model code for concrete structures – *Comité Euro-International du Béton/Fédération Internationale de la Précontrainte*). Accordingly, the transition rules from *BAEL* to *EC2* have changed significantly the calculation of design strength for building applications (15%), at least for

the French National Annexes. One argument would be that the partial factor γ_c already included these time-dependent effects.

The strength tension parameters are also given, even if they are not used for the sectional design at ULS (as the tension contribution of concrete is neglected).

$$f_{ctu} = f_{ctd} = \alpha_{ct} \frac{f_{ctk,0.05}}{\gamma_{ct}} \quad [3.97]$$

where $f_{ctk,0.05}$ (see also Table 3.1) is the tensile strength (5% lower tensile strength).

As an example, let us consider a reinforced concrete section, composed of a *C30/37* type concrete, the first *C* stands for concrete. The next digits are related to characteristic strengths. The first characteristic compression strength is the cylinder characteristic strength f_{ck}=30 MPa, whereas the second characteristic compression strength is the cubic characteristic strength.

We calculate:

$$f_{cu} = -\alpha_{cc} \frac{f_{ck}}{\gamma_c} = -1 \times \frac{30}{1.5} = -20 \text{ MPa} \quad [3.98]$$

It can be interesting to also have some other material characteristics for the reinforced concrete material, such as the volumetric weight $\gamma = 25$ kN/m^3, or the thermic dilatation coefficient $\alpha = 10^{-5}$ K^{-1} (the dilatation coefficient for the steel and the concrete part of the reinforced concrete section are almost identical, as outlined in 3.3.1 in the steel chapter).

The constitutive laws available in Eurocode 2 for modeling concrete behavior at the ULS are now presented. Only the monotonic behavior is mentioned.

3.3.2.2. *Parabola–rectangle constitutive law*

The parabola–rectangle constitutive law is composed of a nonlinear parabolic part for small compressive strain and a constant stress part for larger strains (see Figure 3.20).

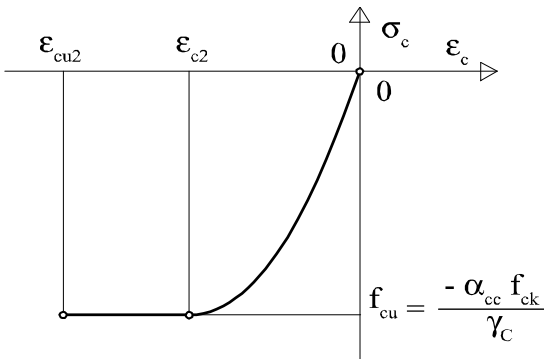

Figure 3.20. *Parabolic rectangular diagram for concrete; typically,* $\varepsilon_{c2} = -2‰$ *and* $\varepsilon_{cu2} = -3.5‰$ *for* $f_{ck} \leq 50$ *MPa*

For $f_{ck} \leq 50$ MPa, the nonlinear constitutive law is mathematically described by the following equations:

$$\frac{\sigma_c}{f_{cu}} = 1 - \left(1 - \frac{\varepsilon_c}{\varepsilon_{c2}}\right)^2 \text{ for } \varepsilon_c \in [\varepsilon_{c2}; 0] \text{ and } \frac{\sigma_c}{f_{cu}} = 1 \text{ for } \varepsilon_c \in [\varepsilon_{cu2}; \varepsilon_{c2}] \quad [3.99]$$

The material parameters are defined in Table 3.2. Note that Eurocode 2 allows the use of some other nonlinear constitutive laws for high concrete strength $f_{ck} \geq 55$ MPa, with power strain function different from $n = 2$, as considered for the parabola–rectangle law.

3.3.2.3. *Rectangular simplified constitutive law*

For simplifying design purposes, a much simpler constitutive law called rectangular simplified constitutive law can be used in Eurocode 2, instead of the parabola–rectangle law. Both laws were already available in the old French rules *Béton Armé aux Etats Limites BAEL 83*.

This law is similar to a rigid plastic constitutive law that acts only on a reduced part λy of the compression block, namely along a portion $\lambda y = \lambda \alpha d$ from the upper (compressed) fiber of the cross-section (see Figure 3.21). ($\lambda = 0.8$ for $f_{ck} \leq 50$ MPa in Eurocode 2). For comparison, the 0.8 factor

appearing for the size of the compression block is changed to 0.85 for ordinary concrete in the American ACI design rules (see, for instance, [MAC 97]).

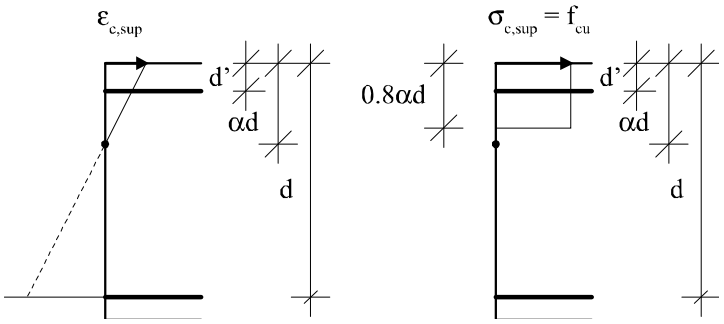

Figure 3.21. *Rectangular simplified diagram for concrete; strain and stress evolution along the cross-section*

The fundamental assumptions of the so-called simplified rectangular constitutive law can also be represented in the stress–strain diagrams for both Pivot *A* (maximum strain capacity of the tensile steel reinforcement) and Pivot *B* (maximum strain capacity of the compression concrete fiber) – see Figure 3.22.

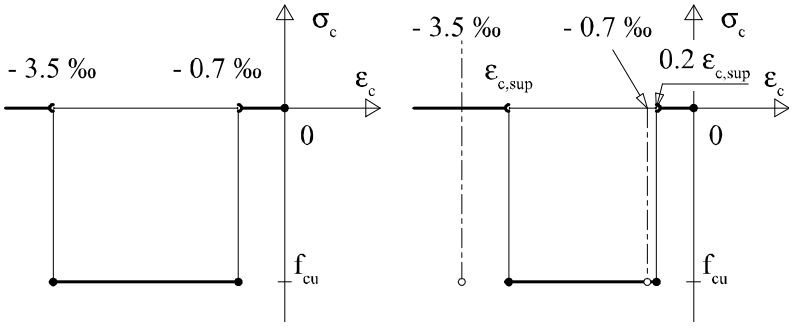

Figure 3.22. *Rectangular simplified diagram for concrete; stress–strain representation*

In the stress–strain diagram, the stress is vanishing up to a strain value equal to $0.2\varepsilon_{c,sup}$. In pivot *B*, as the strain capacity of the concrete is fully

reached, $\varepsilon_{c,sup}$ is equal to –3.5‰ and then the minimum strain value with zero stress value is equal to 0.2 × 3.5‰ = 0.7‰. However, in Pivot *A*, as $\varepsilon_{c,sup}$ is larger than –3.5‰, this minimum strain value will depend on the concrete strain of the upper fiber (see Figure 3.22).

This constitutive law is different in Pivot *A* or Pivot *B*, and is mathematically described by the following single equation:

$$\frac{\sigma_c}{f_{cu}} = 0 \text{ for } \varepsilon_c \in \left[0.2\varepsilon_{\sup};0\right] \text{ and } \frac{\sigma_c}{f_{cu}} = 1 \text{ for } \varepsilon_c \in \left[\varepsilon_{cu2};0.2\varepsilon_{c\sup}\right] \quad [3.100]$$

where $\varepsilon_{c\sup} = \varepsilon_{cu2} = -3.5‰$ in Pivot *B*, and $\varepsilon_{c\sup} = -\alpha\varepsilon_{ud}/(1-\alpha)$ in Pivot *A*.

3.3.2.4. *Bilinear constitutive law*

The bilinear constitutive law is composed of a linear elastic part for small compressive strain and a constant stress part for larger strains (see Figure 3.23). This kind of model can be typically classified as an elastic-perfectly plastic constitutive law, even if for concrete, this ductile classification should be used with precaution.

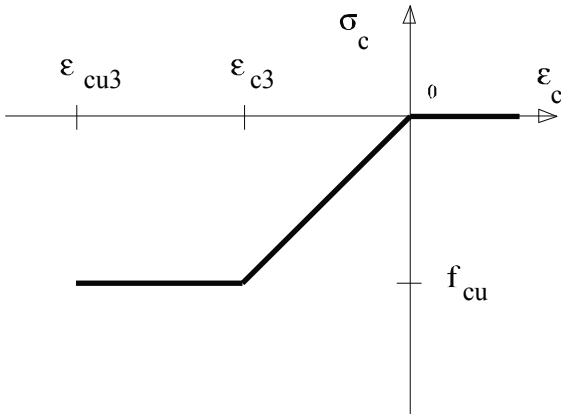

Figure 3.23. *Bilinear constitutive law for concrete; typically,* $\varepsilon_{c3} = -1.75‰$ *and* $\varepsilon_{cu3} = -3.5‰$ *for* $f_{ck} \leq 50$ *MPa*

This constitutive law is mathematically described by the following equations:

$$\frac{\sigma_c}{f_{cu}} = \frac{\varepsilon_c}{\varepsilon_{c3}} \text{ for } \varepsilon_c \in [\varepsilon_{c3}; 0] \quad \text{and} \quad \frac{\sigma_c}{f_{cu}} = 1 \text{ for } \varepsilon_c \in [\varepsilon_{cu3}; \varepsilon_{c3}] \qquad [3.101]$$

The material parameters are defined in Table 3.2. This law is simpler than the parabolic law, as it avoids any piecewise nonlinear stress–strain, but only piecewise linear stress–strain laws. The bilinear law can be considered as a good compromise between the parabola–rectangle constitutive law and the rectangular simplified constitutive law.

3.3.2.5. *Sargin's constitutive law*

According to Eurocode 2, it is also possible to use a nonlinear stress–strain constitutive law introduced by Sargin [SAR 68] – see also [SAR 69], and sometimes called "Sargin's parabola" in some textbooks (see also [SAR 71]; also cited in [OTT 05]). Sargin's law can be used for the structural analysis with respect to the buckling design. Even if Eurocode 2 does not explicitly mention the reference of Sargin, the mentioned nonlinear stress–strain law is referred to the CEB 90, which is based on Sargin's law.

This nonlinear stress–strain constitutive law can be written as (see also [THO 09]):

$$\frac{\sigma_c}{f_{cd}} = \frac{k\eta - \eta^2}{1 + (k-2)\eta} \text{ with } \eta = \frac{\varepsilon_c}{\varepsilon_{c1}} \text{ and } \varepsilon_c \in [\varepsilon_{cu1}; 0] \qquad [3.102]$$

with ε_{cu1} = –3.5‰ for concrete class lower than C55. The characteristics strain variables of Sargin's law are given in Table 3.1.

f_{ck} (MPa)	20	25	30	35	40
ε_{c1} (‰)	–2	–2.1	–2.2	–2.25	–2.3
ε_{cu1} (‰)	–3.5	–3.5	–3.5	–3.5	–3.5

Table 3.1. *Concrete material parameters of Sargin's law at Eurocode 2 for* $f_{ck} \leq 50$ *MPa*

This law is parameterized by one dimensionless coefficient k, which controls the ductility of the concrete. It is easy to check that:

$$\frac{\sigma_c}{f_{cd}}(\eta = 1) = 1 \text{ and } \frac{\sigma'_c}{f_{cd}}(\eta = 1) = 0 \qquad [3.103]$$

The parameter k can be theoretically identified from the initial slope of the undamaged Young's modulus, according to:

$$\sigma'(0) = E_{cm} \quad \Rightarrow \quad k = \frac{E_{cm}\varepsilon_{c1}}{f_{cd}} \geq 0 \qquad [3.104]$$

The Eurocode 2 rules suggested a correction of this law in the evaluation of the second-order effects for stability design, leading to a smaller Young's modulus associated with larger strain and deflection values in a safer design:

$$k = 0.88\frac{E_{cm}\varepsilon_{c1}}{f_{cd}} \geq 0 \qquad [3.105]$$

Sargin's law is represented in Figure 3.24 for a concrete, associated with a k parameter equal to 2.5 (k typically varies between 1.3 and 2.6).

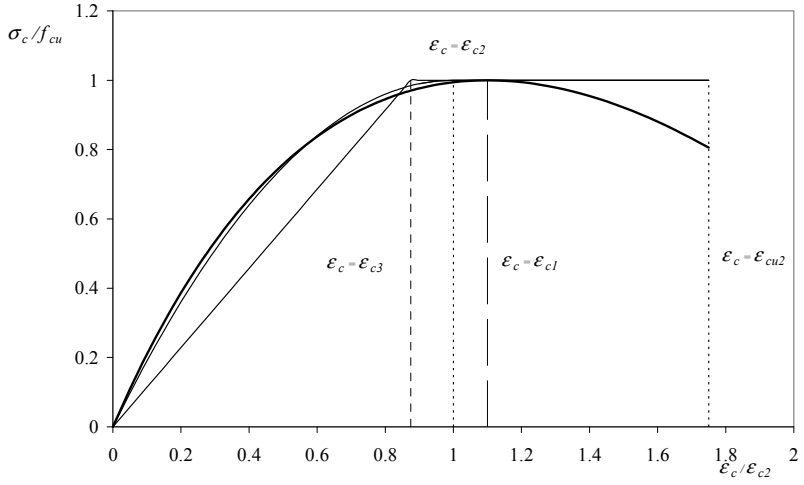

Figure 3.24. *Sargin's law for a C30 concrete with k = 2.5; comparison with the parabolic-rectangular stress-strain relationship*

The three curves (Sargin's law, bilinear constitutive law and parabola–rectangle constitutive laws) are compared in Figure 3.24. It is difficult to distinguish the parabolic part and Sargin's law with these parameters, at least in the hardening part of the nonlinear constitutive law.

More generally, Sargin's law [SAR 68] can be presented in the following form:

$$\frac{\sigma_c}{f_{cd}} = \frac{k\eta + (\alpha - 1)\eta^2}{1 + (k-2)\eta + \alpha\eta^2} \text{ with } \eta = \frac{\varepsilon_c}{\varepsilon_{c1}} \qquad [3.106]$$

The nonlinear equation [3.102] of Eurocode 2 is obviously a particular case of Sargin's law [SAR 68] with $\alpha = 0$.

Some other nonlinear laws are available in the literature such as the law of Desayi and Krishnan [DES 64] suggested in the old French rules *Béton Armé aux Etats Limites* for the structural analyses (see also [ROB 74]), and obtained from Sargin's law by setting $\alpha = 1$ and $k = 2$:

$$\frac{\sigma_c}{f_{cd}} = \frac{2\eta}{1 + \eta^2} \text{ with } \eta = \frac{\varepsilon_c}{\varepsilon_{c1}} \qquad [3.107]$$

Unfortunately, this last nonlinear law has no degree of adjustment of the Young's modulus identification. In fact, with such a law [DES 64], we necessarily have:

$$\sigma'(0) = E_{cm} \quad \Rightarrow \quad E_{cm} = \frac{2f_{cd}}{\varepsilon_{c1}} \geq 0 \qquad [3.108]$$

which can be quite unrealistic.

Another classical law is the parabolic law often used in reinforced concrete design, which is simply obtained as a particular case with $\alpha = 0$ and $k = 2$:

$$\frac{\sigma_c}{f_{cd}} = \eta(2 - \eta) \qquad [3.109]$$

We have only presented a few engineering laws that are recommended in Eurocode 2. Of course, some more refined models have been published in the literature for concrete modeling. CDM models have been found to be very powerful with respect to these reinforced concrete structural problems. The CDM model of Mazars ([MAZ 86], [MAZ 96], see also [MAZ 09], for instance) can be cited, for instance, for a good representation of the strong asymmetry of concrete in the tension and in the compression domain. One loading function is used for the compression behavior and another loading function is used for the tension behavior. Some other tensorial CDM models have been developed in the literature (see, for instance, [HAL 96], [MUR 97], [CHA 05b], [LEM 05] and [MUR 12]); the model of [CHA 05b] presents the advantage to describe the strong unsymmetrical behavior in tension and in compression with a single damage loading function.

We also note that the constitutive laws available in Eurocode 2 have no softening parts, except eventually in Sargin's law that is mainly used for stability designs. Hence, for practical bending design, the softening phenomenon from both local and global state variables does not appear and non-locality mechanics is not needed, in fact, in the evolution problem for the strain range of interest in the design process. However, the post-cracking process of the bending beam needs the use of non-local mechanics as already presented in this chapter.

3.3.2.6. *Synthesis – material parameters for concrete*

The material parameters for the concrete at the ULS are summarized in Table 3.2, based on Eurocode 2 rules.

f_{cm} (MPa)	$f_{cm} = f_{ck} + 8$ MPa ; f_{ck} in MPa
f_{ctm} (MPa)	$f_{ctm} = 0.3\left(f_{ck}\right)^{2/3}$; f_{ck} in MPa
$f_{ctk,0.05}$ (MPa)	$f_{ctk,0.05} = 0.7 f_{ctm}$; f_{ctm} in MPa
E_{cm} (GPa)	$E_{cm} = 22\times\left(f_{cm}/10\right)^{0.3}$; f_{cm} in MPa
ε_{c2}	–2‰
ε_{cu2}	–3.5‰
ε_{c3}	–1.75‰
ε_{cu3}	–3.5‰

Table 3.2. *General concrete material parameters at Eurocode 2 for* $f_{ck} \leq 50$ *MPa*

3.3.3. *Dimensionless parameters at ULS*

A rectangular reinforced concrete cross-section is considered, with both tensile and compression steel reinforcement, respectively, in the lower part and upper part of the cross-section (see Figure 3.25).

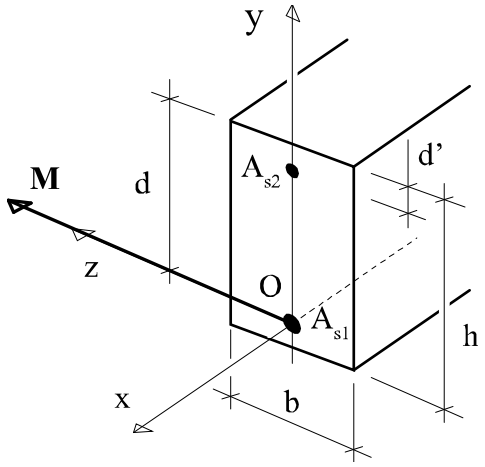

Figure 3.25. *Rectangular cross-section with compression and tensile steel reinforcement*

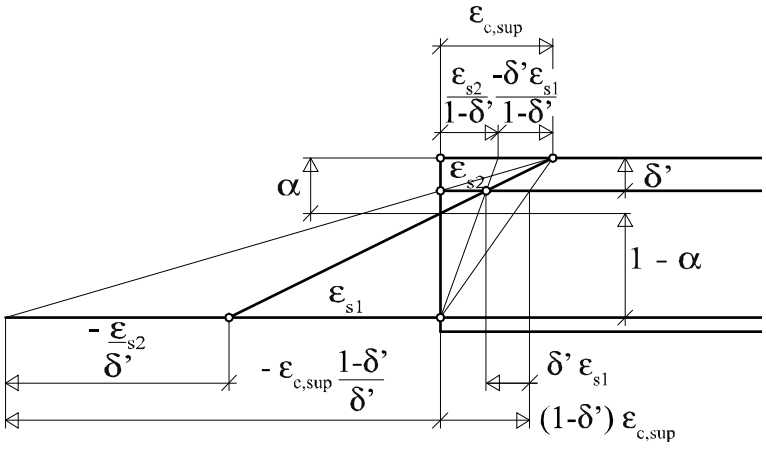

Figure 3.26. *Strain profile at ultimate limit state according to the plane cross-section assumption (Navier–Bernoulli assumption)*

According to Navier–Bernoulli assumption (plane cross-section assumption), the strain is linearly varying along the cross-section, as shown by the geometrical relationship in Figure 3.26.

Using the notations of Figure 3.25, the two equilibrium equations both for the normal force and the bending moment (only two equations for symmetrical reasons) are written with respect to the center of gravity of the tensile steel reinforcement as:

$$N_{act} = A_{s1}\sigma_{s1} + A_{s2}\sigma_{s2} + \alpha\psi bdf_{cu} \qquad [3.110]$$

$$M_{act} = -A_{s2}\sigma_{s2}(d-d') - \alpha\psi(1-\alpha\delta_g)bd^2 f_{cu} \qquad [3.111]$$

where the dimensionless parameters ψ and μ are defined from:

$$\psi = \frac{N_c}{f_{cu}\,A_c} \text{ and } \mu = \alpha\psi(1-\alpha\delta_g) = \frac{-M_c}{bd^2 f_{cu}} \qquad [3.112]$$

N_c and M_c are, respectively, the normal force component of the compression block of concrete and the moment component of this compression block.

The dimensionless parameters ψ and μ can be also introduced in an integral format as:

$$N_c = \int_{d(1-\alpha)}^{d} b\ \sigma_c(y)\,dy \text{ and } M_c = -\int_{d(1-\alpha)}^{d} b\ \ y\ \ \sigma_c(y)\,dy \qquad [3.113]$$

where the stress in concrete σ_c is generally a nonlinear function of the strain ε_c, which is itself a linear decreasing function of the vertical axis, as a result of the kinematics. The origin of the y-axis is here taken at the center of gravity of the tensile steel reinforcement. The coefficients of this linear function depend on the Pivot considered:

$$\varepsilon_c(y) = \frac{d(1-\alpha)-y}{d(1-\alpha)}\varepsilon_{ud} \text{ in Pivot A;}$$
$$\text{whereas } \varepsilon_c(y) = -\frac{d(1-\alpha)-y}{\alpha d}\varepsilon_{cui} \text{ in Pivot B} \qquad [3.114]$$

ε_{cui} is the maximum strain capacity of concrete in compression for each constitutive law (parabola–rectangle, simplified rectangular, bilinear or Sargin's law).

As for the SLS, it is possible to define the pivot rules at the ULS:

– the point "pivot *A*", which corresponds to the maximum strain capacity ε_{ud} of the most tensioned steel reinforcement bars;

– the point "pivot *B*", which corresponds to the maximum strain capacity ε_{cui} in the most compressed fiber in concrete.

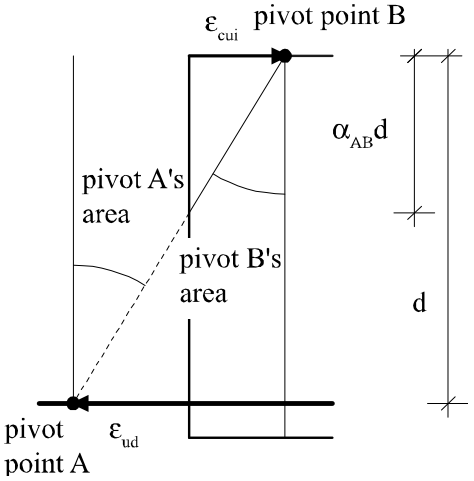

Figure 3.27. *Working zone of the composite cross-section in Pivot A and Pivot B at ULS – strain profile*

At the cross-sectional ULS, the strain diagram should cross one of the two pivot points (Pivot *A* and Pivot *B*) and should also respect the limit strain requirement for the extremal point at the other pivot point (see Figure 3.27).

The limit case between the two pivots is referred to as pivot *AB*, and is characterized by the limit value for the relative position of the neutral axis α_{AB} defined from the upper fiber of the cross-section as:

$$\alpha_{AB} = \frac{-\varepsilon_{cui}}{\varepsilon_{ud} - \varepsilon_{cui}} \qquad [3.115]$$

Pivot *AB* sometimes is often referred to as the balance section, because at the ULS, the concrete and tensioned steel reinforcement reach their ultimate limit strains at the same time.

ε_{cui}, which takes negative values, is explicitly given in Table 3.2, according to the Eurocode 2 rules.

A third case is Pivot *C*, where all parts of the section is in compression, even the lower part of the cross-section. Pivot *C* can also be understood as a particular case of Pivot *B*, as the section is controlled by the maximum strain capacity of concrete in compression. The boundary between Pivot *B* and Pivot *C*, also denoted by Pivot *BC*, is obtained for:

$$\alpha_{BC} = \frac{h}{d} \qquad [3.116]$$

Figure 3.28 shows the nonlinear stress profile along the cross-section, at Pivot *B*, to be integrated to calculate the normal force and bending moment components in concrete at ULS.

Figure 3.28. *Stress profile at Ultimate Limit State – Pivot B*

3.3.4. *Calculation of the concrete resultant for the rectangular simplified diagram*

According to Figure 3.21, the normal force and bending moment components induced by the concrete compression block are calculated as:

$$\begin{cases} N_c = 0.8byf_{cu} \\ M_c = -0.8byf_{cu}\left(d - 0.4y\right) \end{cases} \quad [3.117]$$

We note that these expressions are independent on the Pivot considered (valid for both Pivot *A* and Pivot *B*).

The dimensionless parameters ψ and μ are then easily identified for this simplified constitutive law:

$$\psi = 0.8 \text{ and } \mu = 0.8\alpha\left(1 - 0.4\alpha\right) \quad [3.118]$$

3.3.5. *Calculation of the concrete resultant for the bilinear diagram*

3.3.5.1. *Introduction, Pivot A1, Pivot A2 and Pivot B*

It is useful to distinguish Pivot *A*, characterized by $\varepsilon_s = \varepsilon_{ud}$ and Pivot *B*, characterized by $\varepsilon_{c,\sup} = \varepsilon_{cu3}$, for the bilinear concrete constitutive law. However, Pivot *A* itself can be decomposed into Pivot *A*1 (where the compression block has only linear elastic behavior) and Pivot *A*2 (where the compression block has an elastic and a "perfectly plastic" part). Figure 3.29 represents the stress in the compression block at Pivot *AB*, for a concrete modeling by the bilinear constitutive law.

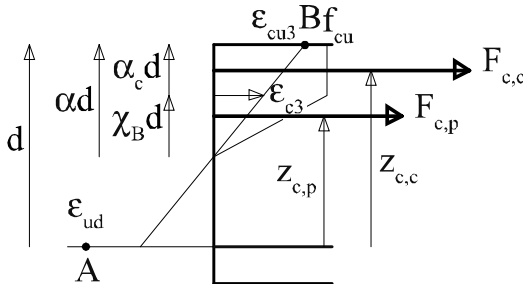

Figure 3.29. *Calculation of the normal force and bending moment components in the compression block of concrete*

3.3.5.2. *Pivot A1 – bilinear diagram*

Pivot *A*1 is a part of Pivot *A*, meaning that the maximum strain capacity of the tensile steel reinforcement is reached $\varepsilon_s = \varepsilon_{ud}$, but the concrete part in compression has only an elastic behavior:

$$\alpha \in \left[0; \alpha_{A_1A_2}\right] \text{ with } \alpha_{A_1A_2} = \frac{-\varepsilon_{c3}}{\varepsilon_{ud} - \varepsilon_{c3}} \quad [3.119]$$

In this case, we only have to integrate the linearly increasing part of the concrete stress along the cross-section, and the problem is the elastic one.

The bending moment is calculated from equation [3.113] as:

$$M_c = -\frac{\alpha b d \sigma_{c,\sup}}{2}\left[(1-\alpha)d + \frac{2}{3}\alpha d\right] \text{ with } \sigma_{c,\sup} = f_{cu}\frac{\alpha}{\alpha - 1}\frac{\varepsilon_{ud}}{\varepsilon_{c3}} \quad [3.120]$$

leading to the dimensionless reduced moment coefficient μ:

$$\mu_{A1} = \frac{\alpha^2}{2(1-\alpha)}\left(1 - \frac{\alpha}{3}\right)\left(\frac{\varepsilon_{ud}}{-\varepsilon_{c3}}\right) \quad [3.121]$$

The shape coefficient ψ is equal to:

$$\alpha\psi_{A1} = \frac{\alpha^2}{2(1-\alpha)}\left(\frac{\varepsilon_{ud}}{-\varepsilon_{c3}}\right) \quad [3.122]$$

3.3.5.3. *Pivot A2 – bilinear diagram*

Pivot *A*2 is also a part of Pivot *A*, meaning that the maximum strain capacity of the tensile steel reinforcement is reached $\varepsilon_s = \varepsilon_{ud}$, but the concrete part in compression has now an elastic and a constant stress component:

$$\alpha \in \left[\alpha_{A_1A_2}; \alpha_{AB}\right] \text{ with } \alpha_{AB} = \frac{-\varepsilon_{cu3}}{\varepsilon_{ud} - \varepsilon_{cu3}} \quad [3.123]$$

We need to decompose the stress variation into a linearly decreasing one and a constant one (see Figure 3.29). $\alpha_c d$ is the distance from the upper fiber to the fiber associated with the transition from the elastic part to the constant part (or plastic part) of the compression block. Applying Thales geometrical relationship, we obtain for this characteristic parameter:

$$\frac{-\varepsilon_{c3}}{(\alpha-\alpha_c)d}=\frac{\varepsilon_{ud}}{(1-\alpha)d} \quad \Rightarrow \quad \alpha_c=\alpha-(1-\alpha)\left(\frac{-\varepsilon_{c3}}{\varepsilon_{ud}}\right) \qquad [3.124]$$

The bending moment is calculated from equation [3.113] as:

$$M_c=-bdf_{cu}\alpha_c\left(d-\frac{\alpha_c d}{2}\right)-\frac{1}{2}bdf_{cu}(\alpha-\alpha_c)\left[\frac{2d}{3}(\alpha-\alpha_c)+(1-\alpha)d\right] \qquad [3.125]$$

leading to the dimensionless reduced moment coefficient μ:

$$\begin{aligned}\mu_{A2}=&\left[\alpha-(1-\alpha)\left(\frac{-\varepsilon_{c3}}{\varepsilon_{ud}}\right)\right]\times\left[1-\frac{\alpha}{2}+\frac{1-\alpha}{2}\left(\frac{-\varepsilon_{c3}}{\varepsilon_{ud}}\right)\right]\\&+\frac{1-\alpha}{2}\left(\frac{-\varepsilon_{c3}}{\varepsilon_{ud}}\right)\left[\frac{2}{3}(1-\alpha)\left(\frac{-\varepsilon_{c3}}{\varepsilon_{ud}}\right)+1-\alpha\right]\end{aligned} \qquad [3.126]$$

The reduced moment can also be simplified as:

$$\mu_{A2}=\alpha\left(1-\frac{\alpha}{2}\right)-\frac{(1-\alpha)^2}{2}\left(\frac{-\varepsilon_{c3}}{\varepsilon_{ud}}\right)-\frac{1}{6}(1-\alpha)^2\left(\frac{-\varepsilon_{c3}}{\varepsilon_{ud}}\right)^2 \qquad [3.127]$$

The shape coefficient ψ is equal to:

$$\alpha\psi_{A2}=\left[\alpha-(1-\alpha)\left(\frac{-\varepsilon_{c3}}{\varepsilon_{ud}}\right)\right]+\frac{1-\alpha}{2}\left(\frac{-\varepsilon_{c3}}{\varepsilon_{ud}}\right)=\alpha-\frac{1-\alpha}{2}\left(\frac{-\varepsilon_{c3}}{\varepsilon_{ud}}\right) \qquad [3.128]$$

3.3.5.4. *Pivot B – bilinear diagram*

In Pivot *B*, the maximum strain capacity of the upper fiber of concrete in compression is reached $\varepsilon_{c,\sup} = \varepsilon_{cu3}$ such as:

$$\alpha \geq \alpha_{AB} \text{ with } \alpha_{AB} = \frac{-\varepsilon_{cu3}}{\varepsilon_{ud} - \varepsilon_{cu3}} \quad [3.129]$$

We also need to decompose the stress variation into a linearly decreasing one and a constant one (see Figure 3.29). $\alpha_c d$ is the distance from the upper fiber to the fiber associated with the transition from the elastic part to the constant part (or plastic part) of the compression block. Applying Thales geometrical relationship, we obtain for this characteristic parameter:

$$\frac{-\varepsilon_{c3}}{(\alpha - \alpha_c)d} = \frac{-\varepsilon_{cu3}}{\alpha d} \quad \Rightarrow \quad \alpha_c = \alpha\left(1 - \frac{\varepsilon_{c3}}{\varepsilon_{cu3}}\right) \quad [3.130]$$

The bending moment expression is the same as in equation [3.125], leading to the dimensionless reduced moment coefficient μ:

$$\mu_{\mathrm{B}} = \alpha\left(1 - \frac{\varepsilon_{c3}}{\varepsilon_{cu3}}\right) \times \left[1 - \frac{\alpha}{2}\left(1 - \frac{\varepsilon_{c3}}{\varepsilon_{cu3}}\right)\right] + \frac{\alpha}{2}\frac{\varepsilon_{c3}}{\varepsilon_{cu3}}\left(\frac{2}{3}\alpha\frac{\varepsilon_{c3}}{\varepsilon_{cu3}} + 1 - \alpha\right) \quad [3.131]$$

The reduced moment can also be simplified as:

$$\mu_B = \alpha\left(1 - \frac{\alpha}{2}\right) - \left(\frac{\varepsilon_{c3}}{\varepsilon_{cu3}}\right)\frac{\alpha(1-\alpha)}{2} - \frac{\alpha^2}{6}\left(\frac{\varepsilon_{c3}}{\varepsilon_{cu3}}\right)^2 \quad [3.132]$$

The shape coefficient ψ is equal to:

$$\alpha\psi_{\mathrm{B}} = \alpha\left(1 - \frac{\varepsilon_{c3}}{\varepsilon_{cu3}}\right) + \frac{\alpha}{2}\frac{\varepsilon_{c3}}{\varepsilon_{cu3}} = \alpha\left(1 - \frac{\varepsilon_{c3}}{2\varepsilon_{cu3}}\right) \quad [3.133]$$

3.3.5.5. *Pivot C – bilinear diagram*

Pivot *C* is reached when the overall section is in compression, which is mathematically equivalent to:

$$\alpha \geq \frac{h}{d} \qquad [3.134]$$

In this case, the lower fiber is in compression and its strain is equal to:

$$\frac{\varepsilon_{c,\inf}}{\alpha d - h} = \frac{\varepsilon_{cu3}}{\alpha d} \Rightarrow \varepsilon_{c,\inf} = \frac{\alpha d - h}{\alpha d}\varepsilon_{cu3} \text{ and } \alpha_c = \alpha\left(1 - \frac{\varepsilon_{c3}}{\varepsilon_{cu3}}\right) \qquad [3.135]$$

where α_c also defined the fiber associated with the transition from the elastic part to the constant part (or plastic part) of the compression block.

The bending moment is calculated from equation [3.113] as:

$$\begin{aligned} M_c = &-bdf_{cu}\alpha_c\left(d - \frac{\alpha_c d}{2}\right) - b\sigma_{c,\inf}\left(h - \alpha_c d\right)\left[\frac{h - \alpha_c d}{2} - \left(h - d\right)\right] \\ &-b\left(f_{cu} - \sigma_{c,\inf}\right)\frac{h - \alpha_c d}{2}\left[\frac{2}{3}\left(h - \alpha_c d\right) - \left(h - d\right)\right] \end{aligned} \qquad [3.136]$$

Assuming that the lower fiber is in the elastic range, the reduced moment is finally calculated as:

$$\begin{aligned} \mu_C = &\alpha\left(1 - \frac{\varepsilon_{c3}}{\varepsilon_{cu3}}\right)\left[1 - \frac{\alpha}{2}\left(1 - \frac{\varepsilon_{c3}}{\varepsilon_{cu3}}\right)\right] \\ &+ \frac{\alpha - \frac{h}{d}}{\alpha}\frac{\varepsilon_{cu3}}{\varepsilon_{c3}}\left[\frac{h}{d} - \alpha\left(1 - \frac{\varepsilon_{c3}}{\varepsilon_{cu3}}\right)\right]\left[-\frac{h}{2d} + 1 - \frac{\alpha}{2}\left(1 - \frac{\varepsilon_{c3}}{\varepsilon_{cu3}}\right)\right] \\ &+ \frac{1}{2}\left(1 - \frac{\alpha - \frac{h}{d}}{\alpha}\frac{\varepsilon_{cu3}}{\varepsilon_{c3}}\right)\left[\frac{h}{d} - \alpha\left(1 - \frac{\varepsilon_{c3}}{\varepsilon_{cu3}}\right)\right]\left[-\frac{h}{3d} + 1 - \frac{2\alpha}{3}\left(1 - \frac{\varepsilon_{c3}}{\varepsilon_{cu3}}\right)\right] \end{aligned} \qquad [3.137]$$

The reduced moment can also be simplified as:

$$\mu_C = \alpha\left(1-\frac{\alpha}{2}\right)-\left(\frac{\varepsilon_{c3}}{\varepsilon_{cu3}}\right)\frac{\alpha(1-\alpha)}{2}\left[1-\left(\frac{h}{d}-\alpha\right)\right]-\frac{\alpha^2}{6}\left(\frac{\varepsilon_{c3}}{\varepsilon_{cu3}}\right)^2 + \frac{1}{\alpha}\frac{\varepsilon_{cu3}}{\varepsilon_{c3}}\left(\frac{h}{d}-\alpha\right)^2\left[\frac{h}{3d}-\frac{1}{2}+\frac{\alpha}{6}\right] \quad [3.138]$$

The shape coefficient ψ is equal to:

$$\alpha\psi_C = \alpha\left(1-\frac{\varepsilon_{c3}}{\varepsilon_{cu3}}\right) + \frac{\alpha-\frac{h}{d}}{\alpha}\frac{\varepsilon_{cu3}}{\varepsilon_{c3}}\left[\frac{h}{d}-\alpha\left(1-\frac{\varepsilon_{c3}}{\varepsilon_{cu3}}\right)\right]+ \frac{1}{2}\left(1-\frac{\alpha-\frac{h}{d}}{\alpha}\frac{\varepsilon_{cu3}}{\varepsilon_{c3}}\right)\left[\frac{h}{d}-\alpha\left(1-\frac{\varepsilon_{c3}}{\varepsilon_{cu3}}\right)\right] \quad [3.139]$$

The shape coefficient ψ can be also simplified as:

$$\alpha\psi_C = \alpha\left(1-\frac{\varepsilon_{c3}}{2\varepsilon_{cu3}}\right)+\frac{\varepsilon_{cu3}}{\varepsilon_{c3}}\left[\frac{h}{d}-\frac{\alpha}{2}-\frac{1}{2\alpha}\left(\frac{h}{d}\right)^2\right] \quad [3.140]$$

It is easy to check the continuity of Pivot *B* and *C* at the boundary between the two behaviors.

3.3.6. *Calculation of the concrete resultant for the parabola–rectangle diagram*

3.3.6.1. *Pivot A1 – parabola–rectangle law*

Pivot *A*1 is a part of Pivot *A*, meaning that the maximum strain capacity of the tensile steel reinforcement is reached $\varepsilon_s = \varepsilon_{ud}$, but the concrete part in compression has only a parabolic behavior (the strength capacity of concrete has not been reached):

$$\alpha \in \left[0;\alpha_{A_1A_2}\right] \text{ with } \alpha_{A_1A_2} = \frac{-\varepsilon_{c2}}{\varepsilon_{ud}-\varepsilon_{c2}} \quad [3.141]$$

The bending moment and the normal forces in the concrete compression block are obtained by integration of the nonlinear stress–strain relationship from equation [3.113] presented as:

$$N_c = \int_0^{dd} b\,\sigma_c(z)\,dz \quad \text{and}$$

$$M_c = -\int_0^{\alpha d} b \quad \left(z + d(1-\alpha)\right)\sigma_c(z)\,dz \quad \text{with}$$

$$\sigma_c(z) = -f_{cu}\left[\left(\frac{\varepsilon_c(z)}{\varepsilon_{c2}}\right)^2 - 2\left(\frac{\varepsilon_c(z)}{\varepsilon_{c2}}\right)\right] \qquad [3.142]$$

where the stress in concrete σ_c is now a nonlinear function of the strain ε_c, which is itself a linear decreasing function of the vertical axis, as a result of the kinematics. The origin of the z-axis is here taken at the location of the neutral axis, in order to make the calculation much easier. The coefficients of this linear function depend on the Pivot considered:

$$\varepsilon_c(z) = \frac{-z}{d(1-\alpha)}\varepsilon_{ud} \text{ in Pivot A ; whereas } \varepsilon_c(z) = \frac{z}{\alpha d}\varepsilon_{cu2} \text{ in Pivot B} \quad [3.143]$$

The dimensionless normal force component in the concrete compression block is calculated from the shape coefficient ψ:

$$\alpha\psi_{A1} = \frac{\alpha^2\varepsilon_{ud}[-3\varepsilon_{c2} - \alpha(\varepsilon_{ud} - 3\varepsilon_{c2})]}{3(1-\alpha)^2\varepsilon^2_{c2}} \qquad [3.144]$$

In pivot $A1$, the reduced moment is calculated from the integral equation:

$$\mu_{A1} = \frac{\alpha^2\varepsilon_{ud}(-12\varepsilon_{c2} + 16\alpha\varepsilon_{c2} - 4\alpha^2\varepsilon_{c2} - 4\alpha\varepsilon_{ud} + \alpha^2\varepsilon_{ud})}{12(1-\alpha)^2\varepsilon^2_{c2}} \qquad [3.145]$$

3.3.6.2. *Pivot A2 – parabola–rectangle law*

Pivot $A2$ is also a part of Pivot A, meaning that the maximum strain capacity of the tensile steel reinforcement is reached $\varepsilon_s = \varepsilon_{ud}$, but the concrete part in compression has now a parabolic and a constant stress component:

$$\alpha \in \left[\alpha_{A_1 A_2} ; \alpha_{AB} \right] \text{ with } \alpha_{AB} = \frac{-\varepsilon_{cu2}}{\varepsilon_{ud} - \varepsilon_{cu2}} \quad [3.146]$$

We need to decompose the stress variation into a parabolic one and a constant one (as already suggested for the bilinear constitutive law). $\alpha_c d$ is the distance from the upper fiber to the fiber associated with the transition from the elastic part to the constant part (or plastic part) of the compression block. Applying Thales geometrical relationship, we obtain for this characteristic parameter:

$$\frac{-\varepsilon_{c2}}{(\alpha - \alpha_c) d} = \frac{\varepsilon_{ud}}{(1-\alpha) d} \quad \Rightarrow \quad \alpha_c = \alpha - (1-\alpha)\left(\frac{-\varepsilon_{c2}}{\varepsilon_{ud}} \right) \quad [3.147]$$

The bending moment is calculated from equation [3.113] as:

$$M_c = b f_{cu} \int_0^{(\alpha-\alpha_c)d} \left(z + d(1-\alpha) \right) \left[\left(\frac{z}{d(1-\alpha)} \frac{\varepsilon_{ud}}{\varepsilon_{c2}} \right)^2 + \frac{2z}{d(1-\alpha)} \frac{\varepsilon_{ud}}{\varepsilon_{c2}} \right] dz$$
$$- b d^2 f_{cu} \left[\alpha + (1-\alpha) \frac{\varepsilon_{c2}}{\varepsilon_{ud}} \right] \left[1 - \frac{\alpha}{2} - \frac{1-\alpha}{2} \frac{\varepsilon_{c2}}{\varepsilon_{ud}} \right] \quad [3.148]$$

where the first term is the associated with the parabolic part of the constitutive law, whereas the second term is related to the maximum capacity strength f_{cu}. After some lengthy manipulations, we finally obtain for the dimensionless reduced moment coefficient μ:

$$\mu_{A2} = \frac{\varepsilon_{c2} (4\varepsilon_{ud} - \varepsilon_{c2}) (1 - \alpha)^2 + 6\alpha\varepsilon_{ud}^2 (2 - \alpha)}{12\varepsilon_{ud}^2} \quad [3.149]$$

The shape coefficient ψ can be shown to be equal to:

$$\alpha\psi_{A2} = \frac{\varepsilon_{c2} - \alpha\varepsilon_{c2} + 3\alpha\varepsilon_{ud}}{3\varepsilon_{ud}} \quad [3.150]$$

3.3.6.3. *Pivot B – parabola–rectangle law*

In Pivot *B*, the maximum strain capacity of the upper fiber of concrete in compression is reached $\varepsilon_{c,\sup} = \varepsilon_{cu3}$ such as:

$$\alpha \geq \alpha_{AB} \text{ with } \alpha_{AB} = \frac{-\varepsilon_{cu2}}{\varepsilon_{ud} - \varepsilon_{cu2}} \quad [3.151]$$

We also need to decompose the stress variation into parabolic stress variation and rectangular stress variation. $\alpha_c d$ is the distance from the upper fiber to the fiber associated with the transition from the elastic part to the constant part (or plastic part) of the compression block. Applying Thales geometrical relationship, we also obtain for this characteristic parameter:

$$\frac{-\varepsilon_{c2}}{(\alpha - \alpha_c)d} = \frac{-\varepsilon_{cu2}}{\alpha d} \quad \Rightarrow \quad \alpha_c = \alpha\left(1 - \frac{\varepsilon_{c2}}{\varepsilon_{cu2}}\right) \quad [3.152]$$

The bending moment is calculated from equation [3.113] as:

$$M_c = bf_{cu}\int_0^{(\alpha-\alpha_c)d} \left(z + d(1-\alpha)\right)\left[\left(\frac{z}{\alpha d}\frac{\varepsilon_{cu2}}{\varepsilon_{c2}}\right)^2 - \frac{2z}{\alpha d}\frac{\varepsilon_{cu2}}{\varepsilon_{c2}}\right]dz$$
$$-bd^2 f_{cu}\alpha \left(1 - \frac{\varepsilon_{c2}}{\varepsilon_{cu2}}\right)\left(1 - \frac{\alpha}{2} + \frac{\alpha}{2}\frac{\varepsilon_{c2}}{\varepsilon_{cu2}}\right) \quad [3.153]$$

leading to the dimensionless reduced moment coefficient μ:

$$\mu_B = \frac{-\alpha\{\alpha\varepsilon_{c2}^2 + \varepsilon_{cu2}[4(1-\alpha)\varepsilon_{c2} - 6(2-\alpha)\varepsilon_{cu2}]\}}{12\varepsilon_{cu2}^2} \quad [3.154]$$

The shape coefficient ψ can be shown to be equal to:

$$\alpha\psi_B = \frac{-\alpha(\varepsilon_{c2} - 3\varepsilon_{cu2})}{3\varepsilon_{cu2}} \quad [3.155]$$

3.3.6.4. *Pivot C – parabola–rectangle law*

For Pivot *C*, the dimensionless reduced moment coefficient μ is calculated as:

$$\alpha\psi_C = \left(\frac{h}{d}\right)\left\{1 - \frac{\left(\frac{h}{d}\right)^2 \varepsilon^3{}_{c2}}{3\,\varepsilon_{cu2}\left[-\alpha\,\varepsilon_{cu2} + (-\varepsilon_{c2} + \varepsilon_{cu2})\left(\frac{h}{d}\right)\right]^2}\right\} \qquad [3.156]$$

The shape coefficient ψ can be shown to be equal to:

$$\mu_C = \left(\frac{h}{d}\right)\left(1 - \frac{h}{2d}\right) + \frac{\left(\frac{h}{d}\right)^3 \varepsilon^3{}_{c2}\left[-4\,\varepsilon_{cu2} + (-\varepsilon_{c2} + 4\,\varepsilon_{cu2})\left(\frac{h}{d}\right)\right]}{12\,\varepsilon^2{}_{cu2}\left[-\alpha\,\varepsilon_{cu2} + (-\varepsilon_{c2} + \varepsilon_{cu2})\left(\frac{h}{d}\right)\right]^2} \qquad [3.157]$$

3.3.7. *Calculation of the concrete resultant for the law of Desayi and Krishnan*

3.3.7.1. *Law of Desayi and Krishnan – introduction*

Sargin's law is defined in one single equation, and there is no need to separate Pivot $A1$ and Pivot $A2$, as introduced for the parabola–rectangle law or the bilinear law. In this section we use the particular version of Sargin's law given by equation [3.107], which is the law of Desayi and Krishnan [DES 64]. This particular case of Sargin's law with $\alpha = 1$ and $k = 2$ leads to an easier analytical determination of the dimensionless concrete resultant parameters (see also [ROB 74]). The more general integration results valid for Sargin's law in the other cases can be obtained from the integration results presented in [THO 09].

The bending moment and the normal forces in the concrete compression block are obtained by integration of the nonlinear stress–strain relationship from equation [3.113] presented as:

$$N_c = \int_0^{dd} b\,\sigma_c(z)\,dz \quad \text{and}$$

$$M_c = -\int_0^{\alpha d} b\left(z + d(1-\alpha)\right)\sigma_c(z)\,dz$$

$$\text{with} \quad \sigma_c(z) = 2 f_{cu} \frac{\frac{\varepsilon_c(z)}{\varepsilon_{c1}}}{1 + \left(\frac{\varepsilon_c(z)}{\varepsilon_{c1}}\right)^2} \qquad [3.158]$$

where the stress in concrete σ_c is now a nonlinear function of the strain ε_c, which is itself a linear decreasing function of the vertical axis, as a result of the kinematics.

The origin of the z-axis is here taken at the location of the neutral axis, in order to make the calculation much easier. The coefficients of this linear function depend on the Pivot considered:

$$\varepsilon_c(z) = \frac{-z}{d(1-\alpha)}\varepsilon_{ud} \text{ in Pivot A; whereas } \varepsilon_c(z) = \frac{z}{\alpha d}\varepsilon_{cu1} \text{ in Pivot } B \quad [3.159]$$

3.3.7.2. *Pivot A – law of Desayi and Krishnan*

The dimensionless normal force component in the concrete compression block is calculated from the shape coefficient ψ:

$$\alpha\psi_A = \int_0^\alpha 2\frac{\left(\frac{\varepsilon_{ud}}{-\varepsilon_{c1}}\right)\frac{\eta}{1-\alpha}}{1+\left[\left(\frac{\varepsilon_{ud}}{-\varepsilon_{c1}}\right)\frac{\eta}{1-\alpha}\right]^2} \quad d\eta \text{ with } \eta = \frac{z}{d} \quad [3.160]$$

which can be easily integrated leading to:

$$\alpha\psi_A = (1-\alpha)\left(\frac{-\varepsilon_{c1}}{\varepsilon_{ud}}\right)\ln\left[1+\left(\frac{\varepsilon_{ud}\alpha}{\varepsilon_{c1}(1-\alpha)}\right)^2\right] \quad [3.161]$$

In pivot A, the reduced moment is calculated from the integral equation:

$$\mu_A = \int_0^\alpha 2(\eta+1-\alpha)\frac{\left(\frac{\varepsilon_{ud}}{-\varepsilon_{c1}}\right)\frac{\eta}{1-\alpha}}{1+\left[\left(\frac{\varepsilon_{ud}}{-\varepsilon_{c1}}\right)\frac{\eta}{1-\alpha}\right]^2} d\eta \quad [3.162]$$

which is also equivalent to:

$$\mu_A = (1-\alpha)\alpha\psi_A - 2\left[\frac{\varepsilon_{c1}(1-\alpha)}{\varepsilon_{ud}}\right]^2\left[\left(\frac{\varepsilon_{ud}\alpha}{\varepsilon_{c1}(1-\alpha)}\right) - \arctan\left(\frac{\varepsilon_{ud}\alpha}{\varepsilon_{c1}(1-\alpha)}\right)\right] \quad [3.163]$$

3.3.7.3. *Pivot B – law of Desayi and Krishnan*

The dimensionless normal force component in the concrete compression block is calculated from the shape coefficient ψ:

$$\alpha\psi_B = \int_0^{\alpha} 2\frac{\left(\frac{\varepsilon_{cu1}}{\varepsilon_{c1}}\right)\frac{\eta}{\alpha}}{1+\left[\left(\frac{\varepsilon_{cu1}}{\varepsilon_{c1}}\right)\frac{\eta}{\alpha}\right]^2} \quad d\eta \text{ with } \eta = \frac{z}{d} \quad [3.164]$$

which can be easily integrated leading to:

$$\alpha\psi_B = \alpha\left(\frac{\varepsilon_{c1}}{\varepsilon_{cu1}}\right)\ln\left[1+\left(\frac{\varepsilon_{cu1}}{\varepsilon_{c1}}\right)^2\right] \quad [3.165]$$

which is also the value presented by Carreira and Chu [CAR 86] who presented the case of Pivot *B* with some additional tension effects for the cracked concrete in tension.

In pivot *B*, the reduced moment is calculated from the integral equation:

$$\mu_B = \int_0^{\alpha} 2(\eta+1-\alpha)\frac{\frac{\varepsilon_{cu1}\eta}{\varepsilon_{c1}\alpha}}{1+\left(\frac{\varepsilon_{cu1}\eta}{\varepsilon_{c1}\alpha}\right)^2} \quad d\eta \text{ with } \eta = \frac{z}{d} \quad [3.166]$$

which is also equivalent to:

$$\mu_B = (1-\alpha)\alpha\psi_B + 2\left(\frac{\varepsilon_{c1}\alpha}{\varepsilon_{cu1}}\right)^2\left[\left(\frac{\varepsilon_{cu1}}{\varepsilon_{c1}}\right) - \arctan\left(\frac{\varepsilon_{cu1}}{\varepsilon_{c1}}\right)\right] \qquad [3.167]$$

In Pivot *B*, these results are also coincident with the results of Carreira and Chu [CAR 86], who calculated the bending moment with respect to the neutral axis, whereas the moment of the compression block is presented here with respect to the center of gravity of the tensile steel reinforcement.

3.3.7.4. *Pivot C – law of Desayi and Krishnan*

The dimensionless normal force component in the concrete compression block is calculated from the shape coefficient ψ:

$$\alpha\psi_C = \int_0^{\frac{h}{d}} 2\frac{\left(\frac{\varepsilon_{cu1}}{\varepsilon_{c1}}\right)\frac{\eta - \frac{h}{d} + \alpha}{\alpha}}{1 + \left[\left(\frac{\varepsilon_{cu1}}{\varepsilon_{c1}}\right)\frac{\eta - \frac{h}{d} + \alpha}{\alpha}\right]^2} \quad d\eta \text{ with } \eta = \frac{z}{d} \qquad [3.168]$$

which can be easily integrated leading to:

$$\alpha\psi_C = \alpha\left(\frac{\varepsilon_{c1}}{\varepsilon_{cu1}}\right)\left\{\ln\left[1 + \left(\frac{\varepsilon_{cu1}}{\varepsilon_{c1}}\right)^2\right] - \ln\left[1 + \left(\frac{\varepsilon_{cu1}}{\varepsilon_{c1}\alpha}\left(\alpha - \frac{h}{d}\right)\right)^2\right]\right\} \qquad [3.169]$$

The reduced moment μ_C is given by:

$$\mu_C = (1-\alpha)\alpha\psi_C + 2\left(\frac{\varepsilon_{c1}\alpha}{\varepsilon_{cu1}}\right)^2\left\{\frac{\varepsilon_{cu1}}{\varepsilon_{c1}} - \arctan\left(\frac{\varepsilon_{cu1}}{\varepsilon_{c1}}\right)\right.$$
$$\left. - \frac{\varepsilon_{cu1}}{\varepsilon_{c1}\alpha}\left(\alpha - \frac{h}{d}\right) + \arctan\left[\frac{\varepsilon_{cu1}}{\varepsilon_{c1}\alpha}\left(\alpha - \frac{h}{d}\right)\right]\right\} \qquad [3.170]$$

The integral calculations are given in [THO 09] for Sargin's law given in equation [3.102], which is possible to use for nonlinear structural analysis according to Eurocode 2.

3.3.8. *Calculation of the concrete resultant for Sargin's law of Eurocode 2*

3.3.8.1. *Sargin's law of Eurocode 2 – introduction*

Sargin's law in Eurocode 2 is a particular case of Sargin's law [SAR 68] with $\alpha = 0$. The integration results valid for Sargin's law are also presented in [THO 09].

The bending moment and the normal forces in the concrete compression block are obtained by integration of the nonlinear stress–strain relationship from equation [3.113] presented as:

$$N_c = \int_0^{dd} b\,\sigma_c(z)\,dz \quad \text{and}$$

$$M_c = -\int_0^{\alpha d} b\big(z + d(1-\alpha)\big)\,\sigma_c(z)\,dz \quad \text{with}$$

$$\sigma_c(z) = f_{cu}\,\frac{k\dfrac{\varepsilon_c(z)}{\varepsilon_{c1}} - \left[\dfrac{\varepsilon_c(z)}{\varepsilon_{c1}}\right]^2}{1 + (k-2)\dfrac{\varepsilon_c(z)}{\varepsilon_{c1}}} \qquad [3.171]$$

where the stress in concrete σ_c is now a nonlinear function of the strain ε_c, which is itself a linear decreasing function of the vertical axis, as a result of the kinematics. The origin of the z-axis is here taken at the location of the neutral axis, in order to make the calculation much easier. The coefficients of this linear function depend on the Pivot considered, as given by equation [3.159].

3.3.8.2. *Pivot A – Sargin's law of Eurocode 2*

The dimensionless normal force component in the concrete compression block is calculated from the shape coefficient ψ:

$$\alpha\psi_A = (1-\alpha)\left(\frac{-\varepsilon_{c1}}{\varepsilon_{ud}}\right)\int_0^{\frac{\varepsilon_{ud}}{-\varepsilon_{c1}}\frac{\alpha}{1-\alpha}} \frac{k\eta-\eta^2}{1+(k-2)\eta}\,d\eta \qquad [3.172]$$

which can be easily integrated leading to:

$$\alpha\psi_A = \frac{1-\alpha}{k-2}\left(\frac{-\varepsilon_{c1}}{\varepsilon_{ud}}\right)\left\{\begin{array}{l} -\frac{1}{2}\left(\frac{\varepsilon_{ud}}{-\varepsilon_{c1}}\frac{\alpha}{1-\alpha}\right)^2+\left(k+\frac{1}{k-2}\right)\left(\frac{\varepsilon_{ud}}{-\varepsilon_{c1}}\frac{\alpha}{1-\alpha}\right) \\ -\frac{1}{k-2}\left(k+\frac{1}{k-2}\right)\ln\left[1+(k-2)\left(\frac{\varepsilon_{ud}}{-\varepsilon_{c1}}\frac{\alpha}{1-\alpha}\right)\right] \end{array}\right\} \qquad [3.173]$$

In pivot *A*, the reduced moment is calculated from the integral equation:

$$\mu_A = (1-\alpha)\alpha\psi_A + (1-\alpha)^2\left(\frac{-\varepsilon_{c1}}{\varepsilon_{ud}}\right)^2 \int_0^{\frac{\varepsilon_{ud}}{-\varepsilon_{c1}}\frac{\alpha}{1-\alpha}} \eta\frac{k\eta-\eta^2}{1+(k-2)\eta}\,d\eta \qquad [3.174]$$

which is also equivalent to:

$$\mu_A = (1-\alpha)\alpha\psi_A + (1-\alpha)^2\left(\frac{-\varepsilon_{c1}}{\varepsilon_{ud}}\right)^2 \left[\begin{array}{l} \frac{-1}{3(k-2)}\left(\frac{\varepsilon_{ud}}{-\varepsilon_{c1}}\frac{\alpha}{1-\alpha}\right)^3+\frac{1}{2(k-2)}\left(k+\frac{1}{k-2}\right)\left(\frac{\varepsilon_{ud}}{-\varepsilon_{c1}}\frac{\alpha}{1-\alpha}\right)^2 \\ -\frac{1}{(k-2)^2}\left(k+\frac{1}{k-2}\right)\left(\frac{\varepsilon_{ud}}{-\varepsilon_{c1}}\frac{\alpha}{1-\alpha}\right)+\frac{1}{(k-2)^3}\left(k+\frac{1}{k-2}\right)\ln\left[1+(k-2)\left(\frac{\varepsilon_{ud}}{-\varepsilon_{c1}}\right)\frac{\alpha}{1-\alpha}\right] \end{array}\right]$$

[3.175]

3.3.8.3. *Pivot B – Sargin's law of Eurocode 2*

The dimensionless normal force component in the concrete compression block is calculated from the shape coefficient ψ:

$$\alpha\psi_B = \alpha\left(\frac{\varepsilon_{c1}}{\varepsilon_{cu1}}\right)\int_0^{\frac{\varepsilon_{cu1}}{\varepsilon_{c1}}} \frac{k\eta-\eta^2}{1+(k-2)\eta}\,d\eta \qquad [3.176]$$

which can be easily integrated, leading to:

$$\alpha\psi_B = \frac{\alpha}{k-2}\left(\frac{\varepsilon_{c1}}{\varepsilon_{cu1}}\right)\times \left\{-\frac{1}{2}\left(\frac{\varepsilon_{cu1}}{\varepsilon_{c1}}\right)^2+\left(k+\frac{1}{k-2}\right)\left(\frac{\varepsilon_{cu1}}{\varepsilon_{c1}}\right)-\frac{1}{k-2}\left(k+\frac{1}{k-2}\right)\ln\left[1+(k-2)\left(\frac{\varepsilon_{cu1}}{\varepsilon_{c1}}\right)\right]\right\} \quad [3.177]$$

Typically, for k = 2.5, the shape coefficient is equal to:

$$k=\frac{5}{2} \quad \Rightarrow \quad \psi_B = 2\frac{\varepsilon_{c1}}{\varepsilon_{cu1}}\left\{-\frac{1}{2}\left(\frac{\varepsilon_{cu1}}{\varepsilon_{c1}}\right)^2+\frac{9}{2}\left(\frac{\varepsilon_{cu1}}{\varepsilon_{c1}}\right)-9\ln\left[1+\frac{\varepsilon_{cu1}}{2\varepsilon_{c1}}\right]\right\} \quad [3.178]$$

In this last case, for a C30 type concrete, the shape coefficient factor is equal to:

$$k=\frac{5}{2} \text{ and } \frac{\varepsilon_{cu1}}{\varepsilon_{c1}}=\frac{3.5}{2.2} \Rightarrow \psi_B = 0.787 \quad [3.179]$$

The shape coefficient $\psi_B = 0.787$ is an intermediate value between $\psi_B = 0.75$ obtained for the bilinear diagram and $\psi_B = 0.8$ obtained for the rectangular simplified diagram.

In pivot *B*, the reduced moment is calculated from the integral equation:

$$\mu_B = (1-\alpha)\alpha\psi_B + \alpha^2\left(\frac{\varepsilon_{c1}}{\varepsilon_{cu1}}\right)^2 \int_0^{\frac{\varepsilon_{cu1}}{\varepsilon_{c1}}} \eta\frac{k\eta-\eta^2}{1+(k-2)\eta}\,d\eta \quad [3.180]$$

which can be developed as following:

$$\mu_B = (1-\alpha)\alpha\psi_B + \left(\alpha\frac{\varepsilon_{c1}}{\varepsilon_{cu1}}\right)^2 \times \left[\begin{array}{l}\dfrac{-1}{3(k-2)}\left(\dfrac{\varepsilon_{cu1}}{\varepsilon_{c1}}\right)^3+\dfrac{1}{2(k-2)}\left(k+\dfrac{1}{k-2}\right)\left(\dfrac{\varepsilon_{cu1}}{\varepsilon_{c1}}\right)^2 \\ -\dfrac{1}{(k-2)^2}\left(k+\dfrac{1}{k-2}\right)\left(\dfrac{\varepsilon_{cu1}}{\varepsilon_{c1}}\right)+\dfrac{1}{(k-2)^3}\left(k+\dfrac{1}{k-2}\right)\ln\left[1+(k-2)\dfrac{\varepsilon_{cu1}}{\varepsilon_{c1}}\right]\end{array}\right] \quad [3.181]$$

Typically, for $k = 2.5$, the reduced moment is equal to:

$$k = \frac{5}{2} \Rightarrow \mu_B = (1-\alpha)\alpha\psi_B + \left(\alpha\frac{\varepsilon_{c1}}{\varepsilon_{cu1}}\right)^2 \times \left[\frac{-2}{3}\left(\frac{\varepsilon_{cu1}}{\varepsilon_{c1}}\right)^3 + \frac{9}{2}\left(\frac{\varepsilon_{cu1}}{\varepsilon_{c1}}\right)^2 - 18\left(\frac{\varepsilon_{cu1}}{\varepsilon_{c1}}\right) + 36\ln\left[1+\frac{\varepsilon_{cu1}}{2\varepsilon_{c1}}\right]\right] \quad [3.182]$$

3.3.8.4. *Pivot C – Sargin's law of Eurocode 2*

The dimensionless normal force component in the concrete compression block is calculated from the shape coefficient ψ:

$$\alpha\psi_C = \alpha\left(\frac{\varepsilon_{c1}}{\varepsilon_{cu1}}\right)\int_{\frac{\varepsilon_{cu1}}{\varepsilon_{c1}\alpha\left(\alpha-\frac{h}{d}\right)}}^{\frac{\varepsilon_{cu1}}{\varepsilon_{c1}}} \frac{k\eta-\eta^2}{1+(k-2)\eta}\,d\eta \quad [3.183]$$

which can be easily integrated, leading to:

$$\alpha\psi_C = \frac{\alpha}{k-2}\left(\frac{\varepsilon_{c1}}{\varepsilon_{cu1}}\right)\left\{\begin{array}{l} -\frac{1}{2}\left(\frac{\varepsilon_{cu1}}{\varepsilon_{c1}}\right)^2 + \frac{1}{2}\left[\frac{\varepsilon_{cu1}}{\varepsilon_{c1}}\left(1-\frac{h}{\alpha d}\right)\right]^2 + \left(k+\frac{1}{k-2}\right)\left(\frac{\varepsilon_{cu1}}{\varepsilon_{c1}}\right)\frac{h}{\alpha d} \\ -\frac{1}{k-2}\left(k+\frac{1}{k-2}\right)\ln\left[\frac{1+(k-2)\left(\frac{\varepsilon_{cu1}}{\varepsilon_{c1}}\right)}{1+(k-2)\left(\frac{\varepsilon_{cu1}}{\varepsilon_{c1}}\right)\left(1-\frac{h}{\alpha d}\right)}\right] \end{array}\right\} \quad [3.184]$$

The reduced moment μ_C is given by:

$$\mu_C = (1-\alpha)\alpha\psi_C + \left(\alpha\frac{\varepsilon_{c1}}{\varepsilon_{cu1}}\right)^2 \times \left[\begin{array}{l} \frac{-1}{3(k-2)}\left[\left(\frac{\varepsilon_{cu1}}{\varepsilon_{c1}}\right)^3 - \left(\frac{\varepsilon_{cu1}}{\varepsilon_{c1}}\left(1-\frac{h}{\alpha d}\right)\right)^3\right] + \frac{1}{2(k-2)}\left(k+\frac{1}{k-2}\right)\left[\left(\frac{\varepsilon_{cu1}}{\varepsilon_{c1}}\right)^2 - \left(\frac{\varepsilon_{cu1}}{\varepsilon_{c1}}\left(1-\frac{h}{\alpha d}\right)\right)^2\right] \\ -\frac{1}{(k-2)^2}\left(k+\frac{1}{k-2}\right)\left(\frac{\varepsilon_{cu1}}{\varepsilon_{c1}}\right)\frac{h}{\alpha d} + \frac{1}{(k-2)^3}\left(k+\frac{1}{k-2}\right)\ln\left[\frac{1+(k-2)\frac{\varepsilon_{cu1}}{\varepsilon_{c1}}}{1+(k-2)\left(\frac{\varepsilon_{cu1}}{\varepsilon_{c1}}\right)\left(1-\frac{h}{\alpha d}\right)}\right] \end{array}\right] \quad [3.185]$$

3.3.9. *On the use of the reduced moment parameter*

In absence of additional steel compression reinforcement, the neutral axis position is calculated from the nonlinear equation:

$$\mu(\alpha) = \mu_{act} \text{ with } \mu_{act} = \frac{M_u}{-bd^2 f_{cu}} \qquad [3.186]$$

which is always a second-order equation for the rectangular simplified constitutive law, and still remains a second-order equation in Pivot *B* for the constitutive law presented in detail (bilinear, parabola–rectangle or Sargin's law). Only the law of Desayi and Krishnan is presented in Table 3.3, for the clarity of presentation, but the parameters of Sargin's law for EC2 can also be deduced from the formula presented in section 3.3.2.5 devoted to this law.

The dimensionless parameters of interest are presented for each model in Table 3.3 (see also [THO 09] for the presentation of these parameters).

For a reinforced cross-section without additional compression steel reinforcement, the dimensionless steel area in the case of simple bending (without axial force) can be given in a dimensionless format as:

$$\left(\frac{f_{su}}{-f_{cu}}\right)\rho'(\mu_{act}) = \alpha(\mu_{act})\psi \text{ with } \rho' = \frac{A_{s1}}{bd} \qquad [3.187]$$

The tensile steel reinforcement is assumed in plasticity, with a tensile stress equal to f_{su}. It is shown in Figure 3.30, that the four models are in fact very close. The rectangular simplified law gives the lower steel area (unsafe design), whereas Sargin's nonlinear law gives the largest steel area, or the safer design (both Sargin's law for EC2, or Desayi and Krishnan law which is also a particular case of Sargin's law). Both the bilinear and the parabola–rectangle constitutive laws lead to very close results.

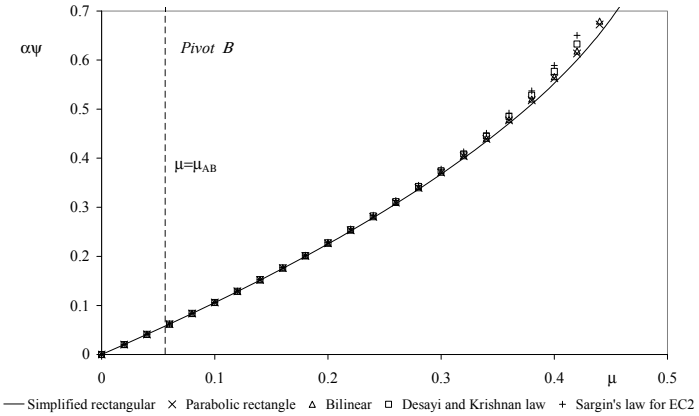

Figure 3.30. *Comparison of the steel reinforcement area for each model*

	Rectangular simplified	Parabolic rectangle	Bilinear	Desayi and Krishnan – C30
ψ_B	0.8	$(3\varepsilon_{cu2} - \varepsilon_{c2})/(3\varepsilon_{cu2})$	$1 - \varepsilon_{c3}/(2\varepsilon_{cu3})$	$(\varepsilon_{c1}/\varepsilon_{cu1}) \times \ln$ $[1 + (\varepsilon_{cu1}/\varepsilon_{c1})^2]$
ψ_B	0.8	17/21 ≈ 0.810	3/4 = 0.75	≈0.793
μ_B	$0.8\alpha(1 - 0.4\alpha)$	$(17/21)\alpha \times$ $[1 - (99/238)\alpha]$	$0.75\alpha \times$ $[1 - (7/18)\alpha]$	$0.793\alpha \times$ $[1 - 0.421\alpha]$
α	$1.25(1 - \sqrt{1 - 2\mu})$	$(119/99)\times$ $(1 - \sqrt{1 - (594/289)\mu})$	$9/7(1 - \sqrt{1 - (56/27)\mu})$	$1.187(1 - \sqrt{1 - 2.125\mu})$

Table 3.3. *Comparison of the characteristics of the constitutive laws in pivot B at ultimate limit state for* $f_{ck} \leq 50$ *MPa*

These results obtained from a second-order polynomial equation for the determination of the position of the neutral axis, for a given acting moment, are based on Pivot *B*. However, in Pivot *A*, the nonlinear equation of the neutral axis position can be a cubic equation for the bilinear constitutive law, a fourth-order equation for the parabola–rectangle constitutive law and a transcendal equation for Sargin's constitutive law.

Chapter 4

Bending-Curvature at Ultimate Limit State (ULS)

4.1. On the bilinear approximation of the moment-curvature relationship of reinforced concrete beams

4.1.1. *Phenomenological approach*

The behavior of a reinforced concrete beam in bending up to the ultimate limit state (ULS) is composed of different complex inelastic stages (cracking of concrete in tension, plasticity phenomena in steel, cracking of concrete in compression), as shown in Figure 4.1 (see also [MAC 97]). First, we start from a phenomenological approach describing qualitatively the main phenomena involved at the ULS of a reinforced concrete beam. Second, some bending-curvature's models are analyzed based on both the local constituent behaviors and a global simplified bending-curvature constitutive law.

Figures 4.1 and 4.2 show two typical responses of reinforced concrete beams with different steel reinforcements. Both curves are linear in the initial stages. Initially, for the low loading level, the beam can be considered as uncracked. The strains at this stage are very small, and the stress distribution is essentially linear. The moment-curvature diagram at this stage is essentially linear. When the stress of the lower fiber reaches the tensile

strength of the concrete, cracking occurs at the lower part of the reinforced concrete beam, for positive bending moment. After cracking, the tensile force in the concrete is transferred to the steel reinforcement. The result is that the lower part of a concrete section is involved in resistance to the acting moment: a decrease in the beam stiffness is observed. However, it is experimentally observed that the beam stiffness is slightly larger than the stiffness totally neglecting the concrete in tension. This phenomenon, already described in Chapter 2, is called the tension stiffening effect. Although potentially significant for the deflection calculation at the serviceability limit state (SLS), the tension stiffening effect will be neglected in the following for the ULS design. When neglecting the concrete behavior in tension, the stress distribution in the concrete is still linear at this stage.

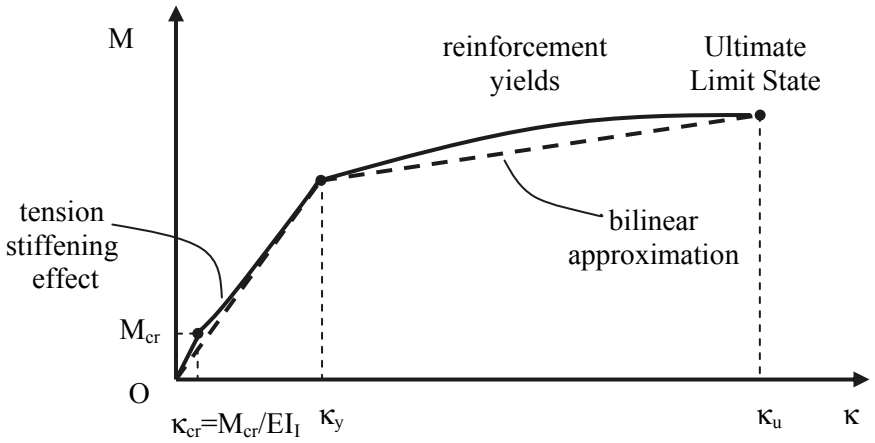

Figure 4.1. *Typical experimental moment-curvature diagram for a the bending of a ductile reinforced concrete beam – bilinear approximation – lightly reinforced sections*

The behavior of the section after cracking is dependent mainly on the steel content (see also [PAR 75]). For lightly reinforced sections, after a certain loading level, the tensile steel reinforcement reaches the yield point and enters into the plasticity range. Even during this plasticity stage of the

steel reinforcement, the concrete in compression can still behave in a linear range. This step is associated with a drastic change of slope in the bending-curvature diagram. Once yielding occurs in the tensile steel reinforcement, the curvature increases rapidly with a small increase in moment (see also [MAC 97]). Finally, the beam mainly fails due to crushing of the concrete at the top of the beam, meaning that Pivot *B* mostly controls the ULS of the bending behavior of reinforced concrete beams for high-ductility steel (even if the tension steel reinforcements are in the plasticity stage). However, Pivot *A* failure can also be potentially observed with a strain of the tensile steel reinforcement, which has reached the ultimate strain of steel in tension. Pivot *A*-type failure leads to higher ductilities than Pivot *B*-type failure, as also mentioned in [PAR 75].

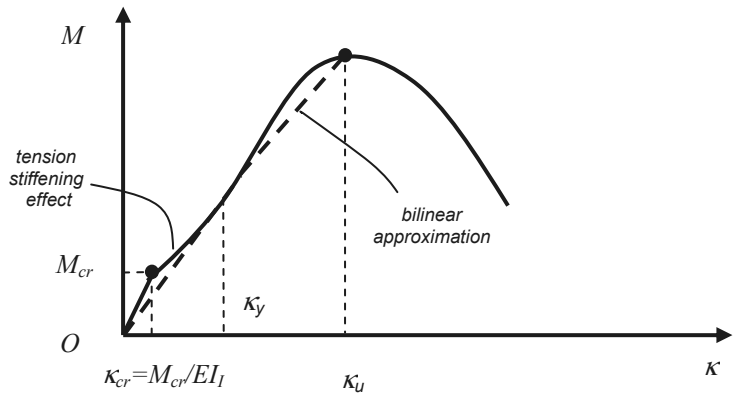

Figure 4.2. *Typical experimental moment-curvature diagram for a the bending of a quasi-brittle reinforced concrete beam – heavily reinforced sections*

In heavily reinforced concrete sections, the bending-curvature response is highly nonlinear, due to the nonlinearity of the stress–strain response induced by the micro-cracking phenomena. A quasi-brittle response is then observed unless the concrete is confined by closed stirrups at close centers. If the concrete is not confined, the concrete crushes at a relatively small curvature before the steel yields leading to the softening behavior in the bending-curvature diagram (see Figure 4.2). To ensure ductility behavior, it can be required to design the reinforced concrete beams with a steel content less than the balanced design value leading to quasi-brittle responses.

The nature of failure at ULS depends on the design of the reinforced concrete section. In the following, the characteristic material parameters associated with different kind of behaviors at failure will be analyzed.

As outlined in [PAR 75] or [MAC 97], although concrete is not a ductile material (concrete is typically a quasi-brittle material), reinforced concrete beams can exhibit large ductilities in bending as shown in Figure 4.1. Typically, the curvature at ULS can be larger than five to six times the curvature at SLS, due to the abrupt change of slope of the bending-curvature constitutive law after the yielding of the tensile reinforcement.

A bilinear approximation of this complex nonlinear bending-curvature constitutive law can model the different nonlinear stages with sufficient accuracy (see also the bilinear approximation in Figure 4.1). The tension stiffening effect is neglected for the bending modeling of reinforced concrete beams at ULS.

4.1.2. *Moment-curvature relationship for concrete – brief overview*

The moment-curvature relationships can be obtained from the local constitutive laws for both the concrete and the steel part, integrating over the cross-section. Most of the results in the literature are focused on the numerical investigation of the bending-curvature relationship for different amount of axial forces. For instance, Pfrang *et al*. [PFR 64] numerically derived the moment-curvature relationship of reinforced concrete sections for different axial load level. The concrete modeling was based on the law of Hognestad [HOG 51]. Hognestad's law [HOG 51] is composed of the usual parabolic law up to the maximum compressive strength and a linearly decreasing (softening) branch up to the ultimate strain failure. Hognestad's law is given by [HOG 51]:

$$\begin{aligned} &\frac{\sigma_c}{f_{cd}} = \eta(2-\eta) \text{ for } \eta = \frac{\varepsilon_c}{\varepsilon_{c1}} \in [0;1] \text{ and} \\ &\frac{\sigma_c}{f_{cd}} = 1 - 0.15\frac{\eta - 1}{\frac{\varepsilon_u}{\varepsilon_{c1}} - 1} \text{ for } \eta = \frac{\varepsilon_c}{\varepsilon_{c1}} \in \left[1; \frac{\varepsilon_u}{\varepsilon_{c1}}\right] \end{aligned} \qquad [4.1]$$

The assumptions used by Pfrang *et al*. [PFR 64] are quite usual: the tension part of concrete was neglected. Strain hardening in plasticity was also neglected for the steel reinforcement. Some bending-curvature relationship and normal force-bending moment interaction diagrams were numerically obtained for symmetrically reinforced concrete beams. The sections have shown a large amount of ductility at low axial load level (axial load in compression). As the load level increased, ductility decreased markedly. Furthermore, the reinforced concrete beam became stiffer with increasing axial load up to a critical load called the balance load.

Since the paper of Pfrang *et al*. [PFR 64], many papers have been published on the theoretical moment-curvature determination in reinforced concrete design (see, for instance, [CAR 86]; or more recently the papers coauthored by Professor Chandrasekaran [CHA 09e], [CHA 10d], [CHA 11d]).

Carreira and Chu [CAR 86] also neglect the strain hardening in the steel reinforcements. The concrete law in compression was modeled by the following nonlinear stress–strain law:

$$\frac{\sigma_c}{f_{cd}} = \frac{\beta\eta}{\beta - 1 + \eta^{\beta}} \text{ with } \eta = \frac{\varepsilon_c}{\varepsilon_{c1}} \qquad [4.2]$$

Even if the law of Carreira and Chu cannot be cast in the framework of Sargin's law in the general case [CAR 86], we recognize the law of Desayi and Krishnan [DES 64] for $\beta = 2$, which is itself a particular case of Sargin's law [SAR 71]. Carreira and Chu take into account some contribution of concrete in tension, with a model expressed by a similar homothetic nonlinear law normalized by the tension strength and expressed with respect to the dimensionless tension strain [CAR 86].

Chandrasekaran *et al*. [CHA 11d] derived the analytical bending-moment curvature relationship with the effect of normal force. Strain hardening was neglected for the steel reinforcement, and a limitation of the tensile strain to 10‰ was taken into account. The concrete was modeled with a parabola–rectangle constitutive law in compression (and as usual the tension part in concrete is neglected).

4.1.3. *Analytical moment-curvature relationship for concrete*

4.1.3.1. *General formulation*

The bending-curvature relationship is studied in this part assuming an elastic and perfect-plastic constitutive law for the steel reinforcement ($\sigma_{s1} = f_{su}$ at ULS), and a bilinear constitutive law for concrete ($\sigma_{c,\sup} = f_{cu}$ at ULS). The contribution of concrete in tension is neglected, which is a reasonable assumption for ULS design. An unsymmetrical reinforced concrete section is analyzed (see Figure 4.3), with tensile steel reinforcement of steel area A_{s1}, but without compression steel reinforcement $A_{s2} = 0$. The presence of the additional compression steel reinforcement does not change fundamentally the complexity of the mathematical problem.

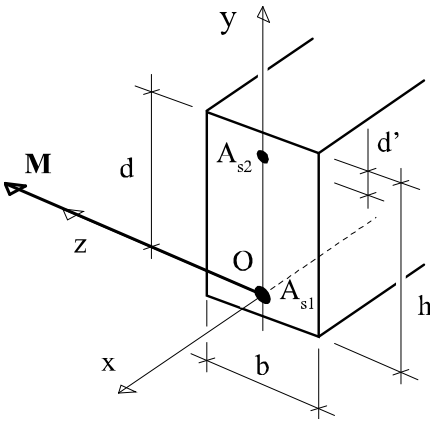

Figure 4.3. *Rectangular cross-section at Ultimate Limit State*

The bending-curvature can be obtained in closed-form solution for this problem, with the bilinear constitutive law for the concrete in compression. We outline that bending-curvature constitutive laws have also been analytically investigated by Chandrasekaran *et al.* [CHA 11d] for parabola–rectangle constitutive laws, leading to some more complex calculations. The detailed equations of the nonlinear bending-curvature constitutive law of a rectangular reinforced concrete section with a parabola–rectangle constitutive law for concrete can be also available in closed-form solutions for this problem, even if the solutions are more difficult to manipulate [CHA 11d].

As already detailed both at SLS and ULS, the Navier–Bernoulli kinematics assumptions are written as:

$$\frac{\varepsilon_{c,\sup}}{\alpha d} = \frac{\varepsilon_{s1}}{d(\alpha - 1)} = -\kappa = \frac{\varepsilon_c(y)}{y} \qquad [4.3]$$

where κ is the curvature and y is the distance of the considered fiber to the neutral axis ($y = 0$ defines the position of the neutral axis).

As we are only presenting results for the case of a simple bending behavior ($N = 0$), the equilibrium equations are:

$$\begin{aligned} M &= -\int_0^{\alpha d} b\sigma_c(y)(y + d - \alpha d)\,dy \text{ and} \\ N &= \int_0^{\alpha d} b\sigma_c(y)\,dy + A_{s1}\sigma_{s1} = 0 \end{aligned} \qquad [4.4]$$

4.1.3.2. *Elasticity for both the steel and the concrete parts*

For sufficiently small bending moments, the behavior is linear. We first assume that both the concrete and the steel are in the elasticity range (but concrete in tension is neglected at ULS as already specified):

$$\sigma_c = E_c\varepsilon_c \text{ and } \sigma_{s1} = E_s\varepsilon_{s1} \qquad [4.5]$$

where E_c and E_s are, respectively, the Young's modulus of concrete and steel. Introducing the concrete constitutive law in the bending equilibrium equation, and using the kinematic relationship between the strain in concrete and the curvature leads to the bending-curvature equation in the linear range:

$$M = bE_c\kappa\int_0^{\alpha d} y^2 + yd(1-\alpha)\ dy = bd^3E_c\frac{\alpha^2}{2}\left(1 - \frac{\alpha}{3}\right)\kappa \qquad [4.6]$$

The position α of the neutral axis is still an unknown of the problem. The normal force equilibrium equation leads to the necessary additional equation for resolution of the problem.

$$\frac{(\alpha d)^2}{2} = \frac{A_{s1}\sigma_{s1}}{b\kappa E_c} \qquad [4.7]$$

Note that in the reasoning, up to now, the steel constitutive law has not been used in the bending-curvature equation presented in equation [4.6], or in the axial equilibrium equation presented in equation [4.7].

Now introducing the elastic constitutive law of steel with the curvature dependence of the strain in the tensile reinforcement gives a second-order equation for the neutral axis, which is nothing more than the "static moment equation":

$$\frac{(\alpha d)^2}{2} = \frac{A_{s1}\alpha_e d(1-\alpha)}{b} \text{ with } \alpha_e = \frac{E_s}{E_c} \qquad [4.8]$$

which can be also written in a more classical equation as:

$$\frac{\alpha^2}{2} + \alpha_e \rho'_{s1}\alpha - \alpha_e \rho'_{s1} = 0 \text{ with } \rho'_{s1} = \frac{A_{s1}}{bd} \qquad [4.9]$$

In the elastic range, the neutral axis position does not depend on the solicitation (as already shown in the part devoted to the SLS), and is equal to:

$$\alpha = -\alpha_e \rho'_{s1} + \sqrt{(\alpha_e \rho'_{s1})^2 + 2\alpha_e \rho'_{s1}} \qquad [4.10]$$

The elastic moment-curvature constitutive law, neglecting the tension stiffening effect (cracked section), is then equal to:

$$M = EI_{eq}\kappa \text{ with } EI_{eq} = E_c I_{II} = E_c b\frac{(\alpha d)^3}{3} + E_s A_{s1} d^2 (1-\alpha)^2 \qquad [4.11]$$

The equivalent stiffness EI_{eq} was also denoted by $E_c I_{II}$ in Chapter 2, and is the equivalent stiffness of the homogeneous cracked section.

From this quasi-elastic state (the section is assumed to be fully cracked and tension behavior is neglected), by increasing the curvature, the section will reach the elastic domain of the concrete or the steel part of the section.

4.1.3.3. *Pivot A1 – linear behavior of concrete*

We first assume that the inelastic part of the section is reached for the tensile steel reinforcement, whereas the concrete part in compression of the section remains in its elastic range. This can also be referred to as Pivot *A1*. This kind of behavior is typical of a low steel reinforcement ratio and is associated with very high-ductility behavior.

It is possible to define a critical curvature κ_y associated with a strain ε_{s1} in the tensile steel reinforcement, equal to the maximum elastic strain ε_{su}, such as:

$$\varepsilon_{s1} = \varepsilon_{su} = \frac{f_{su}}{E_s} \Rightarrow \kappa_y = \frac{\varepsilon_{su}}{d\left(1-\alpha_y\right)} \text{ with}$$
$$\alpha_y = -\alpha_e \rho'_{s1} + \sqrt{\left(\alpha_e \rho'_{s1}\right)^2 + 2\alpha_e \rho'_{s1}} \qquad [4.12]$$

The dimensionless critical curvature can be easily defined as:

$$\kappa_y^* = \kappa_y d = \frac{\varepsilon_{su}}{\left(1-\alpha_y\right)} \qquad [4.13]$$

The reduced moment parameters can be also introduced as:

$$\mu = \frac{M}{-bd^2 f_{cu}} \text{ and } \mu_y = -\frac{\alpha_y^2}{2}\left(1-\frac{\alpha_y}{3}\right)\left(\frac{\kappa_y^*}{\varepsilon_{c3}}\right) \qquad [4.14]$$

In the elastic range (neglecting tension stiffening effect), the bending-curvature constitutive law can be presented with dimensionless variables as:

$$\frac{\mu}{\mu_y} = \frac{\kappa}{\kappa_y} \text{ for } \frac{\kappa}{\kappa_y} \in [0;1] \qquad [4.15]$$

Once the tensile steel reinforcements have yielded ($\sigma_{s1} = f_{su}$), the position of the neutral axis is no more constant but depends on the bending moment solicitation. The normal force equilibrium equation gives in fact:

$$\frac{(\alpha d)^2}{2} = \frac{A_{s1} f_{su}}{b\kappa E_c} \Rightarrow \alpha d = \sqrt{\frac{2 f_{su} A_{s1}}{b\kappa E_c}} \qquad [4.16]$$

The position of the neutral axis given by the dimensionless parameter α is then proportional to the inverse of the square root of the curvature:

$$\frac{\alpha}{\alpha_y} = \sqrt{\frac{\kappa_y}{\kappa}} \qquad [4.17]$$

Replacing the neutral axis variable as a nonlinear function of the curvature in the bending moment equilibrium equation leads to the nonlinear bending moment-curvature constitutive law as:

$$M = bd^3 E_c \frac{\alpha^2}{2}\left(1 - \frac{\alpha}{3}\right)\kappa \Rightarrow M = A_{s1} f_{su}\left(d - \frac{1}{3}\sqrt{\frac{2 f_{su} A_{s1}}{b\kappa E_c}}\right) \qquad [4.18]$$

The bending moment-curvature constitutive law can be also presented in a dimensionless format as:

$$\frac{\mu}{\mu_y} = \frac{1}{1 - \frac{\alpha_y}{3}}\left(1 - \frac{\alpha_y}{3}\sqrt{\frac{\kappa_y}{\kappa}}\right) \text{ for } \frac{\kappa}{\kappa_y} \in \left[1; \frac{\kappa_u}{\kappa_y}\right] \qquad [4.19]$$

where κ_u is the ultimate curvature associated with Pivot *A*1. The ULS at Pivot *A* is defined from the ultimate strain condition:

$$\begin{aligned} \varepsilon_{s1} = \varepsilon_{ud} &= -\kappa_u d\left(\alpha_u - 1\right) = -\kappa_u^*\left(\sqrt{\frac{2 f_{su} A_{s1}}{bd^2 \kappa_u E_c}} - 1\right) \\ &= -\kappa_u^*\left(\sqrt{\frac{2 f_{su} \rho'_{s1}}{\kappa_u^* E_c}} - 1\right) \end{aligned} \qquad [4.20]$$

The calculation of the ultimate curvature κ_u can be achieved from the resolution of this ultimate strain condition, which is a nonlinear equation expressed with respect to the curvature:

$$\varepsilon_{ud} = -\kappa_u^* \left(\alpha_y \sqrt{\frac{\kappa_y^*}{\kappa_u^*}} - 1 \right) \qquad [4.21]$$

This nonlinear equation is in fact a second-order polynomial equation of the dimensionless curvature:

$$\kappa_u^{*2} - \left(2\varepsilon_{ud} + \alpha_y^2 \kappa_y^* \right) \kappa_u^* + \varepsilon_{ud}^2 = 0 \qquad [4.22]$$

The ultimate curvature is then obtained as the solution of this second-order polynomial equation:

$$\begin{aligned} \kappa_u^* &= \varepsilon_{ud} + \frac{\alpha_y^2}{2} \kappa_y^* \pm \sqrt{\left(\varepsilon_{ud} + \frac{\alpha_y^2}{2} \kappa_y^* \right)^2 - \varepsilon_{ud}^2} \\ &= \varepsilon_{ud} + \rho'_{s1} \alpha_e \varepsilon_{su} \pm \sqrt{\left(\varepsilon_{ud} + \rho'_{s1} \alpha_e \varepsilon_{su} \right)^2 - \varepsilon_{ud}^2} \end{aligned} \qquad [4.23]$$

Among these two solutions, only one verifies the constraint condition induced by equation [4.21], and written as:

$$\kappa_u^* \geq \varepsilon_{ud} \qquad [4.24]$$

We finally calculate the ultimate curvature for this reinforced concrete section as the largest solution of the second-order polynomial equation:

$$\kappa_u^* = \varepsilon_{ud} + \rho'_{s1} \alpha_e \varepsilon_{su} + \sqrt{\left(\varepsilon_{ud} + \rho'_{s1} \alpha_e \varepsilon_{su} \right)^2 - \varepsilon_{ud}^2} \qquad [4.25]$$

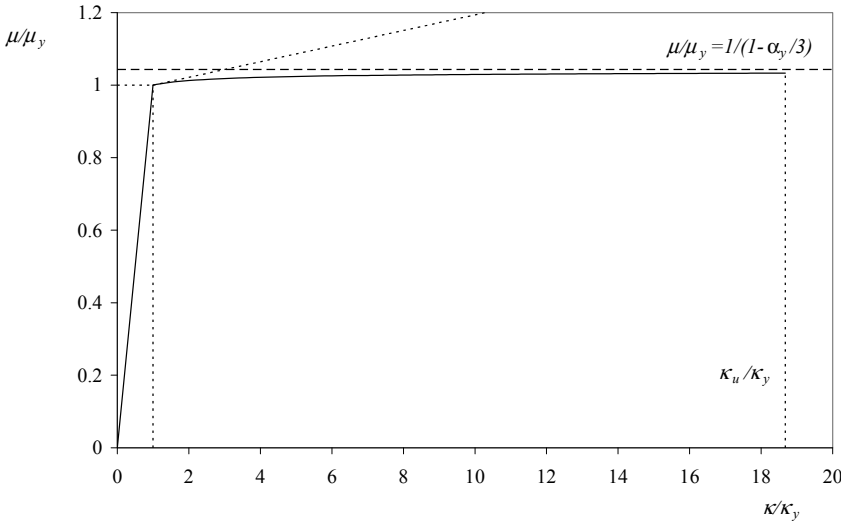

Figure 4.4. *Bending moment-curvature relationship of a reinforced concrete beam – failure with Pivot A1 – linear behavior of concrete; C30-37 for the concrete; B500B for the steel;* $\alpha_e = 17.5$; $\rho'_{s1} = 5 \times 10^{-4}$; $\alpha_y = 0.124$; $\mu_y = 0.01$; $\kappa_u / \kappa_y = 18.67$

It has been shown that the bending moment-curvature response of the reinforced concrete beam is nonlinear in the post-yield regime, as shown by equation [4.19]. It is however possible to linearize this nonlinear function around the yield point, and the linear approximation is written as:

$$\frac{\mu}{\mu_y} = \frac{\frac{\alpha_y}{6}}{1-\frac{\alpha_y}{3}}\frac{\kappa}{\kappa_y} + \frac{1-\frac{\alpha_y}{2}}{1-\frac{\alpha_y}{3}} \text{ for } \frac{\kappa}{\kappa_y} \in \left[1; \frac{\kappa_u}{\kappa_y}\right] \qquad [4.26]$$

As shown in Figure 4.4, this linear approximation solution is not very accurate for a sufficiently large curvature, as can be the case for this ductile section in Pivot *A* (low steel reinforcement ratio). The asymptotic value of the dimensionless bending moment is quite accurate in fact as highlighted in Figure 4.4:

$$\lim_{\frac{\kappa}{\kappa_y} \to \infty} \frac{\mu}{\mu_y} = \frac{1}{1-\frac{\alpha_y}{3}} \qquad [4.27]$$

This solution (Pivot *A* failure with only elastic behavior of concrete, i.e. Pivot *A*1) is valid as long as the strain of the upper fiber has not reached the elastic concrete strain denoted by ε_{c3}, which is mathematically expressed by the inequality:

$$\varepsilon_{c,\text{sup}} = -\kappa_u \alpha_u d \geq \varepsilon_{c3} \Rightarrow \kappa_u^* \alpha_u \leq -\varepsilon_{c3} \quad [4.28]$$

This inequality is also equivalent to the following inequality:

$$\kappa_u^* \leq \frac{\varepsilon_{c3} f_{cu}}{2 f_{su} \rho'_{s1}} = \frac{\varepsilon_{c3}^2}{\alpha_y^2 \kappa_y^*} \quad [4.29]$$

This solution is in fact equivalent to consider that the steel reinforcement ratio has to be lower than a critical ratio given by:

$$\rho'_{s1} \leq \frac{f_{cu}}{f_{su}} \frac{\frac{\varepsilon_{c3}}{2}}{\varepsilon_{ud} - \varepsilon_{c3}} \quad [4.30]$$

We calculate for a C30-37 type concrete and for a B500B steel the steel reinforcement ratio limit as:

$$\rho'_{s1} \leq \frac{30 \times 1.15}{500 \times 1.5} \times \frac{\frac{1.75}{2}}{45 + 1.75} = 8.61 \times 10^{-4} \quad [4.31]$$

The numerical results presented in Figure 4.4 show the bending curvature constitutive law for a Pivot *A*1 failure response with a reinforcement density equal to $\rho'_{s1} = 5 \times 10^{-4}$, which is lower than the one computed above $\rho'_{s1} = 8.61 \times 10^{-4}$ and associated with the transition to Pivot *A*2.

4.1.3.4. *Pivot A2 – bilinear behavior of concrete*

It is however possible to have a Pivot *A*-type failure governed by the maximum capacity strain in the tensile steel reinforcement with some nonlinear behaviors of the concrete. This behavior can be also referred as Pivot *A*2. For this kind of cross-section, typically for:

$$\rho'_{s1} \geq \frac{f_{cu}}{f_{su}} \frac{\frac{\varepsilon_{c3}}{2}}{\varepsilon_{ud} - \varepsilon_{c3}} \qquad [4.32]$$

the section behaves like in Pivot *A*1 (elastic behavior of the concrete) up to a critical curvature and then the section will fail in Pivot *A*2 (nonlinear behavior of concrete).

Linear behavior of concrete for $\frac{\kappa^*}{\kappa_y^*} \leq \frac{\varepsilon_{c3}^2}{\alpha_y^2 \kappa_y^{*2}}$ and

Bilinear behavior of concrete for $\frac{\kappa^*}{\kappa_y^*} \geq \frac{\varepsilon_{c3}^2}{\alpha_y^2 \kappa_y^{*2}}$ [4.33]

In this case, the equilibrium equations [4.4] are written as:

$$\begin{aligned} M &= -\int_0^{(\alpha-\alpha_c)d} bE_c\varepsilon_c(y)(y+d-\alpha d)\,dy - \\ &\quad \int_{(\alpha-\alpha_c)d}^{\alpha d} bf_{cu}(y+d-\alpha d)\,dy \text{ and} \\ N &= \int_0^{(\alpha-\alpha_c)d} bE_c\varepsilon_c(y)\,dy + \int_{(\alpha-\alpha_c)d}^{\alpha d} bf_{cu}\,dy + A_{s1}f_{su} = 0 \end{aligned} \qquad [4.34]$$

As usual, αd is the distance from the upper fiber of the cross-section to the neutral axis, and $\alpha_c d$ is the distance from the upper fiber of the cross-section to the fiber in concrete associated with the maximum elastic strain (see Figure 3.29).

The integral equations can be easily developed as:

$$M = E_c b\kappa \left[\frac{y^3}{3} + (d-\alpha d)\frac{y^2}{2}\right]_0^{(\alpha-\alpha_c)d} - f_{cu} b \left[\frac{y^2}{2} + (d-\alpha d)y\right]_{(\alpha-\alpha_c)d}^{\alpha d} \text{ and}$$
$$N = \frac{b(\alpha-\alpha_c)d}{2} f_{cu} + b\alpha_c d f_{cu} + A_{s1} f_{su} = 0 \quad [4.35]$$

associated with the strain compatibility equation given by:

$$\frac{\varepsilon_{c3}}{(\alpha-\alpha_c)d} = \frac{\varepsilon_{c,\sup}}{\alpha d} = \frac{\varepsilon_{s1}}{d(\alpha-1)} = -\kappa = \frac{\varepsilon_c(y)}{y} \quad [4.36]$$

The dimensionless neutral axis parameters can be expressed with respect to the curvature variables from the normal force equilibrium equation as:

$$\alpha = \frac{-\varepsilon_{c3}}{2\kappa^*} - \rho'_{s1}\frac{f_{su}}{f_{cu}} \text{ and } \alpha_c = \frac{\varepsilon_{c3}}{2\kappa^*} - \rho'_{s1}\frac{f_{su}}{f_{cu}} \quad [4.37]$$

Introducing these neutral axis parameters in the bending moment equilibrium equation leads to the reduced moment nonlinear function of the curvature:

$$\mu = -\frac{1}{24}\left(\frac{\varepsilon_{c3}}{\kappa^*}\right)^2 - \rho'_{s1}\frac{f_{su}}{f_{cu}} - \frac{1}{2}\left(\rho'_{s1}\frac{f_{su}}{f_{cu}}\right)^2 \text{ for } \frac{\kappa}{\kappa_y} \in \left[\frac{\varepsilon_{c3}^2}{\alpha_y^2 \kappa_y^{*2}}; \frac{\kappa_u}{\kappa_y}\right] \quad [4.38]$$

where κ_u is the ultimate curvature associated with Pivot *A*2. The ULS at Pivot *A*2 is defined from the ultimate strain condition:

$$\varepsilon_{s1} = \varepsilon_{ud} = -\kappa_u d(\alpha_u - 1) = \frac{\varepsilon_{c3}}{2} + \kappa_u^*\left(1 + \frac{f_{su}}{f_{cu}}\rho'_{s1}\right) \quad [4.39]$$

The calculation of the ultimate curvature κ_u can be achieved from the resolution of this ultimate strain condition, which is a linear equation expressed with respect to the curvature:

$$\kappa_u^* = \frac{\varepsilon_{ud} - \frac{\varepsilon_{c3}}{2}}{1 + \frac{f_{su}}{f_{cu}}\rho'_{s1}} \quad [4.40]$$

This solution (Pivot *A*2 failure) is valid as long as the strain of the upper fiber has not reached the ultimate concrete strain denoted by ε_{cu3}, which is mathematically expressed by the inequality:

$$\varepsilon_{c,\sup} = -\kappa_u \alpha_u d \geq \varepsilon_{cu3} \Rightarrow \kappa_u^* \alpha_u \leq -\varepsilon_{cu3} \quad [4.41]$$

This solution is in fact equivalent to consider that the steel reinforcement ratio has to be lower than a critical ratio given by:

$$\rho'_{s1} \leq \frac{f_{cu}}{f_{su}} \frac{\varepsilon_{cu3} - \frac{\varepsilon_{c3}}{2}}{\varepsilon_{ud} - \varepsilon_{cu3}} \quad [4.42]$$

This upper bound is clearly associated with the Pivot *AB* boundary. For higher reinforcement steel density, the beam fails with Pivot *B*, meaning that the strain capacity in the section is controlled by the strain capacity in the compression concrete block.

We calculate for a C30-37 type concrete and for a B500B steel the steel reinforcement ratio limit as:

$$\rho'_{s1} \leq \frac{30 \times 1.15}{500 \times 1.5} \times \frac{3.5 - \frac{1.75}{2}}{45 + 3.5} = 2.49 \times 10^{-3} \quad [4.43]$$

At the critical steel reinforcement ratio:

$$\rho'_{s1} = \frac{f_{cu}}{f_{su}} \frac{\varepsilon_{cu3} - \frac{\varepsilon_{c3}}{2}}{\varepsilon_{ud} - \varepsilon_{cu3}} \quad [4.44]$$

The beam fails at Pivot *AB*, that is the ultimate state is characterized by both the maximum strain capacity of the tensile steel reinforcement and the maximum strain capacity of the concrete block in compression. At the ULS associated with this critical steel reinforcement, we clearly have:

$$\alpha_{AB} = \frac{-\varepsilon_{cu3}}{\varepsilon_{ud} - \varepsilon_{cu3}} \text{ and } \mu_{AB} = \alpha_{AB}\left(1 - \frac{\alpha_{AB}}{2}\right) - \left(\frac{\varepsilon_{c3}}{\varepsilon_{cu3}}\right)\frac{\alpha_{AB}\left(1-\alpha_{AB}\right)}{2} - \frac{\alpha_{AB}^2}{6}\left(\frac{\varepsilon_{c3}}{\varepsilon_{cu3}}\right)^2 \quad [4.45]$$

Figure 4.5. shows the typical response of a reinforced concrete section that is controlled by Pivot *A*2 failure, for low steel reinforcement density ratio. The two stages of Pivot *A*1 and Pivot *A*2 are clearly seen with the initial yielding of the tensile steel reinforcement, and then the contribution of the micro-cracking effect in the compression block, even if the failure is still a Pivot *A* failure controlled by the tensile strain capacity in the steel reinforcement

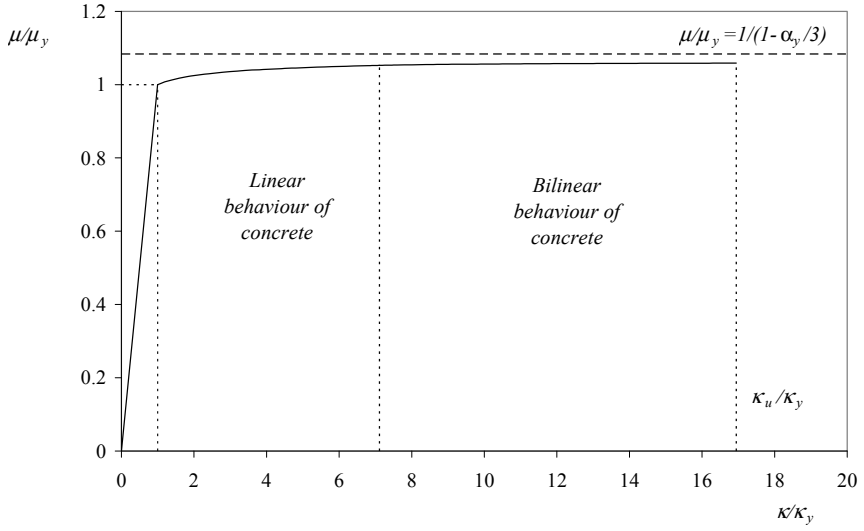

Figure 4.5. *Bending moment-curvature relationship of a reinforced concrete beam – failure with Pivot A2 – bilinear behavior of concrete; C30-37 for the concrete; B500B for the steel;* $\alpha_e = 17.5$; $\rho'_{s1} = 2 \times 10^{-3}$; $\alpha_y = 0.232$; $\mu_y = 0.04$; $\kappa_u / \kappa_y = 16.95$

4.1.3.5. *Pivot B – elastoplastic behavior of the tensile steel reinforcement*

We will now study the case of a Pivot *B*-type of failure, for the steel reinforcement ratio larger than the characteristic density:

$$\rho'_{s1} \geq \frac{f_{cu}}{f_{su}} \frac{\varepsilon_{cu3} - \frac{\varepsilon_{c3}}{2}}{\varepsilon_{ud} - \varepsilon_{cu3}} \qquad [4.46]$$

For this kind of reinforced concrete cross-section, the section behaves like in Pivot *A*1 (elastic behavior of the concrete) up to a critical curvature and then the section will behave in Pivot *B* (failure at Pivot *B* with plasticity in the tensile steel reinforcement).

$$\text{Linear behavior of concrete for } \frac{\kappa^*}{\kappa_y^*} \leq \frac{\varepsilon_{c3}^2}{\alpha_y^2 \kappa_y^{*2}} \text{ and}$$

$$\text{bilinear behavior of concrete for } \frac{\kappa^*}{\kappa_y^*} \geq \frac{\varepsilon_{c3}^2}{\alpha_y^2 \kappa_y^{*2}} \qquad [4.47]$$

The Pivot *B* branch is detailed below. The reduced moment equation is still valid, if the tensile steel reinforcement is in the elasticity range, and is given again below:

$$\mu = -\frac{1}{24}\left(\frac{\varepsilon_{c3}}{\kappa^*}\right)^2 - \rho'_{s1}\frac{f_{su}}{f_{cu}} - \frac{1}{2}\left(\rho'_{s1}\frac{f_{su}}{f_{cu}}\right)^2 \text{ for } \frac{\kappa}{\kappa_y} \in \left[\frac{\varepsilon_{c3}^2}{\alpha_y^2 \kappa_y^{*2}}; \frac{\kappa_u}{\kappa_y}\right] \qquad [4.48]$$

where κ_u is the ultimate curvature associated with Pivot *B*. The ULS at Pivot *B* is defined from the ultimate strain condition:

$$\varepsilon_{c,\sup} = \varepsilon_{cu3} = -\kappa_u \alpha_u d = \frac{\varepsilon_{c3}}{2} + \kappa_u^* \frac{f_{su}}{f_{cu}} \rho'_{s1} \qquad [4.49]$$

The calculation of the ultimate curvature κ_u can be achieved from the resolution of this ultimate strain condition, which is a linear equation expressed with respect to the curvature:

$$\kappa_u^* = \frac{(-f_{cu})}{\rho'_{s1} f_{su}} \left(-\varepsilon_{cu3} + \frac{\varepsilon_{c3}}{2} \right) \qquad [4.50]$$

Figure 4.6 shows a typical failure at Pivot *B*, which clearly shows the lower ductility of the response with a failure at Pivot *B* (failure in compression), as compared to the failure at Pivot *A* (failure in tension in the tensile steel reinforcement).

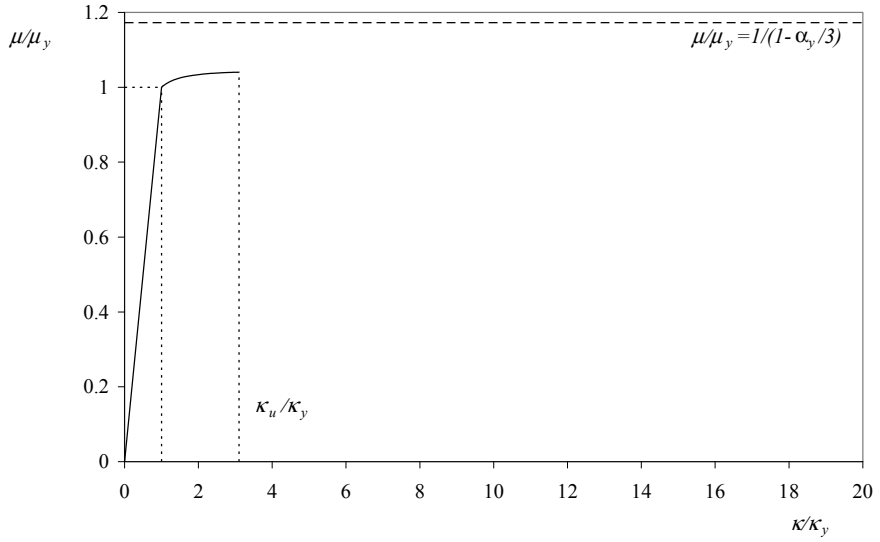

Figure 4.6. *Bending moment-curvature relationship of a reinforced concrete beam – failure with pivot B – bilinear behavior of concrete; C30-37 for the concrete; B500B for the steel;* $\alpha_e = 17.5$; $\rho'_{s1} = 1 \times 10^{-2}$; $\alpha_y = 0.442$; $\mu_y = 0.185$; $\kappa_u / \kappa_y = 3.10$

In this case, with the parameters of interest, the ductility that can be measured as the ratio between the ultimate curvature and the elastic curvature is approximately three, which is significantly different from the ductility observed in Pivot *A*. Furthermore, it is also observed that the asymptotic approximation of the reduced moment suggested for pivot *A* is no more relevant in this case.

4.13.6. *Pivot B – elastic behavior of the tensile steel reinforcement*

For very high steel reinforcement density, the concrete still remains in the linear range. The equilibrium equations are now written as:

$$M = E_c b\kappa \left[\frac{y^3}{3} + (d-\alpha d)\frac{y^2}{2}\right]_0^{(\alpha-\alpha_c)d} -$$

$$f_{cu} b \left[\frac{y^2}{2} + (d-\alpha d)\, y\right]_{(\alpha-\alpha_c)d}^{\alpha d} \text{ and}$$

$$N = \frac{b(\alpha-\alpha_c)d}{2} f_{cu} + b\alpha_c d f_{cu} + A_{s1}\sigma_{s1} = 0 \text{ with}$$

$$\sigma_{s1} = E_s \varepsilon_{s1} = E_s \kappa d (1-\alpha) \qquad [4.51]$$

Introducing the relationship between the neutral axis parameters (see also Figure 3.29):

$$\alpha - \alpha_c = -\frac{\varepsilon_{c3}}{\kappa^*} \qquad [4.52]$$

the normal force equilibrium equation gives the neutral axis position with respect to the curvature as:

$$\alpha = \frac{A_{s1}E_s\kappa d + \dfrac{bf_{cu}\varepsilon_{c3}}{2\kappa}}{A_{s1}E_s\kappa d - bdf_{cu}} \qquad [4.53]$$

The other parameter α_c, which defines the limit of the elastic domain in the compression concrete block along the cross-section, is deduced as:

$$\alpha_c = \frac{A_{s1}E_s(\kappa d + \varepsilon_{c3}) - \dfrac{bf_{cu}\varepsilon_{c3}}{2\kappa}}{A_{s1}E_s\kappa d - bdf_{cu}} \qquad [4.54]$$

The bending moment-curvature is obtained using the bending moment equilibrium equation that gives a nonlinear function as:

$$M = E_c b\kappa \left[\frac{1}{3}\left(\frac{-\varepsilon_{c3}}{\kappa} \right)^3 + \frac{1}{2}\left(\frac{\varepsilon_{c3}}{\kappa} \right)^2 \frac{bdf_{cu} + bf_{cu}\dfrac{\varepsilon_{c3}}{2\kappa}}{-A_{s1}E_s\kappa + bf_{cu}} \right] -$$
$$f_{cu}bd^2 \left[\left(\frac{A_{s1}E_s\left(\kappa d + \varepsilon_{c3}\right) - \dfrac{bf_{cu}\varepsilon_{c3}}{2\kappa}}{A_{s1}E_s\kappa d - bdf_{cu}} \right) - \right.$$
$$\left. \frac{1}{2}\left(\frac{A_{s1}E_s\left(\kappa d + \varepsilon_{c3}\right) - \dfrac{bf_{cu}\varepsilon_{c3}}{2\kappa}}{A_{s1}E_s\kappa d - bdf_{cu}} \right)^2 \right] \qquad [4.55]$$

It is possible to define a new critical curvature κ_y associated with a strain $\varepsilon_{c,\sup}$ in the upper fiber of the cross-section, equal to the maximum elastic strain ε_{c3} in the compression block of concrete, such as:

$$\varepsilon_{c,\sup} = \varepsilon_{c3} \Rightarrow \kappa_y = \frac{-\varepsilon_{c3}}{d\alpha_y} \text{ with}$$
$$\alpha_y = -\alpha_e\rho'_{s1} + \sqrt{\left(\alpha_{\acute{e}}\rho'_{s1}\right)^2 + 2\alpha_e\rho'_{s1}} \qquad [4.56]$$

The dimensionless critical curvature can be easily defined as:

$$\kappa_y^* = \kappa_y d = \frac{-\varepsilon_{c3}}{\alpha_y} \qquad [4.57]$$

The reduced moment parameters can be also introduced as:

$$\mu_y = -\frac{\alpha_y^2}{2}\left(1 - \frac{\alpha_y}{3}\right)\left(\frac{\kappa_y^*}{\varepsilon_{c3}}\right) = \frac{\alpha_y}{2}\left(1 - \frac{\alpha_y}{3}\right) \qquad [4.58]$$

The reduced moment can be rewritten as:

$$\mu = \left(\frac{\kappa^*}{-\varepsilon_{c3}}\right)\left[\frac{1}{3}\left(\frac{-\varepsilon_{c3}}{\kappa^*}\right)^3 + \frac{1}{2}\left(\frac{\varepsilon_{c3}}{\kappa^*}\right)^2 \frac{1+\dfrac{\varepsilon_{c3}}{2\kappa^*}}{1+\alpha_e\rho'_s\left(\dfrac{\kappa^*}{-\varepsilon_{c3}}\right)}\right] + \left[\left(\frac{-\alpha_e\rho'_{s1}\left(\dfrac{\kappa^*}{\varepsilon_{c3}}+1\right)+\dfrac{\varepsilon_{c3}}{2\kappa^*}}{-\alpha_e\rho'_{s1}\left(\dfrac{\kappa^*}{\varepsilon_{c3}}\right)+1}\right) - \frac{1}{2}\left(\frac{-\alpha_e\rho'_{s1}\left(\dfrac{\kappa^*}{\varepsilon_{c3}}+1\right)+\dfrac{\varepsilon_{c3}}{2\kappa^*}}{-\alpha_e\rho'_{s1}\left(\dfrac{\kappa^*}{\varepsilon_{c3}}\right)+1}\right)^2\right]$$

$$\text{for } \frac{\kappa}{\kappa_y} \in \left[1; \frac{\kappa_u}{\kappa_y}\right] \qquad [4.59]$$

where κ_u is the ultimate curvature associated with Pivot *B*. The ULS at Pivot *B* is defined from the ultimate strain condition:

$$\varepsilon_{c,\text{sup}} = \varepsilon_{cu3} \Rightarrow \kappa_u = \frac{-\varepsilon_{cu3}}{d\alpha_u} \text{ with } \alpha_u = \frac{A_{s1}E_s\kappa_u d + \dfrac{bf_{cu}\varepsilon_{c3}}{2\kappa_u}}{A_{s1}E_s\kappa_u d - bdf_{cu}} \qquad [4.60]$$

The calculation of the ultimate curvature κ_u can be achieved from the resolution of this ultimate strain condition, which is a nonlinear equation expressed with respect to the curvature:

$$\kappa_u^{*2} + \varepsilon_{cu3}\kappa_u^* - \frac{f_{cu}}{\rho'_{s1}E_s}\left(\varepsilon_{cu3} - \frac{\varepsilon_{c3}}{2}\right) = 0 \qquad [4.61]$$

The ultimate curvature is then obtained as the positive solution of this second-order polynomial equation, which is:

$$\kappa_u^* = \frac{-\varepsilon_{cu3} + \sqrt{\varepsilon_{cu3}^2 + \dfrac{4f_{cu}}{\rho'_{s1}E_s}\left(\varepsilon_{cu3} - \dfrac{\varepsilon_{c3}}{2}\right)}}{2} \qquad [4.62]$$

This solution (Pivot *B* failure with only elastic behavior of the tensile steel reinforcement) is valid as long as the strain in the tensile steel

reinforcement ε_{s1} has not reached the elastic steel strain denoted by ε_{su}, which is mathematically expressed by the inequality:

$$\varepsilon_{s1} = \kappa_u^* \left(1 - \alpha_u\right) \le \varepsilon_{su} = \frac{f_{su}}{E_s} \Rightarrow \kappa_u^* \le \varepsilon_{su} - \varepsilon_{cu3} \qquad [4.63]$$

This solution is in fact equivalent to consider that the steel reinforcement ratio has to be larger than a critical ratio given by:

$$\rho'_{s1} \ge \frac{f_{cu}}{f_{su}} \frac{\varepsilon_{cu3} - \frac{\varepsilon_{c3}}{2}}{\varepsilon_{su} - \varepsilon_{cu3}} \qquad [4.64]$$

We calculate for a C30-37 type concrete and for a B500B steel the steel reinforcement ratio limit as:

$$\rho'_{s1} \ge \frac{30 \times 1.15}{500 \times 1.5} \times \frac{3.5 - \frac{1.75}{2}}{2.17 + 3.5} = 2.13 \times 10^{-2} \qquad [4.65]$$

The numerical results presented in Figure 4.7 show the bending-curvature constitutive law for a Pivot *B* failure response with a reinforcement density equal to $\rho'_{s1} = 2.5 \times 10^{-2}$, which is larger than the one computed above $\rho'_{s1} = 2.13 \times 10^{-2}$ and associated with the transition to Pivot *B*.

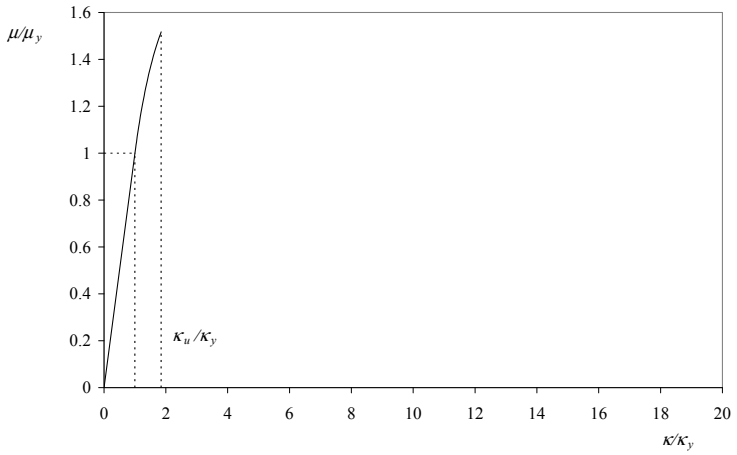

Figure 4.7. *Bending moment-curvature relationship of a reinforced concrete beam – failure with pivot B – bilinear behavior of concrete; C30-37 for the concrete; B500B for the steel;* $\alpha_e = 17.5$; $\rho'_{s1} = 2.5 \times 10^{-2}$; $\alpha_y = 0.595$; $\mu_y = 0.239$; $\kappa_u / \kappa_y = 1.85$

4.1.3.7. *Synthesis of the bending-curvature constitutive laws*

Each kind of reinforced cross-section is associated with a specific bending-curvature constitutive law. Table 4.1 summarizes the main results on the ductility formulae depending on the steel content of the reinforced concrete cross-section.

Pivot	Pivot *A*	Pivot *A*	Pivot *B*	Pivot *B*
ρ'_{s1}	$\rho'_{s1} \le \frac{f_{cu}}{f_{su}} \frac{\frac{\varepsilon_{c3}}{2}}{\varepsilon_{ud} - \varepsilon_{c3}}$	$\frac{f_{cu}}{f_{su}} \frac{\frac{\varepsilon_{c3}}{2}}{\varepsilon_{ud} - \varepsilon_{c3}} \le \rho'_{s1} \le \frac{f_{cu}}{f_{su}} \frac{\varepsilon_{cu3} - \frac{\varepsilon_{c3}}{2}}{\varepsilon_{ud} - \varepsilon_{cu3}}$	$\frac{f_{cu}}{f_{su}} \frac{\varepsilon_{cu3} - \frac{\varepsilon_{c3}}{2}}{\varepsilon_{ud} - \varepsilon_{cu3}} \le \rho'_{s1} \le \frac{f_{cu}}{f_{su}} \frac{\varepsilon_{cu3} - \frac{\varepsilon_{c3}}{2}}{\varepsilon_{su} - \varepsilon_{cu3}}$	$\rho'_{s1} \ge \frac{f_{cu}}{f_{su}} \frac{\varepsilon_{cu3} - \frac{\varepsilon_{c3}}{2}}{\varepsilon_{su} - \varepsilon_{cu3}}$
Numerical values: C30-37 and B500B	$\rho'_{s1} \le 8.61 \times 10^{-4}$	$8.61 \times 10^{-4} \le \rho'_{s1} \le 2.49 \times 10^{-3}$	$2.49 \times 10^{-3} \le \rho'_{s1} \le 2.13 \times 10^{-2}$	$\rho'_{s1} \ge 2.13 \times 10^{-2}$
κ_u	$\kappa_u^* = \varepsilon_{ud} + \rho'_{s1}\alpha_e\varepsilon_{su} + \sqrt{\left(\varepsilon_{ud} + \rho'_{s1}\alpha_e\varepsilon_{su}\right)^2 - \varepsilon_{ud}^2}$	$\kappa_u^* = \frac{\varepsilon_{ud} - \frac{\varepsilon_{c3}}{2}}{1 + \frac{f_{su}}{f_{cu}}\rho'_{s1}}$	$\kappa_u^* = \frac{\left(-f_{cu}\right)}{\rho'_{s1} f_{su}} \left(-\varepsilon_{cu3} + \frac{\varepsilon_{c3}}{2}\right)$	$\kappa_u^* = \frac{-\varepsilon_{cu3} + \sqrt{\varepsilon_{cu3}^2 + \frac{4 f_{cu}}{\rho'_{s1} E_s}\left(\varepsilon_{cu3} - \frac{\varepsilon_{c3}}{2}\right)}}{2}$
Numerical values: C30-37 and B500B	$\frac{\kappa_u^*}{\kappa_y^*} \ge 18.08$	$16.62 \le \frac{\kappa_u^*}{\kappa_y^*} \le 18.08$	$1.84 \le \frac{\kappa_u^*}{\kappa_y^*} \le 16.62$	$\frac{\kappa_u^*}{\kappa_y^*} \ge 1.84$

Table 4.1. *Ductility* κ_u / κ_y *with respect to the dimensionless steel reinforcement quantity* ρ'_{s1}

The calculation of the dimensionless elastic curvature κ_y^* is controlled by the steel content ρ'_{s1} in the reinforced concrete section, and the steel and concrete strain capacities as:

$$\kappa_y^* = \frac{\varepsilon_{su}}{1 - \alpha_y} \text{ if } \alpha_y \le \frac{-\varepsilon_{c3}}{\varepsilon_{su} - \varepsilon_{c3}}, \kappa_y^* = \frac{-\varepsilon_{c3}}{\alpha_y} \text{ if } \alpha_y \ge \frac{-\varepsilon_{c3}}{\varepsilon_{su} - \varepsilon_{c3}} \text{ with}$$
$$\alpha_y = -\alpha_e\rho'_{s1} + \sqrt{\left(\alpha_e\rho'_{s1}\right)^2 + 2\alpha_e\rho'_{s1}} \qquad [4.66]$$

In a certain sense, this calculation is linked to the determination of Pivot *A* or Pivot *B* at SLS. We note that the determination of the pivot nature at ULS can be different from the pivot nature at SLS, the elastic SLS can be controlled, for instance, by the steel strain capacity at SLS associated accompanied with a Pivot *B* failure (ULS). These inequalities conditions can be expressed directly with respect to the steel content as:

$$\kappa_y^* = \frac{\varepsilon_{su}}{1+\alpha_e\rho'_{s1}-\sqrt{\left(\alpha_{\acute{e}}\rho'_{s1}\right)^2+2\alpha_e\rho'_{s1}}} \text{ if } \rho'_{s1} \le \frac{1}{2}\left(\frac{-f_{cu}}{f_{su}}\right)\frac{-\varepsilon_{c3}}{\varepsilon_{su}-\varepsilon_{c3}};$$
$$\kappa_y^* = \frac{-\varepsilon_{c3}}{-\alpha_e\rho'_{s1}+\sqrt{\left(\alpha_{\acute{e}}\rho'_{s1}\right)^2+2\alpha_e\rho'_{s1}}} \text{if } \rho'_{s1} \ge \frac{1}{2}\left(\frac{-f_{cu}}{f_{su}}\right)\frac{-\varepsilon_{c3}}{\varepsilon_{su}-\varepsilon_{c3}} \qquad [4.67]$$

4.1.3.8. *Ductility of the reinforced concrete section*

Figure 4.8 shows the decrease in ductility with the steel reinforcement density, and the transition from Pivot *A* failure to Pivot *B* failure. The ductility is very sensitive to the reinforcement design, and it is not recommended to have heavily reinforced sections, to avoid quasi-brittle or brittle responses of the reinforced beams. In practice, to avoid the quasi-brittle responses of the reinforced concrete beams, it is required that the steel content is bounded by a critical ratio ρ_b, calculated as:

$$\rho'_{s1} \le \rho_b = \frac{f_{cu}}{f_{su}}\frac{\varepsilon_{cu3}-\frac{\varepsilon_{c3}}{2}}{\varepsilon_{su}-\varepsilon_{cu3}} \qquad [4.68]$$

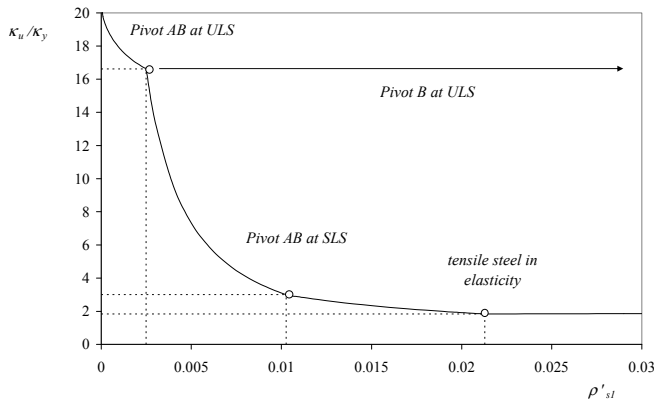

Figure 4.8. *The ductility κ_u / κ_y strongly depends on the steel content ρ'_{s1}; C30-37 for the concrete; B500B for the steel; $\alpha_e = 17.5$*

This condition expressed the need of inelastic strains in the tensile steel reinforcement to guaranty a minimum amount of ductility.

The strength capacity evolution with respect to the steel content is studied in Figures 4.9 and 4.10. The curves have been drawn due to the analytical expressions of the reduced moment presented in this chapter for each kind of behavior, and piecing together each solution. The inelastic strength reserve measured by the dimensionless factor μ_u / μ_y is close to unity in Pivot *A* and in Pivot *B* at ULS up to the critical point where the section behaves in Pivot *AB* at SLS, where the inelastic strength reserve significantly increases. Once the section has reached its behavior characterized by the elastic behavior of the tensile steel reinforcement, the strength capacity is stable and is no more sensitive to the steel content. More generally, as the ductility κ_u / κ_y decreases with the steel content ρ'_{s1}, the strength capacity of the reinforced cross-section measured by the ultimate reduced moment μ_u monotonically increases (see Figure 4.10). However, a singular point is clearly exhibited in Figure 4.10 for a steel content ρ'_{s1} equal to the critical ratio ρ_b associated with the elasticity behavior of the tensile steel reinforcement at ULS. This point is classified as the balance failure (see, for instance, [PAR 75]). This point is located in Pivot *B* where the section is controlled by the strain capacity in concrete at ULS, and is associated with a change of behavior of the tensile steel reinforcement from the plateau range in plasticity to the elasticity range.

It is shown in Figure 4.10 that the ultimate reduced moment increases almost linearly up to the point corresponding to the balance failure $\rho'_{s1} \leq \rho_b$. In the compression failure region for $\rho'_{s1} \geq \rho_b$, the increase in moment with steel area is extremely small because both the steel stress and the lever arm decrease with increase in the steel content for this regime. Hence, there is a change of slope in the diagram of the reduced moment with respect to the steel content at this specific point and there is only a little additional strength to be gained by an increase in the steel area (see Figure 4.10).

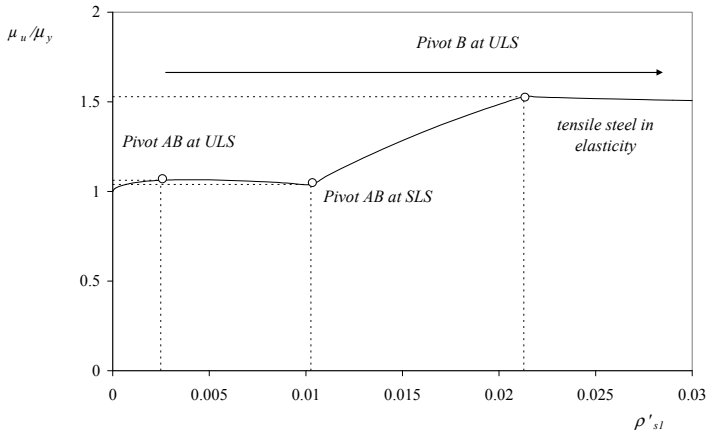

Figure 4.9. *The inelastic strength reserve μ_u / μ_y strongly depends on the steel content ρ'_{s1}; C30-37 for the concrete; B500B for the steel; $\alpha_e = 17.5$*

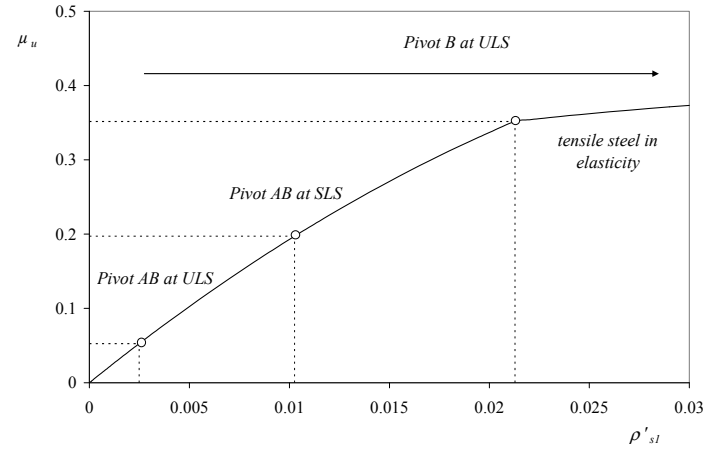

Figure 4.10. *The strength capacity μ_u strongly depends on the steel content ρ'_{s1}; C30-37 for the concrete; B500B for the steel; $\alpha_e = 17.5$*

4.1.3.9. *Condition of non-fragility*

For ductility reasons, it has been shown that it is required for the steel content ρ'_{s1} to be less than a critical steel content ρ_b corresponding to the balance failure point. It is also required to stipulate a minimum reinforcement ratio that should always be exceeded to avoid a brittle

response of the reinforced concrete beam. This condition is called the condition of non-fragility. This is because if the reinforcement ratio is too small, the calculated flexural strength of the reinforced concrete section M_u becomes lower than the bending moment required to crack the section M_{cr} (see Chapter 2), and on cracking, failure becomes sudden and brittle. This condition is mathematically expressed by:

$$M_u \geq M_{cr} = \frac{f_{ctm} I_1}{h - y_1} \qquad [4.69]$$

It can also be a requirement that the elastic moment of the cracked section M_y has to be larger than the critical moment of the uncracked section M_{cr}:

$$M_y \geq M_{cr} = \frac{f_{ctm} I_1}{h - y_1} \qquad [4.70]$$

As shown in this chapter, these two last inequalities are very close in Pivot *A*, which is the Pivot concerned for low steel density. For the unsymmetrical reinforced concrete section with only tensile steel reinforcement, this inequality in Pivot *A* (or in Pivot *B* with an SLS in Pivot *A*) is equivalent to:

$$\rho'_{s1}\left(1 - \frac{\alpha_y}{3}\right) \geq \frac{M_{cr}}{bd^2 f_{su}} \text{ with } \alpha_y = -\alpha_e \rho'_{s1} + \sqrt{\left(\alpha_e \rho'_{s1}\right)^2 + 2\alpha_e \rho'_{s1}} \qquad [4.71]$$

The nonlinear inequality has then to be solved as:

$$\rho'_{s1}\left(1 - \frac{\alpha_y}{3}\right) \geq \frac{f_{ctm}}{f_{su}} \frac{\frac{1}{3}\alpha_1^3 + \frac{1}{3}\left(\frac{h}{d} - \alpha_1\right)^3 + \alpha_e \rho'_{s1}\left(1 - \alpha_1\right)^2}{\frac{h}{d} - \alpha_1} \text{ with}$$

$$\alpha_1 = \frac{\frac{1}{2}\left(\frac{h}{d}\right)^2 + \alpha_e \rho'_{s1}}{\frac{h}{d} + \alpha_e \rho'_{s1}} \text{ and } \alpha_y = -\alpha_e \rho'_{s1} + \sqrt{\left(\alpha_e \rho'_{s1}\right)^2 + 2\alpha_e \rho'_{s1}} \qquad [4.72]$$

Figure 4.11 shows the evolution of the minimum steel reinforcement ρ'_{s1} with respect to the tension strength ratio f_{ctm}/f_{su}, and this curve was obtained from the non-linear function defined by [4.72].

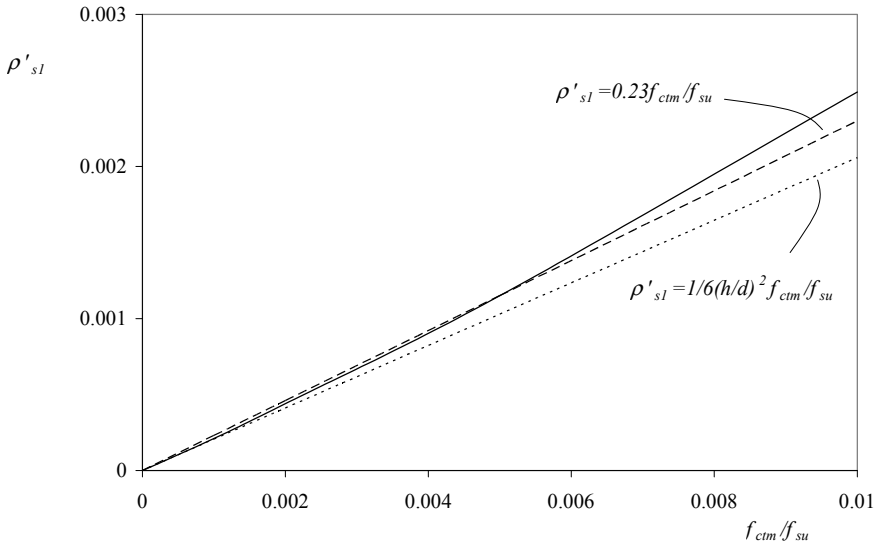

Figure 4.11. *Condition of non-fragility expressed with the minimum steel reinforcement* ρ'_{s1} *with respect to the tension strength ratio* f_{ctm}/f_{su}; $\alpha_e = 17.5$; $d/h = 0.9$

An approximated formula can be obtained by assuming that the critical moment is independent of the steel content and is expressed by:

$$M_{cr} \approx \frac{bh^2}{6} f_{ctm} \Rightarrow \rho'_{s1}\left(1-\frac{\alpha_y}{3}\right) \geq \frac{1}{6}\left(\frac{h}{d}\right)^2 \frac{f_{ctm}}{f_{su}} \qquad [4.73]$$

Hence, for sufficiently small values of the steel content, the lower bound is obtained as:

$$\rho'_{s1} \geq \frac{1}{6}\left(\frac{h}{d}\right)^2 \frac{f_{ctm}}{f_{su}} \qquad [4.74]$$

This lower bound is calculated below for different geometrical d/h ratios as:

$$\frac{d}{h}=0.9 \Rightarrow \rho'_{s1} \geq 0.21\frac{f_{ctm}}{f_{su}}; \frac{d}{h}=0.85 \Rightarrow \rho'_{s1} \geq 0.23\frac{f_{ctm}}{f_{su}} \quad [4.75]$$

It is shown in Figure 4.11 that the linear approximation with the proportionality coefficient 0.21 corresponding to $d/h=0.9$ is relevant only for small steel content. However, for larger steel content, the proportionality coefficient 0.23 is more accurate, due to the weak nonlinearity of the curve. This coefficient 0.23 is, in fact, the coefficient that corresponds to $d/h=0.85$. The same coefficient 0.23 is used as a correction coefficient for the condition of non-fragility of the old French rules *Béton Armé aux Etats Limites*:

$$\frac{d}{h}=0.9 \Rightarrow \frac{A_{s1}}{bd} \geq 0.21\frac{f_{ctm}}{f_{su}}$$

$$\Rightarrow \frac{A_{s1}}{bd} \geq 0.21\gamma_s \frac{f_{ctm}}{f_{yk}} = 0.237\frac{f_{ctm}}{f_{yk}} \text{ with } \gamma_s = 1.15 \quad [4.76]$$

The condition of non-fragility of the old French rules *Béton Armé aux Etats Limites* is normalized with respect to the uniaxial tensile limit strength f_{yk}:

$$\frac{f_{ctm}}{f_{yk}} = 0.23\frac{f_{ctm}}{f_{yk}} \quad [4.77]$$

4.1.4. *A model based on the bilinear moment-curvature approximation*

The bending-curvature relationship is strongly dependent on the steel content and the material constitutive laws. The normalized bending-curvature relationship of each studied bending-curvature law can be presented in Figure 4.12.

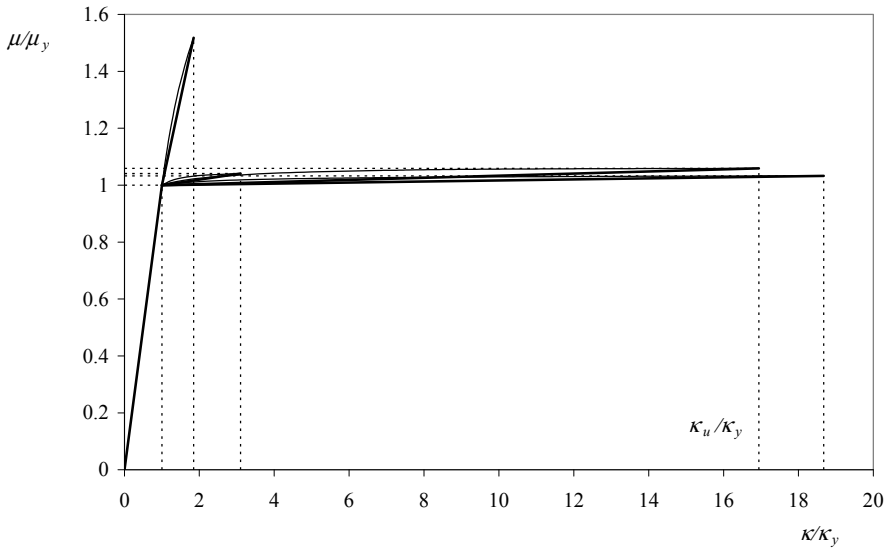

Figure 4.12. *Normalized bending-curvature constitutive law as a function of the steel content* ρ'_{s1}; *C30-37 for the concrete; B500B for the steel;* $\alpha_e = 17.5$

Each curve, numerically obtained with bilinear constitutive laws for both the steel reinforcement and the compression block, can be reasonably approximated by a global bilinear constitutive law (at the beam scale), with a linear elastic stage and a linear hardening bending-curvature constitutive law. Such kinds of bilinear bending-curvature constitutive laws have also been obtained in the literature with some other constitutive laws for the concrete. Park and Paulay [PAR 75] (with a Hognestad constitutive law for the concrete part), Carreira and Chu [CAR 86] (with the generalization of Sargin's law for the concrete part) or Chandrasekaran *et al*. [CHA 09e] (with a parabola–rectangle constitutive law for the concrete part) also found that the bending moment-curvature relationship is close to a bilinear approximation (with hardening range). Furthermore, Chandrasekaran *et al*. gave the exact analytical expressions of the bending-curvature constitutive law with a rectangle-parabolic constitutive law for the concrete ([CHA 09e], [CHA 10d] and [CHA 11d]).

This kind of bilinear bending moment-curvature constitutive law is also used by Challamel [CHA 03] for steel sections, and, in fact, many engineering applications are concerned by such a mathematical bilinear

modeling. The bilinear approximation can be modeled by a plasticity model at the beam scale with a linear hardening law (see Figure 4.13).

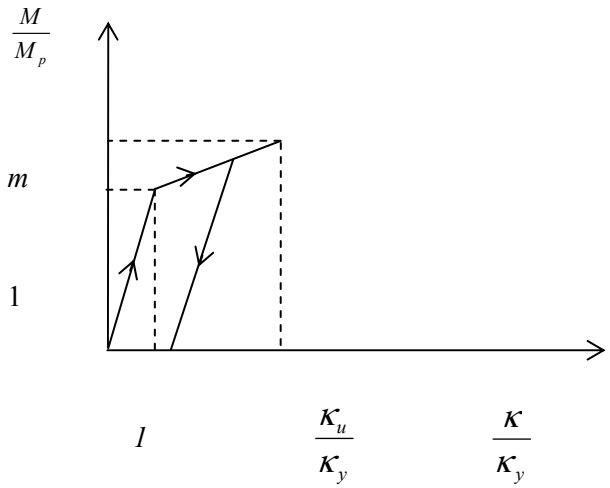

Figure 4.13. *Normalized bending-curvature constitutive law;* $M_p = M_y$ *and* $m = M_u / M_y = \mu_u / \mu_y$

For a monotonic loading, the bilinear constitutive law is given by:

$$\frac{\mu}{\mu_y} = \frac{\kappa}{\kappa_y} \text{ for } \frac{\kappa}{\kappa_y} \in [0;1] \text{ and}$$

$$\frac{\mu}{\mu_y} = \frac{(m-1)\frac{\kappa}{\kappa_y} + \frac{\kappa_u}{\kappa_y} - m}{\frac{\kappa_u}{\kappa_y} - 1} \text{ for } \frac{\kappa}{\kappa_y} \in \left[1; \frac{\kappa_u}{\kappa_y}\right] \qquad [4.78]$$

The parameters of the constitutive law κ_y, μ_y, κ_u and μ_u are given for each steel content and for each behavior of the reinforced concrete cross-section (see, for instance, Table 4.1 for the identification of each parameter from the local steel and concrete constitutive laws based on bilinear approximations).

The local moment-curvature relationship (M, κ) considered is bilinear with a linear elastic part and a linear softening part (Figure 4.13). This model

is first considered in a local form, that is standard plasticity model with negative hardening. The non-local extension will be investigated later in this chapter. M_p is the limit elastic moment, and κ_y is the limit elastic curvature, related through $M_p / \chi_y = EI_{eq} = EI$, which is the equivalent stiffness of the homogeneous cracked section

The elastoplastic model represented in Figure 4.13 is a standard plasticity model with positive plasticity hardening, associated with the yield function f given by equation [3.12], with the plasticity flow rule given by equation [3.13]. The hardening being linear, the following relation holds for the "local" case:

$$M^*\left(\kappa_p\right) = k^+ \left| \ \kappa_p \ \right| \text{ with } k^+ > 0 \qquad [4.79]$$

Using equation [3.16], the hardening branch of the bending moment-curvature constitutive law can be presented in the following form:

$$\frac{\mu}{\mu_y} = \frac{EI}{EI + k^+} + \frac{k^+}{EI + k^+}\frac{\kappa}{\kappa_y} \text{ for } \frac{\kappa}{\kappa_y} \in \left[1; \frac{\kappa_u}{\kappa_y}\right] \qquad [4.80]$$

The hardening modulus can then be calculated from:

$$\frac{k^+}{EI} = \frac{m-1}{\frac{\kappa_u}{\kappa_y} - m} \qquad [4.81]$$

The plasticity hardening modulus k^+ associated with the macroscopic bending response of the reinforced concrete beam depends on the material constituent of the cross-section, and especially on the ductility of the reinforced cross-section, which is very sensitive to the steel content (see Figure 4.14). Figure 4.14 shows the dependence of the equivalent hardening modulus of an unsymmetrical reinforced concrete section, calculated from the bilinear constitutive law for concrete at the local state, and an elastic-perfect plasticity law for the tensile steel reinforcement.

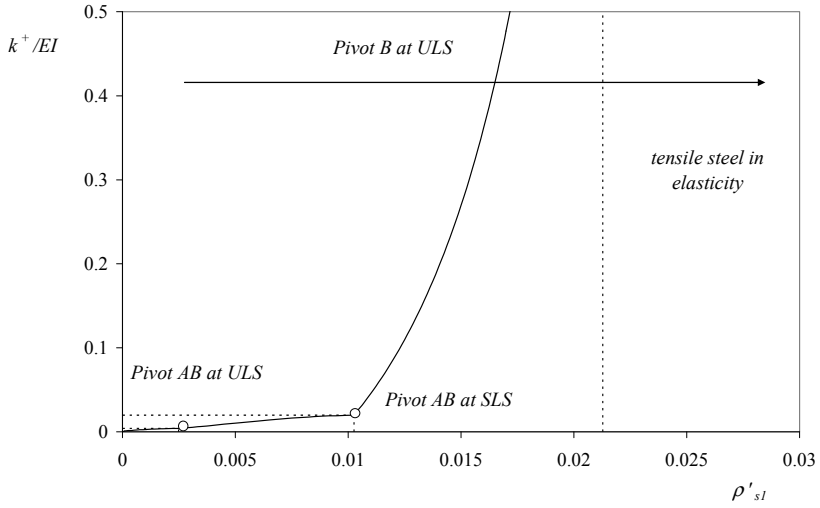

Figure 4.14. *Evolution of the equivalent hardening modulus k^+/EI with respect to the steel content ρ'_{s1} for an unsymmetrical reinforced concrete section with bilinear response for concrete*

4.2. Postfailure of reinforced concrete beams with the initial bilinear moment-curvature constitutive law

4.2.1. *Elastic-hardening constitutive law*

In this chapter, the bending response of a reinforced concrete cantilever beam will be theoretically investigated up to the failure. The cantilever is shown in Figure 3.2, as already investigated with an elastic-softening response. Following the theoretical developments for the justification of the macroscopic bending response from the local steel and concrete constitutive laws, an elastic-hardening response will be first considered. This reinforced concrete cantilever problem has also been investigated by Park and Paulay [PAR 75] with a bilinear bending-curvature constitutive law associated with positive hardening (see, for instance, Figure 4.13). This problem, with elastic-hardening bending-curvature constitutive law, has been recently studied by Challamel *et al*. [CHA 10b] for the cantilever structural case, and by Chandrasekaran *et al.* [CHA 09e] for fixed–fixed beams or simply supported beams under concentrated and distributed loading.

The cantilever beam problem is a statically determinate problem with a bending moment evolution given by equation [3.2]. For monotonic increasing loading, the beam behaves in the elastic range, for P smaller than $P_y = M_p / L$. In the hardening range, the load is increasing such as:

$$P \in \left[P_Y ; mP_Y \right] \text{ with } P_Y = \frac{M_p}{L} \qquad [4.82]$$

For increasing value of the load outside the elastic domain, the plastic regime starts and the beam can be split into an elastic and a plastic domain (see also Figure 3.2). The size of the plastic zone is denoted by l_0^+. In the plastic zone, the plastic curvature is linearly increasing:

$$x \in \left[0; l_0^+ \right] : \left| \ \kappa_p (x) \ \right| = \frac{1}{k^+} \left[P(L-x) - M_p \right] \qquad [4.83]$$

The continuity of the plastic curvature at the elastic–plastic interface leads to the plastic zone-load relationship:

$$\kappa_p \left(l_0^+ \right) = 0 \Rightarrow \frac{l_0^+}{L} = 1 - \frac{P_Y}{P} \qquad [4.84]$$

Note that the propagation of the local hardening process zone is equivalent to the linear relationship between previously used dimensionless parameters:

$$\beta = \xi \text{ with } \beta = \left(1 - \frac{P_Y}{P} \right) \frac{L}{l_c} \geq 0 \text{ and } \xi = \frac{l_0^+}{l_c} \geq 0 \qquad [4.85]$$

The displacement field in the plastic zone is obtained using the boundary conditions (clamped beam):

$$x \in \left[0; l_0^+ \right] : EIw^- (x) = -\left(1 + \frac{EI}{k^+} \right) P \frac{x^3}{6} + \left[\left(1 + \frac{EI}{k^+} \right) PL - M_p \frac{EI}{k^+} \right] \frac{x^2}{2} \qquad [4.86]$$

The displacement in the elastic zone is obtained by enforcing the continuity of the displacement and the rotation at the interface:

$$x \in \left[l_0^+ ; L \right] : EIw^+(x) = -P\frac{x^3}{6} + PL\frac{x^2}{2} + \frac{EI}{k^+}P\frac{\left(l_0^+\right)^2}{2}x - \frac{EI}{k^+}P\frac{\left(l_0^+\right)^3}{6} \quad [4.87]$$

The load-deflection relationship is finally deduced in the hardening range from:

$$\frac{v}{v_Y} = \frac{P}{P_Y} + 3\frac{EI}{k^+}\frac{P}{P_Y}\left[\frac{1}{2}\left(\frac{l_0^+}{L}\right)^2 - \frac{1}{6}\left(\frac{l_0^+}{L}\right)^3\right] \text{ with } \frac{l_0^+}{L} = 1 - \frac{P_Y}{P} \quad [4.88]$$

Figure 4.15 shows the hardening range for the cantilever beam. It can be easily checked from equation [4.88] that the load-deflection relationship is not linear, even for the local hardening constitutive behavior considered in this paragraph (see also Figure 4.15).

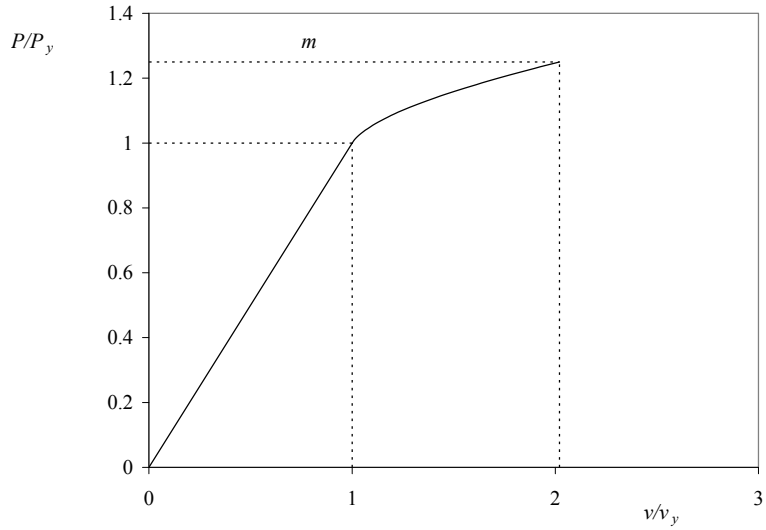

Figure 4.15. *Load-deflection relationship for the cantilever reinforced concrete beam with a bilinear bending-curvature constitutive law;* $m = 5/4$; $EI/k^+ = 11$

A remarkable result is that the plastic curvature distribution depends on the hardening law but the propagation law (equation [4.84] or

equation [4.85]) does not depend on the model of the hardening law. In fact, whatever the hardening model (even in case of nonlinear hardening), the same equality is valid:

$$\kappa_p\left(l_0^+\right)=0 \Rightarrow M^*\left(l_0^+\right)=0 \Rightarrow M\left(l_0^+\right)=P\left(L-l_0^+\right)=M_p \qquad [4.89]$$

The total curvature along the beam is calculated from:

$$x\in\left[0;l_0^+\right]:\frac{\left|\kappa(x)\right|}{\kappa_y}=-\left(1+\frac{EI}{k^+}\right)\frac{P}{P_y}\frac{x}{L}+\left(1+\frac{EI}{k^+}\right)\frac{P}{P_y}-\frac{EI}{k^+};$$
$$x\in\left[l_0^+;L\right]:\frac{\left|\kappa(x)\right|}{\kappa_y}=\frac{P}{P_y}\left(1-\frac{x}{L}\right) \qquad [4.90]$$

The curvature increases drastically inside the inelastic plasticity zone that occurs in an equivalent "plastic hinge" in the vicinity of the critical section (see Figure 4.16).

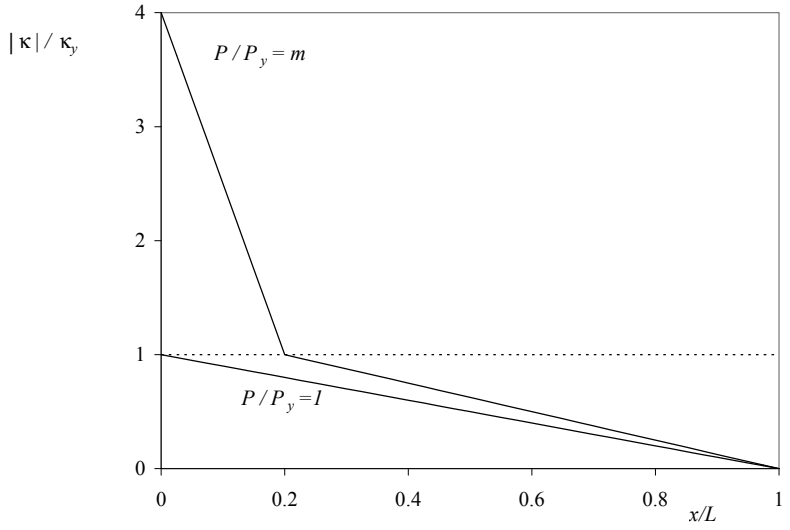

Figure 4.16. *Evolution of the total curvature along the beam* $m=5/4;\ EI/k^+=11$

Using equation [4.81] with the sectional parameters $m=5/4$ and $EI/k^+=11$, we calculate $\kappa_u/\kappa_y=4$, which is the curvature value obtained in

the clamped section with the associated loading parameter. The maximum size of the plastic length in the hardening process is obtained from:

$$\frac{l_0^+}{L} = 1 - \frac{1}{m} = 1 - \frac{\mu_y}{\mu_u} \qquad [4.91]$$

The value of m that controls the strength capacity reserve beyond the elastic moment depends on the design of the reinforced concrete section and the considered Pivot. In the present reasoning, the phenomenon of increase in steel forces due to inclined diagonal tension cracks is neglected. This additional phenomenon can be taken into account by some correction of the linearly decreasing curvature (see [PAR 75], [PAU 92]). Diagonal tension cracks in the plasticity zone increase the available plastic rotation by spreading the zone of yielding along the member (tension shift effect).

4.2.2. *Plastic hinge approach*

A simplified plastic hinge approach can be used, associated with an equivalent length of the plastic hinge over which the plastic curvature is considered to be constant and equal to the mean value of the exact curvature field $\hat{\kappa}_p$:

$$\hat{\kappa}_p = \frac{\kappa_p(0) + \kappa_p\left(l_0^+\right)}{2} = \frac{1}{2}\kappa_p(0) = \frac{M_p - PL}{2k^+} \qquad [4.92]$$

The equivalent plastic rotation θ_p can be calculated as:

$$\theta_p = l_p \left| \hat{\kappa}_p \right| = \frac{LM_p}{2k^+}\left(\frac{P}{P_y} - 1\right)\left(1 - \frac{P_y}{P}\right) = \frac{LM_p}{2k^+}\frac{P_y}{P}\left(\frac{P}{P_y} - 1\right)^2 \qquad [4.93]$$

where $l_p = l_0^+$ is the length of the "equivalent" plastic hinge, which is load-dependent according to equation [4.84]. It is clearly seen from equations [4.92] and [4.93] that the length of the "equivalent" plastic hinge, the mean value of the plastic curvature and the plastic rotation are all dependent on the loading parameter, which has been also reported by [CHA 09a] or Challamel *et al*. [CHA 10b] for the bending of elastoplastic hardening beams. Lee and

Filippou [LEE 09] also used a similar load-dependent hinge model to compute the post-failure response of reinforced concrete beam-columns.

The equivalent load-dependent hinge model can be computed from the elastic differential equations with the following boundary conditions:

$$EIw'' = P\left(L - x\right) \text{ with } w\left(0\right) = 0 \text{ and } w'\left(0\right) = \theta_p \quad [4.94]$$

This model is in fact equivalent to a loading-dependent bending-rotation constitutive law for the concentrated hinge, obtained from equation [4.93] as:

$$\left|M\right| = M_p + \frac{2k^+}{L\left(1 - \frac{P_y}{P}\right)}\left|\theta_p\right| \quad [4.95]$$

The "simplified" nonlinear load-deflection relationship, associated with the load-dependent hinge model, is obtained as:

$$v = \frac{PL^3}{3EI} + \theta_p\left(P\right)L \Rightarrow \frac{v}{v_y} = \frac{P}{P_y} + \frac{3}{2}\frac{EI}{k^+}\frac{P_y}{P}\left(\frac{P}{P_y} - 1\right)^2 \quad [4.96]$$

This deflection-load relationship can be also expressed with respect to the variable hinge length as:

$$\frac{v}{v_y} = \frac{1}{1 - \frac{l_p}{L}} + 3\frac{l_p}{L}\frac{\left|\hat{\kappa}_p\right|}{\kappa_y} \text{ with } \theta_p = l_p\left|\hat{\kappa}_p\right| \quad [4.97]$$

This relationship is valid in the plasticity branch, and especially at the ULS:

$$\frac{v_u}{v_y} = \frac{1}{1 - \frac{l_{p,u}}{L}} + 3\frac{l_{p,u}}{L}\frac{\left|\hat{\kappa}_{p,u}\right|}{\kappa_y} \text{ with } \theta_{p,u} = l_{p,u}\left|\hat{\kappa}_{p,u}\right| \quad [4.98]$$

A more simplified approach would be based on the hinge bending-rotation constitutive law with a constant global hardening modulus calculated from the maximum size of the hardening plasticity zone at ULS as:

$$\left|M\right| = M_p + \frac{2k^+}{l_{p,u}}\left|\theta_p\right| \quad \text{with} \quad \frac{l_{p,u}}{L} = 1 - \frac{1}{m} \qquad [4.99]$$

The "simplified" nonlinear load-deflection relationship, associated with a load-independent hinge model, is obtained as:

$$\frac{v}{v_y} = \frac{P}{P_y} + \frac{3}{2}\frac{EI}{k^+}\left(\frac{P}{P_y} - 1\right)\left(1 - \frac{1}{m}\right) \qquad [4.100]$$

At the ULS, equation [4.98] is also valid, and both equivalent hinge methods coincide.

Although not exact, the approximations based on the equivalent hinge methods provide good engineering results, especially the one based on the loading-dependent hinge model analysis (see Figure 4.17). The hinge model based on a load-independent hardening moment-rotation constitutive law leads to the linear curve in Figure 4.17, and leads to relevant results especially in the vicinity of the ULS (for $\kappa = \kappa_u$ at the section basis).

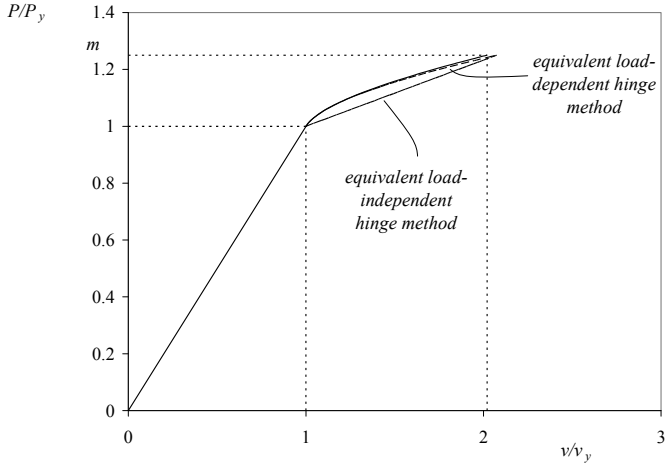

Figure 4.17. *Comparison of the exact bilinear moment curvature model with the hinge models;* $m = 5/4$; $EI/k^+ = 11$

There is a large discussion in the literature on the identification of the finite hinge length (see, for instance, [PAR 75], [BAZ 03], [MEN 01], [BAE 08], [ZHA 12] and [BAR 12]). As mentioned by Park and Paulay [PAR 75]: "The difference between the various empirical expressions emphasizes that the rotation capacity of plastic hinges in reinforced concrete members can only be approximated at present. Most research is needed to clear the differences between the various empirical expressions".

As shown in Figure 4.18 based on the bending-curvature constitutive law obtained from the bilinear constitutive law, the plastic hinge length strongly depends on the steel content, and the mode of failure.

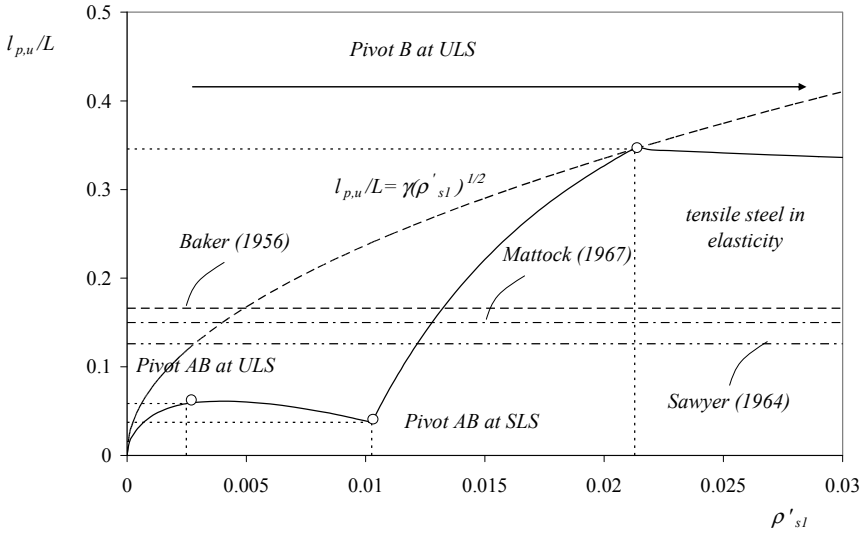

Figure 4.18. *Evolution of the finite plasticity hinge length l_{pu}/L with respect to the steel content ρ'_{s1} for an unsymmetrical reinforced concrete section with bilinear response for concrete; $L/d = 5$; C30-37 for the concrete; B500B for the steel; $\alpha_e = 17.5$*

Park and Paulay [PAR 75] presented various empirical expressions for the correlation of this finite hinge length, based on experimental results (see, for instance, [BAK 56], [SAW 65] and [MAT 67]). Baker [BAK 56] defined an empirical rule expressed by:

$$l_p = k_1 k_2 k_3 \left(\frac{z}{d}\right)^{\frac{1}{4}} d \qquad [4.101]$$

where z is the distance of the critical section to the point of contraflexure; $z = L$ for the cantilever beam studied in this chapter. k_1, k_2 and k_3 are empirical coefficients that depend on the steel and concrete used in the section. For $L/d = 5$, we typically obtain $l_p/d = 0.83$ with this model. Sawyer [SAW 65] used a linear regression law with respect to *d* and *z* as:

$$l_p = 0.25d + 0.075z \qquad [4.102]$$

For $L/d = 5$, we typically obtain $l_p/d = 0.63$ with this model. Mattock [MAT 67] used a slightly different correlation expression:

$$l_p = 0.5d + 0.05z \qquad [4.103]$$

For $L/d = 5$, we typically obtain $l_p/d = 0.75$ with this model. These three models based on experimental results are compared in Figure 4.18 with the theoretical model based on the strain capacity of the cross-section defined by Eurocode 2 rules. In the theoretical analysis, the phenomenon of increase in steel forces due to inclined diagonal tension cracks is neglected, and the post-failure analysis is not included. It can be observed in Figure 4.18 that the empirical correlation expressions mainly give higher plasticity length than the theoretical one in Pivot *A* (or for tension failure), whereas the correlation length can underesti-mate the theoretical plasticity length in Pivot *B* (or for compression failure).

It is also shown in Figure 4.18 that the theoretical plasticity hinge length is sensitive to the steel content and is globally an increasing function of the steel content. Priestley and Park [PRI 87], or Paulay and Priestley [PAU 92] suggested another empirical law for the plastic hinge length, which is sensitive to the steel content and can be presented as:

$$l_p = l_{p,0} + \gamma_1 \phi = l_{p,0} + \gamma_1 \sqrt{\frac{4bd}{\pi}} \sqrt{\rho'_{s1}} \qquad [4.104]$$

where $l_{p,0}$ and γ_1 are two fitting parameters. Priestley and Park [PRI 87], or Paulay and Priestley [PAU 92] suggested the value $l_{p,0} = 0.08L$ whereas

Eurocode 8, for instance, gives the close value $l_{p,0} = 0.10L$. According to Figure 4.18, a new simple proposal could be based on:

$$l_p = \gamma\sqrt{\rho'_{s1}} \qquad [4.105]$$

where the fitting parameter γ is chosen to be equal to $\gamma = 2.37$, for a *C30-37* type concrete, with a *B500B* for steel, in order to enforce the square root approximation function (equation [4.103]) to pass through the balanced failure point defined by $\rho'_{s1} = \frac{f_{cu}}{f_{su}} \frac{\varepsilon_{cu3} - \frac{\varepsilon_{c3}}{2}}{\varepsilon_{su} - \varepsilon_{cu3}}$. Equation [4.105] is a particular case of equation [4.104] where the constant parameter $l_{p,0}$ has been assumed to vanish. Figure 4.18 shows that the new proposal gives the correct tendency for the matching of the theoretical results based on the theoretical strain capacity section.

Finally, as outlined by Park and Paulay [PAU 75], the plastic hinge within the span of a symmetrically loaded beam will have a total equivalent length twice the length found for the cantilever (see also [CHA 08a]).

4.2.3. *Elastic-hardening constitutive law and local softening collapse: Wood's paradox*

It has been shown how the reinforced concrete beam can be designed with respect to the ULS, which is a strain-controlled ULS, compatible with the allowable behavior of the beam with respect to the specificities.

However, the rules including Eurocode 2 do not question the behavior beyond this ultimate limit. We will try to understand now what happens beyond the peak, or during the initiation of collapse. The tri-linear bending-moment curvature diagram is now considered with a softening branch associated with the failure behavior (see Figure 4.19).

It is assumed that the softening branch starts at the ultimate curvature κ_u but the reasoning can be generalized by considering a starting branch at a higher value.

The hardening/softening rule is now given in the following form:

$$\begin{cases} M^*(\lambda) = k^+\lambda \ \ if \ \ \lambda \in [0;\kappa_c] \\ M^*(\lambda) = \left\langle k^-(\lambda - \kappa_c) + mM_p \right\rangle \ -M_p \ \ if \ \ \lambda \geq \kappa_c \end{cases} \text{ with}$$
$$\kappa_c = (m-1)\frac{M_p}{k^+}; \lambda = |\kappa_p| \text{ and } \begin{cases} k^+ \geq 0 \\ k^- \leq 0 \end{cases} \qquad [4.106]$$

M_p is the limit elastic moment, and κ_y is the limit elastic curvature, related through $M_p / \kappa_y = EI$. m is the ratio between the maximum moment reached during positive hardening and the limit elastic moment (m is necessarily greater than unity), and κ_c is the plastic curvature reached before the initialization of the softening process. The hardening modulus k^+ is positive whereas the softening modulus k^- is negative.

We first studied the "local" softening process in the sense that the softening constitutive law is expressed only with respect to the local plastic curvature.

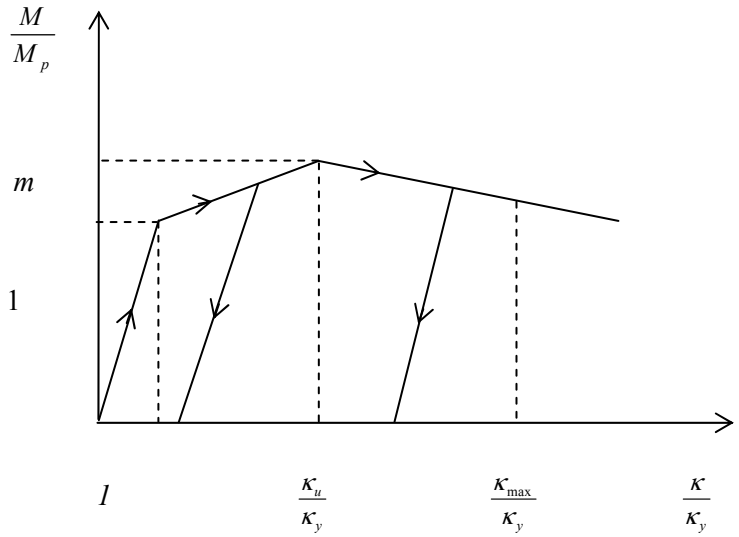

Figure 4.19. *Elastic–plastic hardening–softening moment-curvature law*

The plastic softening response may start once the load P reaches the maximum value mP_Y. Enforcing that κ_p is a continuous function of x $\left(\kappa_p\left(l_0^-\right)=\kappa_c\right)$ leads to:

$$\begin{cases} P\left(L-l_0^-\right)=mM_p \\ PL\le mM_p \end{cases} \Rightarrow l_0^-=0 \qquad [4.107]$$

This additional assumption gives the new Wood's paradox for hardening–softening local constitutive relationship. The unloading elastic solution is the only possible solution of the local softening problem (Figure 4.20).

In this case again, the paradox can be interpreted as the appearing of plastic curvature increments localized into one single section, leading to physically no reasonable phenomenon of failure with zero dissipation.

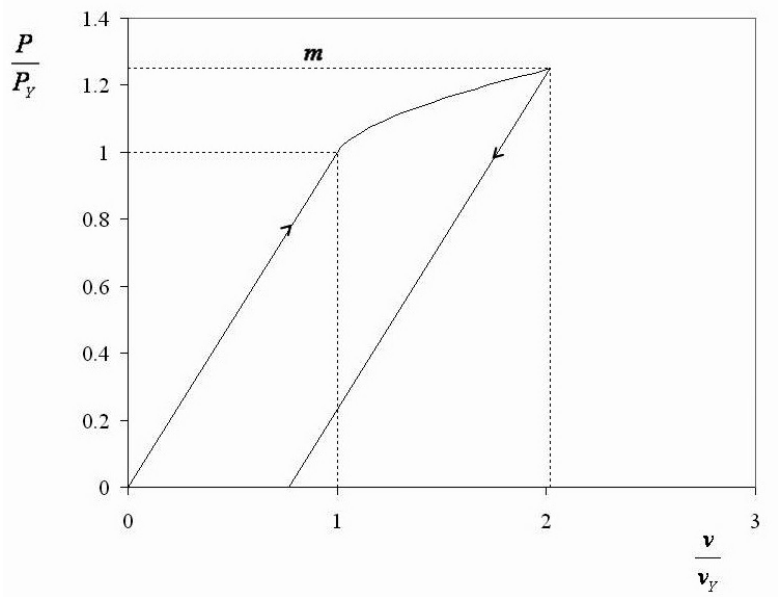

Figure 4.20. *Wood's paradox – local hardening/softening plasticity models; $m=5/4$; $EI/k^+=11$*

4.2.4. *Elastic-hardening constitutive law and non-local local softening collapse*

Wood's paradox for the hardening–softening beam can be solved by using a non-local softening moment-curvature law, as in the case of the elastic-softening beams. Once the bending moment in the clamped section $\left| M(x=0) \right| = PL$ reaches the yield strength mM_p, the softening zone can propagate from the clamped section, whereas unloading is observed in the hardening plastic zone and in the elastic zone. The local hardening and non-local softening constitutive relationship are given by:

$$\begin{cases} M^*(\lambda) = k^+ \lambda \quad if \quad \lambda \in [0;\kappa_c] \\ M^*(\lambda) = \left\langle k^- \left(\tilde{\lambda} - \kappa_c \right) + mM_p \right\rangle - M_p \quad if \quad \lambda \notin [0;\kappa_c] \end{cases} \text{ with } \tilde{\lambda} = \overline{\lambda} + {l_c}^2 \overline{\lambda}'' \qquad [4.108]$$

The problem of the continuity requirement between hardening and softening constitutive laws (a local law and a non-local law) will be implicitly solved by the fact that the length of the softening zone at the yield strength mM_p will vanish as we will see (as for the elastic-softening problem). Furthermore, the non-local plastic variable is integrated over the active plastic domain, that is the softening zone, as the hardening zone is in unloading during this final process.

As introduced in equation [3.55], the non-local softening measure is also equivalent to:

$$\tilde{\lambda} = -\lambda + 2\overline{\lambda} \text{ with } \overline{\lambda} - l_c^2 \overline{\lambda}'' = \lambda \qquad [4.109]$$

By considering the yield function in the softening area, the linear differential equation is obtained in the softening domain:

$$x \in \left[0; l_0^- \right] : \overline{\lambda} + {l_c}^2 \overline{\lambda}'' = \frac{P(L-x) - mM_p}{k^-} + \kappa_c \qquad [4.110]$$

with the boundary conditions associated with the higher order boundary conditions of the non-local model and the continuity requirement of the plastic curvature:

$$\lambda(l_0) = \kappa_c,\ \bar{\lambda}'\left(l_0^-\right) = 0 \text{ and } \bar{\lambda}'(0) = 0 \qquad [4.111]$$

The general solution of the differential equation [4.110] is written as:

$$x \in \left[0; l_0^-\right] : \bar{\lambda}(x) = A\cos\frac{x}{l_c} + B\sin\frac{x}{l_c} + \frac{P(L-x) - mM_p}{k^-} + \kappa_c \qquad [4.112]$$

The nonlinear system of three equations with three unknowns A, B and l_0^- is finally obtained:

$$\begin{cases} 2A\cos\dfrac{l_0^-}{l_c} + 2B\sin\dfrac{l_0^-}{l_c} + \dfrac{P\left(L-l_0^-\right) - mM_p}{k^-} = 0 \\ -\dfrac{A}{l_c}\sin\dfrac{l_0^-}{l_c} + \dfrac{B}{l_c}\cos\dfrac{l_0^-}{l_c} - \dfrac{P}{k^-} = 0 \\ \dfrac{B}{l_c} - \dfrac{P}{k^-} = 0 \end{cases} \qquad [4.113]$$

The following dimensionless parameters may be introduced as:

$$\beta = \left(1 - m\frac{P_Y}{P}\right)\frac{L}{l_c} \le 0 \text{ and } \xi = \frac{l_0^-}{l_c} \ge 0 \qquad [4.114]$$

leading to the localization relation of equation [3.61].

A remarkable result is that the plastic diffusion in the softening range does not depend on the hardening range. In other words, the hardening modulus (or the material history in the hardening domain) does not affect the localization process, from a qualitative point of view. The deflection in

the plastic zone $x \in \left[0; l_0^-\right]$ is obtained by integrating twice the elastic curvature:

$$w^-(x) = \left(\frac{PL}{EI} + \frac{PL - mM_p}{k^-} + \kappa_c\right)\frac{x^2}{2} - \left(\frac{P}{EI} + \frac{P}{k^-}\right)\frac{x^3}{6} - 2\frac{Pl_c^3}{k^-}\frac{\cos\left(\frac{l_0^-}{l_c}\right) - 1}{\sin\left(\frac{l_0^-}{l_c}\right)}\left[\cos\left(\frac{x}{l_c}\right) - 1\right] - 2\frac{Pl_c^3}{k^-}\left[\sin\left(\frac{x}{l_c}\right) - \frac{x}{l_c}\right] \quad [4.115]$$

The deflection in the elastic zone $x \in \left\lfloor l_0^-; l_0^+ \right\rfloor$ is derived from the kinematics continuity condition, along the active softening–passive hardening zone, whereas the plastic curvature distribution is constant in the unloading phase:

$$w_1^+(x) = \left(\frac{PL}{EI} + (m-1)\frac{M_p}{k^+}\right)\frac{x^2}{2} - \left(\frac{P}{EI} + m\frac{P_Y}{k^+}\right)\frac{x^3}{6} + \left[w^{-\prime}\left(l_0^-\right) - \frac{PLl_0^-}{EI} + \frac{P\left(l_0^-\right)^2}{2EI} - (m-1)\frac{M_p l_0^-}{k^+} + m\frac{P_Y\left(l_0^-\right)^2}{2k^+}\right]x + \left[w^-\left(l_0^-\right) - \left(l_0^-\right)w^{-\prime}\left(l_0^-\right) + \frac{PL\left(l_0^-\right)^2}{2EI} - \frac{P\left(l_0^-\right)^3}{3EI} + (m-1)\frac{M_p\left(l_0^-\right)^2}{2k^+} - \frac{mP_Y}{k^+}\frac{\left(l_0^-\right)^3}{3}\right] \quad [4.116]$$

The deflection in the elastic zone $x \in \left\lfloor l_0^+; L \right\rfloor$ is derived from the kinematics continuity condition along the passive hardening–elastic interface:

$$w_2^+(x)=\frac{PLx^2}{2EI}-\frac{Px^3}{6EI}+\left[w_1^{+\prime}\left(l_0^+\right)-\frac{PLl_0^+}{EI}+\frac{P\left(l_0^+\right)^2}{2EI}\right]x+$$

$$\left[w_1^+\left(l_0^+\right)-\left(l_0^+\right)w_1^{+\prime}\left(l_0^+\right)+\frac{PL\left(l_0^+\right)^2}{2EI}-\frac{P\left(l_0^+\right)^3}{3EI}\right] \text{ with} \qquad [4.117]$$

$$l_0^+=\frac{m-1}{m}L$$

Generally speaking, the plastic zone grows in the hardening range until the maximum load, then a more localized softening zone arises from the clamped section and controls the mode of collapse. The global softening is then observed after the hardening behavior (Figure 4.21) and Wood's paradox is solved within the non-local plasticity constitutive law.

Figure 4.21. *Response of the elastoplastic hardening – non-local softening beam;* $EI/k^-=-5$; $l_c/L=0.1$; $m=5/4$; $EI/k^+=11$

l_0^+ related to the hardening domain is the length of the hardening plasticity zone that propagates along the beam without any material limits, whereas the softening localization zone, denoted by l_0^-, is increasing during the softening process, until a finite length, which depends on the material-section model. Of course, these two localization zones are strongly different $\left(l_0^+\neq l_0^-\right)$. For

the non-local models studied in this chapter, the plastic variable is integrated on an active plastic domain. In particular, during the softening process, the non-local plastic variable is integrated on the localization length l_0^-, even if the plasticity zone is generally much larger $\left(l_0^+ > l_0^-\right)$. In fact, the hardening and the softening plastic zones are given by:

$$\frac{l_0^+}{L} = 1 - \frac{1}{m} \text{ and } \frac{l_0^-}{L} \leq \pi \frac{l_c}{L} \qquad [4.118]$$

where the hardening zone has been calculated from the local hardening model. Therefore, the softening plastic zone is necessarily smaller than the hardening plastic zone for a sufficiently small characteristic length, that is:

$$\frac{l_c}{L} \leq \frac{1}{\pi}\left(1 - \frac{1}{m}\right) \Rightarrow l_0^- \leq l_0^+ \qquad [4.119]$$

It is not excluded, however, the softening localization zone is influenced by the overall plasticity phenomena in the precracked reinforced concrete beam, and the simple non-local model presented in this chapter has its own limits. The calibration of the characteristic length l_c, which includes material and cross-sectional properties, should certainly merit further investigations. The research on the global modeling of the collapse of reinforced concrete beams is still open, and would merit further studies, especially including the coupling mode of collapse between the shear and the bending modes.

4.3. Bending moment-curvature relationship for buckling and postbuckling of reinforced concrete columns

4.3.1. *A continuum damage mechanics-based moment curvature relationship*

The buckling and postbuckling behaviors of reinforced concrete softening columns composed of quasi-brittle materials such as concrete and composite materials are of interest in this section. Such members must be designed taking into account the second-order effects produced by the axial loads on the deformed member. The main international rules, including, for instance, the European code for reinforced concrete design, Eurocode 2 [EUR 04], are based on this concept, even though they may allow second-order effects to be neglected when the column slenderness does not exceed certain limits.

Such limits have been investigated (e.g. [HEL 05a], [HEL 08] and [MAR 05]) and included in most reinforced concrete codes. Various empirical or theoretical based methods have been published in the past, which all introduced some necessary realistic imperfections through additional load eccentricities ([ROB 75], [BAZ 03]). This is typical and necessary, from a theoretical stability point of view, for nonlinear structural systems that belong to the field of imperfection sensitive systems. There have been numerous textbooks devoted to the elastic or inelastic buckling of columns (see, for instance, [LHE 76] or [BAZ 03]), but the link between the imperfection sensitivity of the structural models and the buckling phenomenon of reinforced concrete columns was not clearly highlighted in the authors' point of view, at least not from simple physically based models.

In such analyses, it is necessary to include some nonlinearity in the bending-curvature constitutive law. Such nonlinearities may lead to unstable post-bifurcation and post-buckling branches in the buckling problem. As a result, and rather well known, the buckling of softening systems may lead to the imperfection sensitivity phenomenon. This study will focus on such problems based on continuum damage mechanics (CDM) models that may specifically be applied in a qualitative sense to reinforced concrete sections.

The problem handled in this study is not so different from the elastic problem of a softening column, as already numerically investigated by [ODE 70], [MON 74], [YU 82], [HAS 85], [KOU 87], [LEW 87], [WAN 96], [VIR 04], [BRO 07] or [LAC 08]. These authors studied the post-buckling of columns modeled with a nonlinear bending-curvature constitutive law, with different potential applications including steel or composite structures. A major observation by these authors is that the local stiffness softening of the constitutive law (associated with a decrease in the secant stiffness) may induce some global softening of the post-buckling behavior, that is the axial load must decrease with increasing deflection during the post-buckling range in order to maintain equilibrium. This kind of post-buckling behavior is, as mentioned, typically responsible for imperfection sensitivity phenomena.

The continuous clamped-free cantilever column considered is shown in Figure 4.22. A similar problem has been recently studied by Krauberger *et al.* [KRA 11] for reinforced concrete columns without any imperfection. However, in the presence of softening induced by the micro-cracking in concrete, the buckling load of the perfect system may overestimate

significantly the limit load of the imperfect column. An imperfection analysis is needed, as previously shown for the single-degree-of-freedom softening structural system. The imperfection is, as before, introduced through an additional eccentricity of the axial load.

Figure 4.22. *Eccentrically loaded, continuous cantilever column, and definition of parameters and variables used in the buckling and postbuckling study of softening reinforced concrete columns*

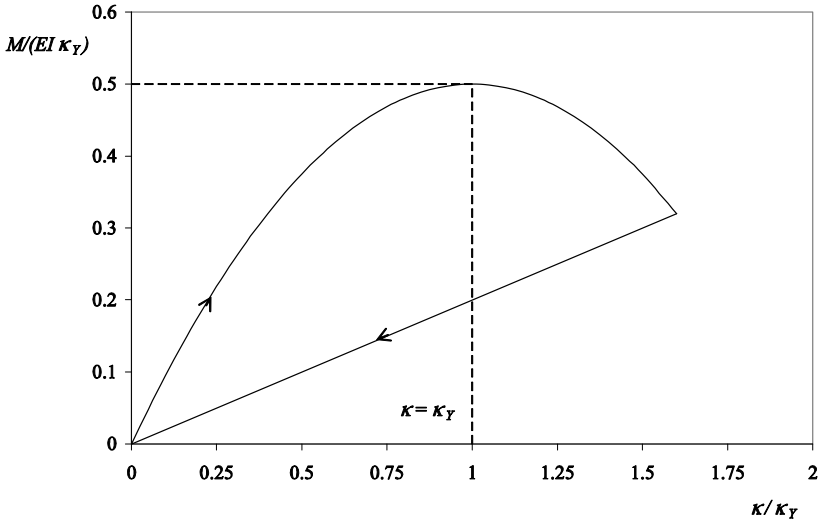

Figure 4.23. *CDM constitutive law of the inelastic spring*

The bending-curvature relationship is assumed to be inelastic and behaves with a damage law illustrated in Figure 4.23 and defined by:

$$M = EI(1-D)\kappa \qquad [4.120]$$

where M is the bending moment, κ is the curvature of the cross-section, EI is the initial stiffness of the spring and D is the damage variable that measures the integrity of the cross-section (see also [CHA 07] for a similar damage bending constitutive law). D evolves from 0 for a virgin cross-section to 1 for the totally broken cross-section. As seen in the figure, plasticity effects are neglected, as there is no remaining rotation at completed unloading. The damage loading function is postulated as:

$$f(\theta', D) = \frac{|\kappa|}{\kappa_Y} - 2D \text{ and } \kappa = \frac{d\theta}{ds} = \theta' \qquad [4.121]$$

where κ is the curvature, θ is the rotation of the cross-section and s is the curvilinear abscissa (coordinate along the deformed axis). The curvature κ_Y is the only material parameter, and is associated with the maximum moment capacity of the cross-section. The irreversible damage constitutive law including the loading–unloading conditions can be written as:

$$\dot{D} \geq 0,\ f(\kappa, D) \leq 0,\ \dot{D}\, f(\kappa, D) = 0 \qquad [4.122]$$

Equation [4.122] can be viewed as the so-called optimality Kuhn–Tucker conditions where the Lagrange multiplier is equal to the damage rate (see, for instance, [JIR 02] for a discussion on Kuhn–Tucker conditions for inelastic analysis). First, monotonic loading behavior will be considered, without any unloading phenomena. Unloading will be discussed in a subsequent section of the chapter.

4.3.2. *Governing equations of the problem and numerical resolution*

Application of the principle of virtual work in the so-called geometrically exact configuration for the inextensible softening column leads to:

$$\int_0^L \left[EI(1-D)\theta'\delta\theta' - P\sin\theta\delta\theta \right] ds - Pe_0 \cos\theta(L)\delta\theta(L) = 0 \qquad [4.123]$$

where e_0 is the eccentricity of the applied axial load at the column top. An integration by part gives the differential equation:

$$\left[EI\left(1-D\right)\theta'\right]' + P\sin\theta = 0 \qquad [4.124]$$

and the natural and essential boundary conditions:

$$\left[EI\left(1-D\right)\theta'\delta\theta\right]_0^L - Pe_0\cos\theta\left(L\right)\delta\theta\left(L\right) = 0 \qquad [4.125]$$

For the clamped-free column studied in this chapter, these boundary conditions become:

$$\theta\left(0\right) = 0 \text{ and } EI\ \left[1-D\left(L\right)\right]\ \theta'\left(L\right) = Pe_0\cos\theta\left(L\right) \qquad [4.126]$$

In case of monotonic loading in the hardening regime, uniqueness prevails. Hill's uniqueness criterion [HIL 58] at the beam scale (see also [CHA 07]) can be applied:

$$\int_0^L \frac{\partial M}{\partial t}\frac{\partial \kappa}{\partial t} > 0 \qquad [4.127]$$

For this loading range, the column behaves as a nonlinear elastic column with a damage loading function given by $f\left(\kappa, D\right)$ from equation [4.121]. In the monotonic loading case, $f\left(\kappa, D\right) = 0$, implying $D = \left|\kappa\right| / \left(2\kappa_Y\right)$, the nonlinear constitutive law is assumed in the same form:

$$M = EI\kappa\ \left[1 - \frac{1}{2}\left(\frac{\kappa}{\kappa_Y}\right)\right] \qquad [4.128]$$

This is typically a hyperelastic constitutive law whose potential π^0 is given by:

$$M = \frac{\partial \pi^0}{\partial \kappa} \text{ with } \pi^0 = \frac{1}{2}EI\kappa^2 - \frac{1}{6}EI\frac{\kappa^3}{\kappa_Y} \qquad [4.129]$$

By substituting the damage parameter into equation [4.124], the nonlinear differential equation governing the hardening (increasing moment) path of the nonlinear material and geometrical problem is then given by:

$$\left[EI\left(1-\frac{\theta'}{2\kappa_Y}\right)\ \theta' \right]' + P\sin\theta = 0 \qquad [4.130]$$

The general solution of such a nonlinear differential equation is difficult to achieve analytically.

With the dimensionless parameters:

$$p = \frac{PL^2}{EI}; s^* = \frac{s}{L}, x^* = \frac{x}{L}, \kappa_Y^* = \kappa_Y L \text{ and } e_0^* = \frac{e_0}{L} \qquad [4.131]$$

where κ_Y^* typically has an order of magnitude of 0.05 or 0.1 for reinforced concrete columns, the nonlinear boundary value problem for the hardening path can be expressed by the nonlinear differential equation and boundary conditions given by:

$$\frac{d^2\theta}{ds^{*2}}\left(1-\frac{1}{\kappa_Y^*}\frac{d\theta}{ds^*}\right)+p\sin\theta=0$$

$$\text{with } \theta(0)=0 \text{ and } \left[1-\frac{1}{2\kappa_Y^*}\frac{d\theta}{ds^*}(1)\right]\ \frac{d\theta}{ds^*}(1)=pe_0^*\cos\theta(1) \qquad [4.132]$$

For a curvature $d\theta/ds$ equal to κ_Y (or $\kappa^* = \kappa_Y^*$), equation [4.132] shows that the tangent modulus vanishes, and the differential equation above becomes singular, leading to the loss of well posedness of the structural problem. In order to proceed for curvatures beyond κ_Y, it is necessary to introduce non-local consideration in a region of the column instead of local sectional considerations alone. This will be dealt with in detail later.

It is theoretically possible to express the above nonlinear differential equation as a first-order differential equation. Multiplying the nonlinear differential equation by the curvature and integrating one time leads to the following nonlinear first-order differential equation:

$$\frac{1}{2}\left(\frac{d\theta}{ds^*}\right)^2-\frac{1}{3\kappa_Y^*}\left(\frac{d\theta}{ds^*}\right)^3-p\left[\cos\theta-1\right]=0 \qquad [4.133]$$

This is a cubic equation with respect to the curvature. It can be theoretically solved using Cardano's method, but then the post-buckling behavior investigated from the first-order nonlinear differential equation still needs some numerical computations. In the paper of Haslach [HAS 85], based on a cubic moment-curvature constitutive law, a quartic equation in the curvature was obtained by integration, leading to an easier analytical solution of the curvature, even if the final integration process was numerically performed.

For the parabolic constitutive law adopted in this chapter, a different approach is required. In the hardening range, that is for $\kappa < \kappa_Y$, the nonlinear boundary value problem (equation [4.132]) can, in order to facilitate a computational format, be rewritten in an explicit form with respect to the second derivative:

$$\frac{d^2\theta}{ds^{*2}} = -\frac{p\sin\theta}{1-\dfrac{1}{\kappa_Y^*}\dfrac{d\theta}{ds^*}} \text{ with } \theta(0)=0 \text{ and}$$

$$\frac{d\theta}{ds^*}(1) = \kappa_Y^* - \sqrt{\kappa_Y^{*2} - 2p\kappa_Y^* e_0^* \cos\theta(1)}$$

$$\text{for } \frac{d\theta}{ds^*} < \kappa_Y^* \text{ and } pe_0^*\cos\theta(1) < \frac{\kappa_Y^*}{2} \qquad [4.134]$$

The rotation α at the column end with the applied load is taken as the control parameter.

Simplifications of the above formulations, in the geometrically exact framework, will often give sufficiently accurate results for cases with small rotations. For this reason, we will derive some approximate solutions for the so-called "second-order analysis" of the considered problem. Introducing ($\sin\theta \approx \theta$ and $\cos\theta \approx 1$) in the differential equations [4.134], they can be written as:

$$\frac{d^2\theta}{dx^{*2}} = -\frac{p\theta}{1-\dfrac{1}{\kappa_Y^*}\dfrac{d\theta}{dx^*}} \text{ with } \theta(0)=0 \text{ and}$$

$$\frac{d\theta}{dx^*}(1) = \kappa_Y^* - \sqrt{\kappa_Y^{*2} - 2p\kappa_Y^* e_0^*} \text{ for } \frac{d\theta}{dx^*} < \kappa_Y^* \text{ and } pe_0^* < \frac{\kappa_Y^*}{2} \qquad [4.135]$$

where derivatives are now with respect to the abscissa (longitudinal axis) x (rather than with respect to the curvilinear s).

Figure 4.24 shows numerical load-rotation results obtained for the unstable, softening post-bifurcation branches of the perfect system (with no load eccentricity). The abscissa α in the figure is the rotation at the top of the cantilever column. Results based on the geometrically exact and on the second-order approximated analysis were found to be identical within three decimals. In the figure, this difference is not visible. Similar correspondence between the two analyses was found for load-rotation results for imperfect columns, for a range of load eccentricities $e_0^* \in [0;0.01]$. Such results are presented in Figure 4.25. Hence, the second-order analysis is sufficient for most engineering applications, including the analysis and design of reinforced concrete columns.

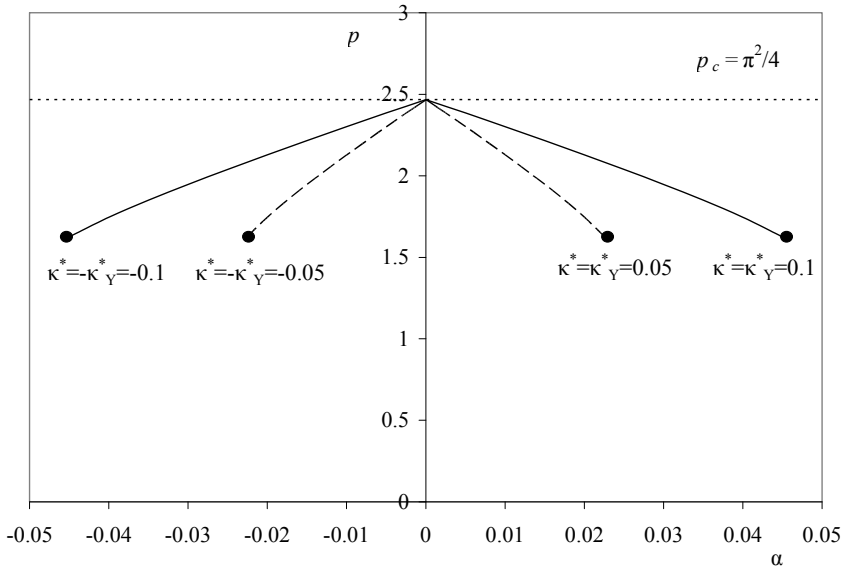

Figure 4.24. *Bifurcation diagram for the perfect softening buckling system showing unstable branches with a singular point;* $\kappa_Y^* = 0.05$ *and* $\kappa_Y^* = 0.1$

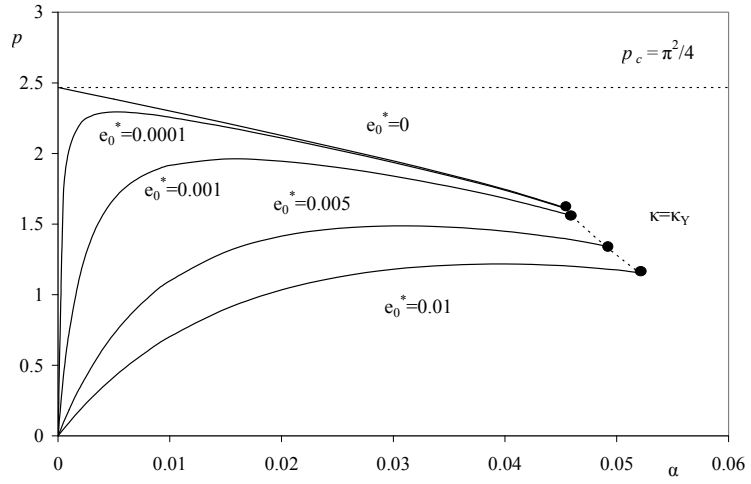

Figure 4.25. *Eccentricity effect on the pre- and post-buckling response of the softening column;* $\kappa_Y^* = 0.1$

In the numerical computation of these figures, κ_Y^* was chosen to be equal to either 0.05 or 0.1. This range is of an order of magnitude that is typical for reinforced concrete columns. With these material parameters, the curvature corresponding to the section moment capacity, $\kappa(0) = \kappa_Y$, is reached for a column end rotation of approximately $\alpha_Y \approx 0.0228$ in the case of $\kappa_Y^* = 0.05$, and for $\alpha_Y \approx 0.0455$ in the case of $\kappa_Y^* = 0.1$. Thus, in both cases, α_Y is approximately equal to half of the curvature κ_Y^*, $\alpha_Y \approx \kappa_Y^*/2$. This is an interesting result. It can be checked in a simplified manner based on an assumed linear moment distribution along the cantilever column. This gives

$$EI\theta'(x) = M_0\left(1 - \frac{x}{L}\right) \Rightarrow EI\theta(x) = M_0\left(x - \frac{x^2}{2L}\right) \qquad [4.136]$$

where $M_0 = M(0)$ is the moment at the column base. Then, from equation [4.136]:

$$\frac{\theta(L)}{L\theta'(0)} = \frac{\alpha}{\kappa^*(0)} = \frac{1}{2} \qquad [4.137]$$

which, as an approximation, confirms the results above from the second-order analysis.

For the continuous column, the unstable post-bifurcation branches (Figure 4.24) can be seen to have a singular bifurcation point, a phenomenon also noticed for the softening single-degree-of-freedom system. Figure 4.25 reflects the strong load sensitivity of the imperfect column with respect to the load eccentricity at the column end. The limit points of the imperfect column, as well as the complete softening (descending) post-buckling branches shown in the figures, are all obtained for section curvatures that are in the hardening (ascending) range of the moment-curvature law, that is for $\kappa \le \kappa_Y$. In engineering design contexts, it is often the limit loads that are of prime interest. Since these are reached prior to or at $\kappa = \kappa_Y$, as shown above, the presented analyses (limited to $\kappa \le \kappa_Y$) are sufficient. However, if the response beyond this value is of interest, which it often is, a non-local CDM approach can be used, as we will see later, in the postfailure range $\kappa \ge \kappa_Y$.

4.3.3. *Second-order analysis – some analytical arguments*

In an effort to derive imperfection sensitivity results, in an analytical form, an asymptotic method based on a linearization of an integral formulation of the boundary value problem is suggested in this section, which still is limited to $\kappa \le \kappa_Y$. A numerical comparison of the exact and the linearized solution will be presented in a second step.

Small rotations are assumed in order to simplify the nonlinear differential equation [4.130] as:

$$\left[EI\left(1-\frac{w''}{2\kappa_Y} \right) w'' \right]' + Pw' = 0 \text{ where } \theta = w' \qquad [4.138]$$

where the prime derivative is now expressed with respect to the spatial abscissa x (in the length direction). An integration of equation [4.138] leads to the differential equation:

$$EI\left(1-\frac{w''}{2\kappa_Y} \right) w'' + Pw = C_1 \qquad [4.139]$$

The constant C_1 can be identified from the boundary conditions at the loaded end of the column:

$$M(L) = Pe \Rightarrow C_1 = P\left[w(L) + e\right] \qquad [4.140]$$

equation [4.140] can then be written as:

$$w''^2 - 2\kappa_Y w'' + \frac{2P\kappa_Y}{EI}\left[w(L) + e - w\right] = 0 \text{ with } w(0) = w'(0) = 0 \qquad [4.141]$$

which is a quadratic nonlinear differential equation, from which the roots (curvatures) can readily be extracted. The smallest root is important for the hardening moment-curvature regime studied in this section. Thus,

$$w'' = \kappa_Y - \sqrt{\kappa_Y^2 - \frac{2P\kappa_Y}{EI}\left[w(L) + e - w\right]} \qquad [4.142]$$

Note that the expression under the square root is positive in the curvature hardening range. This can be argued physically, but also mathematically as shown below.

$$M(0) = P\left[w(L) + e - w\right] \le M_Y = EI\frac{\kappa_Y}{2}$$

$$\Rightarrow \kappa_Y^2 - \frac{2P\kappa_Y}{EI}\left[w(L) + e - w\right] \ge 0 \qquad [4.143]$$

The mathematical problem can be simplified by introducing the variables *A* and *B* as follows:

$$w'' = \kappa_Y - \sqrt{A + Bw} \text{ with } \begin{cases} A = \kappa_Y^2 - \dfrac{2P\kappa_Y}{EI}\left[w(L) + e\right] > 0 \\ B = \dfrac{2P\kappa_Y}{EI} > 0 \end{cases} \qquad [4.144]$$

By multiplying each term in this nonlinear differential equation by the rotation, such that:

$$w''w' = \kappa_Y w' - \sqrt{A + Bw}\, w' \qquad [4.145]$$

and then integrating this equation, the nonlinear first-order differential equation below is obtained.

$$\frac{w'^2}{2} = \kappa_Y w - \frac{2}{3B}\left(A + Bw\right)^{\frac{3}{2}} + C_1 \qquad [4.146]$$

The constant C_1 is easily identified from the introduction of the boundary conditions at the clamped section:

$$w(0) = w'(0) = 0 \Rightarrow C_1 = \frac{2}{3B}A^{\frac{3}{2}} \qquad [4.147]$$

We finally obtain the following nonlinear differential equation:

$$w' = \sqrt{2\kappa_Y w + \frac{4}{3B}\left[A^{\frac{3}{2}} - \left(A + Bw\right)^{\frac{3}{2}}\right]} \qquad [4.148]$$

that can be presented in an integral format by:

$$L = \int_0^{w(L)} \frac{dw}{\sqrt{2\kappa_Y w + \frac{4}{3B}\left[A^{\frac{3}{2}} - \left(A + Bw\right)^{\frac{3}{2}}\right]}} \qquad [4.149]$$

By incorporating the dimensionless parameters:

$$p = \frac{PL^2}{EI}, x^* = \frac{x}{L}, w^* = \frac{w}{L}, \kappa_Y^* = \kappa_Y L, e_0^* = \frac{e_0}{L},$$
$$A^* = \kappa_Y^{*2} - 2p\kappa_Y^*\left[w^*(1) + e_0^*\right] \text{ and } B^* = 2p\kappa_Y^* \qquad [4.150]$$

the integral equation [4.149] can then be expressed in dimensionless format by:

$$1 = \int_0^{w^*(1)} \frac{dw^*}{\sqrt{2\kappa_Y^* w^* + \frac{4}{3B^*}\left[A^{*\frac{3}{2}} - \left(A^* + B^* w^*\right)^{\frac{3}{2}}\right]}} \qquad [4.151]$$

In an integral format, equation [4.151] gives the exact load-displacement relationship of the imperfect softening column based on the second-order analysis.

It is now investigated to see if it is possible to develop a suitable approximate imperfection sensitive law based on the second-order analysis, integral-formulation of equation [4.151]. For sufficiently small deflection values $w^* << 1$, an asymptotic expansion of equation [4.151] yields:

$$\left(A^* + B^* w^*\right)^{\frac{3}{2}} = A^{*\frac{3}{2}}\left(1 + \frac{3B^*}{2A^*} w^* + \ldots\right) \Rightarrow$$

$$1 = \int_0^{w^*(1)} \frac{dw^*}{\sqrt{2\kappa_Y^* - 2\sqrt{A^*}}\sqrt{w^*}} \qquad [4.152]$$

From equation [4.152], the top defection $w^*(1)$ can be calculated and expressed by:

$$w^*(1) = \frac{\kappa_Y^* - \sqrt{A^*}}{2} = \frac{1}{2}\left[\kappa_Y^* - \sqrt{\kappa_Y^{*2} - 2p\kappa_Y^*\left[w^*(1) + e_0^*\right]}\right] \qquad [4.153]$$

from which the dimensionless load *p* can be solved for and expressed by:

$$\frac{p}{p_0} = \frac{w^*(1)\left[1 - \dfrac{w^*(1)}{\kappa_Y^*}\right]}{w^*(1) + e_0^*} \text{ with } p_0 = 2 = \frac{8}{\pi^2} p_E \approx 0.8105... \times p_E \qquad [4.154]$$

From this equation, the critical (bifurcation) load of the perfect column becomes $p = p_0$ (for $e_0^* = 0$). The analysis above gave $p_0 = 2$, which clearly only represents an approximation of the correct buckling load of the clamped-free linearly elastic column, $p_E = \pi^2/4$. The difference between p_0 and p_E is due to the expansion approximation. For the perfect problem $e_0^* = 0$, the post-bifurcation branch is typically an unstable branch. For the imperfect problem, with $e_0^* \neq 0$, the deflection at the limit loads can be calculated from:

$$\frac{\partial p}{\partial w^*(1)} = 0 \Rightarrow \left[w^*(1)\right]^2 + 2e_0^* w^*(1) - e_0^* \kappa_Y^* = 0 \qquad [4.155]$$

which for the larger root gives:

$$w_c^*(1) = -e_0^* + \sqrt{e_0^{*2} + e_0^* \kappa_Y^*} \qquad [4.156]$$

By substituting this expression into equation [4.154], the imperfection sensitive rule is obtained as:

$$\frac{p_c}{p_0} = 1 + \frac{p_0}{\kappa_Y^*}\left[e_0^* - \sqrt{e_0^{*2} + \frac{2}{p_0} e_0^* \kappa_Y^*} \right] \text{ with } p_0 = 2 \qquad [4.157]$$

The inaccuracy implied by $p_0 = 2$ will be corrected in a simple manner in the following, simply by taking p_0 equal to the correct value $p_E = \pi^2/4$. Thus, with $p_0 = p_E = \pi^2/4$, the final imperfection sensitive rule becomes:

$$\frac{p_c}{p_0} = 1 + \frac{p_0}{\kappa_Y^*}\left[e_0^* - \sqrt{e_0^{*2} + \frac{2}{p_0} e_0^* \kappa_Y^*} \right] \text{ with } p_0 = p_E = \frac{\pi^2}{4} \qquad [4.158]$$

Other closely related imperfection sensitivity rules can be derived by means of the Rayleigh–Ritz approach or the Galerkin method based on only one-term sinusoidal approximate function. An approximation formula can also be derived from the application of Rayleigh–Ritz method, starting from Rayleigh's quotient:

$$Q = \frac{\int_0^L \frac{EI}{2} w''^2 - \frac{EI}{6} \frac{w''^3}{\kappa_Y} dx}{\int_0^L \frac{w'^2}{2} dx + e_0 w'(L)} \qquad [4.159]$$

Note that the energy term π^0 defined in equation [4.159] is convex for curvature κ lesser than κ_Y, which is the case considered for the initial postbuckling behavior considered here. Introducing the initial buckling mode

$$w = w(L)\left[1 - \cos\frac{\pi x}{2L} \right] \qquad [4.160]$$

in Rayleigh's quotient leads to the upper bound:

$$\frac{p}{p_E}=\frac{w^*(1)\left[1-\frac{2\pi}{9}\frac{w^*(1)}{\kappa_Y^*}\right]}{w^*(1)+\frac{8}{\pi}e_0^*} \text{ with } p_E=\frac{\pi^2}{4} \qquad [4.161]$$

Another upper bound can be obtained from Galerkin's method based on the weak form of the differential equations [4.141] written as:

$$\int_0^L\left\{w''^2-2\kappa_Y w''+\frac{2P\kappa_Y}{EI}\left[w(L)+e_0-w\right]\right\}\tilde{w}\,dx=0 \qquad [4.162]$$

Using again the comparison function equation [4.160] in equation [4.162] leads to a close upper bound:

$$\frac{p}{p_E}=\frac{w^*(1)\left[1-\pi^2\frac{\frac{\pi}{16}-\frac{1}{6}}{2-\frac{\pi}{2}}\frac{w^*(1)}{\kappa_Y^*}\right]}{w^*(1)+\frac{\pi-2}{2-\frac{\pi}{2}}e_0^*} \text{ with } p_E=\frac{\pi^2}{4} \qquad [4.163]$$

The two bounds, Rayleigh's bound and Galerkin's bound, are very close as:

$$0.6981=\frac{2\pi}{9}\approx\pi^2\frac{\frac{\pi}{16}-\frac{1}{6}}{2-\frac{\pi}{2}}=0.6825 \text{ and}$$

$$2.546=\frac{8}{\pi}\approx\frac{\pi-2}{2-\frac{\pi}{2}}=2.6598 \qquad [4.164]$$

More terms in the use of these approximated variationally based methods would be probably needed for a more accurate description of the analytical post-buckling response of the softening column (see, for instance, [LAC 08]

or [YU 12] for the use of Galerkin's method with several comparison functions). It is sufficient at this stage to compare the structure of the post-buckling equation issued of the variationally based methods with the previous asymptotic one for a correct understanding of the physical problem.

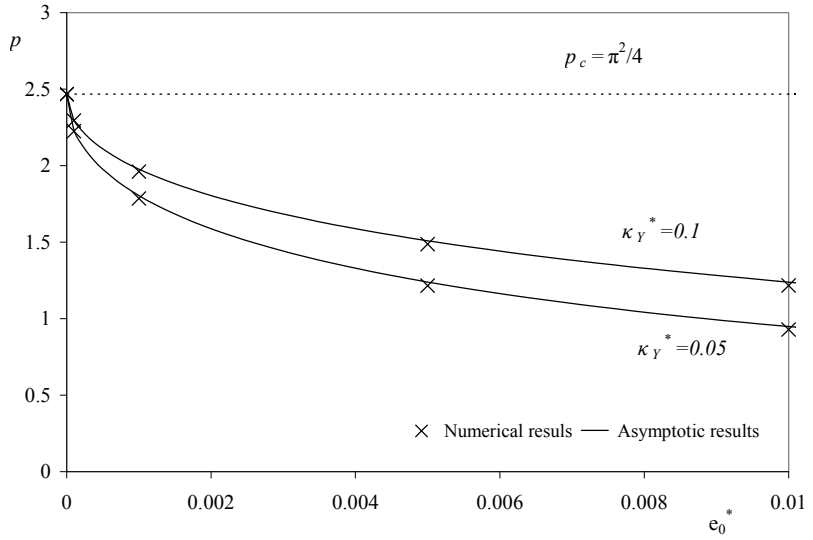

Figure 4.26. *Comparison of the exact numerical imperfection results from the nonlinear boundary value problem, and the asymptotic analytical rule (equation [4.158])*

Figure 4.26 compares numerical results from the exact imperfection sensitivity rule to those from the corrected asymptotic imperfection sensitivity rule (equation [4.158]) given by the full lines. The results for both $\kappa_Y^* = 0.05$ and $\kappa_Y^* = 0.1$ are in very good agreement. For sufficiently small eccentricities, equation [4.158] can be simplified to the following rule:

$$\frac{p_c}{p_0} = 1 - \sqrt{\frac{2p_0}{\kappa_Y^*}}\sqrt{e_0^*} + \ldots \qquad [4.165]$$

which is identical to Koiter's ½ power law (see [KOI 45] or [BAZ 03]). It reflects a rather extreme sensitivity of the limit load on the eccentricities, or the imperfection, that is generally found in asymmetrical structural systems, as pointed out by Bažant and Cedolin [BAZ 03]. It is remarkable that this strong imperfection sensitivity appears in the present damage problem,

which is initially a symmetrical structural problem, where a sharp angular bifurcation branch intersection characterizes the post-buckling system.

4.3.4. *Postfailure of the non-local continuum damage mechanics column*

As far as the calculation of the limit point calculation is concerned, a local bending curvature constitutive law (applicable at each local section) is sufficient. However, once the bending moment at the clamped, maximum moment section has reached the bending moment capacity M_Y (at the apex of the moment-curvature relationship), the local law is adequate for calculating unloading (decreasing P) for decreasing rotations (and curvatures), but not for the calculation of continued unloading associated with increasing induced rotations (or deflections). This phenomenon is discussed in some detail in this section.

This limitation of a local section model may be explained physically. Consider first the column state at which the clamped, maximum moment section has just reached the moment M_Y (capacity) and corresponding curvature $\kappa = \kappa_Y$ for an axial load $P = P_Y$. For simple reference, this state in this chapter will be denoted by the "local modeling limit state" (LMLS). Unloading from P_Y for an imposed increasing column rotation will require the curvature to increase at the clamped section and its moment to decrease, since $\kappa > \kappa_Y$. A reduced moment at the base section requires (from equilibrium) the moments and curvatures at all other sections of the column to decrease along an unloading (elastic) moment-curvature curve (similar to that shown in Figure 4.2). Considering that an increased curvature at the base section, which may be considered as a localized damage zone of zero (infinitesimal, or "vanishing") length, will not contribute to an increased column rotation, while at the same time the curvature (unloading) reductions at all of the other sections will call for a reduced rotation, it is clear that unloading for increasing rotations is impossible. Therefore, local modeling methods are limited to $\kappa \leq \kappa_Y$. This problem is also encountered in material nonlinear finite element analysis ([BAZ 76], [HEL 81], [BAZ 03]).

This phenomenon is sometimes referred to as Wood's paradox [WOO 68], and implies that the softening, damage localization zone vanishes in local modeling methods, leading to the zero dissipation

phenomenon ([WOO 68], [BAZ 76], [BAZ 03], [CHA 05d], [CHA 08b], [CHA 08c]).

Wood's paradox can be mathematically proven in this post-buckling problem, by assuming a softening damage zone (or damage localization zone) over a length adjacent to the clamped section of size l_0, where $x \in [0; l_0]$. Inside this zone, the constraint $\kappa > \kappa_Y$ implies a positive derivative (curvature gradient), ensuring an increasing curvature. From equation [4.135], the curvature inside the softening zone can be given by:

$$\frac{d\kappa^*}{dx^*} = -\frac{p\theta}{1-\frac{\kappa^*}{\kappa_Y^*}} \text{ and } \kappa^* > \kappa_Y^* \Rightarrow \frac{d\kappa^*}{dx^*} > 0 \text{ for } x^* \in \left[0;\ l_0^*\right] \qquad [4.166]$$

where $l_0^* = l_0 / L$. The continuity of the curvature at the softening damage boundary implies that:

$$\kappa^*\left(x^* = l_0^*\right) = \kappa_Y^* \text{ and } \frac{d\kappa^*}{dx^*} > 0 \Rightarrow \kappa^* < \kappa_Y^* \text{ for } x^* \in \left[0;\ l_0^*\right] \qquad [4.167]$$

As the curvature κ is increasing inside the softening damage zone, the curvature κ should be necessarily lower than the characteristic curvature κ_Y, which is in contradiction to the fact that the curvature should be larger than the characteristic curvature κ_Y from the adopted constitutive law for the softening branch.

As a reference for later, the LMLS, defined by $P=P_Y$ and the local limit rotation function $\theta_Y(s^*)$ corresponding to $\kappa(0) = \kappa_Y$ and $M(0)=M_Y$, can be calculated for small rotations, which for this case becomes:

$$\frac{d^2\theta_Y}{dx^{*2}} = -\frac{p_Y\theta_Y}{1-\frac{1}{\kappa_Y^*}\frac{d\theta_Y}{dx^*}} \text{ with } \theta_Y(0) = 0,\ \frac{d\theta_Y}{dx^*}(0) = \kappa_Y^* \text{ and}$$

$$\frac{d\theta_Y}{dx^*}(1) = \kappa_Y^* - \sqrt{\kappa_Y^{*2} - 2p_Y\kappa_Y^* e_0^*} \qquad [4.168]$$

The damage function $D(x)$ at this state is denoted by $D_Y(x)$. It can be obtained from equation [4.121] for $f(\theta, D) = 0$. This leads to the proportional equation:

$$D_Y(x^*) = \frac{\frac{d\theta_Y}{dx^*}}{2\kappa_Y^*} \qquad [4.169]$$

which relates the damage function $D_Y(x^*)$ and the positive curvature $\kappa_Y(x^*)$.

It is of interest to study what unloading implies within the local model framework. As mentioned, at the limit, damage localization vanishes to a "zone" consisting of a single section in such models. Consequently, unloading from this state implies elastic unloading along secants stiffnesses defined by $EI(x) = EI_0[1 - D_Y(x)]$. The resulting unloading analysis therefore becomes equivalent to an analysis of a non-uniform column with varying (non-uniform) stiffness.

$$\left[EI\left(1 - D_Y(x)\right)\ \theta'\right]' + P\theta = 0 \qquad [4.170]$$

Typical numerical results are presented in Figure 4.27 for a perfect column and an imperfect column. The figure shows the hysteresis loop linked to the loading and unloading phase. The hysteresis is due to the damage dissipation associated with the damage constitutive law. In both cases, unloading implies rotation reversals (after the $\kappa = \kappa_Y$ curvature state). For the perfect column, unloading from the post-bifurcation branch follows a horizontal line to θ = 0, and then along the ordinate to p = 0.

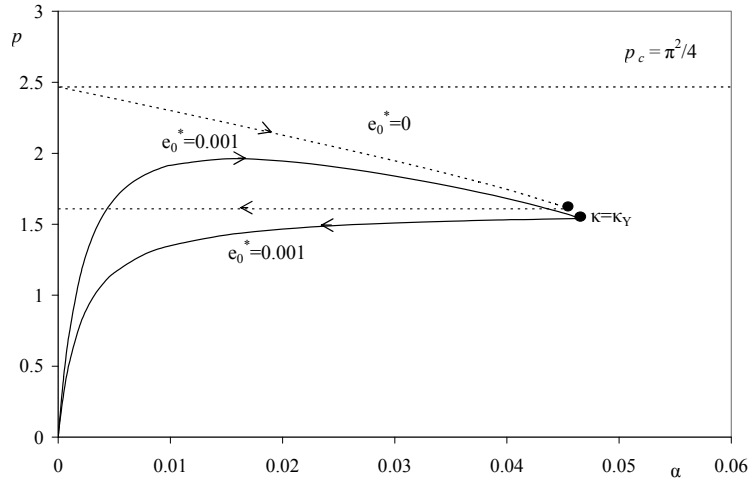

Figure 4.27. *Lod-rotation response including unloading behavior of columns modeled with local damage law (curvature reversal at the clamped section from* $\kappa^* = \kappa_Y^* = 0.1$ *); Wood's paradox found in the postbuckling range*

In order to extend the analysis validity beyond $\kappa = \kappa_Y$ at the base (clamped) section, it is necessary to develop a non-local formulation of the boundary value problem. This is contemplated in this part with the use of non-local damage mechanics for bending-curvature constitutive law, as shown, for instance, by Challamel [CHA 10a]. We start from the generalized version of the principle of virtual work for gradient damage systems defined by:

$$\int_0^L \left[EI(1-D)\theta'\delta\theta' - P\sin\theta\delta\theta \right] ds + \lambda \int_0^{l_0} \left[\left(\overline{\kappa} - \kappa \right) \delta D + l_c^2 \overline{\kappa}' \delta D' \right] ds -$$
$$Pe_0 \cos\theta(L)\delta\theta(L) = 0 \text{ with } \kappa = \theta' \qquad [4.171]$$

where $\overline{\kappa}$ is a non-local curvature, l_c is an additional internal length, specific of the non-local damage model needed for the softening propagation (caused by micro-cracking), and l_0 is the active region of the damage softening process, here denoted as the *damage localization zone* (see also [CHA 10a] in case of non-local hardening–softening plasticity). λ has the dimension of a moment variable. The presentation of the weak formulation as considered

in equation [4.171] may rigorously justify the use of higher order boundary conditions associated with the higher order damage model. For a more detailed presentation, the reader is referred to various papers for the generalized principle of virtual work applied to non-local or gradient damage systems (see, for instance, [FRE 96], [LOR 99], [FOR 09], [PHA 10a], [PHA 10b], [NGU 11a]). An integration by parts of equation [4.171] gives the following coupled system of differential equations:

$$\left[EI\left(1-D\right)\theta'\right]' + P\sin\theta = 0 \text{ and } \overline{\kappa} - l_c^2\overline{\kappa}'' = \kappa \qquad [4.172]$$

The second equation above is similar to Eringen's differential equation [ERI 83] used for non-local elastic models, and later used by Peerlings *et al*. [PEE 96] for non-local damage models. Note that the present model expressed by equation [4.172] cannot be derived from a single energy functional in this case, even if alternative variationally consistent non-local damage models also can be used as shown by Challamel [CHA 10a], for instance. The non-local curvature $\overline{\kappa}$, which controls the non-local damage process, is calculated over the active part l_0 of the damage process, as also suggested by Challamel *et al*. [CHA 10a] from variational arguments or Nguyen *et al*. [NGU 11b] from micromechanics and numerical arguments.

The natural and essential boundary conditions are given by:

$$\begin{aligned} &\left[EI\left(1-D\right)\theta'\delta\theta\right]_0^L - Pe_0\cos\theta\left(L\right)\delta\theta\left(L\right) = 0 \text{ and} \\ &\left[l_c^2\overline{\kappa}'\,\delta D\right]_0^{l_0} = 0 \end{aligned} \qquad [4.173]$$

The non-local damage loading function, valid for $D \geq 1/2$, is chosen as:

$$f\left(\theta', D\right) = \frac{\left|\overline{\kappa}\right|}{\kappa_Y} - 2D \text{ and } \kappa = \frac{d\theta}{ds} = \theta' \qquad [4.174]$$

The damage loading function is expressed with respect to the non-local curvature-driven parameter. This model typically belongs to the class of strain-based non-local damage models developed by Pijaudier-Cabot and Bažant [PIJ 87], where the non-local operator in this work is chosen from Eringen's kernel, as adopted, for instance, by Peerlings *et al.* [PEE 96]. In

the present analysis, the implication of $f(\bar{\kappa},D)=0$ in the damage localized zone is that the non-local curvature $\bar{\kappa}$ can be equivalently replaced by the damage variable D. Inserting the damage variable in the implicit differential equation [4.172] dealing with the non-local curvature variable leads to the equivalent damage loading function defined by:

$$g(\theta',D)=\frac{|\kappa|}{\kappa_Y}-2\left(D-l_c^2D''\right) \qquad [4.175]$$

We recognize in this case that this is a typical gradient damage model where the second derivative of the damage variable appears in the loading function (see, for instance, [FRE 96]; see more recently [PHA 10b], [NGU 11a]). Therefore, in the present problem, there is an equivalence between the non-local integral strain (curvature)-driven damage model (equation [4.174]) and the gradient damage model (equation [4.175]). Note that the gradient of the damage variable vanishes at the boundary ($x = l_0$) of the active damage zone with the present model.

In view of the above, the multipoint (three-point) nonlinear boundary value problem can now be presented with second-order analysis assumptions by:

$$\left[EI(1-D)\theta'\right]'+P\theta=0 \text{ and } D-l_c^2D''=\frac{\theta'}{2\kappa_Y} \text{ for } x\in[0;l_0],$$
$$\text{and } \left[EI\left(1-D_Y(x)\right)\theta'\right]'+P\theta=0 \text{ for } x\in[l_0;L] \qquad [4.176]$$

with the boundary conditions:

$$\theta^-(0)=0,\ D'^-(0)=0,\ D^-(l_0)=\frac{1}{2},\ D'^-(l_0)=0,\ \theta^-(l_0)=\theta^+(l_0),$$
$$EI\left[1-D^-(l_0)\right]\theta'^-(l_0)=EI\left[1-D^+(l_0)\right]\theta'^+(l_0) \text{ and}$$
$$EI\left[1-D_Y(L)\right]\frac{d\theta^+}{dx}(L)=Pe_0 \qquad [4.177]$$

The rotation and the moment variables are continuous variables along the column. Note that the equivalence between the non-local integral strain (curvature)-driven damage model and the gradient damage model both

concern the loading function and the higher order boundary conditions at the softening, damage localization interface as reflected by:

$$\left[\; l_c^2 \overline{\kappa}' \delta D \; \right]_0^{l_0} = 0 \text{ or } \left[\; l_c^2 D' \delta D \; \right]_0^{l_0} = 0 \qquad [4.178]$$

It is found numerically that the gradient of the damage parameter is not vanishing at the free-end boundary of the column, as we generally have $D'(L) = D'_Y(L) \neq 0$.

This (three-point) nonlinear boundary value problem can be numerically solved with the Matlab® program bvp4c, using a first-order vectorial differential equation with four components $(\theta, d\theta/dx, D, dD/dx)$. As before, solutions are obtained for specified (controlled or imposed) rotations at the column's free end (α).

The non-local problem depends on the additional length scale parameter $l_c^* = l_c / L$ that controls the extension of the localization zone l_0 and the post-failure regime (see also [CHA 03] or later [CHA 10b] for non-local plasticity beam models, see also [CHA 09b] or [CHA 10a] for non-local damage beam models). The determination of the characteristic length l_c (or the maximum length of the localization zone l_0) is related to the question of the finite-length hinge model, which is a central question of the present non-local model. Wood [WOO 68] inspired by the works of Barnard and Johnson [BAR 65] suggested the term discontinuity length. Many works have been published on the experimental or theoretical investigation of such a length for reinforced concrete beams [BAZ 03]. It is generally acknowledged that the value of l_c (affecting the maximum localization zone l_0) must be related to the depth of the cross-section h. Therefore, it is recommended that the maximum length of the localization zone l_0 should be chosen to be in the order of the magnitude of the cross-section depth h ([BAZ 87], [BAZ 03]).

In the present numerical calculations, the order of magnitude of $l_c^* = l_c / L$ is chosen equal to 0.1. The damage localization zone propagates (increases) with increasing values of the control parameter α. The simulation was arbitrarily stopped for a value of α giving $l_0^* \approx 0.3$. Figure 4.28 shows column softening results obtained with the non-local damage model for $\kappa >$

κ_Y. It is observed that the local and non-local analysis regimes have a common tangent at the transition between the two regimes.

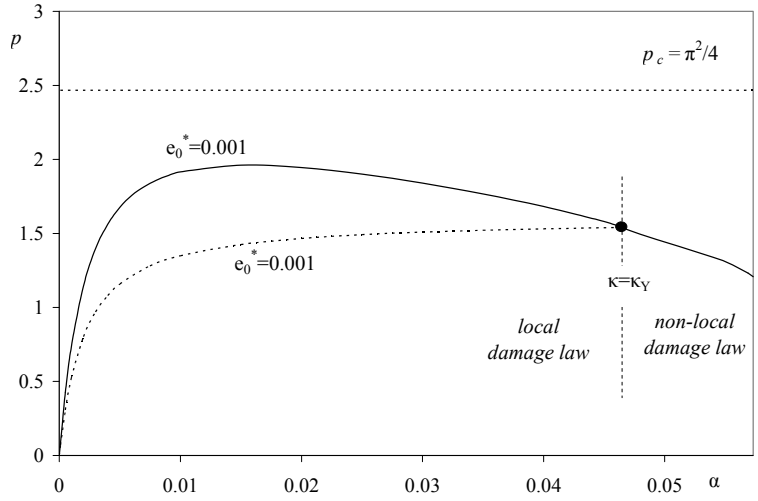

Figure 4.28. *Pre- and post-buckling response according to local damage law for $\kappa < \kappa_Y$, and continued column softening for increasing rotations (due to increasing curvatures in the damage localization zone) as predicted by the non-local damage law; $\kappa_Y^* = 0.1$; $e_0^* = 0.001$; $l_c^* = 0.1$*

Some further studies would probably be needed in the future to investigate the possible coexistence of multiple solutions for this propagating problem, and more specifically the bifurcation from this fundamental solution, for large rotations. In this chapter, we have mainly been concerned about showing the possibility of modeling the post-buckling, softening column response with a non-local CDM model for curvatures in the softening moment-curvature range.

The need of introducing non-locality in the problem formulation has been discussed for the post-buckling response for increasing curvatures in the softening range. A local bending-curvature constitutive law leads to the unloading Wood's paradox, a phenomenon well known for the bending of local softening beams (see Chapter 3). By including some non-locality in the moment-curvature constitutive law, the propagation phenomenon of damage localization has been solved. However, non-locality needs not to be necessary, as far as the limit load calculations are concerned, as these are obtained for local curvatures in the hardening regime.

Appendix 1

Cardano's Method

A1.1. Introduction

This appendix gives the mathematical method to solve the roots of a polynomial of degree 3, called a cubic equation. Some results in this section can be found, for instance, in [ART 04].

As a useful extension, we also give the methodology to determine the roots of a polynomial of degree 4, called a quartic equation. The roots of a cubic equation, like those of a quartic equation, can be found algebraically. It can be shown that this property is no more valid, in general, for a quintic equation (equation of the fifth order) or equations of higher degrees. This is known as the Abel–Ruffini theorem, which was first published in 1824.

Referring to the French dictionary *Le Robert*, the complete method for the general resolution of a cubic is probably due to Tartaglia (Niccolo Fontana, 1500–1557, also called Tartaglia) from his works concluded in 1537, based on the first approach of Gerolamo Cardano (1501–1576). In 1539, Tartaglia revealed his method to Cardano on the condition that Cardano would never reveal it. Some years later, Cardano learned about Ferro's prior work and published Ferro's method in his book *Ars magnasive de regulis algebraicis, liner unus* in 1545. These works, which are produced by the Italian mathematics school, are also based on:

– Rafael Bombelli (1526–1572) was the one who finally managed to address the resolution of polynomial equations with imaginary numbers.

– Lodovico Ferrari (1522–1565), as Cardano's student, gave the solution of a quartic equation, which was published in one chapter of *Ars magnasive de regulis algebraicis, liner unus* written by Cardano in 1545.

– Scipione del Ferro (1465–1526) first discovered the method to solve the canonical form of a cubic equation ($x^3 + px + q = 0$), the first step toward the more general method of a cubic equation.

In the following, we use the mathematical function sgn(x) for the sign function of a real x, and we also use:

$$\sqrt[3]{x} = |x|^{1/3}.sgn(x) \text{ with } |x|=sgn(x).x \qquad \text{[A1.1]}$$

A1.2. Roots of a cubic function – method of resolution

A1.2.1. *Canonical form*

We consider the cubic equation with real coefficients:

$$g(t) = at^3 + bt^2 + ct + d = 0 \text{ with } a \neq 0 \qquad \text{[A1.2]}$$

Each term can be divided by the first coefficient, leading to:

$$t^3 + \frac{b}{a}\ t^2 + \frac{c}{a}\ t + \frac{d}{a} = 0 \qquad \text{[A1.3]}$$

This cubic equation can be factorized as:

$$(t + \frac{b}{3a}\ )^3 + \frac{ac - b^2}{3a^2}(t + \frac{b}{3a}) + \frac{27a^2d + 2b^3 - 9abc}{27a^3} = 0 \qquad \text{[A1.4]}$$

which is known as the canonical form:

$$f(x) = x^3 + px + q = 0 \text{ by setting}$$
$$x = t + \frac{b}{3a}\ ;\ p = \frac{3ac - b^2}{3a^2} \text{ and } q = \frac{27a^2d + 2b^3 - 9abc}{27a^3} \qquad \text{[A1.5]}$$

This canonical equation is solved from the introduction of two numbers y and z such that $x = y + z$ are roots of the cubic equation $f(x) = 0$, by imposing some constraint equalities:

$$\begin{cases} y^3 + z^3 = -q \\ yz = -\frac{p}{3} \end{cases} \Leftrightarrow \begin{cases} f(y+z) = 0 \\ y^3 + z^3 = -q \\ yz = -\frac{p}{3} \end{cases} \Leftrightarrow \begin{cases} (y^3 + z^3) + (p + 3yz)(y+z) + q = 0 \\ y^3 + z^3 = -q \\ yz = -\frac{p}{3} \end{cases} \quad [A1.6]$$

The following change of variable can be chosen as:

$$\begin{cases} Y = y^3 \\ Z = z^3 \end{cases} \text{ and then } \begin{cases} Y + Z = -q \\ (YZ)^{1/3} = -\frac{p}{3} \end{cases} \quad [A1.7]$$

Knowing the sum and the product of Y and Z, these numbers are necessarily the roots U_1 and U_2 of the quadratic equation: $U^2 + qU - \frac{p^3}{27} = 0$. If U_1 and U_2 are known, then y and z are calculated from $(e^{2kip}\ U_1)^{1/3}$ and $(e^{2kip}\ U_2)^{1/3}$, which should be associated by a pair such that the product yz is a real number. We can distinguish several possible cases using the discriminant concept, depending on the sign of $D = q^2 + \frac{4p^3}{27}$ or equivalently, depending on the sign of $4p^3 + 27q^2$.

A1.2.2 *Resolution – one real and two complex roots*

Case $4p^3 + 27q^2 > 0$ (one real and two complex conjugate roots for $f(x) = 0$).

This case includes the case $p = 0$.

In this case, both U_1 and U_2 are real numbers:

$$U_1 = \frac{-q + \sqrt{q^2 + \frac{4p^3}{27}}}{2} = -\frac{q}{2} + \sqrt{\frac{q^2}{4} + \frac{p^3}{27}} \text{ and}$$

$$U_2 = -\frac{q}{2} - \sqrt{\frac{q^2}{4} + \frac{p^3}{27}} \quad [A1.8]$$

To have the product yz as a real number, the possible couples (y, z) (or equivalently (z,y)) are then:

$$(\sqrt[3]{U_1} ; \sqrt[3]{U_2}), (j \sqrt[3]{U_1} ; j^2 \sqrt[3]{U_2}), (j^2 \sqrt[3]{U_1} ; j \sqrt[3]{U_2}) \qquad [A1.9]$$

where j denotes the complex number that is the cubic root of unity. The solutions in x are then:

$$x_1 = \sqrt[3]{-\frac{q}{2} + \sqrt{\frac{q^2}{4} + \frac{p^3}{27}}} + \sqrt[3]{-\frac{q}{2} - \sqrt{\frac{q^2}{4} + \frac{p^3}{27}}}$$

$$x_2 = j \sqrt[3]{-\frac{q}{2} + \sqrt{\frac{q^2}{4} + \frac{p^3}{27}}} + j^2 \sqrt[3]{-\frac{q}{2} - \sqrt{\frac{q^2}{4} + \frac{p^3}{27}}}$$

with $j=e^{2i\pi/3}$ [A1.10]

$$x_3 = j^2 \sqrt[3]{-\frac{q}{2} + \sqrt{\frac{q^2}{4} + \frac{p^3}{27}}} + j \sqrt[3]{-\frac{q}{2} - \sqrt{\frac{q^2}{4} + \frac{p^3}{27}}}$$

In reinforced concrete design, we are only concerned with real solutions, and then only x_1 will be of interest, which finally leads to the root of the initial cubic equation [A1.2], as:

$$t = \frac{1}{3a} \sqrt[3]{-\frac{27a^2d+2b^3-9abc}{2} + \sqrt{\left(\frac{27a^2d+2b^3-9abc}{2}\right)^2 + (3ac-b^2)^3}} + \frac{1}{3a} \sqrt[3]{-\frac{27a^2d+2b^3-9abc}{2} - \sqrt{\left(\frac{27a^2d+2b^3-9abc}{2}\right)^2 + (3ac-b^2)^3}} - \frac{b}{3a}$$

[A1.11]

In the specific case p = 0, this real root is simply reduced to

$$t = \frac{1}{3a} \sqrt[3]{-27a^2d-2b^3+9abc} - \frac{b}{3a}$$

A1.2.3. *Resolution – two real roots*

Case $4p^3 + 27q^2 = 0$ (one real and one double real roots for $f(x) = 0$).

In this case, U_1 and U_2 are real numbers with $U_1 = U_2 = -\frac{q}{2} = \left(\frac{3q}{2p}\right)^3 = U$. The product yz being real, the possible couples (y, z) (or equivalently (z,y)) are given by:

$$(\sqrt[3]{U}\ ;\sqrt[3]{U}\ ),\ (j\sqrt[3]{U}\ ;j^2\sqrt[3]{U}\ ),\ (j^2\sqrt[3]{U}\ ;j\sqrt[3]{U}\ ) \qquad \text{[A1.12]}$$

where j denotes the complex number that is the cubic root of unity. Using the fundamental property $1 + j + j^2 = 0$, the solutions in x are given by:

$$\text{simple root: } x_1 = 2\sqrt[3]{-\frac{q}{2}} = \frac{3q}{p};$$
$$\text{double root: } x_2 = x_3 = -\frac{3q}{2p} \qquad \text{[A1.13]}$$

The real roots of the initial cubic equation $g = 0$ in "t" (equation [A1.2]) are then:

$$t_1 = \frac{3q}{p} - \frac{b}{3a} = \frac{9a^2d + b^3 - 4abc}{a(3ac - b^2)} \quad \text{and}$$
$$t_2 = t_3 = -\frac{3q}{2p} - \frac{b}{3a} = \frac{-9ad + bc}{2(3ac - b^2)} \qquad \text{[A1.14]}$$

A1.2.4. *Resolution – three real roots*

Case $4p^3 + 27q^2 < 0$ (three real roots for $f(x) = 0$).

In this case, U_1 and U_2 are conjugate imaginary numbers. It can be checked that if y is a cubic root of the complex number U_1, then $z = -\frac{p}{3y}$ is the imaginary conjugate number of y; and $x = y+z$ is a real number. Practically, we use the fact that a necessary and sufficient condition for two polynomial equations to have the same roots is that the coefficients of these polynomial equations are proportional. We use the equality $4\cos^3 a - 3\cos$

a - $cos\ 3a = 0$ which is always true. The unknown $y = cos\ a$ is a root of $4\ y^3$ - $3\ y$ - $cos\ 3a = 0$. We are looking for the conditions to have both equations $x^3 + px + q = 0$ and $4\ y^3$ - $3\ y$ - $cos\ 3a = 0$ with proportional coefficients. In this case, if x is a root of the first cubic, kx would be the root of the second cubic, with k as a proportional coefficient, leading to the equivalence principle:

$$\frac{1}{4\,k^3} = -\frac{p}{3\,k} = -\frac{q}{\cos 3a} \quad \text{for } k \neq 0 \qquad \text{[A1.15]}$$

These two equations are equivalent to the conditions:

$$\begin{cases} k^2 = -\dfrac{3}{4p} \\ k^3 = -\dfrac{\cos 3a}{4q} \end{cases} \text{ or equivalently } \begin{cases} k = \sqrt{-\dfrac{3}{4p}} \\ k^3 = -\dfrac{\cos 3a}{4q} \end{cases} \text{ when } p < 0 \qquad \text{[A1.16]}$$

The elimination of k gives: $\cos 3a = \dfrac{3q}{2p}\sqrt{-\dfrac{3}{p}}$ which should be comprised between –1 and +1, leading to $\left(\dfrac{3q}{2p}\sqrt{-\dfrac{3}{p}}\right)^2 \leq 1 \Leftrightarrow \dfrac{27q^2}{-4p^3} \leq 1$ with $-4p^3 > 0$. We recognize the condition that the discriminant is negative, that is $4p^3 + 27q^2 \leq 0$. In this case, and from equation [A1.16], we have the inverse relationship:

$$k = \sqrt{-\frac{3}{4p}} \quad \text{and} \quad a = \frac{1}{3}\left[\text{Arc}\cos\left(\frac{3q}{2p}\sqrt{-\frac{3}{p}}\right) + 2k\pi\right] \qquad \text{[A1.17]}$$

As the roots of the cubic equation $4\ y^3$ - $3\ y$ - $cos\ 3a = 0$ are $y = cos\ a$, the roots of the cubic equation $x^3 + px + q = 0$ are $1/k$ proportional to the previous ones (with $x_1 < x_2 < x_3$):

$$x_1 = 2\sqrt{-\frac{p}{3}} \cos\left[\frac{\text{Arc}\cos\left(\dfrac{3q}{2p}\sqrt{-\dfrac{3}{p}}\right) + 2\pi}{3}\right]$$

$$x_2 = 2\sqrt{-\frac{p}{3}} \cos\left[\frac{\text{Arc}\cos\left(\dfrac{3q}{2p}\sqrt{-\dfrac{3}{p}}\right) + 4\pi}{3}\right] \qquad \text{[A1.18]}$$

$$x_3 = 2\sqrt{-\frac{p}{3}} \quad \cos\left[\frac{\text{Arc}\cos\left(\frac{3q}{2p}\sqrt{-\frac{3}{p}}\right)}{3}\right]$$

The roots of the initial cubic equation [A1.2] g(t) = 0 are then (with $t_1 < t_2 < t_3$):

$$t_1 = \frac{2}{3|a|}\sqrt{b^2 - 3ac}\ \cos\left\{\frac{\text{Arc}\cos\left[\frac{\text{sgn}(-a)\,(27a^2d+2b^3-9abc)(b^2-3ac)^{-1.5}}{2}\right] + 2\pi}{3}\right\} - \frac{b}{3a}$$

$$t_2 = \frac{2}{3|a|}\sqrt{b^2 - 3ac}\ \cos\left\{\frac{\text{Arc}\cos\left[\frac{\text{sgn}(-a)\,(27a^2d+2b^3-9abc)(b^2-3ac)^{-1.5}}{2}\right] + 4\pi}{3}\right\} - \frac{b}{3a}$$

$$t_3 = \frac{2}{3|a|}\sqrt{b^2 - 3ac}\ \cos\left\{\frac{\text{Arc}\cos\left[\frac{\text{sgn}(-a)\,(27a^2d+2b^3-9abc)(b^2-3ac)^{-1.5}}{2}\right]}{3}\right\} - \frac{b}{3a} \quad \text{[A1.19]}$$

A1.3. Roots of a cubic function – synthesis

A1.3.1. *Summary of Cardano's method*

Considering the cubic equation now expressed in terms of the unknown α that is related to the dimensionless neutral axis position in reinforced concrete design:

$$a\alpha^3 + b\alpha^2 + c\alpha + d = 0 \quad \text{[A1.20]}$$

The parameters p and q can be introduced as:

$$p = \frac{3ac - b^2}{3a^2} \text{ and } q = \frac{27a^2d + 2b^3 - 9abc}{27a^3} \quad \text{[A1.21]}$$

If $4p^3 + 27q^2 > 0,$ the unique real solution of the cubic equation is obtained from:

$$\alpha_1 = \sqrt[3]{-\frac{q}{2} + \sqrt{\frac{q^2}{4} + \frac{p^3}{27}}} + \sqrt[3]{-\frac{q}{2} - \sqrt{\frac{q^2}{4} + \frac{p^3}{27}}} - \frac{b}{3a} \quad \text{[A1.22]}$$

If $4p^3 + 27q^2 < 0$, the three real solutions are given by:

$$\begin{cases} \alpha_1 = 2\sqrt{\dfrac{-p}{3}}\cos\left[\dfrac{Arc\cos\left(\dfrac{3q}{2p}\sqrt{\dfrac{3}{-p}}\right)+2\pi}{3}\right]-\dfrac{b}{3a} \\ \alpha_2 = 2\sqrt{\dfrac{-p}{3}}\cos\left[\dfrac{Arc\cos\left(\dfrac{3q}{2p}\sqrt{\dfrac{3}{-p}}\right)+4\pi}{3}\right]-\dfrac{b}{3a} \\ \alpha_3 = 2\sqrt{\dfrac{-p}{3}}\cos\left[\dfrac{Arc\cos\left(\dfrac{3q}{2p}\sqrt{\dfrac{3}{-p}}\right)}{3}\right]-\dfrac{b}{3a} \end{cases} \quad [A1.23]$$

A1.3.2. *Resolution of a cubic equation – example*

We give here a small example to illustrate our purpose. Let us consider the following cubic equation:

$$\alpha^3 - 2\alpha^2 - \alpha + 2 = 0 \quad [A1.24]$$

The coefficients (a,b,c,d) are identified from equation [A1.20] as:

$$a = +1, b = -2, c = -1 \text{ and } d = +2 \quad [A1.25]$$

We calculate now p and q for determining the nature of the solutions:

$$p = c - \frac{b^2}{3} = -\frac{7}{3} \text{ and } q = d + \frac{2}{27}b^3 - \frac{bc}{3} = \frac{20}{27} \quad [A1.26]$$

We calculate the discriminant as:

$$4p^3 + 27q^2 = -36 \le 0 \quad [A1.27]$$

Hence, we have three real solutions for this cubic equation. It can be relevant to compute the following number for the root calculation:

$$Arc\cos\left(\frac{3q}{2p}\sqrt{-\frac{3}{p}}\right)=Arc\cos\left(-\frac{10}{7\sqrt{7}}\right)\approx 2.141173137... \qquad [A1.28]$$

We then compute the three roots of the cubic from equation [A1.23] as:

$$\begin{cases} \alpha_1=2\sqrt{\frac{7}{3}}\cos\left[\frac{2.141173137...+2\pi}{3}\right]+\frac{2}{3}=-1 \\ \alpha_2=2\sqrt{\frac{7}{3}}\cos\left[\frac{2.141173137...+4\pi}{3}\right]+\frac{2}{3}=1 \\ \alpha_3=2\sqrt{\frac{7}{3}}\cos\left[\frac{2.141173137...}{3}\right]+\frac{2}{3}=2 \end{cases} \qquad [A1.29]$$

Of course, it is easy to check that $\alpha^3-2\alpha^2-\alpha+2=.$ $(\alpha+1)(\alpha-1)(\alpha-2)$

A1.4. Roots of a quartic function – principle of resolution

We now consider the quartic equation with real coefficients:

$$f(x)=x^4+ax^3+bx^2+cx+d=0 \text{ with a}\neq 0 \qquad [A1.30]$$

It can be postulated that the quartic corresponds to the beginning of the square of a second-order polynomial equation like:

$$f(x)=\left(x^2+\frac{a}{2}x+y\right)^2+\left(-2y-\frac{a^2}{4}+b\right)\ x^2+(-ay+c)x+(d-y^2) \qquad [A1.31]$$

where *y* is a real number. For the following, we will assume that:

$$-\alpha^2=-2y-\frac{a^2}{4}+b \text{ and } -\beta^2=d-y^2 \qquad [A1.32]$$

y is chosen such that the second trinome of f(x), constituted of the three last terms of f(x), could be considered in a square format. It is then necessary that:

$$(-ay+c)^2 - 4\left(-2y - \frac{a^2}{4} + b\right)(d-y^2) = 0 \qquad \text{[A1.33]}$$

We recognize a cubic equation expressed with the unknown y:

$$\left(2y - \frac{b}{3}\right)^3 + \left(ac - \frac{b^2}{3} - 4d\right)\left(2y - \frac{b}{3}\right) + \frac{abc}{3} - \frac{2b^3}{27}$$

$$+ \frac{8bd}{3} - a^2d - c^2 = 0 \qquad \text{[A1.34]}$$

which can be solved with the previous Cardano's cubic method. Let y_1, y_2 and y_3 be the three roots of this cubic equation. The parameters α and β will be chosen as:

$$\alpha = \sqrt{2y_1 + \frac{a^2}{4} - b} \quad \text{and } \beta = \sqrt{y_1^2 - d} \quad \text{if } ay_1 - c \geq 0 \text{ and}$$
$$\beta = -\sqrt{y_1^2 - d} \quad \text{if } ay_1 - c < 0 \qquad \text{[A1.35]}$$

Once the cubic root y is calculated $y = y_1$, the quartic function $f(x)$ has the following form:

$$f(x) = \left(x^2 + \frac{a}{2}x + y_1\right)^2 - (\alpha x + \beta)^2$$

$$= \left[x^2 + \left(\frac{a}{2} - \alpha\right)x + y_1 - \beta\right]\left[x^2 + \left(\frac{a}{2} + \alpha\right)x + y_1 + \beta\right] = 0 \qquad \text{[A1.36]}$$

Then, the determination of the roots of the quartic function is reduced to the determination of the roots of two quadratic functions.

Appendix 2

Steel Reinforcement Table

	Number of bars and steel area (in cm^2)									
Φ (mm)	1	2	3	4	5	6	7	8	9	10
5	0.196	0.393	0.589	0.785	0.982	1.178	1.374	1.571	1.767	1.963
6	0.283	0.565	0.848	1.131	1.414	1.696	1.979	2.262	2.545	2.827
8	0.503	1.005	1.508	2.011	2.513	3.016	3.519	4.021	4.524	5.027
10	0.785	1.571	2.356	3.142	3.927	4.712	5.498	6.283	7.069	7.854
12	1.131	2.262	3.393	4.524	5.655	6.786	7.917	9.048	10.179	11.310
14	1.539	3.079	4.618	6.158	7.697	9.236	10.776	12.315	13.854	15.394
16	2.011	4.021	6.032	8.042	10.053	12.064	14.074	16.085	18.096	20.106
20	3.142	6.283	9.425	12.566	15.708	18.850	21.991	25.133	28.274	31.416
25	4.909	9.817	14.726	19.635	24.544	29.452	34.361	39.270	44.179	49.087
32	8.042	16.085	24.127	32.170	40.212	48.255	56.297	64.340	72.382	80.425
40	12.566	25.133	37.699	50.265	62.832	75.398	87.965	100.53	113.10	125.66

Table A2.1. *Abacus of the steel area A_s in cm^2 for each bar diameter **Φ** (mm)*

Bibliography

[AAS 73] AAS-JAKOBSEN K., Design of slender reinforced concrete frames, Bericht Nr. 48, Institut für Baustatik, ETH, Zurich, Switzerland, 1973.

[AIF 03] AIFANTIS E.C., "Update on a class of gradient theories", *ACI Structural Journal*, vol. 35, pp. 259–280, 2003.

[AIF 11] AIFANTIS E.C., "On the gradient approach – relation to Eringen's nonlocal theory", *International Journal of Engineering Science*, vol. 49, no. 12, pp. 1367–1377, 2011.

[ALB 81] ALBIGES M., MINGASSON M., *Théorie et pratique du béton armé aux états limites*, Eyrolles, Paris, 1981.

[AME 11] AMERICAN CONCRETE INSTITUTE (ACI Committee 318), Building code requirements for structural concrete (ACI 318-11), and commentary, Farmington Hills, MI, 2011.

[ARI 95] ARISTIZABAL-OCHOA J.D., "Story stability and minimum bracing in RC framed structures: a general approach", *ACI Structural Journal*, vol. 92, no. 6, pp. 735–744, 1995.

[ART 04] ARTEMIADIS N.K., *History of Mathematics: From a Mathematician's Vantage Point*, American Mathematical Society, Paris, 2004.

[AUS 61] AUSTIN W.J., "Strength and design of metal beam columns", *Journal of the Structural Division, ASCE*, vol. 87, no. ST4, pp. 1–32, 1961.

[BAE 08] BAE S., BAYRAK O., "Plastic hinge length of reinforced concrete columns", *ACI Structural Journal*, vol. 105, no. 3, pp. 290–300, 2008.

[BAI 83] BAILOV V., SIGALOV E., *Reinforced Concrete Structures*, MIR, 1983.

[BAK 56] BAKER A.L.L., *Ultimate Load Theory Applied to the Design of Reinforced and Prestressed Concrete Frames*, Concrete Publications Ltd, London, 1956.

[BAR 65] BARNARD P.R., JOHNSON R.P., "Plastic behaviour of continuous composite beams", *Proceedings – Institution of Civil Engineers*, vol. 32, pp. 161–210, 1965.

[BAR 12] BARRERA A.C., BONET J.L., ROMERO M.L., FERNÁNDEZ M.A., "Ductility of slender reinforced concrete columns under monotonic flexure and constant axial load", *Engineering Structures*, vol. 40, pp. 398–412, 2012.

[BAŽ 76] BAŽANT Z.P., "Instability, ductility and size effect in strain-softening concrete", *Journal of Engineering Mechanics, ASCE*, vol. 102, pp. 331–344, 1976.

[BAŽ 87] BAŽANT Z.P., PIJAUDIER-CABOT G., PAN J., "Ductility, snap-back, size effect, and redistribution in softening beams or frames", *Journal of Structural Engineering, ASCE*, vol. 113, no. 12, pp. 2348–2364, 1987.

[BAŽ 03] BAŽANT Z.P., CEDOLIN L., *Stability of Structures – Elastic, Inelastic, Fracture, and Damage Theories*, Dover Publications, Inc., New York, NY, 2003.

[BEN 07] BENALLAL A., MARIGO J.J., "Bifurcation and stability issues in gradient theories with softening", *Modelling and Simulation in Materials Science and Engineering*, vol. 15, pp. 283–295, 2007.

[BIJ 53] BIJLAARD P.P., FISHER P.P., WINTER G., "Strength of columns elastically restrained and eccentrically loaded", *Proceedings, ASCE*, volume 79, separate no. 292, pp. 1–52, 1953.

[BRI 86] BRIDGE R.Q., FRASER, D.J., "Improved G-factor method for evaluating effective lengths of columns", *Journal of Structural Engineering, ASCE*, vol. 113, no. 6, pp. 1341–1356, 1986.

[BRO 07] BROJAN M., PUKSIC A., KOSEL F., "Buckling and post-buckling of a nonlinearly elastic column", *Zeitschrift für Angewandte Mathematik Mechanik*, vol. 87, no. 7, pp. 518–527, 2007.

[CAL 05] CALGARO J., CORTADE J., *Application de l'Eurocode 2: calcul des bâtiments en béton*, Presses de l'Ecole Nationale des Ponts et Chaussées, 2005.

[CAR 86] CARREIRA D., CHU K.H., "The moment-curvature relationship of RC members", *Advanced Computing: An International Journal,* vol. 83, pp. 191–198, 1986.

[CAS 89] CASANDJIAN C., "Calculs de section en Té en flexion non déviée à l'aide de coefficients adimensionnés", *Rencontres Universitaire de Génie Civil, AUGC* – French Civil Engineering Congress, Rennes, 1989.

[CHA 03] CHALLAMEL N., "A gradient plasticity approach for steel structures", *Comptes-Rendus Mécanique*, vol. 331, no. 9, pp. 647–654, 2003.

[CHA 05a] CHALLAMEL N., LANOS C., CASANDJIAN C., "Creep failure in concrete as a bifurcation phenomenon", *International Journal of Damage Mechanics*, vol. 14, pp. 5–24, 2005.

[CHA 05b] CHALLAMEL N., LANOS C., CASANDJIAN C., "Strain-based anisotropic damage modelling and unilateral effects", *International Journal of Mechanical Sciences*, vol. 47, no. 3, pp. 459–473, 2005.

[CHA 05c] CHALLAMEL N., LANOS C., CASANDJIAN C., "Creep damage modelling for quasi-brittle materials", *European Journal of Mechanics A/Solids*, vol. 24, pp. 593–613, 2005.

[CHA 05d] CHALLAMEL N., HJIAJ M., "Non-local behavior of plastic softening beams", *Acta Mechanica*, vol. 178, pp. 125–146, 2005.

[CHA 06a] CHALLAMEL N., LANOS C., CASANDJIAN C., "Stability analysis of quasi-brittle materials – creep under multiaxial loading", *Mechanics of Time-Dependent Materials*, vol. 10, no. 1, pp. 35–50, 2006.

[CHA 06b] CHALLAMEL N., PIJAUDIER-CABOT G., "Stability and dynamics of a plastic softening oscillator", *International Journal of Solids and Structures*, vol. 43, pp. 5867–5885, 2006.

[CHA 07] CHALLAMEL N., LANOS C., CASANDJIAN C., "Creep failure of a simply-supported beam through a uniaxial continuum damage mechanics model", *Acta Mechanica*, vol. 192, no. 1–4, pp. 213–234, 2007.

[CHA 08a] CHALLAMEL N., WANG C.M., "The small length scale effect for a non-local cantilever beam: a paradox solved", *Nanotechnology*, vol. 19, p. 345703, 2008.

[CHA 08b] CHALLAMEL N., LANOS C., CASANDJIAN C., "Plastic failure of nonlocal beams", *Physics Review E*, vol. 78, p. 026604, 2008.

[CHA 08c] CHALLAMEL N., "A regularization study of some ill-posed gradient plasticity softening beam problems", *Journal of Engineering Mathematics*, vol. 62, pp. 373–387, 2008.

[CHA 09a] CHALLAMEL N., "An application of large displacement limit analysis to frame structures", *Structural Engineering & Mechanics*, vol. 33, no. 2, pp. 169–177, 2009.

[CHA 09b] CHALLAMEL N., LANOS C., CASANDJIAN C., "Some closed-form solutions to simple beam problems using non-local (gradient) damage theory", *International Journal of Damage Mechanics*, vol. 18, no. 6, pp. 569–598, 2009.

[CHA 09c] CHALLAMEL N., LANOS C., CASANDJIAN C., "Comment une poutre peut-elle casser?", *Annales du Bâtiment et des Travaux Publics*, vol. 6, pp. 42–46, 2009.

[CHA 09d] CHALLAMEL N., RAKOTAMANANA L., LE MARREC L., "A dispersive wave equation using non-local elasticity", *Comptes-Rendus Mécanique*, vol. 337, pp. 591–595, 2009.

[CHA 09e] CHANDRASEKARAN S., NUNZIANTE L., SERINO G., CARANNANTE F., *Seismic Design Aids for Nonlinear Analysis of Reinforced Concrete Structures*, CRC Press/Taylor and Francis, Florida, FL, 2009.

[CHA 10a] CHALLAMEL N., "A variationally-based nonlocal damage model to predict diffuse microcracking evolution", *International Journal of Mechanical Sciences*, vol. 52, pp. 1783–1800, 2010.

[CHA 10b] CHALLAMEL N., LANOS C., CASANDJIAN C., "On the propagation of localization in the plasticity collapse of hardening-softening beams", *International Journal of Engineering Science*, vol. 48, no. 5, pp. 487–506, 2010.

[CHA 10c] CHALLAMEL N., MEFTAH S.A., BERNARD F., "Buckling of elastic beams on nonlocal foundation: a revisiting of Reissner model", *Mechanics Research Communications*, vol. 37, pp. 472–475, 2010.

[CHA 10d] CHANDRASEKARAN S., NUNZIANTE L., SERINO G., CARANNANTE F., "Axial force bending moment limit domain and flow rule for reinforced concrete elements using Eurocode", *International Journal of Damage Mechanics*, vol. 19, no. 5, pp. 523–558, 2010.

[CHA 11a] CHALLAMEL N., GIRHAMMAR U.A., "Boundary layer effect in composite beams with interlayer slip", *Journal of Aerospace Engineering, ASCE*, vol. 24, no. 2, pp. 199–209, 2011.

[CHA 11b] CHALLAMEL N., GIRHAMMAR U.A., "Variationally-based theories for buckling of partially composite beam-columns including shear and axial effects", *Engineering Structures*, vol. 33, no. 8, pp. 2297–2319, 2011.

[CHA 11c] CHALLAMEL N., HELLESLAND J., "Simplified buckling analysis of imperfection sensitive reinforced concrete columns", *Proceedings of the 24th Nordic Seminar on Computational Mechanics*, 3–4 November 2011, Aalto University, Helsinki, Finland.

[CHA 11d] CHANDRASEKARAN S., NUNZIANTE L., SERINO G., CARANNANTE F., "Curvature ductility of RC sections based on Eurocode: analytical procedure", *KSCE Journal of Civil Engineering*, vol. 15, no. 1, pp. 131–144, 2011.

[CHA 12a] CHALLAMEL N., HELLESLAND J., "Buckling of imperfect CDM structural systems", *International Conference on Damage Mechanics (ICDM)*, Belgrade, Serbia, 25–27 June 2012.

[CHE 99] CHEONG-SIAT-MOY F., "An improved K-factor formula", *Journal of Structural Engineering*, vol. 125, no. 2, pp. 169–174, 1999.

[CIM 07] CIMETIERE A., HALM D., MOLINES E., "A damage model for concrete beam in compression", *Mechanics Research Communications*, vol. 34, pp. 91–96, 2007.

[COM 77] COMITÉ EURO-INTERNATIONAL DU BETON (CEB), "CEB/FIP design manual on buckling and instability", *CEB Bulletin d'Information*, vol. 123, 1977.

[COM 78] COMITÉ EURO-INTERNATIONAL DU BETON (CEB), "CEB-FIP model code for concrete structures", *CEB Bulletin d'Information*, vol. 124–125, 1978.

[COM 93] COMITÉ EURO-INTERNATIONAL DU BETON (CEB), "CEB-FIP model code 1990", *CEB Bull.*, vol. 213–214, 1993.

[DAN 08] DANIELL J.E., OEHLERS D.J., GRIFFITH M.C., MOHAMED ALI M.S., OZBAKKALOGLU T., "The softening rotation of reinforced concrete members", *Engineering Structures*, vol. 30, pp. 3159–3166, 2008.

[DEB 92] de BORST R., MÜHLHAUS H.B., "Gradient-dependent plasticity: formulation and algorithmic aspects", *International Journal for Numerical Methods in Engineering*, vol. 35, pp. 521–539, 1992.

[DES 64] DESAYI P., KRISHNAN S., "Equations for the stress-strain curve of concrete", *Advanced Computing: An International Journal*, vol. 61, no. 3, pp. 345–350, 1964.

[DES 05] Design aids for EC2, Design of concrete structures, Design aids for ENV 1992-1-1 Eurocode 2, Part1, Betonvereniging, The Concrete Society, E & FN Spon, 2005.

[DI 09] DI PAOLA M., MARINO F., ZINGALES M., "A generalized model of elastic foundation based on long-range interactions: integral and fractional model", *International Journal of Solids and Structures*, vol. 46, no. 17, pp. 3124–3137, 2009.

[ELI 12] ELISHAKOFF I., PENTARAS D., DUJAT K., VERSACI C., MUSCOLINO G., STORCH J., BUCAS S., CHALLAMEL N., NATSUKI T., ZHANG Y.Y., WANG C.M., GHYSELINCK G., *Carbon Nanotubes and Nanosensors: Vibrations, Buckling and Ballistic Impact,* ISTE Ltd, London and John Wiley & Sons, New York 2012.

[ENG 03] ENGELEN R.A.B., GEERS M.G.D., BAAIJENS F.P.T., "Nonlocal implicit gradient-enhanced elasto-plasticity for the modelling of softening behaviour", *International Journal of Plasticity*, vol. 19, pp. 403–433, 2003.

[ERI 83] ERINGEN A.C., "On differential equations of nonlocal elasticity and solutions of screw dislocation and surface waves", *Journal of Applied Physics*, vol. 54, pp. 4703–4710, 1983.

[EUR 04] EUROPEAN COMMITTEE FOR STANDARDIZATION (CEN), EN 1992-1-1:2004:E– Eurocode 2: design of concrete structures – Part 1-1: general rules and rules for buildings, Brussels, Belgium, 2004.

[EUR 08a] EUROCODE 2, Worked Examples, European Concrete Platform ASBL, May 2008.

[EUR 08b] EUROPEAN COMMITTEE FOR STANDARDISATION (CEN)/STANDARD NORGE, Eurocode 2: Design of concrete structures -- Part 1-1: General rules and rules for buildings (NS-EN 1992-1-1:2004 + National Annex NA:2008), Oslo, Norway, 2008.

[FAE 73] FAESSEL P., MORISSET A., FOURE B., "Le flambement des poteaux en béton armé", *Annales de l'ITBTP*, p. 305, 1973.

[FOR 09] FOREST S., "Micromorphic approach for gradient elasticity, viscoplasticity, and damage", *Journal of Engineering Mechanics*, vol. 135, no. 3, pp. 117–131, 2009.

[FRE 96] FRÉMOND M., NEDJAR B., "Damage, gradient of damage and principle of virtual power", *International Journal of Solids and Structures*, vol. 33, pp. 1083–1103, 1996.

[FRI 94] FRISLID A., Evaluation of simplified methods for stability analysis of frame structures, Candidatus Scientiarum thesis, Mechanics Division, Department of Mathematics, University of Oslo, Norway, 1994.

[FUE 78] FUENTES A., *Béton armé – Calcul des ossatures – Torsion – Flambement – Oscillations – Déformations plastiques*, Eyrolles, 1978.

[GAL 68] GALAMBOS T.V., *Structural Members and Frames*, Prentice-Hall, Inc., New York, NY, 1968.

[GAL 02] GALILEO, "Discorsi e Dimonstrazioni Matematiche, intorno à due nuove Scienze, 1638", in HAWKINGS S. (ed.), *Sur les épaules des géants – les plus grands textes de physique et d'astronomie*, Dunod, pp. 154–182, 2002.

[GAL 08] GALAMBOS, T.V., SUROVEK, A.E., *Structural Stability of Steel – Concepts and Applications for Structural Engineers*, John Wiley & Sons, Inc., Hoboken, NJ, 2008.

[GIR 07] GIRHAMMAR U.A., PAN D.H., "Exact static analysis of partially composite beams and beam-columns", *International Journal of Mechanical Sciences*, vol. 49, pp. 239–255, 2007.

[GYÖ 88] GYÖRGY F., *Cours de béton armé et constructions hydrauliques, Tome 1 – Béton armé aux états limites*, Presse de l'Ecole Nationale Polytechnique d'Alger, 1988.

[HAL 96] HALM D., DRAGON A., "A model of anisotropic damage by mesocrack growth: unilateral effect", *International Journal of Damage Mechanics*, vol. 5, pp. 384–402, 1996.

[HAS 85] HASLACH H.W., "Post-buckling behaviour of columns with nonlinear constitutive equations", *International Journal of Non-Linear Mechanics*, vol. 20, no. 1, pp. 53–67, 1985.

[HAS 09] HASKETT M., OEHLERS D.J., ALI M.S.M., WU C., "Rigid moment-rotation mechanism for reinforced concrete beam hinges", *Engineering Structures*, vol. 31, pp. 1032–1041, 2009.

[HEL 70a] HELLESLAND J., A study into the sustained and cyclic load behaviour of reinforced concrete columns, PhD Thesis, Department of Civil Engineering, University of Waterloo, Canada, 1970.

[HEL 70b] HELLESLAND J., GREEN R., "Strength characteristics of reinforced concrete columns under sustained loading", *IABSE Symposium on Design of Concrete Structures for Creep, Shrinkage and Temperature Changes*, Madrid, Spain, 1970.

[HEL 72] HELLESLAND J., GREEN R., "A stress and time dependent strength law for concrete", *Cement and Concrete Research*, vol. 2, pp. 261–275, 1972.

[HEL 76] HELLESLAND J., Approximate second order analysis of unbraced frames, Technical report, Dr. Ing. A. Aas-Jakobsen Ltd., Oslo, Norway, pp. 1–43, 1976.

[HEL 81] HELLESLAND J., SCORDELIS A.C., "Analysis of r.c. bridge columns under imposed deformations", *Proceedings, IABSE Colloquium on Advanced Mechanics of Reinforced Concrete*, Delft, Holland, pp. 545–559, June, 1981.

[HEL 85] HELLESLAND, J., CHOUDHURY, D., SCORDELIS, A.C., Nonlinear analysis and design of RC bridge columns subjected to imposed deformations, Report no. UCB/SESM-85/03, Department of Civil Engineering, University of California, Berkeley, CA, 1985.

[HEL 90a] HELLESLAND J., "Ny NS~3473 – Når er en trykkstav slank?", Betongprodukter, *Norges Betongindustriforbund*, vol. 1, 1990.

[HEL 90b] HELLESLAND J., "Øvre slankhetsgrenser for trykkstaver", Betongprodukter, *Norges Betongindustriforbund*, vol. 4, 1990.

[HEL 95] HELLESLAND J., "Simplified system instability analysis", in SHANMUGAN N.E., CHOO Y.S. (eds.), *4th Pacific Structural Steel Conference (PSSC'95)*, vol. 1, Pergamon Press, pp. 95–102, 1995.

[HEL 96a] HELLESLAND J., BJORHOVDE R., "Restraint demand factors and effective lengths of braced columns", *Journal of Structural Engineering, ASCE*, vol. 122, no. 10, pp. 1216–1224, 1996.

[HEL 96b] HELLESLAND J., BJORHOVDE R., "Improved frame stability analysis with effective lengths", *Journal of Structural Engineering, ASCE*, vol. 122, no. 11, pp. 1275–1283, 1996.

[HEL 97] HELLESLAND J., FRISLID A., "Approximate critical load analysis of frame systems with axially compressed beams", in USAMI T. (ed.), *Proceedings, 5th International Colloquium and Ductility of Structures (SDSS'97)*, Japanese Society of Steel Construction, Nagoya University, Japan, vol. 2, pp. 699–706, 1997.

[HEL 98] HELLESLAND J., "Application of the method of means to the stability analysis of unbraced frames", *Journal of Constructional Steel Research*, vol. 46, no. 1–3, 1998. (The full version is available in Preprint Series for Mechanics and Applied Mathematics, no. 4, December 1997, Department of Mathematics, University of Oslo, Norway).

[HEL 02a] HELLESLAND J., Lower slenderness limits for braced end-loaded r.c. compression members, Research report in mechanics, no. 02-2, Mechanics Division, University of Oslo, Oslo, Norway, pp. 1–33, 2002.

[HEL 02b] HELLESLAND J., Lower slenderness limits for unbraced and transversely loaded r.c. compression members, Research report in mechanics, no. 02-1, Mechanics Division, University of Oslo, Oslo, Norway, pp. 1–37, 2002.

[HEL 05a] HELLESLAND J., "Nonslender column limits for braced and unbraced reinforced concrete members", *ACI Structural Journal*, vol. 102, no. 1, pp. 12–21, 2005.

[HEL 05b] HELLESLAND J., Analysis of second-order effects with axial loads, EN 1992-1-1:2004, National Annex, Evaluations and proposals submitted to Standard Norge, Oslo, Norway, pp. 1–10, 2005.

[HEL 07] HELLESLAND J., "Mechanics and effective lengths of columns with positive and negative end restraints", *Engineering Structures*, vol. 29, no. 12, pp. 3464–3474, 2007.

[HEL 08a] HELLESLAND, J. Approximate second order analysis of unbraced frames reflecting inter-storey interaction in single curvature regions, Research report in mechanics, no. 08-2. Mechanics Division, University of Oslo, Oslo, Norway, pp.1–26, 2008.

[HEL 08b] HELLESLAND J., "Mechanics and slederness limits of sway-restricted reinforced concrete columns", *Journal of Structural Engineering, ASCE*, vol. 134, no. 8, pp. 1300–1309, 2008.

[HEL 09a] HELLESLAND J., "Extended second order approximate analysis of frames with sway-braced column interaction", *Journal of Constructional Steel Research*, vol. 65, no. 5, pp. 1075–1086, 2009.

[HEL 09b] HELLESLAND J., "Second order approximate analysis of unbraced multistorey frames with single curvature regions", *Engineering Structures*, vol. 31, no. 8, pp. 1734–1744, 2009.

[HEL 12] HELLESLAND J., "Evaluation of effective length formulas and applications in system instability analysis", *Engineering Structures*, vol. 45, no. 12, pp. 405–420, 2012.

[HEY 99] HEYMAN J., *The Science of Structural Engineering*, Imperial College Press, 1999.

[HIL 58] HILL R., "A general theory of uniqueness and stability in elastic-plastic solids", *Journal of the Mechanics and Physics of Solids*, vol. 6, pp. 236–249, 1958.

[HIL 76] HILLERBORG A., MODEER M., PETERSSON P.E., "Analysis of crack formation and crack growth in concrete by means of fracture mechanics and finite elements", *Cement and Concrete Research*, vol. 6, pp. 773–782, 1976.

[HOG 51] HOGNESTAD E., A study of combined and axial load in reinforced concrete members, Bulletin no. 399, University of Illinois Engineering Experiment Station, Urbana, November 1951.

[HOR 75] HORNE M.R., "An approximate method for calculating the elastic critical loads of multi-storey plane frames", *Journal of Structural Engineering*, vol. 53, no. 6, pp. 242–248, 1975.

[JIR 02] JIRÁSEK M., BAŽANT Z.P., *Inelastic Analysis of Structures*, Wiley, 2002.

[JUN 05] JUNG J.H., KANG T.J., "Large deflection analysis of fibers with nonlinear elastic properties", *Journal of the Textile Institute*, vol. 75, no. 10, pp. 715–723, 2005.

[KAB 66] KABAILA A.P., HALL A.S., "Analysis of instability of unrestrained prestressed concrete columns with end eccentricities", in *Symposium on Reinforced Concrete Columns*, presented at the 61th Annual ACI Convention, San Francisco, California, March 4, 1965, Compiled under the sponsorship of ACI-ASCE Committee 441, American Concrete Institute, Publication SP-13, 1966.

[KOE 07] KOECHLIN P., POTAPOV S., "Global constitutive model for reinforced concrete plates", *Journal of Engineering Mechanics*, vol. 133, no. 3, pp. 257–266, 2007.

[KOE 08] KOECHLIN P., ANDRIEUX S., MILLARD A., POTAPOV S., "Failure criterion for reinforced concrete beams and plates subjected to membrane force, bending and shear", *European Journal of Mechanics A/Solids*, vol. 27, pp. 1161–1183, 2008.

[KOI 45] KOITER W.T., Over de stabiliteit van het elastische evenwicht, Dissertation, Delft, Holland, The Netherlands, 1945.

[KOU 87] KOUNADIS A.N., MALLIS J.G., "Elastica type buckling analysis of bars from non-linearly elastic material", *International Journal of Non-Linear Mechanics*, vol. 22, no. 2, pp. 99–107, 1987.

[KRA 11] KRAUBERGER N., BRATINA S., SAJE M., SCHNABL S., PLANINC I., "Inelastic buckling load of a locally weakened reinforced concrete column", *Engineering Structures*, vol. 34, pp. 278–288, 2011.

[KUH 76] KUHN G.K., An appraisal of the effective length alignment charts, Engineering report for the degree of M.Sc. in engineering, Arizona State University, Tempe, AZ.

[LAC 08] LACARBONARA W., "Buckling and post-buckling of non-uniform non-linearly elastic rods", *International Journal of Mechanical Sciences*, vol. 50, pp. 1316–1325, 2008.

[LAI 83a] LAI S.M.A., MACGREGOR J.G., "Geometric non-linearities in unbraced multistory frames", *Journal of Structural Engineering, ASCE*, vol. 109, no. 11, pp. 2528–2545, 1983.

[LAI 83b] LAI S.M.A., MACGREGOR J.G., HELLESLAND J., "Geometric non-linearities in nonsway frames", *Journal of Structural Engineering, ASCE*, vol. 109, no. 12, pp. 2770–2785, 1983.

[LAR 12] LARSEN K.P., POULSEN P.N., NIELSEN L.O., "Limit analysis of 3D reinforced concrete beam elements", *Journal of Engineering Mechanics*, vol. 138, no. 3, pp. 286–296, 2012.

[LEE 49] LEE A.Y.-W., A study on column analysis, PhD. Thesis, Cornell University, Ithaca, NY, 1949.

[LEE 09] LEE C.L., FILIPPOU F.C., "Efficient beam-column element with variable inelastic end zones", *Journal of Structural Engineering*, vol. 135, no. 11, pp. 1310–1319, 2009.

[LEM 05] LEMAITRE J., DESMORAT R., *Engineering Damage Mechanics: Ductile, Creep, Fatigue and Brittle Failures*, Springer, 2005.

[LEM 77] LEMESSURIER W.M., "A practical method of second order analysis", *Engineering Journal, AISC*, vol. 14, no. 2, pp. 49–67, 1977.

[LEN 81] LENSCHOW R., *Betongkonstruksjoner*, Tapir, 1981.

[LEO 78] LEONHARDT F., *Vorlesungen über Massivbau*; Vierter Teil, Nachweis der Gebrauchsfähigkeit; Rissebeschränkung, Formänderungen, Momentenumlagerung und Bruchlinientheorie im Stahlbetonbau, Springer-Verlag, 1978.

[LEW 87] LEWIS G., MAZILU P., MONASA F., "A variational approach for the deflections and stability behaviour of postbuckled elastic-plastic slender struts", *International Journal of Non-Linear Mechanics*, vol. 22, no. 5, pp. 373–385, 1987.

[LHE 76] L'HERMITE R., *Flambage et stabilité – Le flambage élasto-plastique des colonnes et systèmes de barres droites*, Eyrolles, 1976.

[LOR 99] LORENTZ E., ANDRIEUX S., "A variational formulation for nonlocal damage models", *International Journal of Plasticity*, vol. 15, pp. 119–138, 1999.

[LUI 92] LUI E.M., "A novel approach for K factor determination", *Engineering Journal, AISC*, vol. 29, no. 4, pp. 150–159, 1992.

[MAC 75] MACGREGOR J.G., OELHAFEN V.H., HAGE S.E., "A re-examination of the EI values for slender columns", *Reinforced Concrete Columns*, Special Publication SP-50, American Concrete Institute, pp. 1–40, 1975.

[MAC 97] MAC GREGOR J.G., *Reinforced Concrete Mechanics and Design*, 3rd ed., Prentice Hall, 1997.

[MAG 14] MAGNY M.A.V., *La construction en béton armé, théorie et pratique*, ED Librairie Polytechnique, CH. Béranger, 1914.

[MAN 67] MANUEL R.F., MACGREGOR J.G., "Analysis of restrained reinforced concrete columns under sustained load", *Advanced Computing: An International Journal*, vol. 64, no. 1, pp. 12–23, 1967.

[MAR 03] MARI A., HELLESLAND J., Lower slenderness limits for reinforced concrete columns, Research Report no. 2003-01, Department of Construction Engineering, Universitat Politecnica de Catalunya, Barcelona, Spain, pp. 1–50, 2003.

[MAR 05] MARI A.R., HELLESLAND J., "Lower slenderness limits for rectangular reinforced concrete columns", *Journal of Structural Engineering*, vol. 131, no. 1, pp. 85–95, 2005.

[MAS 59] MASSONNET C., "Stability considerations in the design of steel columns", *Journal of the Structural Division, ASCE*, vol. 85, pp. 75–111, 1959.

[MAT 67] MATTOCK A.H., "Discussion of "rotational capacity of reinforced concrete beams" by W.G. Corley", *Journal of the Structural Division, ASCE*, vol. 93, no. ST2, pp. 519–522, 1967.

[MAZ 86] MAZARS J., "A description of micro and macroscale damage of concrete structures", *Engineering Fracture Mechanics*, vol. 25, no. 5–6, pp. 729–737, 1986.

[MAZ 96] MAZARS J., PIJAUDIER-CABOT G., "From damage to fracture mechanics and conversely: a combined approach", *International Journal of Solids and Structures*, vol. 33, pp. 3327–3342, 1996.

[MAZ 09] MAZARS J., MILLARD A. (eds), *Dynamic Behaviour of Concrete and Seismic Engineering*, ISTE Ltd, London and John Wiley and Sons New York, 2009.

[MEN 01] MENDIS P., "Plastic hinge lengths of normal and high-strength concrete in flexure", *Advances in Structural Engineering*, vol. 4, pp. 189–195, 2001.

[MON 74] MONASA F.E., "Deflections and stability behavior of elastoplastic flexible bars", *Journal of Applied Mechanics*, vol. 96, pp. 537-538, 1974.

[MOS 07] MOSLEY B., BUNGAY J., HULSE R., *Reinforced Concrete Design to Eurocode 2*, 6th ed., Palgrave MacMillan, 2007.

[MUH 91] MÜHLHAUS H.B., AIFANTIS E.C., "A variational principle for gradient plasticity", *International Journal of Solids and Structures*, vol. 28, pp. 845–857, 1991.

[MUR 97] MURAKAMI S., KAMIYA K., "Constitutive and damage evolution equations of elastic-brittle materials based on irreversible thermodynamics", *International Journal of Mechanical Sciences*, vol. 39, no. 4, pp. 473–486, 1997.

[MUR 12] MURAKAMI S., *Continuum Damage Mechanics – A Continuum Mechanics Approach to the Analysis of Damage and Fracture*, Springer, 2012.

[NGU 11a] NGUYEN Q.S., "Variational principles in the theory of gradient plasticity", *Comptes-Rendus Mécanique*, vol. 339, pp. 743–750, 2011.

[NGU 11b] NGUYEN V.P., LLOBERAS-VALLS O., STROEVEN M., SLUYS L.J., "Homogenization-based multiscale crack modelling: from micro-diffusive damage to macro-cracks", *Computer Methods in Applied Mechanics and Engineering*, vol. 200, pp. 1220–1236, 2011.

[NIE 99] NIELSEN M.P., *Limit Analysis and Concrete Plasticity*, CRC, Boca Raton, 1999.

[NOR 89] NORWEGIAN STANDARDS ASSOCIATION (NSF), NS 3473—Concrete Structures. Design Rules, 3rd ed., Oslo, Norway (Standard Norge), 1989; 5th ed., 1998.

[NOR 04] NORME EUROPÉENNE EN 1992-1.1 Eurocode 2 – Calcul des structures en béton, AFNOR, April 2004.

[ODE 70] ODEN J.T., CHILDS S.B., "Finite deflection of a nonlinearly elastic bar", *Journal of Applied Mechanics*, vol. 69, pp. 48–52, 1970.

[OTT 05] OTTOSEN N.S., RISTINMAA M., *The Mechanics of Constitutive Modelling*, Elsevier, 2005.

[PAI 09] PAILLÉ J.M., *Calcul des structures en béton*, Guide d'application, Eyrolles, 2009.

[PAR 75] PARK R., PAULAY T., *Reinforced Concrete Structures*, John Wiley & Sons, New York, NY, 1975.

[PAU 92] PAULAY T., PRIESTLEY M.J.N., *Seismic Design of Reinforced Concrete and Masonry Buildings*, Wiley, New York, NY, 1992.

[PAU 11] PAULTRE P., *Structures en béton armé – Analyse et dimensionnement*, International Polytechnic Press, Polytechnic School of Montreal , 2011.

[PEE 96] PEERLINGS R.H.J., DE BORST R., BREKELMANS W.A.M., DE VREE J.H.P., "Gradient-enhanced damage for quasi-brittle materials", *International Journal for Numerical Methods in Engineering*, vol. 39, pp. 3391–3403, 1996.

[PER 09] PERCHAT J., *Eurocode 2 – Béton armé, Dispositions et données générales*, Techniques de l'Ingénieur, 2009.

[PER 10] PERCHAT J., *Traité de béton armé*, Editions Le Moniteur, 2010.

[PFR 64] PFRANG E.O., SIESS C., SOZEN M.A., "Load-moment-curvature characteristics of RC cross sections", *Advanced Computing: An International Journal*, vol. 61, no. 7, pp. 763–778, 1964.

[PHA 10a] PHAM K., MARIGO J.J., "The variational approach to damage: I. The foundations", *Comptes-Rendus Mécanique*, vol. 338, pp. 191–198, 2010.

[PHA 10b] PHAM K., MARIGO J.J., "The variational approach to damage: II. The gradient damage models", *Comptes-Rendus Mécanique*, vol. 338, pp. 199–206, 2010.

[PIJ 87] PIJAUDIER-CABOT G., BAŽANT Z.P., "Nonlocal damage theory", *Journal of Engineering Mechanics*, vol. 113, pp. 1512–1533, 1987.

[PLA 93] PLANAS J., ELICES M., GUINEA G.V., "Cohesive cracks versus nonlocal models: closing the gap", *International Journal of Fracture*, vol. 63, pp. 173–187, 1993.

[POL 98] POLIZZOTTO C., BORINO G., FUSCHI P., "A thermodynamically consistent formulation of nonlocal and gradient plasticity", *Mechanics Research Communications*, vol. 25, no. 1, pp. 75–82, 1998.

[PRI 87] PRIESTLEY M.J.N., PARK R., "Strength and ductility of concrete bridge columns under seismic loading", *ACI Structural Journal*, vol. 84, no. 1, pp. 61–76, 1987.

[REI 58] REISSNER E., "A note on deflections of plates on a viscoelastic foundation", *Journal of Applied Mechanics*, vol. 25, pp. 144–145, 1958.

[ROB 74] ROBINSON J.R., *Cours de béton armé de l'Ecole Nationale des Ponts et Chaussées*, 1974.

[ROB 75] ROBINSON J., FOURÉ F., BOURGHLI M., "Le flambement des poteaux en béton armé chargés avec des excentricités différentes à leurs extrémités", *Annales de l'ITBTP*, vol. 333, pp. 46–74, 1975.

[ROU 09a] ROUX J., *Pratique de l'Eurocode 2 (Tome 1)*, Eyrolles, 2009.

[ROU 09b] ROUX J., *Pratique de l'Eurocode 2 (Tome 2)*, Eyrolles, 2009.

[ROY 01] ROYER-CARFAGNI G., "Can a moment-curvature relationship describe the flexion of softening beams", *European Journal of Mechanics A/Solids*, vol. 20, pp. 253–276, 2001.

[RUB 73] RUBIN H., "Das QΔ Verfahren zur vereinfachten Berechnung verschieblicher Rahmensysteme nach dem Traglastverfahren der Theorie II. Ordnung", *Der Bauingenieur*, vol. 48, no. 8, pp. 275–285, 1973.

[RÜS 60] RÜSCH H., "Researches toward a general flexural theory for structural concrete", *Advanced Computing: An International Journal*, vol. 57, no. 1, pp. 1–28, 1960.

[SAL 83] SALENÇON J., *Calcul à la rupture et analyse limite*, Presses de l'École Nationale des Ponts et Chaussées, 1983.

[SAL 90] SALENÇON J., "An introduction to the yield design theory and its application to soil mechanics", *European Journal of Mechanics A/Solids*, vol. 9, no. 5, pp. 477–500, 1990.

[SAL 02] SALENÇON J., *De l'élastoplasticité au calcul à la rupture*, Editions de l'Ecole Polytechnique, Ellipses, 2002.

[SAL 06] SALENÇON J., "Revisiting Galileo's insight in structural mechanics", *Conference at the Department of Structural Mechanics*, Budapest University of Technology and Economics, June 2006.

[SAR 68] SARGIN M., Stress-strain relationships for concrete and the analysis of structural concrete sections, PhD Thesis, University of Waterloo, Ontario, Canada, p. 334, submitted March 1968.

[SAR 69] SARGIN M., HANDA V.K., *A General Formulation for the Stress-Strain Properties of Concrete*, University of Waterloo, Canada, Solid Mechanics Division, SM Report No. 3, May 1969.

[SAR 71] SARGIN M., *Stress-Strain Relationships for Concrete and the Analysis of Structural Concrete Sections*, Solid Mechanics Division, University of Waterloo, Ontario, Canada, 1971.

[SAW 65] SAWYER H.A., "Design of concrete frames for two failure states", *Proceedings of the International Symposium on the Flexural Mechanics of Reinforced Concrete*, ASCE-ACI, Miami, pp. 405–431, 1965.

[SIE 10] SIEFFERT Y., *Le béton armé selon les Eurocodes 2*, Dunod, 2010.

[THO 09] THONIER H., *Conception et calcul de structures de bâtiments – l'Eurocode 2 pratique*, Presses de l'Ecole Nationale des Ponts et Chaussées, 2009.

[TIM 61] TIMOSHENKO S.P., GERE J.M., *Theory of Elastic Stability*, McGraw-Hill, 1961.

[TIM 83] TIMOSHENKO S.P., *History of Strength of Materials*, Dover Publications, 1983.

[VER 94] VERMEER P.A., BRINKGREVE R.B.J., "A new effective non-local strain measure for softening plasticity", in CHAMBON, R., DESRUES, J., VARDOULAKIS, I. (eds), Balkema, Rotterdam, pp. 89–100, 1994.

[VIR 04] VIRGIN L.N., PLAUT, R.H., "Postbuckling and vibration of linearly elastic and softening columns under self-weight", *International Journal of Solids and Structures*, vol. 41, pp. 4989–5001, 2004.

[WAL 90] WALTHER R., MIEHLBRADT M., *Dimensionnement des structures en béton, Bases et Technologie*, Treaty of Civil Engineering at the Ecole Polytechnique Fédérale de Lausanne, vol. 7, 1990.

[WAN 96] WANG C.Y., "Global buckling load of a nonlinearly elastic bar", *Acta Mechanica*, vol. 119, pp. 229–234, 1996.

[WES 04] WESTERBERG B., Second-order effects in slender concrete structure – background to rules EC2, TRITA-BKN, Report 77, Betonbyggnad, KTH, Stockholm, Sweden, p. 98, 2004.

[WIN 54] WINTER G., "Compression members in trusses and frames", *The Philosophy of Column Design, Proceedings of the 4th Technical Session*, Column Research Council, Lehigh University, Bethlehem, PA, 1954.

[WOO 68] Wood R.H., "Some controversial and curious developments in the plastic theory of structures", in HEYMAN J., LECKIE F.A. (eds), *Engineering Plasticity*, Cambridge University Press, UK, pp. 665–691, 1968.

[XU 02] XU L., LIU, Y., "Story stability of semi-braced steel frames", *Journal of Constructional Steel Research*, vol. 58, no. 4, pp. 467–491, 2002.

[YU 82] YU T.X., JOHNSON W., "The plastica: the large elastic–plastic deflection of a strut", *International Journal of Non-Linear Mechanics*, vol. 17, no. 3, pp. 195–209, 1982.

[YU 96] YU T.X., ZHANG L.C., *Plastic Bending: Theory and Applications*, World Scientific, Singapore, 1996.

[YU 12] YU Y., WU B., LIM C.W., "Numerical and analytical approximations to large post-buckling deformation of MEMS", *International Journal of Mechanical Sciences*, vol. 55, pp. 95–103, 2012.

[ZHA 10] ZHANG Y.Y., WANG C.M., CHALLAMEL N., "Bending, buckling and vibration of hybrid nonlocal beams", *Journal of Engineering Mechanics*, vol. 136, no. 5, pp. 562–574, 2010.

[ZHA 12] ZHAO X.M., WU Y.F., LEUNG A.Y.T., "Analyses of plastic hinge regions in reinforced concrete beams under monotonic loading", *Engineering Structures*, vol. 34, pp. 466–482, 2012.

Index

B

Bending moment and normal forces, 90
Bending-curvature law, 222
Bilinear behavior of concrete, 206–209
Buckling and post-buckling, 242–258

C

Cantilever, 134
Collapse, 123, 133
Composite cross section, 20, 31, 32, 36, 58
Condition of non-fragility, 220–222
Continuum damage mechanics, 129–133, 242–245
Cubic equation, 54

D

Deflection calculation, 118
Dimensionless parameters, 170–173
Ductility, 217–219

E

Eccentricity, 93–99
Elastic behavior, 32, 36, 71

F

Fundamental analysis, 19

I

Imperfection sensitive law, 254

L

Limit load, 243, 251, 254, 257, 265

N

Neutral axis, 14–15
Non-local mechanics, 155, 169

O

Optimization, 50–53

P

Parabola-rectangle diagram, 179–183
Pivot A, 19–20, 180–181, 201–209
Pivot B, 19–20, 181–182, 210–215
Pivot C, 182–183
Plastic hinge length, 233, 234
Plasticity, 129–133
Post-failure, 133–156

R

Rectangular cross section, 4, 30, 35, 39–65, 67, 74–79, 92–94, 96–98
Reduced moments, 191–192
Reinforced concrete design, 14, 26, 38, 62, 69, 94, 96

S

Sargin's law, 166–169
Serviceability limit state, 1–68, 69–122
Simplified approach, 232
Simplified diagram, 164, 174
Softening, 129–131, 224
Steel reinforcement, 4–6, 14

T

T-cross-section, 58–68, 76–79
Tension stiffening phenomenon, 107–109
Triangular cross section, 82, 85, 86, 87, 88

U

Ultimate limit state, 123–192, 193–276

W

Wood's paradox, 135–137, 235, 237, 238, 241, 258, 259, 261, 265

Y

Yield design, 123–125